Lectures on turbulence

Physics Reports 1021 (2023) 1–106

Contents lists available at ScienceDirect

Physics Reports

journal homepage: www.elsevier.com/locate/physrep

Lectures on turbulence

Roberto Benzi [a], Federico Toschi [b,c,*]

[a] Department of Physics and INFN, University of Rome Tor Vergata, I-00133 Rome, Italy
[b] Department of Applied Physics and Science Education, Eindhoven University of Technology, 5600 MB Eindhoven, The Netherlands
[c] CNR-IAC, I-00185 Rome, Italy

ARTICLE INFO

Article history:
Received 26 February 2023
Accepted 25 May 2023
Available online xxxx
Editor: Itamar Procaccia

Keywords:
Fluid dynamics turbulence

ABSTRACT

Fluid dynamics turbulence refers to the chaotic and unpredictable dynamics of flows. Despite the fact that the equations governing the motion of fluids are known since more than two centuries, a comprehensive theory of turbulence is still a challenge for the scientific community. Rather recently a number of important breakthroughs have clarified many relevant, fascinating, and largely unexpected, statistical features of turbulent fluctuations. In these lectures, we discuss recent advances in the field with the aim of highlighting the physical meaning and implication of these new ideas and their role in contributing to disentangling different parts of our understanding of the turbulence problem. The lectures aim at introducing non-experts to the subject and no previous knowledge of the field is required.

Contents

* Corresponding author at: Department of Applied Physics and Science Education, Eindhoven University of Technology, 5600 MB Eindhoven, The Netherlands.
E-mail address: f.toschi@tue.nl (F. Toschi).

https://doi.org/10.1016/j.physrep.2023.05.001

Introduction

Turbulence can be considered as the most outstanding and classical prototype of complex system and the fascinating complex behaviour of turbulent flows inspired artists like for instance Van Gogh or Hokusai. Understanding the physics of turbulent flows is often considered as the "last grand challenge" of classical physics: we know the equation of motion for a Newtonian fluid since 200 years and we are still facing fundamental challenges to achieve a quantitative description of the statistical and geometrical properties characterising turbulent flows.

The goal of this review is to collect the most basic knowledge and recent advances in the understanding the physics of turbulent flows. The review is addressed to any student, graduate and undergraduate, and researcher that wishes a broader view on the topic. Most of the focus is devoted to homogeneous and isotropic turbulence, as this is usually a good representation of any turbulent flow at small enough scales and far enough from boundaries. The case of most complex flows, where anisotropies and non homogeneities prevail is also shortly discussed towards the end of the review.

Although there exist a number of excellent textbooks on fluid dynamics turbulence, we feel that there is a need for a rather pedagogical introduction to the subject including the recent theoretical and conceptual developments. We assume that the reader does know the basic tools of the theory of dynamical systems and fluid mechanics. The required level of

knowledge is at any rate elementary as it can be easily achieved during undergraduate and graduate courses in scientific disciplines. Starting from this knowledge, we introduced the basic ideas on the subject with no further mathematical and/or physical requirements. We intend to introduce the non-expert reader to these findings focusing on their physical meaning.

The review is divided in 8 Lectures. The first two Lectures deal with the basic features of turbulent flows, namely the viscous anomaly in three-dimensional turbulent flows and Kolmogorov theory. In Lecture 2 we discuss the difference between three and two-dimensional turbulence, while we only consider the case of three-dimensional turbulence in all other Lectures. The Kolmogorov theory plays an important role in turbulence by combining two fundamental ideas: (a) the existence of viscous anomaly, that is to say, the experimental observation that energy dissipation is constant for large *Re* number; (b) the self-similarity of the statistical properties of turbulent fluctuations. It turns out that point (b) is not strictly true and this opens the problem of intermittency in turbulence. Although deviations from self-similarity may be considered small, the existence of intermittency opens a non-trivial problem and it has been considered a major conceptual challenge in the field. This question is detailed in Lecture 3 and a possible solution to the problem is presented in Lecture 4, based on the so-called multifractal theory of turbulence. One basic feature of the multifractal theory is the possibility to explain the observed scaling properties of small-scale fluctuations for *both inertial and dissipative dynamics*. There is evidence from existing experimental and numerical data that anomalous scaling, i.e. deviations from self-similarity, is independent of both large-scale forcing and the detailed dissipation mechanism, i.e. anomalous scaling is universal. In Lecture 5, we introduce the reader to simplified models of intermittency, namely the shell models. Although shell models cannot provide any information on the geometrical features of turbulence, yet they show interesting similarities with the observed intermittency properties of real 3d turbulence and we think they can be used to clarify rather general questions about scaling properties of turbulence fluctuations. Lecture 6 is devoted to a rather non-trivial extension of the multifractal theory for Lagrangian turbulence and it reviews recent developments on the subject. Lecture 7 and Lecture 8 discuss more advanced topics. In Lecture 7 we review the solution of the so-called Kraichnan model for the passive scalar. This particular topic is reviewed in details in [1]. Here we present a simplified version of the results to illustrate the basic physical ideas. Although the Kraichnan model represents a simplified version of the real problem of passive scalar turbulence, its solution highlights the importance of new conceptual ideas like the *zero modes* and the *statistical preserved structures* and demonstrates the universality, with respect to forcing and dissipation, of the small-scale statistical properties of the passive scalar fluctuations. We simplify as much as possible the mathematical treatment of the problem by using shell model version of the full problem. Finally, in Lecture 8 we discuss the effect of non-isotropic forcing, including some implications for turbulence modelling, and more generally how to properly discuss the issue of anisotropic fluctuations.

Lectures 1 to 6 can be used as a trace for teaching turbulence in advanced courses. It is important that, besides the theoretical discussion presented in the Lectures, the students can use numerical and/or experimental data to perform their own statistical analysis and assessment following the guidelines presented in the theoretical Lectures. Whenever possible we made use of the original figures from the original works.

Lecture 1. The very basic law of turbulence

Chaos and turbulence

The word turbulence is derived from latin "*turba*", which means disorder or confusion, and "*ulentus*" which means "in abundance". It was used in the last period of the Roman empire to mean political or crowd turmoils. Although its original meaning is preserved today, one often uses the word turbulence during commercial flights to describe sudden shakes of the aircraft induced by the atmospheric wind. In physics, the word "turbulence" refers to the space and time chaotic behaviour of a fluid. As we shall see in the following, this definition is somehow obscure since we should first define what we mean by chaotic behaviour (assuming we all agree on the definition of fluid). It is the aim of this lecture to introduce the reader to the basic features which characterise turbulent flows and to provide a definition of turbulence in the simplest possible way.

Let us start with our knowledge of fluids. We do know the equation of the motion of a fluid since two hundred years due to the work of Claude–Louis Navier [2] and Gabriel Stokes [3] developed in the period 1822–1850. Upon defining $\boldsymbol{v}(\boldsymbol{x}, t)$ the flow velocity depending on the space position, $\boldsymbol{x}$, and the time, t, the Newton law for a fluid is described by the equation:

$$\frac{d\boldsymbol{v}}{dt} \equiv \frac{\partial \boldsymbol{v}}{\partial t} + \boldsymbol{v}\cdot\boldsymbol{\nabla}\boldsymbol{v} = -\frac{1}{\rho}\boldsymbol{\nabla} p + \nu \Delta \boldsymbol{v} \tag{1}$$

where ρ is the fluid density. Mass conservation requires the continuity equation

$$\frac{d\rho}{dt} \equiv \frac{\partial \rho}{\partial t} + \boldsymbol{\nabla}\cdot(\rho \boldsymbol{v}) = 0 \tag{2}$$

As in the rest of this review, we consider an incompressible fluid with $\rho = const$, then mass conservation implies $\boldsymbol{\nabla}\cdot\boldsymbol{v} = 0$. Eq. (1) is nothing else nothing more than Newton's equation: the l.h.s is the acceleration $d\boldsymbol{v}/dt$ while the r.h.s are the internal forces acting in the fluid. The latter is divided into two parts: the effect of the internal pressure, p, which should

satisfy the equation of state, and the effect of the forces acting between the fluid atoms which lead to the viscous effect proportional to the kinematic viscosity ν. For incompressible flow, the equation of state is simply $\rho = const$ and the pressure is derived by imposing the condition $\nabla \cdot \boldsymbol{v} = 0$. Eq. (1), referred to as the Navier–Stokes equations (NSE), describes a Newtonian fluid, i.e. a fluid where the internal forces due to atom interactions produce a stress proportional to the shear rate. In the following, we assume that the reader is familiar with the basic knowledge of fluid dynamics acquired during undergraduate courses.

The Navier–Stokes equation is our definition of an incompressible Newtonian fluid. The dynamical behaviour of water, air, and other common fluids at constant room temperature is described by Eq. (1) with very good accuracy. We can now use this knowledge to make a first and non-trivial step in the definition of turbulence. To this aim, we consider the following experiment: let us take a cylinder of radius L and height H and let us look at the dynamical behaviour of a fluid that flows around the cylinder. This experiment is easily performed in a wind tunnel and Fig. 1 shows schematically typical flow visualisations looking from the top, assuming that the fluid flows initially at a constant velocity U_0 (left side of the images). We can now exploit an important property of the NSE, i.e. we can use the variables L and U_0 to measure space and time using units L and L/U_0 respectively. Then, in terms of dimensionless variables $\boldsymbol{v} \to \boldsymbol{v}/U_0$, $\boldsymbol{x} \to \boldsymbol{x}/L$, $t \to tU_0/L$, $p/\rho \to p/(\rho U_0^2)$, Eq. (1) can be written as

$$\frac{\partial \boldsymbol{v}}{\partial t} + \boldsymbol{v} \cdot \nabla \boldsymbol{v} = -\frac{1}{\rho}\nabla p + \frac{1}{Re}\Delta \boldsymbol{v} \tag{3}$$

where the number $Re = U_0 L/\nu$, called the Reynolds number, is the only dimensionless variable describing the viscous effect. Upon increasing U_0, in our simple experiment, we are increasing Re. Thus in Fig. 1 the different flow visualisations refer to different incoming flow velocity U_0. The striking result is that the *qualitative* behaviour of the fluid is changing upon increasing Re. For small Re the fluid is flowing smoothly around the cylinder. Then for some Re greater than a critical value, Re_c, two vortices appear downstream and, upon further increasing of Re, the vortices detach from the fluid surface and the flow becomes non-stationary. For very large Re we cannot easily detect any structure in the fluid and the flow appears fully disordered and very *complex* both in space and in time. It is a remarkable experimental fact, due to Osborne Reynolds [4], that by changing U_0, L or ν the fluid behaves exactly in the same way for the same Re number.

Fig. 1 can be used to define turbulence as the dynamical behaviour of a fluid for $Re \to \infty$, which, for all practical purpose, means $Re \gg Re_c$. The question is now to understand the nature of the dynamical behaviour of a fluid for $Re \to \infty$. The problem is highly non-trivial because the Navier–Stokes Eqs. (1) are non-linear equations for the velocity field, $\boldsymbol{v}$. At very small Re, when the flow is smooth, we can assume that the non-linear contribution to the velocity acceleration $\boldsymbol{v} \cdot \nabla \boldsymbol{v}$ can be neglected. If this is correct, then we can solve Eq. (1) almost exactly. However, we cannot use this solution as the starting point of any perturbative expansion in Re. Thus we cannot even dream to obtain an analytical solution of the non-linear problem using any perturbative scheme. The qualitative change in flow behaviour when increasing Re is the signal of a rather non-trivial mechanism in the system. Physically it means that the smooth solution at small Re becomes "unstable".

It is also not obvious how we should describe the flow when $Re \to \infty$ where no clear pattern emerges in the system (both in space and time). One can imagine that this kind of "complex" behaviour can be obtained by some superposition of different patterns in the form:

$$\boldsymbol{v} = \sum_{\alpha} \mathbf{w}_{\alpha}(\boldsymbol{x}, t) \tag{4}$$

Then, if $\boldsymbol{w}_{\alpha}$ are periodic or quasiperiodic functions of time and if there is a large number of possible "patterns" then the resulting velocity field may look very "complex". It was a remarkable achievement in the seventies to show that, in fact, the chaotic behaviour of a fluid can be described by Eq. (4) for moderate Re. Here chaotic means that w_{α} are no longer a periodic or quasiperiodic function of time: the behaviour is characterised by a positive Lyapunov number λ which quantitatively describes the sensitivity to the initial conditions. Let us consider two solutions of Eq. (1) which starts with extremely small but finite difference $E(0)$ of the initial conditions. For Re large enough, $E(t)$ grows exponentially as $\exp(\lambda t)$ where the growing rate $\lambda > 0$ is the Lyapunov number or exponent. For time longer than $1/\lambda$, i.e. the predictability time, we can predict the system behaviour only probabilistically. Chaotic behaviour is found in a number of different physical systems and it properly describes non stationary fluid flows for moderate Re. The case $Re \to \infty$ is just more complicated than chaotic behaviour.

One simple but rather non trivial question is whether or not the Navier–Stokes equations properly describe the complexity of the flow behaviour for $Re \to \infty$. To reach any conclusion on this question, we need to solve Eq. (1) numerically. Due to technological achievement, our ability to perform numerical simulations of the Navier–Stokes equations has been growing exponentially during the last forty years. In Fig. 2 we show the value of Re for the largest numerical simulations obtained as a function of the year when it was performed. Actually in the figure we show $Re_{\lambda} = Re^{1/2}$. The scientific outcome of this non-trivial effort is that Eq. (1) properly describes the complex (space/time) behaviour of turbulent flows in the limit $Re \to \infty$. Does it mean we solve the problem? From a naive point of view, we may say that, since we have the equation of motion, we know the solution to the "turbulence" problem based on the numerical simulations. This is really "naive": although numerical simulations provide accurate information on turbulence, we are left with the non-trivial problem to understand *physically* the nature of turbulence at large Re and its statistical properties.

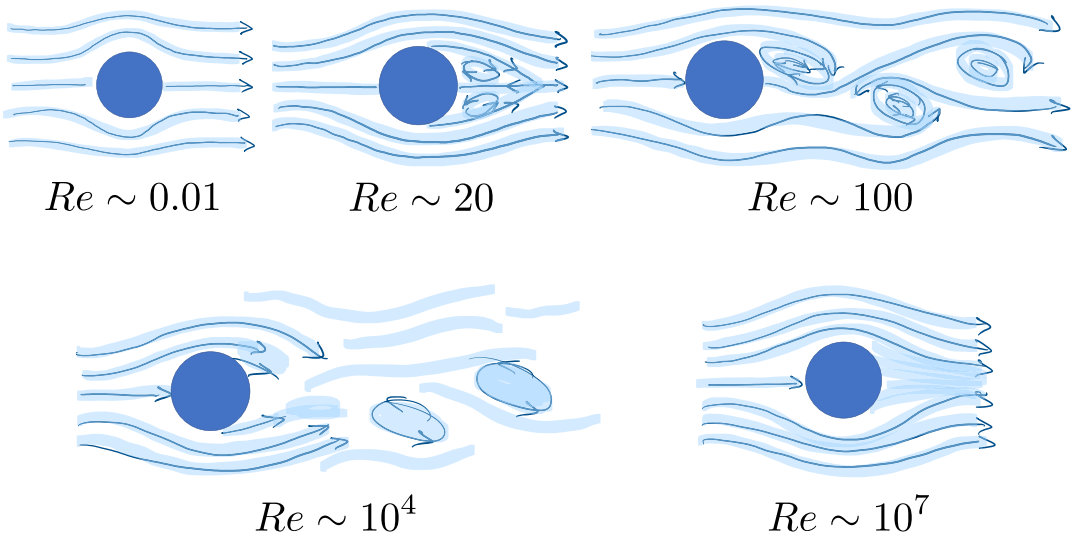

Fig. 1. The picture describes the dynamics of the flow around a cylinder (top view) for different *Re* numbers. Upon increasing the value of *Re* one observes many different qualitative changes in the solution. Eventually, at large *Re* the flow becomes turbulent and no clear pattern is detectable.

Lecture 1.1. The zero-th law of turbulence

To make a first step, let us consider the energy balance in turbulent flows at large *Re*. We assume that the flow is confined in a closed geometry and we generate the flow by using an external forcing $\boldsymbol{F}$ acting on the r.h.s of Eq. (1). For instance, this can be achieved by considering a flow in a Couette geometry, i.e. the flow between two cylinders separated by a distance L, the smaller one at rest and the largest one rotating at velocity U_0.

Then we can look at the kinetic energy $E = v^2/2$ obtained as the space average $\langle \dots \rangle$ over the fluid:

$$\frac{dE}{dt} = \langle \boldsymbol{F} \cdot \boldsymbol{v} \rangle - \epsilon \tag{5}$$

where

$$\epsilon = -\nu \langle \boldsymbol{v} \cdot \Delta \boldsymbol{v} \rangle \tag{6}$$

Note that the rate of the energy dissipation ϵ is expressed in m^2/sec^3 and it is given by:

$$\epsilon = \nu \int d^3x \sum_{i,j} S_{ij}^2 \;\; ; \;\; S_{ij} \equiv \frac{1}{2}(\partial_i v_j + \partial_j v_i) \tag{7}$$

where S_{ij} is the shear rate tensor. To understand the problem we are facing, let us now make use of the previous transformation leading to the definition of the *Re* number. The idea is that the velocity field $\boldsymbol{v}$ can be written as

$$\boldsymbol{v} = U_0 \boldsymbol{w} \left[\frac{\boldsymbol{x}}{L}, \frac{tU_0}{L} \right] \tag{8}$$

Then, dimensional analysis give (where C is a numerical constant) :

$$\epsilon \sim \nu C \frac{U_0^2}{L^2} \sim \frac{C}{Re} \frac{U_0^3}{L} \tag{9}$$

Thus, our first and simple expectation is that the rate of energy dissipation ϵ decreases with *Re*. In fact this is badly wrong: **the remarkable and fundamental experimental and numerical evidence is that the rate of energy dissipation ϵ is independent of *Re* in the limit $Re \to \infty$.** This result is sometime referred to as the zero law of turbulence.

To provide an interpretation of the zero law of turbulence, we can assume that the velocity gradients in the flow are proportional to U_0/λ where now λ is some length scale to be defined. It follows that our estimate of ϵ is given by

$$\epsilon \sim \nu \frac{U_0^2}{\lambda^2} = \frac{1}{Re} \frac{L^2}{\lambda^2} \frac{U_0^3}{L} \tag{10}$$

The zero law of turbulence implies $\lambda = Re^{-1/2} L$, i.e. it implies that, for large *Re*, λ goes to zero (with respect to L) and that the velocity gradients becomes infinite for $Re \to \infty$! The quantity λ is known as the Taylor scale and beside *Re*, one usually consider a "reduced" Reynolds number $Re_\lambda = U_0 \lambda / \nu = Re^{1/2}$.

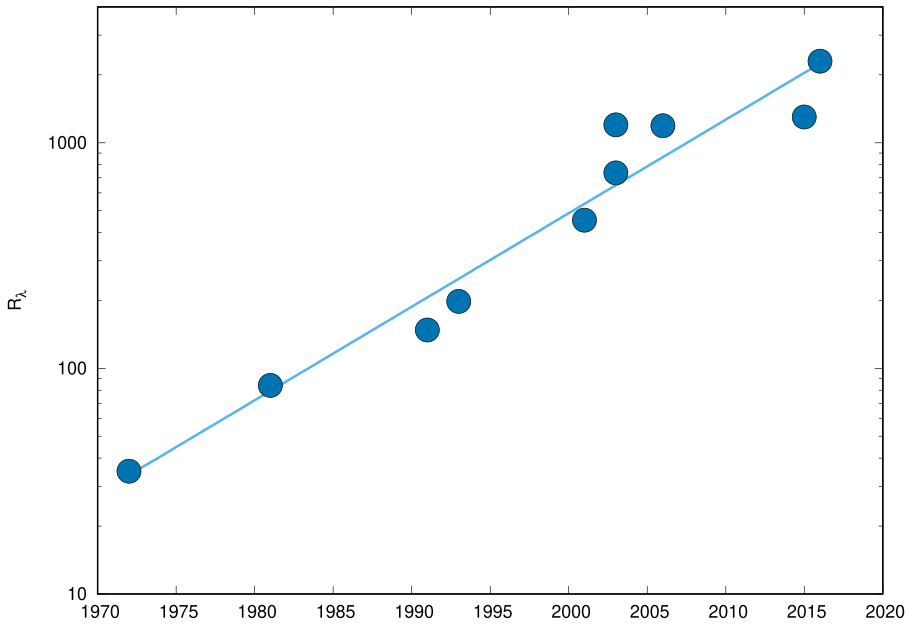

Fig. 2. The value of the $Re_\lambda = Re^{1/2}$ which has been achieved in the numerical simulations over the last four decades. At Re_λ order 10^3 the numerical simulations become comparable with standard laboratory experiments for turbulent flows.

The above result is very surprising. We start with a system defined by a set of partial differential equations (the N.S. equation) and we study the case of relatively large Re or, equivalently, small ν. In this limit, we discover that the velocity gradients go to infinity, i.e. the velocity field becomes very "rough" over space with strong variations in a relatively small (order λ) distance. This feature is rather unique in physics. We are used to considering large spatial gradients of a physical observable whenever external noise acts as perturbations (due to temperature or quantum fluctuations) on the system. Turbulence is the only case where internal non-linear dynamics generate strong gradients for large external forcing (or small viscous effects) without any external small-scale perturbations. In second-order phase transition, the powerful method based on Renormalisation Group enables us to understand the macroscopic behaviour of the system once we average over small scales "strong" fluctuations, i.e. knowing the small-scale dynamics we obtain the "universal" macroscopic behaviour of the large-scale variables. In turbulence we face the opposite problem: we know the large scale behaviour (i.e. the N.S. equation) and we are interested to understand why does the system develop large gradients at small scales and why the rate of energy dissipation is *Re* independent.

In a very general and somehow abstract way, we can state that the turbulence problem is how to derive from the N.S. equation the zeroth law of turbulence. Right now we have some hints on why the zeroth law is true as we will discuss in the following lectures. For the time being we focus on two different issues related to the zeroth law of turbulence: namely (1) whether we do observe the zeroth law in numerical simulations and (2) what are some macroscopic consequences of the zeroth law. The first question tries to answer how much we can trust the N.S. equation when *Re* is very large. After all there may be some physical mechanisms that modify energy dissipation at large Re. Remember that we are not able to obtain experimentally the whole velocity field in any point of space and at any time. We are now able to measure velocity gradients (i.e. velocity difference in space) with high accuracy in one point or we are able to obtain the overall energy balance with high precision. However, if the N.S. equations can develop large gradients, then one should observe this phenomenon very clearly in numerical simulations.

In Fig. 3 we show rather recent numerical results showing the rate of normalised energy dissipation $\epsilon L/U_0^3$ as a function of Re_λ. It is quite clear that, once Re_λ is large enough, the rate of energy dissipation becomes constant.

Lecture 1.2. Consequences of the zero-th law of turbulence

There exist very simple and practical implications from the zero law of turbulence. For instance, let us consider the drag force acting on a body of size L moving at constant velocity U_0. Based on dimensional analysis, the drag force can be written as

$$F = A\rho L^3 \frac{\nu U_0}{L^2} f(Re) \tag{11}$$

where A is a constant and $A\rho L^3$ is proportional to the body mass. The function $f(x)$ is constant for small $\boldsymbol{x}$ so that the drag is proportional to the viscosity and to the velocity. At very large *Re*, however, $f(Re)$ is no longer constant since we must

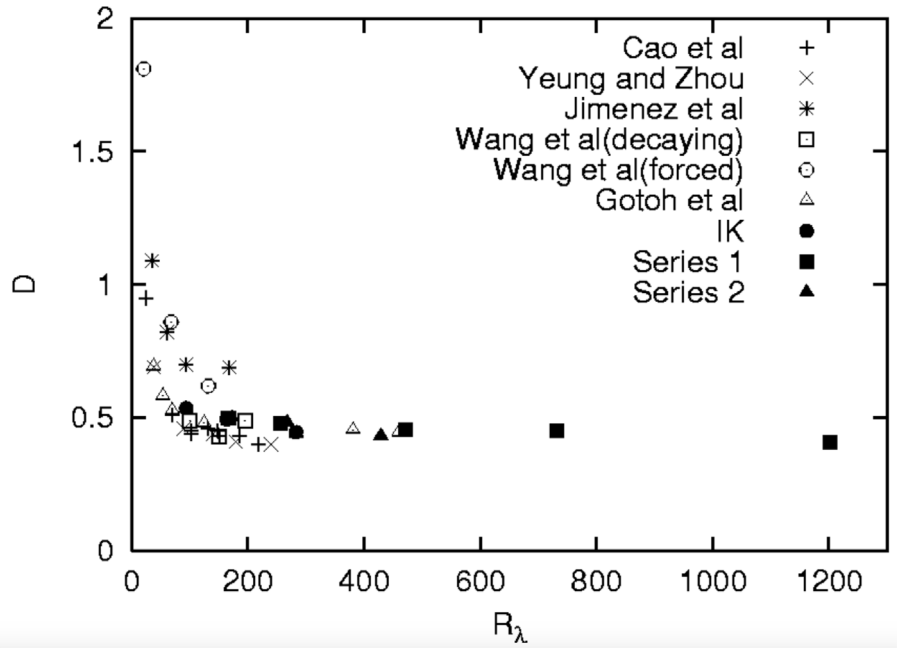

Fig. 3. The normalised energy dissipation rate, ε (indicated as D on the y-axis), versus R_λ. Results from direct numerical simulations Gotoh et al. (2002), Ishihara & Kaneda (2002), and Kaneda et al. (2003), together with the ones compiled by Sreenivasan (1998), i.e., the data from Cao et al. (1999), Jimenez et al. (1993), Wang et al. (1996), and Yeung & Zhou (1997).
Source: Figure reproduced from [5].

satisfy the zero law of turbulence. Using Eq. (11) we can estimate the rate of energy dissipation as FU_0 and we should require that it is independent of Re. This is possible only if $f(Re) \sim Re$ for large Re:

$$F \sim \rho L^3 \frac{\nu U_0}{L^2} Re = C_D \rho L^2 U_0^2 \tag{12}$$

The quantity C_D is called the drag coefficient. Eq. (12) tells us that the drag force for large Re is proportional to U_0^2.

Lecture 1.3. Boundary layer turbulence

The above example is just one of many. Two interesting consequences of the zeroth law of turbulence are the boundary layer flow and the Richardson diffusion. Let us start with the boundary layer flow: we consider a channel in three dimensions or the flow around two cylinders at some distance 2H. The flow is forced by a pressure gradient in the x-direction and we denote y the transverse direction. We assume that the flow is turbulent and we are interested to obtain the velocity profile of $U(y)$ which is the "average" flow in the channel. Furthermore, we assume for theoretical purpose that the channel is so extended that at any point x we can observe the same statistical properties of the turbulent flows. It follows than any average quantity is independent on x. This also implies that any time average should also corresponds to the space average on x (they are supposed to be the same!). Finally, we assume periodic boundary conditions in z.

We consider each velocity component as the sum of an average part and a "turbulent" fluctuating part and we write

$$\boldsymbol{v} = \langle \boldsymbol{v} \rangle + \boldsymbol{v}' \tag{13}$$

where $\langle .. \rangle$ denotes average. Since the average cannot depend on both x and z (because of the periodic boundary conditions), $\langle \mathbf{v} \rangle = U(y)\mathbf{i}$ where $\mathbf{i}$ is the versor in the x direction. Hereafter, we often use the notation a_i, with $i = 1, 2, 3$, to denote the component of the vector $\mathbf{a}$ and the notation on repeated indices, i.e. $\Sigma_i a_i b_i$ is written as $a_i b_i$. Note that in this notation $\boldsymbol{\nabla} \cdot \boldsymbol{v} = \partial_i v_i$. Finally, we assume that the pressure, as any other quantities, can be decomposed as $p = \langle p \rangle + p'$.

Using the above notation we can rewrite the N.S. Eq. (1) as:

$$\partial_t v_i' + \partial_t U \delta_{i,1} + v_j' \partial_j v_i' + U \partial_1 v_i' + v_2' \partial_2 U \delta_{i,1} = -\frac{\partial_i p'}{\rho} + \nu \Delta (v_i' + U \delta_{i1}) \tag{14}$$

Upon average, we obtain:

$$\partial_t U + \partial_y \langle v_y' v_x' \rangle = \frac{v_*^2}{H} + \nu \partial_{yy}^2 U \tag{15}$$

where we denote $-\partial_x\langle p/\rho\rangle \equiv v_*^2/H$, $2H$ being the channel wide, i.e. $0 \le y \le 2H$. Subtracting Eq. (15) from Eq. (14), we obtain an equation for the so called turbulent fluctuations v_i'. For our purpose, it is convenient to consider the turbulent kinetic energy $E_t' = (1/2)\Sigma_i v_i^2$ and in particular its average quantity $E_t = \langle E_t'\rangle$. A straightforward but lengthy computation gives:

$$\partial_t E_t + \partial_y \left\langle \left[v_y' E_t' + \frac{v_y' p'}{\rho} \right] \right\rangle = -\langle v_y' v_x'\rangle \partial_y U - \epsilon_t \tag{16}$$

where ϵ_t is the turbulent energy dissipation defined as $\nu\langle \Sigma_{ij}(\partial_i v_j')^2\rangle$. Upon multiplying Eq. (15) for U we can also obtain the equation for the kinetic energy of the mean flow $E_m \equiv (1/2)U^2$:

$$\partial_t E_m = -U\partial_y\langle v_y' v_x'\rangle + \frac{v_*^2}{H}U - \epsilon_m \tag{17}$$

where now ϵ_m is the energy dissipation due to the mean flow $\epsilon_m = \nu\langle(\partial_y U)^2\rangle$. Hereafter we denote by $W(y) \equiv -\langle v_y' v_x'\rangle$. Next we integrate Eqs. (16) (17) in y from $y = 0$ to $y = 2H$ and use the notation $\bar{....}$ to denote the integral:

$$\partial_t \bar{E}_t = \int_0^{2H} W\partial_y U dy - \bar{\epsilon}_t \tag{18}$$

$$\partial_t \bar{E}_m = \int_0^{2H} U\partial_y W dy + \frac{v_*^2}{H}\bar{U} - \bar{\epsilon}_m \tag{19}$$

The first term on the r.h.s of Eq. (19) can be integrated by part and, using the boundary condition $\boldsymbol{v} = 0$ in $y = 0$ and $y = 2H$, we write

$$\partial_t \bar{E}_m = -\int_0^{2H} W\partial_y U dy + \frac{v_*^2}{H}\bar{U} - \bar{\epsilon}_m \tag{20}$$

Looking at Eqs. (18) and (20) we get a quite clear physical picture: the second term on the r.h.s of (20) is the power input per unit length in the system and energy can be transferred from the mean flow to turbulence only if $W\partial_y U$ is positive. This implies that the momentum flux $\langle v_y' v_x'\rangle$ should be directed towards the wall of the channel, i.e. it is negative when $\partial_y U > 0$ and positive when $\partial_y U < 0$.

The above discussion is just a preliminary analysis of the problem and does not say anything about $U(y)$. We notice that, from a mathematical point of view, Eqs. (15) and (16) do not form a closed system of equations. To make progress we should use some other informations. First, we can safely neglect all the time derivates since we are looking at average quantities. Then we can integrate Eq. (15) in y and, using the boundary conditions, we obtain:

$$\nu\left[\frac{dU}{dy}\right] + W = v_*^2(1 - \frac{y}{H}) \tag{21}$$

Next we discuss the behaviour of the system when y is small so that the last term y/H can be neglected. Then, close to the wall region $y = 0$, using boundary conditions and the continuity equations, it is easy to show that $W(y) = O(y^3)$. Thus Eq. (21) implies, in the limit $y \ll H$:

$$U(y) = \frac{v_*^2 y}{\nu} + \mathcal{O}(y^4) \tag{22}$$

The key observation is now to introduce the scale $\delta \equiv \nu/v_*$. Then *close* to the boundary $y = 0$ means assuming that y is order of few δ which is the length scale to take into account. Furthermore, we can evaluate the *Re* of the flow by using $Re = v_* H/\nu = H/\delta$. Fully developed turbulence is achieved for large value of H/δ. Then, for $y \ll H$ and $Re \gg 1$ we can assume that:

$$U(y) = v_* f\left(\frac{y}{\delta}\right). \tag{23}$$

This implies that we do not need to take into account finite size effects due to H which of course appear when y/H cannot be neglected. Notice that $\xi = y/\delta$ can be interpreted as a *local* Reynolds number. For $1 \ll \xi \ll Re$ we may expect that the term proportional to ν in Eq. (21) can be neglected and $W = v_*^2$.

We now consider Eq. (16). For the time being, we neglect the second term on the l.h.s: it represents a transport of turbulent kinetic energy and we know that it is irrelevant to the overall energy budget. The first term on the r.h.s is a source of energy and it is proportional to $W\partial_y U$ while the second term is the energy dissipation. Then $\xi \gg 1$ we know that energy dissipation is independent on ν. Using Eq. (23) we obtain:

$$W\partial_y U = v_*^2 \frac{v_*}{\delta}\frac{df}{d\xi} \tag{24}$$

Since, on average, energy production $W\partial_y U$ and energy dissipation must balance, we should require that $W\partial_y U$ should be independent on ν. This implies that the function $f(\xi)$ should be of the form $A log(\xi) + B$, with A and B being constants,

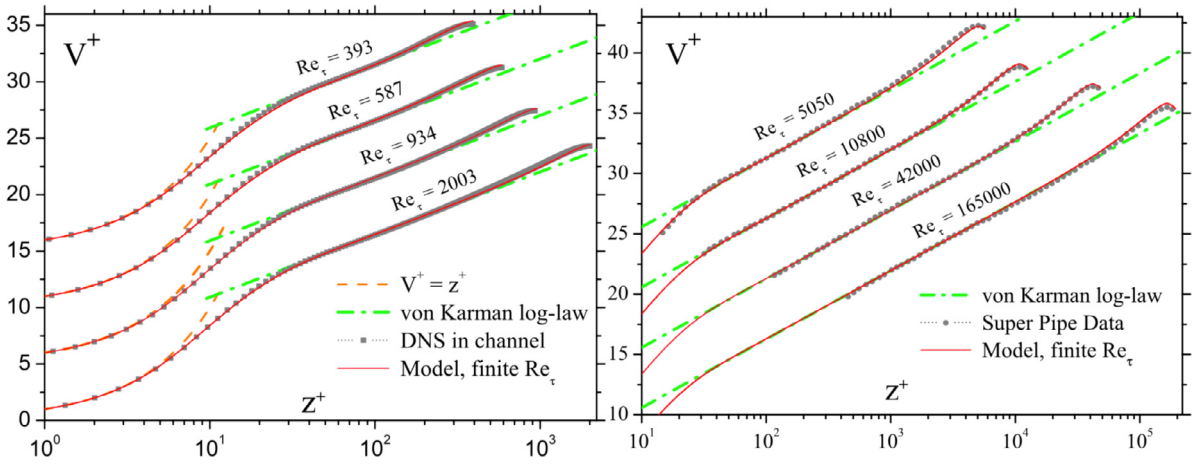

Fig. 4. Comparison of the theoretical mean velocity profiles for a channel flow (red solid lines) at different values of Re_τ against the velocity profiles from a Direct Numerical Simulation (DNS). (Left panel, grey squares; model with $l_{\rm buf} = 49$, $\kappa = 0.415$, $l_s = 0.311$) and with the experimental Super-Pipe data (Right panel, grey circles; model with $l_{\rm buf} = 46$, $\kappa = 0.405$, $l_s = 0.275$). In orange dashed line we plot the viscous solution $V^+ = z^+$. In green dashed–dotted line the von-Karman log-law. Plots are shifted vertically for readability.
Source: Reproduced from [7].

which gives $W\partial_y U = v_*^3/y$ independently on ν. We reach the conclusion that, for $\xi \gg 1$ and $y \ll H$, we should observe a velocity profile

$$U(y) = B + Av_* \log(yv_*/\nu) \tag{25}$$

The above expression is due to von Karman [6]. The derivation we did is not the usual way to introduce the von Karman logarithm profile. It has the advantage to highlight the link between this result and the zeroth law of turbulence caveat the assumption on the local balance between energy production and energy dissipation.

The von Karman result work quite well on data from both experiments and Direct Numerical Simulation (DNS), see Fig. 4 and Ref. [7]. Yet, the constants A and B cannot be derived analytically. In the original derivation of von Karman, there is no argument about energy production and energy dissipation. The basic idea is simply that dU/dy should be independent on ν at large enough y (but not too large). We see, however, that this requirement is also equivalent to assuming that the local rate of turbulent energy production is Re independent (for each y) which is echoing the zeroth law of turbulence.

Lecture 1.4. Richardson diffusion

The next problem we are interested to discuss is the so-called Richardson diffusion [8]. We consider an initial spot of any passive substance. Passive means that the substance is advected by the flow without changing the flow dynamics. A simple example is to consider a smoke cloud in a turbulent flow. The problem we want to solve is the following: given an initial drop of size $R(0)$ we want to compute at time t the value of $R(t)$. Obviously, the initial shape of the drop changes at each time but we assume to make an average over several realisations so that, on average, the shape of the passive substance is well defined by R(t). In principle we can solve our problem by considering the equation for our passive substance $C(x, y, z, t)$ advected by the turbulent flow:

$$\partial_t C + \boldsymbol{u} \cdot \nabla C = D\nabla C \tag{26}$$

The problem pointed out by Richardson was very clear: without advection, the diffusion Eq. (26) predicts that an initial spot of a passive tracer of radius $R(0)$ increase its size $R(t)$ in time according to the equation

$$R(t)^2 = R(0)^2 + Dt \tag{27}$$

In a turbulent flow, we can imagine that D is different from the one due to molecular effects. However, if we compute D using (27) from available data, we find values that differ by nine orders of magnitude! Clearly, something should be changed in our view of diffusion. Even if we do not expect D to be given by molecular effect, nevertheless 9 orders of magnitude mean that we do not capture the physics. Richardson realised that the correct way to look at the problem is completely different. What we are interested in is not how C is changing in time but the distance among different regions of the drop.

The basic idea by Richardson was that what we call diffusion in turbulent flows cannot be parametrises as a simple constant and D should depend in a way or another on the statistical property of the turbulence. At this point, Richardson

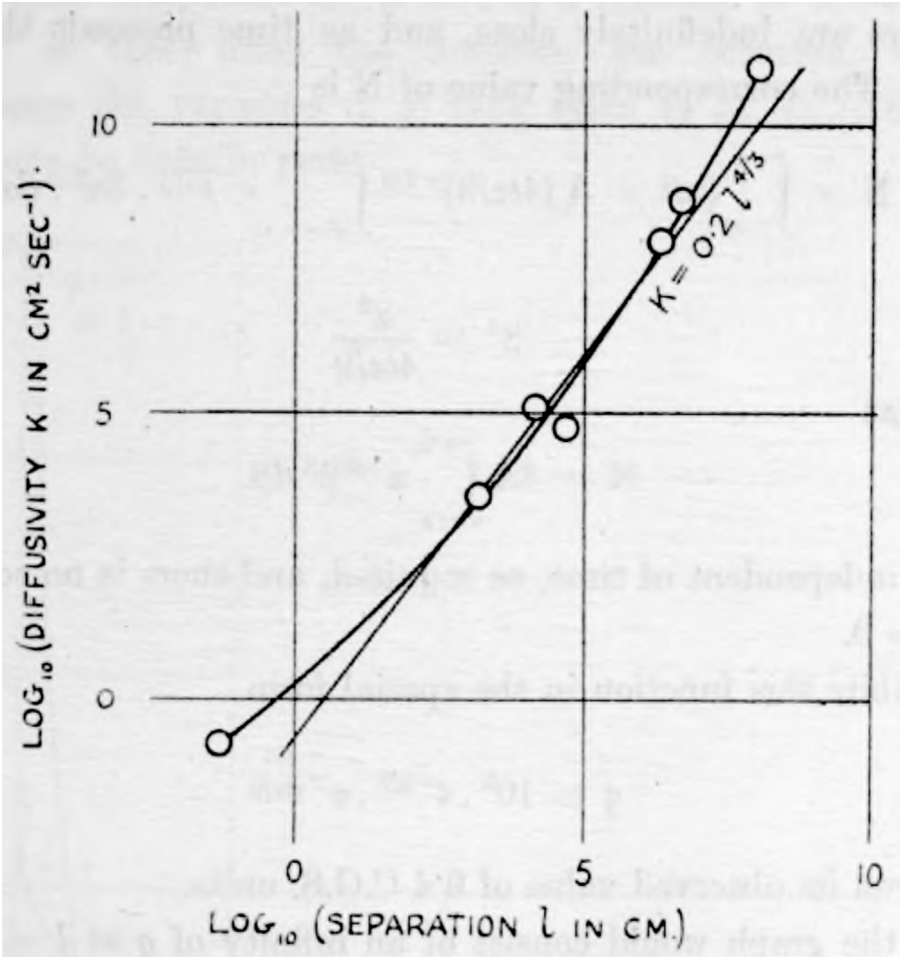

Fig. 5. Figure from the original Richardson's paper [8] representing the experimental results of the diffusivity D measured as a function of l, i.e. the distance separation between two particles. Starting from these data, Richardson proposed his famous 4/3 law drawn in the figure.
Source: Reproduced from [8].

had a brilliant and deep intuition and assumed D to be a function of R. Then, he considered two particles at a distance R and considered the probability distribution $P(R, t)$ to find the particles at distance R at time t. Because the integral of P over the domain should be constant and equal to 1, the equation of P should be of the form:

$$\partial_t P = \frac{1}{R^{d-1}} \frac{\partial}{\partial R} \left[D(R) R^{d-1} \frac{\partial}{\partial R} P(R) \right] \tag{28}$$

assuming isotropy in a d dimensional space. Eq. (28) follows by the continuity equation

$$\partial_t P + \nabla \cdot \boldsymbol{J} = 0 \tag{29}$$

with the "current" $\boldsymbol{J}$ given by the Fickian law $\boldsymbol{J} = -D\nabla P$.

Next, looking at observations and available data, Richardson found that

$$D(R) = \sigma R^{4/3} \tag{30}$$

see Fig. 5. The constant σ was changing only by a factor 10 instead of nine order of magnitude: clearly a big improvement.

It is possible to solve Eqs. (28)–(30) analytically. For our purpose, however, it is simple to get the basic information by using a simple trick. Upon rescaling $R \to \lambda R$ and $t \to \lambda^a t$, Eq. (28) remains invariant if $a = 3/2$. This implies that the solution of Eq. (28) should be of the form $P(R, t) = Z(t)P(\xi)$ with $\xi \equiv R/t^{3/2}$, with $Z(t)$ a suitable normalisation factor. Using this observation we obtain

$$R^2(t) \sim t^3$$

Richardson's finding can be discussed in a different way [9]: let us consider two particle in $\boldsymbol{x}$ and $\boldsymbol{y}$. The two-particle move according to the equations:

$$\frac{d\boldsymbol{x}}{dt} = \boldsymbol{v}(\boldsymbol{x}) \tag{31}$$

$$\frac{d\boldsymbol{y}}{dt} = \boldsymbol{v}(\boldsymbol{y}) \tag{32}$$

Then the relative vector $\boldsymbol{R} \equiv \boldsymbol{x} - \boldsymbol{y}$ satisfies the equation:

$$\frac{d\boldsymbol{R}}{dt} = \boldsymbol{v}(\boldsymbol{x}) - \boldsymbol{v}(\boldsymbol{y}) \equiv \delta\boldsymbol{v}(\boldsymbol{R}) \tag{33}$$

The quantity we are interested to compute is

$$\frac{d\left\langle R^2\right\rangle}{dt} = 2\left\langle \boldsymbol{R}\cdot\delta\boldsymbol{v}(\boldsymbol{R})\right\rangle \tag{34}$$

What Richardson discovered is that the r.h.s of (34) is well approximated by the function

$$\left\langle \boldsymbol{R}\cdot\delta\boldsymbol{v}(\boldsymbol{R})\right\rangle = \sigma R^{4/3} \tag{35}$$

where

$$R^2 \equiv \boldsymbol{R}\cdot\boldsymbol{R} \tag{36}$$

Richardson's result implies something weird, namely that

$$\delta v(R) \sim R^{1/3}. \tag{37}$$

From the Richardson result we obtain something not trivial

$$R(t)^{2/3} \sim R(0)^{2/3} + \sigma t \tag{38}$$

Now we must look at this expression very carefully: even when $R(0) = 0$ (two coinciding particles at t=0) Richardson result implies that $R(t)$ becomes different from 0 in a finite time [1]. This is completely at variance with our intuition that two coinciding particles will stay stuck together no matter what. In other words, there is the breakdown of the lagrangian trajectories, i.e. we are not able to distinguish one trajectory from another one. Notice that our argument can be applied for normal diffusion Eq. (27). However, in the case of normal diffusion, we know, thanks to Einstein's work, that diffusion is induced by molecular collision and two different particles are subjected to different collisions. In the case of Richardson diffusion, there is no molecular diffusion and the effect is entirely due to turbulent fluctuations. We remark that the breakdown of the lagrangian trajectories can occur both forward and backward in time, i.e. two lagrangian particles can meet at the same point even if they start from separate positions.

Next if $\delta V(R) \sim R^{1/3}$ we expect that for the velocity gradients Γ

$$\Gamma \sim \lim_{R\to 0}\frac{\delta V(R)}{R} = \lim_{R\to 0} R^{-2/3} \to \infty \tag{39}$$

This can explain why the energy dissipation

$$\varepsilon = \nu\Gamma^2 \tag{40}$$

becomes finite for $\nu \to 0$. Although very rough and qualitative, it looks like the breakdown of the lagrangian trajectories, as implied by the Richardson law, can eventually explain the zeroth law of turbulence

As a mathematical remark, we notice that the solution of the equation $\frac{dx}{dt} = f(x)$ is unique if $f(x)$ satisfies the Lipschitz condition $f(x) \sim \mathcal{O}(x)$.

For the Richardson law, $f(x) = x^\alpha$ with $\alpha = 1/3$, i.e. $f(x)$ is not Lipschitz but Hölder continuous and multiple solutions can arise. For instance for $\alpha < 1$, the equation $dx/dt = f(x)$ has two possible solutions for $x(0) = 0$

$$x(t) = 0 \tag{41}$$

$$x(t) = [(1-\alpha)t]^{1/(1-\alpha)} \tag{42}$$

Obviously, the situation is more complicated than what we shortly discussed so far. For any finite ν (no matter how small it is) we expect that viscous effects eventually dominate the dynamic of turbulent fluctuations in a way similar to what happens in the boundary layer near to the walls. Then we also expect that the velocity gradient Γ is finite and it can be estimated as $(\varepsilon/\nu)^{1/2}$. This implies that for a small value of R, we have $\delta V(R) = \Gamma R$. Then $R(t)$ for two particles initially separated by a distance $R(0)$ goes as $R(t) = R(0)\exp(t/\tau_\eta)$ where $\tau_\eta \equiv \left(\frac{\nu}{\varepsilon}\right)^{1/2}$.

The point is that τ_η goes to 0 for $\nu \to 0$ if ε is independent on ν. Then $R(t)$ becomes large enough for $\delta V(R)$ to be "rough" i.e. proportional to the Richardson finding $R^{1/3}$. On the contrary, if ε is proportional to ν, then τ_η is constant

and the breakdown of lagrangian trajectories cannot occur in the limit $\nu \to 0$. This highlight why the breakdown of the Lagrangian trajectories can explain the zeroth law of turbulence in the limit of large Reynolds number. Notice that the exponential increases of R(t) is just what we expect from the chaotic behaviour of the lagrangian particles. It is natural to associate $1/\tau_\eta$ to the maximum Lyapunov number Λ of the Lagrangian flow. Then, we understand that turbulence, at large Reynolds number, is not just chaotic because of the breakdown of the Lagrangian trajectories in the limit $\nu \to 0$.

It remains to clarify what it means small enough $R(0)$ for the exponential growth to be observed. As we already said, we expect that at small interparticle separation $R(0)$ viscosity (or it is better to say molecular diffusivity for tracers) is dominant. Leaving aside for the time being the difference between viscosity and molecular diffusivity, we know that "on average" the root mean square distance $l(t)$ between two particles grows as

$$l(t) \sim \sqrt{\nu t} \tag{43}$$

Using this idea, we can identify the scale η at which the viscous or diffusivity effects are dominant:

$$\eta \sim \sqrt{\nu \tau_\eta} \sim \left(\frac{\nu^3}{\varepsilon}\right)^{1/4} \tag{44}$$

For $R(0) < \eta$ we expect exponential growth of the inter-particle separation $R(t)$ while for $R(0) > \eta$ we expect the Richardson law to be valid. Since $\eta \to 0$ for $\nu \to 0$, we can conjecture (at this stage) that the zeroth law of turbulence holds for $\nu \to 0$ because of the breakdown of Lagrangian trajectories. Just to fix some numbers, consider a pipe of 10 m radius where air is flowing at 10 m/s. Knowing $\nu = 10^{-5}$ m^2/s we have $Re = 10^7$, $\tau_\eta = 0.0003$sec, $\eta \sim 0.5$mm

The connection between the Richardson law and the breakdown of the Lagrangian trajectories are due to the breakthrough work done about 20 years ago by Gawedzky and collaborators [1]. Richardson himself did not recognise how his findings may eventually implies the zeroth law of turbulence (not known at his time) or the effect on the Lagrangian trajectories [10]. However, in his 1926 paper on diffusion, Richardson wrote a rather astonishing and remarkable section with the title "Does the wind possess a velocity?". The idea of the breakdown in the Lagrangian trajectories (in a very intuitive way) was there.

Lecture 1.5. Summary of Lecture 1

In this first lecture we started to discuss the peculiar properties of three-dimensional turbulence. First of all, we have stated that turbulence is described by the Navier–Stokes equations and we do not need to discover new equations for turbulence. In the following lectures, we will compare theoretical findings against both experimental and numerical results which support our statements. The second important statement is the zeroth law of turbulence, namely that energy dissipation is independent of the Re number for $Re \to \infty$. This is observed both in numerical simulations and experiments and it is one of the peculiar properties of turbulence. We have exploited two important consequences of the zeroth law: boundary layer turbulence and Richardson diffusion. In particular, Richardson diffusion shows that in the limit of $Re \to \infty$ lagrangian trajectories breakdown, a phenomenon whose consequences we need to understand better. The interested reader is referred to the review by Falkovich, Gawedzki and Vergassola [1], for a detailed discussion of the consequence of the Richardson diffusion. For a basic introduction to fluid mechanics and turbulence, we refer to the books of Landau and Lifschitz [11], Uriel Frisch [12] and Tennekes and Lumley [13]. Although relatively old the book by Landau and Lifshitz is still one of the best books on fluid dynamics where the basic features of laminar and turbulent flows are discussed. A recent review on our knowledge of boundary layer turbulence can be found in [7] whereas it is worthwhile to read the original paper by Richardson [8]. For a historical review of the work by von Karman and Richardson we refer to [10]. Finally, an in-depth analysis of chaotic behaviour can be found in [14].

Lecture 2. The Kolmogorov 1941 theory of turbulence

Neither von Karman nor Richardson said anything about the zeroth law of turbulence in their work. In 1941 A.N. Kolmogorov [15], one of the scientific giants of the last century, pointed out the fundamental issue of fully developed turbulence, namely that energy dissipation is independent on the Reynolds Re number in the limit $Re \to \infty$. The Kolmogorov 1941 theory (K41) is the topic of this lecture.

Lecture 2.1. Homogeneous and isotropic turbulence

Following Kolmogorov, we consider the case of homogeneous and isotropic turbulence (HIT) at a very large Re number (fully developed). Obviously, in all experiments and in many numerical simulations, it is difficult to achieve the case under consideration. The idea is that deviation from homogeneity and isotropy can be considered perturbations. Whether these perturbations are "weak" or "strong" is a matter to be discussed (see in particular Lecture 8).

A rather non-trivial issue is to understand what are the proper quantities to use for describing fully developed homogeneous and isotropic turbulence. The basic idea is that we look at a "random" flow field continuously changing in time as experienced in experiments and numerical simulations. Thus, it seems reasonable to look at the relevant statistical

quantities to describe random fields, namely correlation functions. In our case, we look at the correlation functions of the velocity field. For instance, we consider objects like

$$C_{i_1,i_2\ldots i_n}(\boldsymbol{x}_1,\boldsymbol{x}_2,\ldots,\boldsymbol{x}_n) \equiv \langle v_{i_1}(\boldsymbol{x}_1)v_{i_2}(\boldsymbol{x}_2)\ldots v_{i_n}(\boldsymbol{x}_n)\rangle \tag{45}$$

Here the average $\langle\ldots\rangle$ should be considered as the average over many (infinite!) realisations which, for the statistically stationary case, should be equivalent to *time* average.

The next step is to use the assumption of homogeneity and isotropy to reduce the complexity of the function (45). To understand the previous statement, let us consider the case $n = 2$ in Eq. (45), i.e we study $C_{i,j}(\boldsymbol{x}_1,\boldsymbol{x}_2)$. Because of homogeneity, it is simpler to consider the quantity

$$B_{i,j}(\boldsymbol{r}) \equiv \langle [v_i(\boldsymbol{x}+\boldsymbol{r}) - v_i(\boldsymbol{x})][v_j(\boldsymbol{x}+\boldsymbol{r}) - v_j(\boldsymbol{x})]\rangle \tag{46}$$

Now we can use the assumption of isotropy to write the most general form of Eq. (46):

$$B_{i,j}(\boldsymbol{r}) = A(r)\delta_{ij} + B(r)r_i r_j \tag{47}$$

Using the notation $\boldsymbol{x}_1 = \boldsymbol{x}$ and $\boldsymbol{x}_2 = \boldsymbol{x}+\boldsymbol{r}$, we can also rewrite Eq. (46) in the form

$$B_{i,j} = \langle v_i(\boldsymbol{x}_2)v_j(\boldsymbol{x}_2) - v_i(\boldsymbol{x}_2)v_j(\boldsymbol{x}_1) - v_i(\boldsymbol{x}_1)v_j(\boldsymbol{x}_2) + v_i(\boldsymbol{x}_1)v_j(\boldsymbol{x}_1)\rangle \tag{48}$$

Notice that the first and last term on the r.h.s of (48) are equal upon averaging (for homogeneity) whereas the second and third the term should be equal because of homogeneity and isotropy. Thus we obtain

$$B_{i,j} = 2\langle v_i(x_1)v_j(x_1)\rangle - 2\langle v_i(x_1)v_j(x_2)\rangle \tag{49}$$

At this point we can use the information that $\nabla\cdot\boldsymbol{v} = \partial_j v_j = 0$, i.e. the fluid is incompressible. This means that

$$\frac{\partial B_{i,j}(r)}{\partial x_{2j}} = \frac{\partial B_{i,j}(r)}{\partial r_j} = 0 \tag{50}$$

Since $\partial r/\partial r_i = r_i/r$, applying Eq. (50) to Eq. (47) we obtain:

$$\frac{dA}{dr}\frac{r_j\delta_{ij}}{r} + \frac{dB}{dr}\frac{r_i r_j r_j}{r} + B\delta_{ij}r_j + 3Br_i = 0 \tag{51}$$

where summation over j is understood and $\partial r_j/\partial r_j = 3$. Eq. (51) implies

$$\frac{dA}{dr} + r^2\frac{dB}{dr} + 4rB = 0 \tag{52}$$

We now introduce two quantities

$$B_{rr} = A + Br^2 \tag{53}$$

$$B_{tt} = A \tag{54}$$

B_{rr} is the *longitudinal* correlation functions, i.e. is the correlation function of the velocity field $\boldsymbol{v}$ parallel to the vector $\boldsymbol{r}$ and B_{tt} is the transverse correlation function. Then, Eq. (52) leads to the relation

$$B_{tt} = \frac{1}{2r}\frac{d}{dr}[r^2 B_{rr}] \tag{55}$$

Because of isotropy and incompressibility, the two-point correlation function depends only on one function namely the longitudinal one. In the jargon of turbulence, we define B_{rr} as the *second order longitudinal structure function* while B_{tt} is referred to as the *second order transverse structure function*. Eq. (55) can be used to verify in numerical simulations whether isotropy holds in turbulent flows.

Lecture 2.2. A simpler problem: the Burgers equation

Now we can use the above results and the N.S. equations to write down the *dynamical* equation for B_{rr}. Obviously, because the N.S. equations are non-linear in the velocity field, we must consider the correlation function of three velocity fields and the algebra become more complex. In order to understand our final goal, we consider the N.S. equation in *one dimension* without pressure:

$$\partial_t v + v\partial_x v = \nu\partial^2_{xx} v \tag{56}$$

Eq. (56) is known as the Burgers' equation and it is relevant for many interesting applications [16] (see also next lecture for a short discussion). Here we just want to use (56) as a tool to illustrate how to grasp physics from mathematical manipulation in the simplest possible way. Since we are in one dimension we do not need to consider isotropy. Then we

take two points x_1 and $x_2 = x_1 + r$ and we write the equation of motion for the quantity $\langle v(x_1)v(x_2)\rangle$:

$$\partial_t \langle v(x_1)v(x_2)\rangle = -\frac{1}{2}[\langle v(x_2)\partial_1 v(x_1)^2\rangle + \langle v(x_1)\partial_2 v(x_2)^2\rangle] \tag{57}$$

$$+ \nu\langle[v(x_2)\partial_{11}^2 v(x_1) + v(x_1)\partial_{22}^2 v(x_2)]\rangle \tag{58}$$

where ∂_i means ∂_{x_i} for $i = 1, 2$. Let us now look at the r.h.s of (57). The quantities $\langle v(x_2)v(x_1)^2\rangle$ and $\langle v(x_1)v(x_2)^2\rangle$ are the same quantities is we change x to $-x$. Notice under the transformation $x \to -x$ we also require $v \to -v$ and the Burgers equation remains invariant. Next we observe that $v(x_1)^2 v(x_2)$ should be a function only of r because of homogeneity. Then we can state that $\partial_1 = -\partial_r$ and $\partial_2 = \partial_r$ while $\langle v(x_2)v(x_1)^2\rangle = -\langle v(x_1)v(x_2)^2\rangle$. Using the above information we can write

$$\partial_t \langle v(x_1)v(x_2)\rangle = \partial_r \langle v(x_1)^2 v(x_2)\rangle + 2\nu\partial_{rr}^2 \langle v(x_1)v(x_2)\rangle \tag{59}$$

Finally we consider the following equalities:

$$B_{rr} \equiv \langle (v(x_2) - v(x_1))^2\rangle = 2\langle v^2\rangle - 2\langle v(x_2)v(x_1)\rangle \tag{60}$$

$$B_{rrr} \equiv \langle (v(x_2) - v(x_1))^3\rangle = 3\langle v(x_2)v(x_1)^2\rangle - 3\langle v(x_2)^2 v(x_1)\rangle = 6\langle v(x_1)^2 v(x_2)\rangle \tag{61}$$

where the last term on the r.h.s of Eq. (61) is derived upon using the symmetry $x \to -x$, $v \to -v$. Upon substituting the above definitions in Eq. (59), we obtain:

$$\frac{\partial v^2}{\partial t} - \frac{1}{2}\frac{\partial B_{rr}}{\partial t} = \frac{1}{6}\frac{\partial B_{rrr}}{\partial r} - \nu\frac{\partial^2 B_{rr}}{\partial r^2} \tag{62}$$

At this point, from the Burgers' equation, we know that $\partial_t v^2 = -2\epsilon$ where ϵ is the rate of energy dissipation. Then, upon neglecting $\partial_t B_{rr}$ and integrating once in r, we obtain:

$$B_{rrr} = -12\epsilon r + 6\nu\frac{d}{dr}B_{rr} \tag{63}$$

In deriving Eq. (63) we made the assumption that $\int dr \partial_t B_{rr}$ can be neglected compared to ϵr. This is justified if $B_{rr} \sim r^\alpha$ ($\alpha > 0$) and r small enough. At this stage, for $\nu \to 0$ and ϵ independent of ν, we obtain a very non trivial results namely that

$$B_{rrr} = -12\epsilon r \tag{64}$$

In other words, we obtain an exact expression for the third order longitudinal structure function.

Lecture 2.3. Third order structure function and the Kolmogorov equation

Kolmogorov [15] derived an equation similar to Eq. (63) for three-dimensional homogeneous and isotropic turbulent flows. Obviously, in 3d, the computation is much more complex algebraically. Here we sketch some information useful to obtain the final result. Again we consider two points $\boldsymbol{x}_1$ and $\boldsymbol{x}_2 = \boldsymbol{x}_1 + \boldsymbol{r}$ in three-dimensional space and we denote the vector field at this location with $\mathbf{v}_1$ and $\mathbf{v}_2$. The first problem we need to understand is whether pressure plays any role. The quantity we consider is $\langle \partial_{1i} p(x_1)v_j(x_2)\rangle$. Because of homogeneity and isotropy, we can write:

$$\langle p(x_1)v_i(x_2)\rangle = f(r)r_i \tag{65}$$

Then, because of compressibility, we have $\partial_j(f(r)r_j) = 0$ which leads:

$$\frac{df}{dr}r + 3f = \frac{1}{r^2}\frac{d}{dr}[r^3 f(r)] = 0 \tag{66}$$

Eq. (66) implies $f(r) = Kr^{-3}$. Since $f(r)$ should be finite for $r = 0$ we have $K = 0$. This implies that $\langle p(x_1)v_i(x_2)\rangle = 0$, thus pressure terms can be neglected.

Next we need to consider the third order quantity $B_{ijk}(r) \equiv \langle v_i(x_1)v_j(x_1)v_k(x_2)\rangle$. Note that all combinations of triple products of v in two different points and their derivates can be obtained from B_{ijk} using the invariance $\mathbf{r} \to -\mathbf{r}$, $\mathbf{v} \to -\mathbf{v}$ of the N.S. equations. Assuming isotropy and homogeneity, we can write:

$$B_{ijk}(r) = A(r)r_i r_j r_k + B(r)(r_i\delta_{jk} + r_j\delta_{ik}) + C(r)\delta_{ij}r_k \tag{67}$$

Next we use the incompressibility condition $\partial_{r_k} B_{ijk}(r) = 0$ to obtain:

$$\left[5A + r\frac{dA}{dr} + \frac{2}{r}\frac{dB}{dr}\right]r_i r_j + \left[2B + 3C + r\frac{dC}{dr}\right]\delta_{ij} = 0 \tag{68}$$

Eq. (68) implies that the two terms proportional to $r_i r_j$ and δ_{ij} should vanish independently. This implies that we have two equations in three unknowns. Thus only one function is needed to obtain all the possible combinations of triple products of the velocities. The solutions of Eq. (68) are

$$A = \frac{1}{r}\frac{dC}{dr} \tag{69}$$

$$B = -\frac{1}{2}\left[3C + r\frac{dC}{dr}\right] \tag{70}$$

As before we denote by B_{rrr} the third-order longitudinal structure functions which can be computed by the knowledge of $B_{ijk}(r)$ assuming all components are in the same direction of $\boldsymbol{r}$, i.e. $r^3A + 2rB + Cr$. Using Eqs. (69)–(70), the previous expression becomes $-2C(r)r$.

Although algebraically more complicated, only two functions B_{rr} and B_{rrr} are needed to solve the equations for $\partial_t B_{ij}(r)$. The final result, after a rather long work, is

$$-\frac{2}{3}\epsilon + \frac{1}{2}\frac{\partial}{\partial t}B_{rr} = \frac{1}{6r^4}\frac{\partial}{\partial r}[r^4 B_{rrr}] - \frac{\nu}{r^4}\frac{\partial}{\partial r}[r^4 B_{rr}] \tag{71}$$

Upon multiplying all terms for r^4 and integrating once in r, we obtain the celebrated Kolmogorov 4/5 equation:

$$B_{rrr} = -\frac{4}{5}\epsilon r + 6\nu\frac{d}{dr}B_{rr} \tag{72}$$

Once again, we have neglected the term $\partial_t B_{rr}$ which is supposed to be small for small enough r.

Even if some of the details may be lost in deriving Eq. (72), what it is of interest here is the physical meaning of the final result which we are now going to discuss. First of all, let us notice that there is no forcing in our derivation. Physically we are considering a region of the turbulent flow far away from the one where turbulence is produced. For instance, in the case of very large *Re* number, we can consider turbulence as produced by some obstacle (like a cylinder) and we are looking at a region downstream of the obstacle at a distance far enough so that homogeneity and isotropy are *locally* satisfied. By this, we mean that non-isotropic and non-homogeneity occur on some very large scale L in the system. Next, the basic assumption, as we already notice for Eq. (63), is that ϵ should be independent on *Re* (i.e. on ν). Then for $r \ll L$ and not too small we reach the conclusion that $B_{rrr} = -4\epsilon r/5$. As we shall see, there is a range of value of r where this conclusion should be true.

Lecture 2.4. Inertial range of turbulence

For $r \to 0$ we must require $B_{rr} = G_2 r^2$ and $B_{rrr} = G_3 r^3$ where $G_n \equiv \langle(\partial_x v)^n\rangle$. In other words, we expect that for very small r the velocity difference $\delta v(r)$ should be proportional to $r\partial_x v$. In this case, Eq. (72) reduces to

$$B_{rrr} = G_3 r^3 = -\frac{4}{5}\epsilon r + 12\nu G_2 r \simeq 0 \tag{73}$$

i.e. $\epsilon = 15\nu\langle(\partial_x v)^2\rangle$.

The physical meaning of (72) can be obtained by the following consideration. Let us consider the quantity $B_{rrr} = \langle[\delta v(r)]^3\rangle$ where $\delta v(r)$ is the velocity difference between two points x and $x + r$ in the r direction. Since B_{rrr} is negative, there should be many situations where $\delta v(r)$ is negative with respect to those where $\delta v(r)$ is positive. A negative value of $\delta v(r)$ means that two particles initially in x and $x + r$ tend to become closer in time. This implies that the kinetic energy carried by the two particles tends to be *transferred* from an initial distance r to a smaller *scale*. This *cascade* process of energy transfer, from relatively larger to smaller scales, is the physical interpretation behind the 4/5 Kolmogorov equation. One can make a more phenomenological argument on the energy transfer as follows: a possible measure of the kinetic energy at scale r can be estimated to be proportional to $[\delta v(r)]^2$. Due to non-linear interaction, the characteristic time scale $\tau(r)$ for the energy to be transferred from large to small scales should be of order $r/[\delta v(r)]$. We expect that the rate of energy transfer is on average equal to the rate of energy dissipation ϵ. Thus we should expect $[\delta v(r)]^2/\tau(r) = [\delta v(r)]^3/r \sim \epsilon$ or, equivalently, $[\delta v(r)]^3 \sim \epsilon r$. This kind of argument, as many others obtained in a similar way, is based upon the assumption that the probability distribution of $\delta v(r)$ should depend, for small enough r, only on ϵ and r. This immediately implies for the velocity structure functions $S_n(r)$:

$$S_n(r) \equiv \langle[\delta v(r)]^n\rangle = A_n(\epsilon r)^{n/3} \tag{74}$$

At variance with Eq. (72), the relation Eq. (74) can only be conjectured and it cannot be proved except for $n = 3$. However, Eq. (72) is telling us that for small enough r the statistical properties of B_{rrr} are controlled by ϵ and r in the limit $\nu \to 0$. Then Eq. (74) follows from dimensional analysis. Nothing is known about the dimensionless quantities A_n except for $n = 3$.

An important consequence of Eq. (74) is that $\delta v(r) \sim \epsilon^{1/3} r^{1/3}$ which is precisely what Richardson found in his effective diffusion for turbulent flows! Thus the K41 theory is consistent with Richardson's data analysis for diffusion in turbulence: a very non-trivial achievement from the theoretical point of view. Moreover, we are now able to understand the *window* in r for Eq. (74) to be valid. Using Eq. (74) into Eq. (73) we can estimate the value $r = \eta$ at which the term proportional to ν becomes relevant:

$$\epsilon\eta \sim \nu\epsilon^{2/3}\eta^{-1/3} \tag{75}$$

This lead to the definition of the Kolmogorov scale η

$$\eta \sim [\nu^3/\epsilon]^{1/4} \tag{76}$$

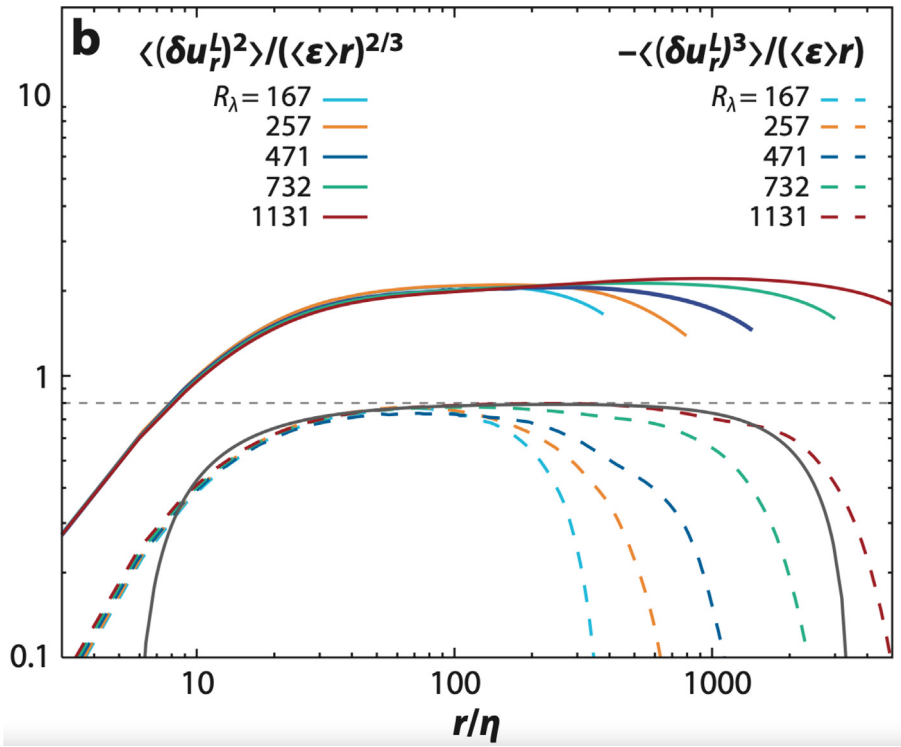

Fig. 6. Normalised second-order (solid coloured lines) and third-order (dashed coloured lines) longitudinal structure functions versus r/η. *Source:* Figure reproduced from [17].

Finally, assuming that $\epsilon \sim v^3/L$, where v^2 is the average kinetic energy and L some (large) scale, we have

$$\frac{\eta}{L} \sim Re^{-3/4} \tag{77}$$

Associated with the space scale η there exists a time scale $\tau_\eta \sim \eta/\delta v(\eta) = \eta/(\epsilon\eta)^{1/3} \sim (\nu/\epsilon)^{1/2}$. Eq. (77) can be used to estimate the computational cost to numerically simulate a turbulent flow: since we are in 4 dimensions (3 space dimension plus 1 time dimension) and since we need to resolve all scales up to $r = \eta$, the computational cost is order Re^3! At the present time the largest numerical simulation reaches $L/\eta \sim 12000$ corresponding to an equivalent Reynolds number $Re \sim 3 \times 10^5$.

In Fig. 6 we show the results obtained from recent numerical simulations [17]: the lower curve shows $-B_{rrr}/(\epsilon r)$ while the upper curve reports $B_{rr}/(\epsilon r)^{2/3}$. The dashed horizontal line shows 4/5: the Kolmogorov 4/5 is well verified in the range $r \in [50, 500]\eta$. Outside this range, finite size effects in Re are observed for small r while large scale effects are observed for $r \geq 500\eta$. The second curve $B_{rr}/(\epsilon r)^{2/3}$ seems to be not exactly flat in r, as expected from Eq. (74). This is an issue to be discussed in the next lecture.

Eq. (72) tells us something non-trivial about the velocity gradient for $\nu = 0$ and $\epsilon = 0$. Using $B_{rrr} = G_3 r^3$ and $B_{rr} = G_2 r^2$ we obtain:

$$\frac{1}{2}\frac{\partial}{\partial t}G_2 r^2 = -\frac{1}{6r^4}\frac{\partial}{\partial r}G_3 r^7 = -\frac{7}{6}G_3 r^2 \rightarrow \frac{dG_2}{dt} = -\frac{7}{3}G_3 \tag{78}$$

Since $G_2 > 0$, Eq. (78) implies that G_2 can grow if G_3 is negative, that is to say, that large velocity longitudinal gradients emerge from the skewness of the probability distribution of the velocity gradients. In fully developed turbulence the quantity $K_3 \equiv G_3/G_2^{3/2}$ (skewness of the velocity gradients) is negative and almost constant with Re. Using this information in Eq. (78) we obtain:

$$G_2(t) = \frac{G_2(0)}{[1 - \frac{7}{6}|K_3|G_2(0)^{1/2}t]^2} \tag{79}$$

The above equation means that G_2 has a finite time singularity and it is consistent with the idea that ϵ is independent of Re for $Re \rightarrow \infty$.

Lecture 2.5. Restricted Euler equation

A better investigation of the behaviour of the velocity gradients can be obtained using directly the N.S. equation. Upon defining $A_{ij} = \partial_j v_i$, it is easy to show that

$$\frac{dA_{ij}}{dt} = \frac{\partial A_{ij}}{\partial t} + v_k \frac{\partial A_{ij}}{\partial x_k} = -A_{ik}A_{kj} - \frac{\partial^2 P}{\partial x_i \partial x_j} + \nu \Delta A_{ij} \tag{80}$$

where now $P \equiv p/\rho$. Since the flow is incompressible, we must require that $A_{ii} = \partial_i v_i = 0$. This implies that $\Delta P = -A_{ik}A_{ki}$. Then Eq. (80) can be rewritten as

$$\frac{dA_{ij}}{dt} = -\left[A_{ik}A_{kj} - \frac{1}{3}A_{km}A_{mk}\delta_{ij}\right] - \left[\frac{\partial^2 P}{\partial x_i \partial x_j} - \frac{1}{3}\Delta P \delta_{ij}\right] + \nu \Delta A_{ij} \tag{81}$$

Eqs. (81) are still not closed and we need some information concerning the effect of pressure (beside imposing the incompressibility) and the effect of viscosity. Neglecting these terms (pressure and viscosity). Eq. (81) becomes

$$\frac{dA_{ij}}{dt} = -\left[A_{ik}A_{kj} - \frac{1}{3}A_{km}A_{mk}\delta_{ij}\right] \tag{82}$$

which are a closed set of equations describing the evolution of the gradients A_{ij} experienced from a lagrangian particle. This is equivalent to say that (besides viscosity) we are neglecting the non-isotropic contribution of the pressure term (second square bracket on the r.h.s. of Eq. (81). Eqs. (82) are referred to as Restricted Euler (RE) system in the literature [18,19]. Using (82) we can get some insights into the dynamic evolution of the velocity gradients. To do that, we introduce the quantities

$$Q \equiv -\frac{1}{2}A_{im}A_{mi} \tag{83}$$

$$R \equiv -\frac{1}{3}A_{im}A_{mk}A_{ki} \tag{84}$$

In terms of Q and R we are able to compute the eigenvalues λ of the matrix A_{ij}. A long but straightforward direct computation gives the equation:

$$\lambda^3 + \lambda Q + R = 0 \tag{85}$$

Most important, multiplying Eq. (82) by A_{ji} and by $A_{jk}A_{ki}$ we can derive (after some computation) a dynamical system for Q and R:

$$\frac{dQ}{dt} = -3R \tag{86}$$

$$\frac{dR}{dt} = \frac{2}{3}Q^2 \tag{87}$$

Using Eqs. (86)–(87), one can easily show that the following condition should be satisfied:

$$F(Q,R) \equiv \frac{1}{27}Q^3 + \frac{1}{4}R^2 = const \tag{88}$$

where the *const* depends on the initial value of Q and R. Finally, without lack of generality we can assume that the eigenvalues of λ of A_{ij} can be written as a couple of complex conjugate $\lambda_R \pm \lambda_I$ and a third eigenvalue equal $-2\lambda_R$ since the trace of A_{ij} is zero. Then, in terms of λ_R and λ_I the value of Q and R are given by

$$Q = \lambda_I^2 - 3\lambda_R^2 \tag{89}$$

$$R = 2\lambda_R(\lambda_I^2 + \lambda_R^2) \tag{90}$$

To better understand the physics behind the above mathematical formulas, as an example, we assume that A_{ij} is given by the sum of a diagonal matrix with elements $A_{11} = \alpha$, $A_{22} = \beta$ and $A_{33} = \gamma$ (with $\alpha + \beta + \gamma = 0$) and an antisymmetric matrix with $A_{12} = -\omega_\gamma/2$, $A_{13} = \omega_\beta/2$ and $A_{23} = -\omega_\alpha/2$. For this example we have

$$Q = -\frac{1}{2}(\alpha^2 + \beta^2 + \gamma^2) + \frac{1}{4}\omega^2 \tag{91}$$

$$R = -\alpha\beta\gamma - \frac{1}{4}(\alpha\omega_\alpha^2 + \beta\omega_\beta^2 + \gamma\omega_\gamma^2) \tag{92}$$

with $\omega^2 = \omega_\alpha^2 + \omega_\beta^2 + \omega_\gamma^2$. We are now ready to understand the physical meaning of the restricted Euler equation. For this purpose we consider the $Q - R$ plane 7.

In the first and fourth quadrant, we can draw the line $F(Q,R) = 0$. For values of Q which are below this line, there are 3 real eigenvalues. For $F(Q,R) > 0$ the evolution on the $Q - R$ diagram is quite simple: Q grows for $R < 0$ up to the

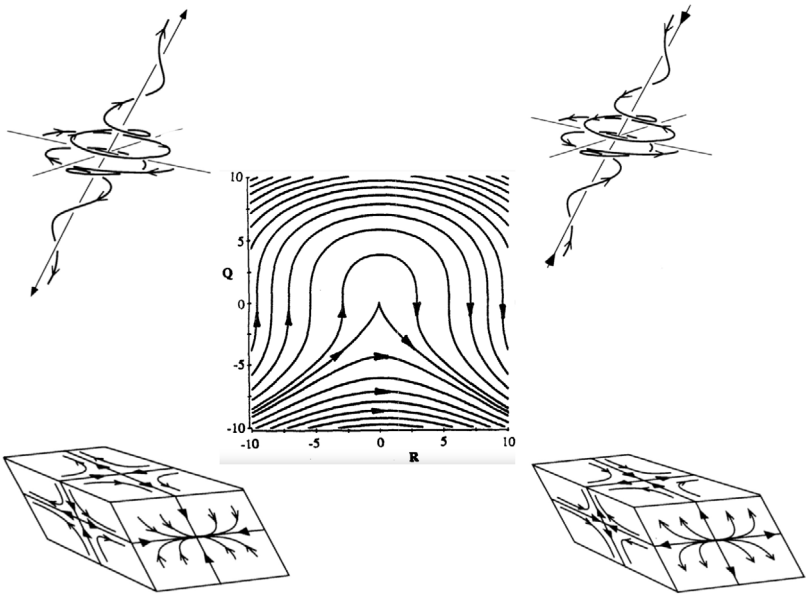

Fig. 7. Phase-space portrait of the restricted Euler model in the R, Q plane, together with sketches of the local flow topology prevalent in each quadrant.
Source: Figure courtesy of Charles Meneveau, adapted from [20] and [21].

point $R = 0$. Then, while R is still growing, Q starts to decreases and eventually becomes negative and the evolution tends asymptotically to the line $F(Q, R) = 0$. In the region $Q > 0$ and $R < 0$, we must have 2 complex conjugate eigenvalues with negative real part (because of (90)) and 1 real eigenvalue equal to $-2\lambda_R$. In this region the λ_I^2 (the vorticity) increases and it is bigger than the "dissipation" $-3\lambda_R^2$. The system experiences what is called vortex stretching in the jargon of fluid dynamics. Thus the quadrant $Q > 0$ and $R < 0$ is dominated by the production of vorticity. In the region $Q > 0$ and $R > 0$ the matrix A_{ij} has 2 complex conjugate eigenvalues with $\lambda_R > 0$ and 1 real and negative eigenvalues $-2\lambda_R$. Eventually when Q becomes negative the effect of dissipation $-3\lambda_R^2$ becomes dominant. The term dissipation means that for finite ν the dissipation effects should be proportional to $3\lambda_R^2$. More properly we should speak in this case of "strain dominated region".

To summarise our findings we can say that the restricted Euler equation shows a quite non-trivial dynamical behaviour of the velocity gradients with two different physical and topological properties: for $\lambda_R < 0$ the dynamics is characterised by a growth of the vorticity induced by the vortex stretching dynamics while at a later time, the system becomes strain dominated $\lambda_R > 0$ and vorticity tend to be negligible $\lambda_I \to 0$. In a real turbulent flow, energy dissipation is due to the strain of the velocity gradients. The restricted Euler equations tell us that large strain can be eventually reached *after* the vortex stretching. It remains to understand whether this picture is correct given the approximation performed to obtain Eq. (82). For this purpose, we can use numerical simulations which can provide a sampling of Q and R in the flow. The result is shown in Fig. 8 where we plot on the $Q - R$ diagram the probability density $P(Q, R)$ obtained from the numerical simulations. The figure agrees quite remarkably with our previous picture: most of the events occur in the second quadrant $[Q > 0 \; ; R] < 0$ and in the fourth one $[Q < 0 \; ; R > 0]$, whereas the third quadrant does not seem to be much populated. Also, we remark that a substantial part of the probability density occurs in the region $F(Q, R) < 0$.

In Fig. 9 we show $P(Q, R)$ conditioned to the region where vorticity grows and to the region where $\left\langle (\partial_x v)^3 \right\rangle < 0$: it is quite clear that the qualitative picture emerging from the restricted Euler equations agrees quite well with the numerical simulations. Now let us recall that Eqs. (82) are supposed to describe the gradient matrix A_{ij} of the velocity field *experienced by a Lagrangian particle*. This implies that in a turbulent flow, there will be a mixture of "vorticity dominated regions" and "strain dominated regions" where energy dissipations mostly occur. Thus energy dissipation has its own fluctuations which may depend on how turbulence has been generated and eventually on the *Re* number. This implies that in Eq. (74), which defines moments of the longitudinal velocity difference $\delta v(r)$, the coefficients A_n may depend on the statistical properties of the energy dissipation. In other words, the probability distribution of $\delta v(r)$ may not be universal with respect to the flow characteristics although its dependence on r can still be the one fixed by the Kolmogorov 4/5 equation. This observation is reported in a famous footnote of the Landau & Lifshitz book [11] on Fluid Dynamics suggesting that a deeper investigation is needed (see Fig. 10).

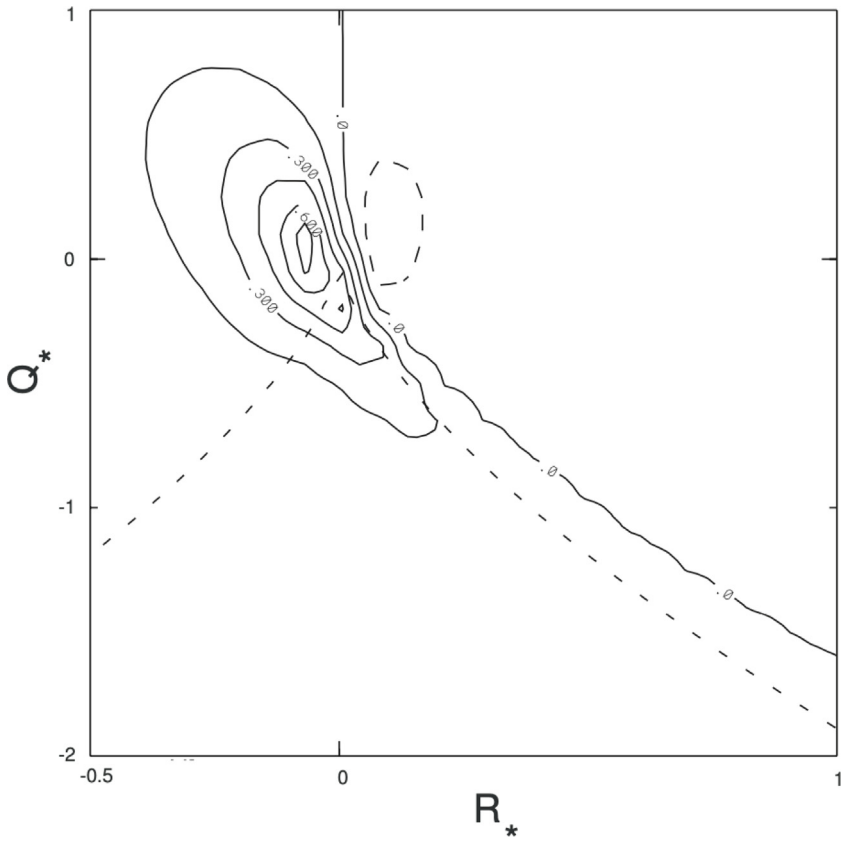

Fig. 8. Enstrophy production density in R, Q plane from the DNS, $R_\lambda = 85$, at $\rho/L = 0.125$. The enstrophy production is normalised by $\langle tr(M^2 M^\dagger)\rangle$. Solid lines correspond to positive values, dashed lines to negative values.
Source: Figure reproduced from [22].

Lecture 2.6. Energy spectrum and scale invariance

Based on Eq. (74) we can also obtain a clear-cut prediction on the energy spectrum of turbulence. Let us define the Fourier transform of the velocity field $\mathbf{v}$ as

$$\hat{\mathbf{v}}(\mathbf{k}) = \int \mathbf{v} \exp(i\boldsymbol{k}\cdot\boldsymbol{x}) d^3x \tag{93}$$

We define the energy spectrum $E(k)$ as

$$\langle v(x)^2\rangle = \int E(k)dk \sim \int k^2 \langle |\hat{\boldsymbol{v}}(\boldsymbol{k})|^2\rangle dk \tag{94}$$

From the properties of the Fourier transform we know that $\left\langle |\hat{\boldsymbol{v}}(\boldsymbol{k})|^2 \right\rangle = \int r^2 \left\langle [\delta v(r)]^2 \right\rangle \exp(-i\boldsymbol{k}\cdot\boldsymbol{r}) dr$. Thus we obtain $\left\langle |\hat{\boldsymbol{v}}(\boldsymbol{k})|^2 \right\rangle \sim \epsilon^{2/3} k^{-3-2/3}$. Using this expression in (94) we have

$$E(k) \sim k^2 \epsilon^{2/3} k^{-3-2/3} = k^{-5/3} \tag{95}$$

Let us remark that (95) can be obtained by dimensional analysis assuming that it depends only on ϵ and k. Eq. (95) is the celebrated prediction of the Kolmogorov theory on the turbulence energy spectrum. In many cases, the scaling with k of the energy spectrum is assumed to be *evidence* of the Kolmogorov-like behaviour. This is mostly due to historical reasons since, before the discovery of chaotic theory, turbulence was often considered as the superposition of Fourier modes with some complex (quasi-periodic) time behaviour. In fact, the $k^{-5/3}$ spectrum is not evidence of the Kolmogorov theory: the crucial evidence is the agreement with the 4/5 law and in particular the validity of the relation $B_{rrr} = -\frac{4}{5}\epsilon r$.

We can compare (95) against numerical simulation as shown in Fig. 11: the $-5/3$ slope in the energy spectrum is quite clear and it is found in many laboratory experiments and numerical simulations.

Let us summarise our findings on the Kolmogorov theory:

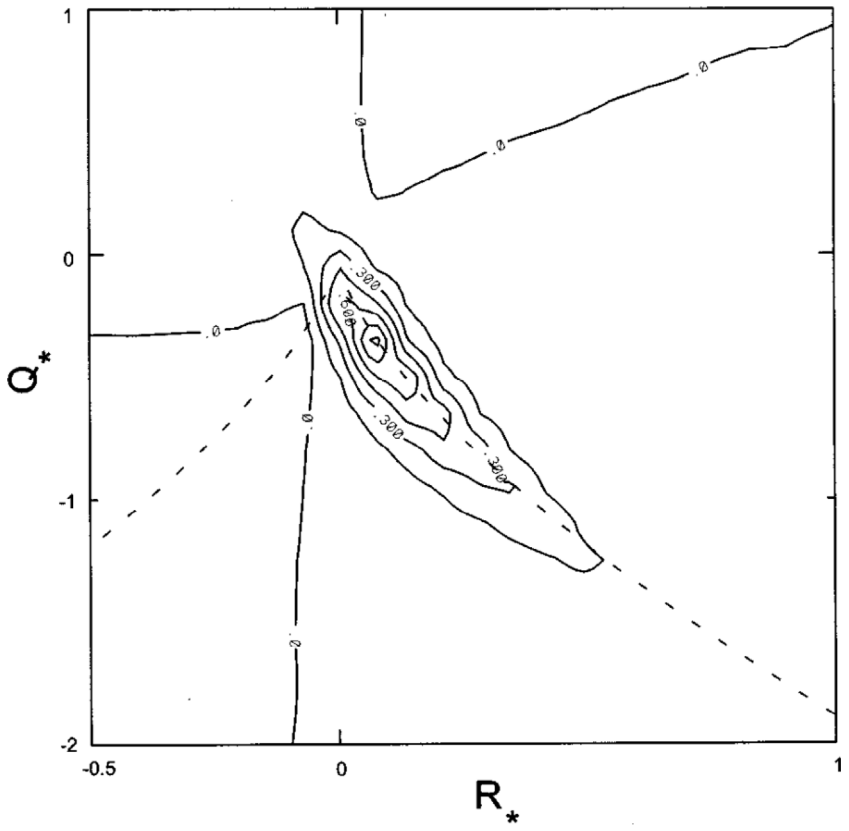

Fig. 9. Strain skewness density, $-tr(S^3)$ in R, Q plane from the DNS, $R_\lambda = 85$, $\rho/L = 0.125$. The strain skewness density is normalised by $\langle tr(M^2M^\dagger)\rangle$. The same convention as in Fig. 8 is used.
Source: Figure reproduced from [22].

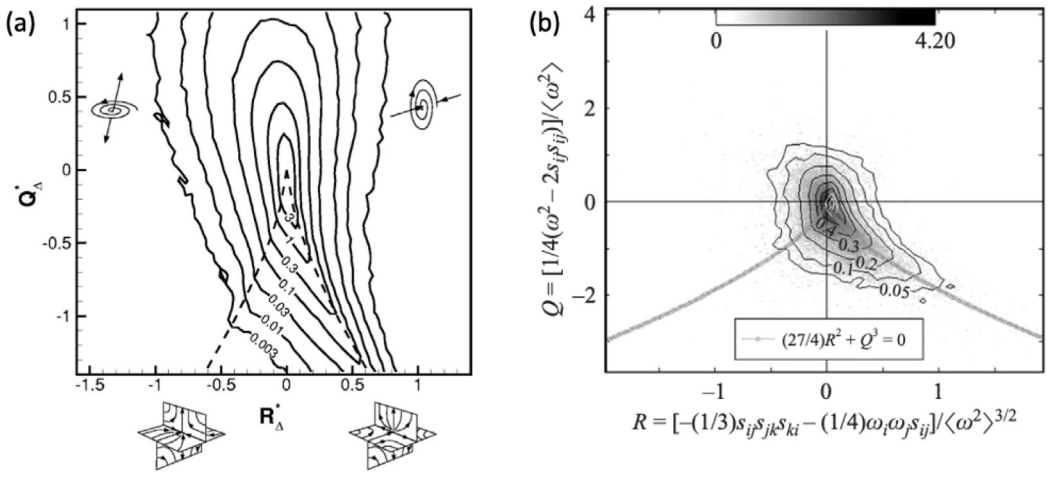

Fig. 10. Joint PDF of R and Q, measured turbulent flows in (a) a moderate Reynolds number experiment in a square pipe using 3D holographic particle image velocimetry (Figure reproduced from [23]) and in (b) a high-Reynolds number atmospheric boundary layer using hot-wire anemometry (Figure reproduced from [24]).

A - there is good evidence that for homogeneous and isotropic turbulence, $\langle[\delta v(r)]^3\rangle = -\frac{4}{5}\epsilon r$ which is based on the idea that ϵ is *Re* independent;

B - the conjecture $\delta v(r) \sim (\epsilon r)^{1/3}$ is consistent with Richardson's finding on diffusion in turbulent flows;

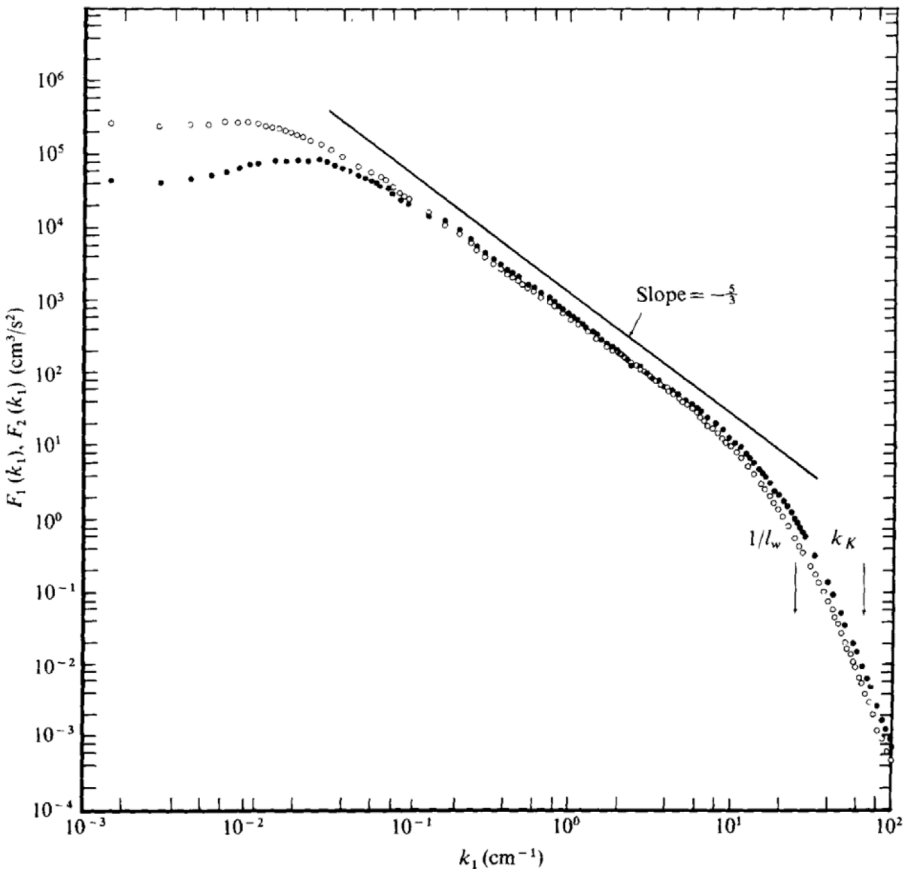

Fig. 11. One-dimensional spectra of streamwise- and lateral-component velocity fluctuations for an axisymmetric jet; $Re = 3.7 \times 10^6$, $x/d = 70$, $r/d = 0$.
Source: Figure reproduced from [25].

C - although the probability distribution $P[\delta v(r)]$ may not be universal, the rescaled probability distribution $P\left[\frac{\delta v(r)}{\langle[\delta v(r)]^2\rangle^{1/2}}\right]$ should be independent of r.

Items (B) and (C) implies that we should observe *scale invariance* in the probability distribution of the velocity field.

The idea of scale invariance can be discussed in a more general way [26]. Let us consider the scale transformation:

$$\mathbf{r} \to \lambda \mathbf{r} \tag{96}$$
$$\mathbf{v} \to \lambda^h \mathbf{v} \tag{97}$$
$$t \to \lambda^{h-1} t \tag{98}$$
$$\nu \to \lambda^{1+h} \nu \tag{99}$$
$$\epsilon \to \lambda^{3h-1} \epsilon \tag{100}$$

Notice that Eqs. (99) and (100) follow from dimensional analysis. It is easy to show that the scale transformation (96)–(99) leaves the N.S. equation invariants. Then if we assume that ϵ is independent on Re, we should ask for ϵ to be invariant under the above scale transformation. This implies that $3h - 1 = 0$, i.e. $h = 1/3$. This is a rather abstract way to obtain the Kolmogorov–Richardson scaling $\delta v(r) \sim r^{1/3}$. In other words, we can think for $\lambda < 1$ the scale transformation is a way to investigate the statistical properties of the N.S. at smaller scales as implied by Eq. (96). Then, this is equivalent to reduce the characteristic velocity fluctuations by a factor λ^h. The requirement of ϵ to be independent on λ is equivalent to say that in the limit $\nu \to 0$ (or $\lambda \to 0$) we require that ϵ does not change. This immediately leads to $h = 1/3$. This is a nice argument *a posteriori* i.e. after we understand the physical meaning of the requirement of ϵ to be Re independent.

Lecture 2.7. Passive scalar

The Kolmogorov *K41* theory provides a quite clear and defined theoretical framework that we can use to investigate new problems. Among them, the first one we consider is the case of a passive scalar advected by a turbulent flow. The

equation for the advection and diffusion of a passive scalar θ are:

$$\partial_t \theta + \boldsymbol{v} \cdot \boldsymbol{\nabla} \theta = \kappa \Delta \theta \tag{101}$$

Where κ is the molecular diffusivity. We assume that $\boldsymbol{v}$ is a turbulent flow and we also assume that the statistical properties of both $\boldsymbol{v}$ and θ are homogeneous and isotropic. One way to have a relative simple picture of Eq. (101) is the following: we describe θ as the equivalent of a large number N of lagrangian particles (tracers) labelled by the index $i = 1, \ldots, N$ and each of one advected by the local velocity field. Each particle is carrying a value θ_i and the value of θ in $\boldsymbol{x}$ is given by the local average of the values θ_i. This microscopic interpretation of Eq. (101) is exactly the case discussed by Richardson in the previous lecture. Because the flow if turbulent, we expect that, for $\nu \to 0$, the considerations highlighted for the Richardson' diffusion can be applied. It follows that the passive gradient $\nabla\theta$ tends to increase for κ and ν small. Using Eq. (101) we can compute the average rate of *passive dissipation* as $N \equiv \kappa \langle [\nabla \theta]^2 \rangle$. The above discussion implies that we expect N to be independent of ν and κ for fully developed turbulence in analogy with our discussion on the zero law of turbulence.

Having said that, we can now follow the Kolmogorov derivation of the 4/5 equation for the passive scalar. The computations are similar to the ones already done and the final results read:

$$\left\langle \delta v(r) [\delta \theta(r)]^2 \right\rangle = -\frac{4}{3} N r + 6\kappa \frac{d}{dr} \left\langle [\delta \theta(r)]^2 \right\rangle \tag{102}$$

where $\delta\theta(r) = \theta(\boldsymbol{x} + \boldsymbol{r}) - \theta(\boldsymbol{x})$ which, due to homogeneity and isotropy, depends only on r. For $\kappa \to 0$, Eq. (102) predicts $\left\langle \delta v(r) [\delta \theta(r)]^2 \right\rangle \sim Nr$. Since $\delta v(r) \sim (\epsilon r)^{1/3}$ we obtain $(\delta\theta(r))^2 \sim (N\epsilon^{-1/3}) r^{2/3}$. This expression can be used to identify the region in r where the scaling $\delta\theta(r) \sim r^{1/3}$ should hold by computing the cutoff scale $r = \eta_\theta$ from the relation:

$$\frac{4}{3} N r \sim 6\kappa \frac{d}{dr} \left(\epsilon^{-1/3} N r^{2/3} \right) \tag{103}$$

This identifies the cutoff scale η_θ by the relation:

$$\eta_\theta = \left[\frac{\kappa^3}{\epsilon} \right]^{1/4} = Pr^{-3/4} \eta \tag{104}$$

where $Pr = \nu/\kappa$ is called the Prandtl number or, in some cases, the Schimdt number. In analogy with the energy spectrum $E(k)$, we can define the spectrum $E_\theta(k)$ such that $\left\langle \theta^2 \right\rangle = \int E_\theta(k) dk$. The range of r or scales where $\delta\theta(r) \sim r^{1/3}$ extends from the large scale to η_θ. For this range of scales we have that both $\delta v(r)$ and $\delta\theta(r)$ are proportional to $r^{1/3}$, i.e we expect that $\langle [\delta\theta(r)]^{2n} \rangle \sim r^{2n/3}$ in analogy with Eq. (74) which also implies $E_\theta(k) \sim k^{-5/3}$ in close analogy with the energy spectrum. At large Pr number η_θ can be much smaller that η. Then for $r \in [\eta; \eta_\theta]$ the velocity field should be smooth, i.e. $\delta v(r) \sim r$, and from Eq. (104) we reach the conclusion that $\delta\theta(r) \sim const$. In this case, called the Batchelor regime, we should expect $E_\theta(k) \sim k^{-1}$ [27]. In summary, the statistical properties of a passive scalar are similar to the one already discussed for the velocity field. The remark on the non-universality of $P[\delta v(r)]$ also applies to the probability distribution of $\delta\theta(r)$. Also in this case, we expect that $P[\delta\theta(r)/\langle [\delta\theta(r)]^2 \rangle^{1/2}]$ is independent on r. A more detailed discussion on passive scalar is postponed to Lecture 7.

Lecture 2.8. Two dimensional turbulence

An important non-trivial extension of the original Kolmogorov's ideas is the case of two-dimensional turbulence. Physically, we can think of two-dimensional turbulence as a turbulent flow in a region of space $L \times L \times h$ where $h \ll L$. This is one way to look experimentally at the problem. Another way is to study turbulent flows on a thin two-dimensional film like, for instance, a soap film. The problem does not arise for numerical investigations where two-dimensional turbulence can be studied in detail. The very large scale of atmospheric or oceanic circulations can be considered, in some cases, as examples of two-dimensional turbulence.

The major difference between three-dimensional turbulence and two dimensional one is that in $d = 2$ vorticity ω is a scalar quantity which satisfies the equation

$$\partial_t \omega + \boldsymbol{v} \cdot \boldsymbol{\nabla} \omega = \nu \Delta \omega \tag{105}$$

From Eq. (105) we see that ω is a conserved quantity when $\nu = 0$. At variance with the three-dimensional case, there is no mechanism similar to vortex stretching in two dimensions and vorticity is bounded. Mathematically, it is possible to show the existence and the unicity of the $d = 2$ Euler equation and that the velocity field is smooth, i.e. $\delta v(r) \sim r$. In two dimensions, there is no breaking of lagrangian trajectories as discussed in the previous lecture. This behaviour implies that the velocity gradients are bounded in the limit $\nu \to 0$ and that the rate of energy dissipation, ϵ, goes to zero. Moreover, from Eq. (105) we obtain the equivalent of the Kolmogorov equation for the vorticity in the very same way we did for a passive scalar (although ω is not at all passive!). The results is

$$\langle \delta v(r) [\delta \omega(r)]^2 \rangle = -2Zr + 6\nu \frac{d}{dr} \langle [\delta \omega(r)]^2 \rangle \tag{106}$$

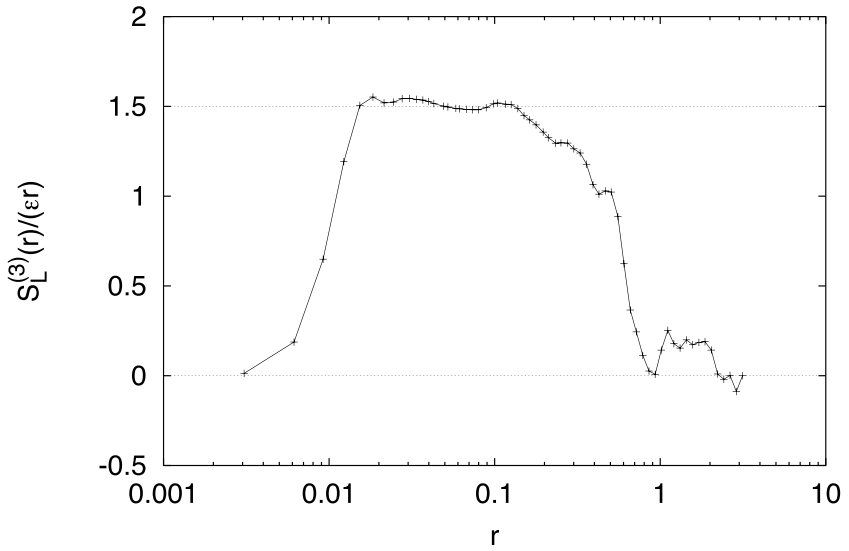

Fig. 12. Compensated third order longitudinal structure function $S_L^3(r)/(\varepsilon r)$. The dotted line is the value 3/2..
Source: Figure reproduced from [28].

where $\delta\omega(r) = \omega(\boldsymbol{x}+\boldsymbol{r}) - \omega(\boldsymbol{x})$ and $Z = \nu\langle[\nabla\omega]^2\rangle$ is the rate of vorticity dissipation. For $\nabla\omega$, mathematically, we have no a priori bounds and Z can remain finite for $\nu \to 0$. What is the physical picture which emerges? In the three-dimensional case, the physical picture we obtained is that exists an energy flux towards small scales which eventually dissipates due to the effect of viscosity. This is the reason why the average rate of energy dissipation ϵ is *Re* independent. In two dimensions there cannot be a flux of energy towards small scales: if we force the system at some characteristic scale, l_f, then $\epsilon \to 0$ for $\nu \to 0$ and $\partial_t\langle v^2\rangle$ should be proportional to the rate of energy input W in the system. Then, for homogeneous and isotropic turbulence, in Eq. (71) and Eq. (72) we should substitute ϵ with $-W$, i.e. the kinetic energy is growing. This leads to the equation:

$$B_{rrr} = \frac{3}{2}Wr + 6\nu\frac{d}{dr}B_{rr} \tag{107}$$

In other words, B_{rrr} changes sign and becomes positive. A positive value of B_{rrr} means that two particles at distance r tend to separate which is consistent with an energy flux towards *large scales*. Obviously, stationarity cannot be obtained unless we assume some dissipation effects (not due to viscosity) at very large scales. For instance, in laboratory experiments, where $d = 2$ turbulence is observed, using a thin layer of fluid forced and confined in a $L \times L$ region, large-scale dissipation is naturally introduced by the friction of the fluid on the confinement walls: the system tends to produce a large-scale, order L, turbulent circulation which dissipates energy due to the walls confining the fluid. Then Eq. (107) is valid for $r \in [l_f : L]$. In this range of scales, we should observe velocity fluctuations $\delta v(r) \sim r^{1/3}$. In this range, one usually speaks of *inverse energy cascade*. For $r \ll l_f$ the velocity fluctuations should be characterised, as already observed, by the scaling $\delta v(r) \sim r$ corresponding to an energy spectrum $E(k) \sim k^{-3}$. For this range of scales, Eq. (106) tells us that there is the flux of the vorticity square, referred to as *enstrophy*, from large to small scales where enstrophy is dissipated.

The existence of an inverse cascade of energy is well documented in numerical simulations, see Fig. 12, as well as the existence of a direct enstrophy cascade. However, the situation is somehow more complicated than we can initially think of. Since the flow is incompressible, the velocity field **v** can be obtained by a stream function Ψ in the form $v_x = -\partial_y\Psi$ and $v_y = \partial_x\Psi$. Then the equation for the vorticity $\omega = \Delta\Psi$ can be written in the form:

$$\partial_t\Delta\Psi + \partial_x\Psi\partial_y\Delta\Psi - \partial_y\Psi\partial_x\Delta\Psi = \nu\Delta\Delta\Psi \tag{108}$$

The key observation is that, if in some space region we have $\Psi = F(\Delta\Psi)$ for some function $F(x)$, then the non linear terms are identical to zero (depletion of non-linearity) and there cannot be a flux of enstrophy towards small scales (for that particular region). For instance, if we consider a circular vortex then upon defining r, the distance from the vortex centre, both Ψ and $\Delta\Psi$ are function of r and $\Psi = F(\Delta\Psi)$ holds. This argument implies that any circular vortex in a turbulent $d = 2$ flows, is a local *stable* structure of the fluid which eventually dissipated enstrophy on extremely long time scales (order $1/\nu$).

To understand the relevance of the above observation, we consider the vorticity field shown in Fig. 13 obtained from a numerical simulation [29,30]. The figure refers to a case of decaying turbulence in $d = 2$ with an initial condition consistent with the energy spectrum $E(k) \sim k^{-3}$. After some time, most of the enstrophy is concentrated in relatively few vortices that survive for a very long time. Strictly speaking, our considerations on enstrophy transfer are valid only

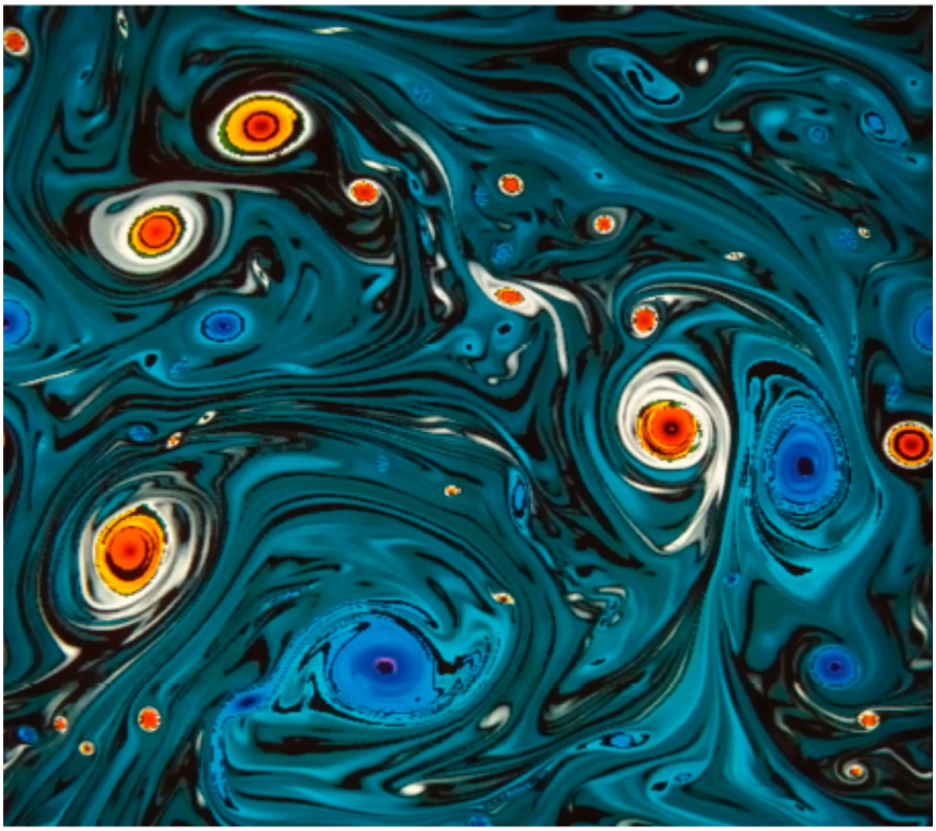

Fig. 13. Colour plot of the vorticity field in a two-dimensional decaying turbulent flow. The velocity field has been initialised with an energy spectrum proportional to k^{-3}. After a short transient regime, the system develops a number of well defined vortices that are stable solutions of the Euler equations, see [29] for details.

outside vortices where the large shear rate (mostly due to the velocity field induced by the vortices themselves) are able to stretch the residual vorticity and increase the vorticity gradients. Moreover, vortices are stable structures (except for the large-scale forcing, see later) and their lifetimes is much longer than the characteristic eddy turnover time scale which can be estimated as Ω^2/Z where Ω^2 is the overall enstrophy of the system. Eventually, strong enstrophy transfer can occur when two vortices of equal sign merge and give rise to a larger vortex.

The situation becomes even more intriguing when we consider the case of *forced* two-dimensional turbulence where the formation and stability of vortices (which form no matter what) depends on the time scale of the forcing [31]. In Fig. 14 we consider three different numerical simulations performed by introducing a forcing at the same scale in three different ways: constant forcing; random forcing and instability. The useful numbers to consider are the characteristic time of the forcing, t_f, and the eddy turnover time, $t_{ed} = \Omega^2/Z$. The dimensionless number t_{ed}/t_f provides a measure of how much the forcing mechanism influences *dynamically* the turbulent flows. It is quite clear from the figure that for $t_{ed}/t_f \to \infty$ the system is characterised by long-lived *coherent structures* which dictate the statistical properties of the system.

The above discussion leads to the following observations: in two-dimensional turbulence viscous anomaly can be observed for the rate of enstrophy dissipation; energy is transferred from small to large scales at variance with three-dimensional turbulence; coherent structures (vortices) play an important role depending on the forcing mechanism. When the flow is dominated by vortices, the statistical properties of turbulence at small scales, as described by a Kolmogorov-like theory, is almost irrelevant to the overall dynamics. In this case, vortex–vortex interactions are the leading contribution to the turbulent field and the effect of the viscous anomaly in the statistical properties of turbulence may be marginal.

We will not investigate any longer the peculiar and interesting properties of two-dimensional turbulence discussed in detail in [33] and [34] for ideas borrowed from conformal field theory.

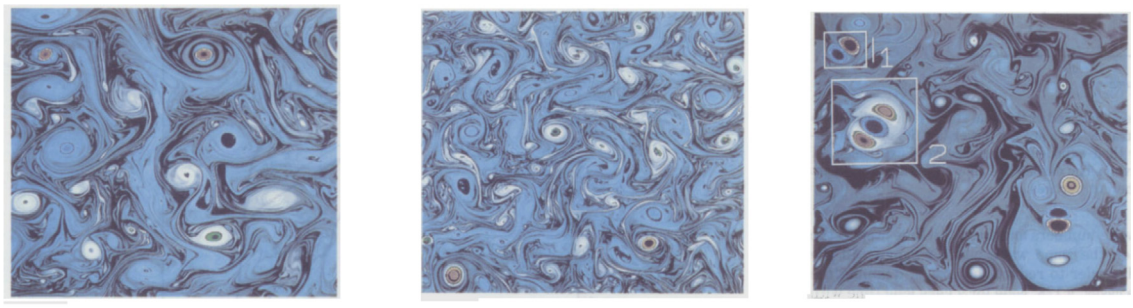

Fig. 14. Numerical simulations of forced two-dimensional turbulence. Three different forcing mechanisms are chosen: constant forcing (left panel); random forcing (middle panel) and instability (right panel).
Source: Reproduced from [32], see the original paper for discussion.

Lecture 2.9. Eddy viscosity

We now turn to a very pragmatic question that may be addressed within the framework of Kolmogorov's theory. To fix the problem in the simplest possible way, let us assume we want to perform numerical simulations for a three-dimensional flow at $Re = 10^8$ in a box or region of size L. Then we know that the number of "grid" points in any direction should be $L/\eta \sim Re^{3/4} = 10^6$. Just to understand the physical meaning of these numbers, let us consider the case of a turbulent flow generated by an atmospheric wind at a speed $U = 10$ m/s flowing at height 100 m from the land. Then $Re = 10^8$ and $\eta = 0.1$ mm. If one is interested to simulate turbulence for this problem, the numerical resolution is prohibitive even with our present technology. Moreover, in many practical situations, it is likely that our interest is to understand the statistical properties of turbulence at scales r order few centimetres, i.e. for $r \gg \eta$. Does Kolmogorov's theory tell any computational trick to turn around the problem?

The basic physical idea is similar, but not equal, to the one discussed for Richardson's turbulent diffusion. Kolmogorov's theory suggests that there exists an energy flux towards small scales which eventually leads to the dissipation of the kinetic energy. We can imagine dividing the computational grid into two different parts the resolved part where numerical simulations are performed using the N.S. equation and a *subgrid* part which is not computationally resolved and which takes care of the energy dissipation. However, we should match the resolved and the subgrid part in some way. The simplest way to do that is to assume that for the resolved part Kolmogorov's theory holds. Then, upon denoting Δ the smallest scale in the resolved computation, we should require that

$$\langle [\delta v(\Delta)]^3 \rangle = -\epsilon \Delta \tag{109}$$

Since the *subgrid* takes care of dissipation, we can introduce an *eddy* viscosity ν_{turb} such that

$$\epsilon = \nu_{turb} \frac{\delta v(\Delta)^2}{\Delta^2} \tag{110}$$

Using Eqs. (109) and (110) we reach the conclusion that

$$\nu_{turb} = \delta v(\Delta) \Delta \tag{111}$$

However this is not the end of the story, since Δ is the smallest size we resolve computationally, for numerical stability we must require $\delta v(\Delta) = S_* \cdot \Delta$ where $S_* \equiv \sqrt{S_{ij} S_{ij}}$, i.e. S_* is the characteristic strain of the velocity field. Obviously S_* depends both on time and space. Using the definition of S_* we finally get

$$\nu_{turb} = S_* \Delta^2 \tag{112}$$

and for the energy dissipation rate we obtain:

$$\epsilon = \nu_{turb} S_*^2 = S_*^3 \Delta^3 \tag{113}$$

Using Eq. (113) it is easy to check that the value of η corresponding to ν_{turb} is $[\nu_{turb}^3/\epsilon]^{3/4} = \Delta$. This idea, originally due to Smagorinsky, has been shown to be very powerful in many applications and it has been investigated and generalised in many ways. It is a standard way to consider turbulence in atmospheric flows. Just to see how this approach works in different cases, let us consider turbulence in a boundary layer and let us assume to resolve turbulence up to a distance y from the boundary. Then in the boundary layer $\nu_{turb} = y v_*$ since in this case, $\delta v(r)$ is just the size of the turbulent fluctuations which, as we know, are of order v_*. Then the momentum conservation at y (i.e. at the scale Δ) implies

that $\nu_{turb}\partial_y U = v_*^2$ as we discussed in the previous lecture. From this relation, we immediately obtain that $\partial_y U = v_*/y$ consistently with the von Karman theory. This is another way to say that the logarithmic profile is consistent with the zeroth law of turbulence as already discussed. Obviously, this is the starting point of possible in-depth analysis and refinement of the problem. A more detailed discussion is done in Lecture 8. Here we want just to point out that, starting from Kolmogorov's framework of homogeneous and isotropic turbulence, we can develop some non-trivial and useful hints for numerical simulations at large *Re*.

Lecture 2.10. Summary of Lecture Lecture 2

The Kolmogorov theory is one of the most important achievements in the study of turbulence flows. Yet it is based on a number of different assumptions (most important homogeneity and isotropy) which are not at all obvious. An in-depth discussion on the subject and the possible outcomes can be found in several textbooks among which we refer to [12,13,35]. The discussion of scale invariance of the NSE can be found in [26]. The possibility to perform high resolution numerical simulations of the NSE opened a new way to understand turbulence. A review on the subject can be found in [17] and in [36] for the passive scalar. The restricted Euler equations were investigated in a number of papers trying to understand the role of flow topology in the dynamics of turbulent flows. A well-documented review on the subject can be found in [19], see also [37,38]. The extension of the Kolmogorov theory for the passive scalar is reviewed in [39]. A recent review on two-dimensional turbulence can be found in [33].

The Kolmogorov theory and, in particular, Eq. (74) is a scaling theory for the structure functions of velocity differences in turbulence, $S_n(r) = \langle[\delta v(r)]^n\rangle$. There is no reference in the theory to any pattern and/or space structures in the statistical description of turbulence. At variance with this point of view, the Restricted Euler equations highlight non-trivial topological features of turbulent flows. In particular, we understand that energy dissipation (the strain-dominated region in the Q, R diagram, arises from the vortex stretching mechanism (region of positive Q and negative R). Thus one can wonder whether there is no sign of the complex topological flow structures in a statistical description of turbulent flows. In other words, the question of whether or not correlation functions are the quantities to study in turbulence is not so straightforward to disentangle. In fact, for two-dimensional turbulence numerical simulations clearly show the relevance of coherent structures (vortices) to properly describe turbulence dynamics. For three-dimensional turbulence, the question is less obvious and we will discuss this problem in more detail in the following lectures. An interesting issue, at least theoretically, is to study turbulence between two and three dimensions [40,41].

Another non-trivial issue arises by a closer look to the Fig. 6. Even if *Re* is rather large, we do observe agreement with the scaling ϵr for only less than one decade. Since we have a theory (the 4/5 Kolmogorov equation) that predicts the scaling, we can definitively state that the scaling is observed. However, for very small scales and very large scales, we observe deviations to the scaling. This is not a surprise and we can consider these deviations as *finite size effects* in *Re*, i.e. we argue these deviations become small for $Re \to \infty$. This argument is supported by looking at the energy spectrum obtained from high *Re* number laboratory experiments, see for instance Fig. 11. However, we must be careful to properly take into account finite-size effects while investigating the scaling properties of turbulence.

Lecture 3. Intermittency in 3D turbulent flows

Lecture 3.1. Violation of the Kolmogorov theory

As we discussed in the previous section, Kolmogorov's theory of homogeneous and isotropic turbulence is based on two different assumptions. The first one is that the rate of energy dissipation ϵ is *Re* independent (zero-*th* law of turbulence) which leads to 4/5 Kolmogorov' equation which predicts $B_{rrr} \sim -\epsilon r$ in the inertial range $r \in [\eta; L]$. The second assumption, or conjecture, is that any moments $S_n(r) \equiv \langle[\delta v(r)]^n\rangle$ scales as $[\epsilon r]^{n/3}$. This implies that the probability distribution $P[X(r)]$, with $X(r) \equiv \delta v(r)/S_2(r)^{1/2}$, although it may be not universal, is independent of r. Physically, this is equivalent to, say, that the statistical properties of the velocity fields in turbulent flows are scale-invariant in the limit $Re \to \infty$. Scale invariance means that going from say r to $r/10$ we observe the same statistical fluctuations of X, i.e. the same physics. Given the complexity of the phenomenon (i.e. turbulence), scale invariance is a very interesting and powerful statement that is worthwhile to investigate in detail.

Let us consider moments of $X(r)$. The first moment $\langle X(r)\rangle$ should be zero for homogeneity, $\langle X^2(r)\rangle = 1$ by definition. Thus we focus on $\langle X^4(r)\rangle \equiv S_4(r)/S_2(r)^2$ which is also called *kurtosis*. This quantity can be computed with better precision than the third moment which, at any rate, is controlled by the Kolmogorov 4/5 equation.

In Fig. 15 [42] (see also [13,35] for a more pedagogical discussion), we show two examples of how $K(r) \equiv \langle X^4(r)\rangle$ depends on r: both numerical simulations and experimental measurements show quite clearly that $K(r)$ is close to 3 at large $r \sim L$ and then increases all the way down for small r becoming flat and large for $r \leq \eta$. Let us remark that for a gaussian distribution of unit variance, the kurtosis is equal to 3. A large value of the kurtosis of $P[X]$ means that there is a relative small probability (compared to a gaussian) for X to be near 0 and a *higher* probability to be large. This interpretation is also supported by a direct measurements of $P[X(r)]$ for different r in turbulent flows, as reported [43] in Fig. 16: at very large scale the probability distribution is close to be gaussian while at small scales we observe long tails in $P[X]$. The qualitative picture we obtain is that the quantity $\delta v(r)$ shows relatively small fluctuations near zero with

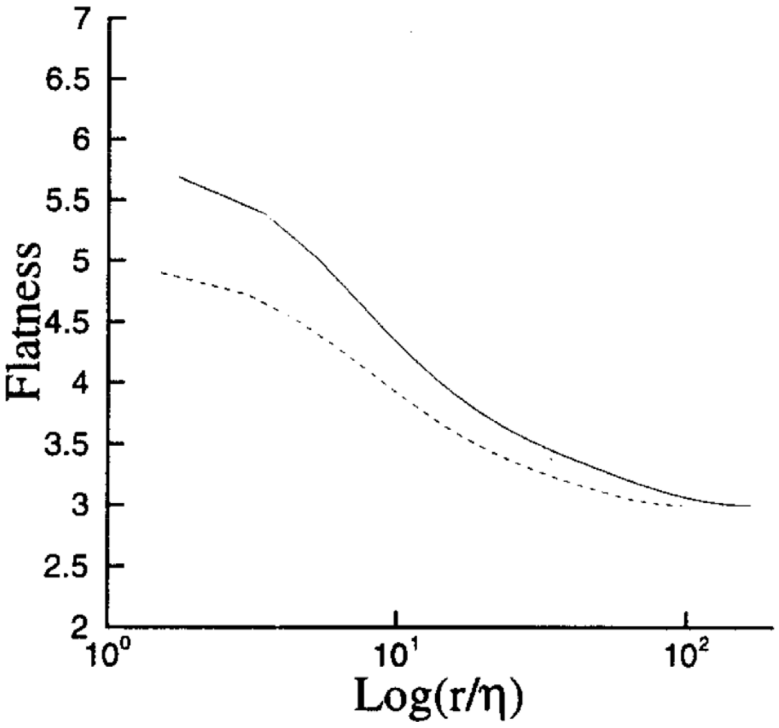

Fig. 15. Flatness of the velocity increments in a homogeneous shear flow, solid line, and in homogeneous and isotropic turbulence, dotted line. *Source:* Figure reproduced from [44].

intermittent bursts of large values: the smaller is r the larger the bursts in the velocity difference. For this reason, we can say that the statistical properties of the velocity fluctuations in a turbulent flow show *intermittency*. This also means that scale invariance does not hold and that the second assumption, or conjecture, of Kolmogorov's theory is wrong (see Fig. 16).

Lecture 3.2. The statistics of lagrangian acceleration

The first question we ask is, why scale invariance is broken? Can we have any physical intuition on the phenomenon of intermittency? One can do many different analyses but, perhaps, the best way to address this question is to look in detail at the probability distribution of the acceleration experienced by a lagrangian particle in a turbulent flows [43,47,48]. The particle is moving according to the equation:

$$\frac{d\boldsymbol{x}}{dt} = \boldsymbol{v}(\boldsymbol{x}, t) \tag{114}$$

Thus the acceleration is given by $d^2\boldsymbol{x}/dt^2$ which depends on the velocity gradients of the turbulent flow. We can compute the acceleration using the estimate of the velocity gradients at scale $r = \eta$. Let us call the acceleration $a(\eta)$, we can then write

$$a(\eta) \sim \frac{\delta v(\eta)}{\tau_\eta} \sim \frac{\delta v(\eta)^2}{\eta} \tag{115}$$

Next, using the Kolmogorov theory we can write:

$$\delta v(r) = \delta v(L)\left[\frac{r}{L}\right]^{1/3} \tag{116}$$

where $\delta v(L)$ is the velocity fluctuations at large scale. From the analysis of existent numerical and experimental data, we can assume that the probability distribution of $\delta v(L)$ is gaussian with some variance σ. Kolmogorov's theory tells us that η is obtained by using the relation $\delta v(\eta) \cdot \eta \sim \nu$. Using the definition of η and Eq. (115) we obtain

$$a(\eta) = \nu^{-1/4} L^{-3/4} \delta v(L)^{9/4} \tag{117}$$

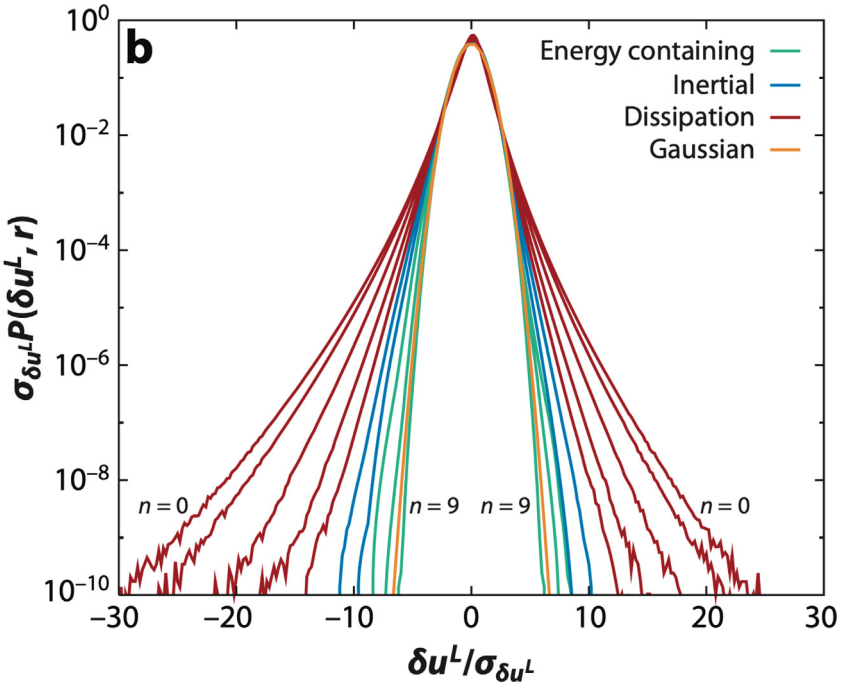

Fig. 16. Probability distribution function P of velocity increment δv_r calculated for different values of $r \propto 2^n$, for $n = 0, \ldots, 9$ (i.e. smaller values of n correspond to shorted distances r).
Source: Reproduced from [17], adapted from [45].

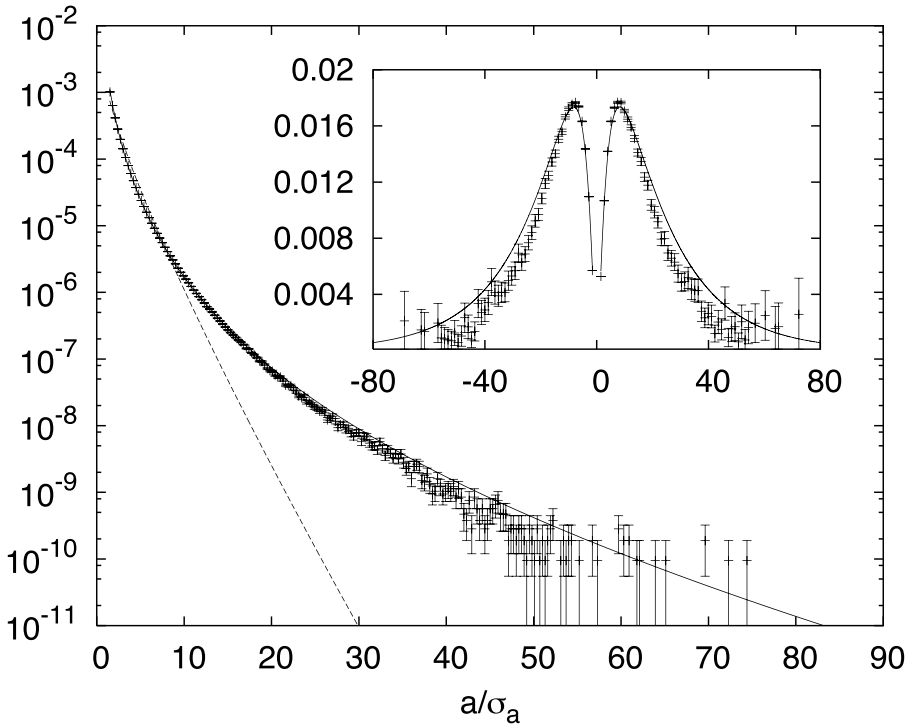

Fig. 17. Log-linear plot of the acceleration PDF. The crosses are the DNS data, the solid line is the multifractal prediction, and the dashed line is the K41 prediction, Eq. (119). The DNS statistics were calculated along the trajectories of 2.0×10^6 particles amounting to 1.06×10^{10} events in total. The statistical uncertainty in the PDF was quantified by assuming that fluctuations grow like the square root of the number of events. Inset: $\tilde{a}^4 \mathcal{P}(\tilde{a})$ for the DNS data (crosses) and the multifractal prediction.
Source: Figure reproduced from [46].

This expression allows us to compute $P[a(\eta)]$:

$$P[a(\eta)] \sim a(\eta)^{-5/9}\nu^{4/9}\exp\left[-\frac{a(\eta)^{8/9}\nu^{2/9}L^{2/3}}{2\sigma^2}\right] \tag{118}$$

Finally, after some algebra, we can compute the probability distribution of $A \equiv a(\eta)/\langle a(\eta)^2\rangle^{1/2}$ which is

$$P[A] = ZA^{-5/9}\exp\left[-\frac{A^{8/9}}{2}\right] \tag{119}$$

with Z a normalising factor. In Fig. 17 we show the probability distribution $P[A]$ obtained from the numerical simulations against the prediction given by Eq. (119): strong deviation at large A are observed. Once again the tail of the probability distribution is much larger than expected.

In order to understand the reason for the large discrepancy between the observed $P[A]$ and the prediction is given by Eq. (119), we look at the time signal of the velocity reported in Figs. 18 and 19: it is quite clear that the large value of the acceleration is due to the fast oscillations experienced by the lagrangian velocity.

In Fig. 18 we show the trajectory of a particle in the three-dimensional space: what happens is that from time to time the particle enters in a region of high vorticity (probably a vortex tube). Then, since ω is large, the acceleration experiences a large value for a relatively short time. Vortex tubes (or vortex filaments) are the coherent structure that appears in any turbulent flow [52,53]. Vortex tubes cannot be described in terms of $\delta v(r)$ and they do not appear in the Kolmogorov theory. Vortex filaments or vortex tubes are unstable structures and do not dissipate energy which obviously implies that large shear rates should occur randomly outside the core of the vortex tube. In other words, the field of energy dissipation is spatially organised for the vortex tubes to appear. This is also in agreement with the discussion in Lecture 2 on the Restricted Euler equations. If the above arguments are correct, then the violations of the Kolmogorov theory are due to structures and/or to some sort of spatial organisation (whatever it means) of the energy dissipation. Then one can reasonably argue that all these effects depend both on the way we force turbulence and/or the detailed mechanism of viscous dissipation. Clearly, we need to understand in a better way what we mean by "space organisation".

Lecture 3.3. Refined Kolmogorov similarity hypothesis

Let us suppose that, upon averaging many realisations, we can still assume that turbulent fluctuations are homogeneous and isotropic. After all, in the Navier–Stokes equations there are nowhere informations about breaking the space isotropy: any space anisotropy must come eventually from the forcing. Then whatever we mean by space organisation it should be related to the correlation properties of the energy dissipation. Numerical simulations are very helpful to clear the picture. Energy dissipation does show non-trivial patterns in space (and in time) as we can see from Fig. 20. Next, we understand from Kolmogorov theory that the quantity $\langle[\delta v(r)]^3\rangle$, at least in some average way, is related to the energy flux from large to small scales which is dictated by the rate of energy dissipation ϵ. However, if the dissipation field is space correlated, then we should also take care of this correlation.

Kolmogorov himself addressed the previous question with a non-trivial first step [56]. The basic idea is to consider the *field* $\epsilon(\mathbf{x})$ and not just its average $\epsilon \equiv \langle\epsilon(\mathbf{x})\rangle$. It is quite clear, from the data analysis discussed so far, that the conjecture $\delta v(r) \sim (\epsilon r)^{1/3}$ is not true. Given the velocity difference $\delta v(r) = v(x+r) - v(x)$, Kolmogorov considered the *local* average $\epsilon(r)$ defined as the space average of $\epsilon(\mathbf{x})$ in a box of size r, computed as:

$$\epsilon(r) \equiv \frac{1}{r^3}\int_{B(r,x_0)} d^3x\epsilon(\mathbf{x}) \tag{120}$$

where $B(r, x_0)$ is three dimensional box of size r around the point x_0. Now, if the average energy dissipation ϵ is physically interpreted as the average flux of energy from large to small scales, then we can reasonably consider $\epsilon(r)$ as the *local* energy flux correlated to the velocity fluctuation $\delta v(r)$. Then, under this assumption, we have

$$\delta v(r)^3 \sim \epsilon(r)r \tag{121}$$

On average Eq. (121) is exactly the 4/5 Kolmogorov' equation. In general, Eq. (121) tells us that the correct quantity to look at is the probability distribution of $Y(r) \equiv \delta v(r)/[\epsilon(r)r]^{1/3}$. This is a major difference with respect to the quantity $X(r)$ previously defined: now we need to look for any r to two different quantities namely $\delta v(r)$ and $\epsilon(r)$. In Fig. 21 [57] we show the results obtained from experimental data: it is now clear that $P[Y(r)]$ is no longer dependent on r, i.e. $Y(r)$ is a scale-independent quantity. Eq. (121) is referred to as *Refined Kolmogorov Similarity Hypothesis* or RKSH and it has been observed to hold in a number of numerical and experimental data of turbulence flows.

Lecture 3.4. Intermittency and fractal dimension

Although the RKSH works very well, the bad news is that we do not know anything about the probability distribution of $\epsilon(r)$ which implies that we have no guess about the probability distribution of the velocity field. We understand that, besides the average rate of energy dissipation ϵ, we need to know something about the statistical properties of $\epsilon(r)$. A first

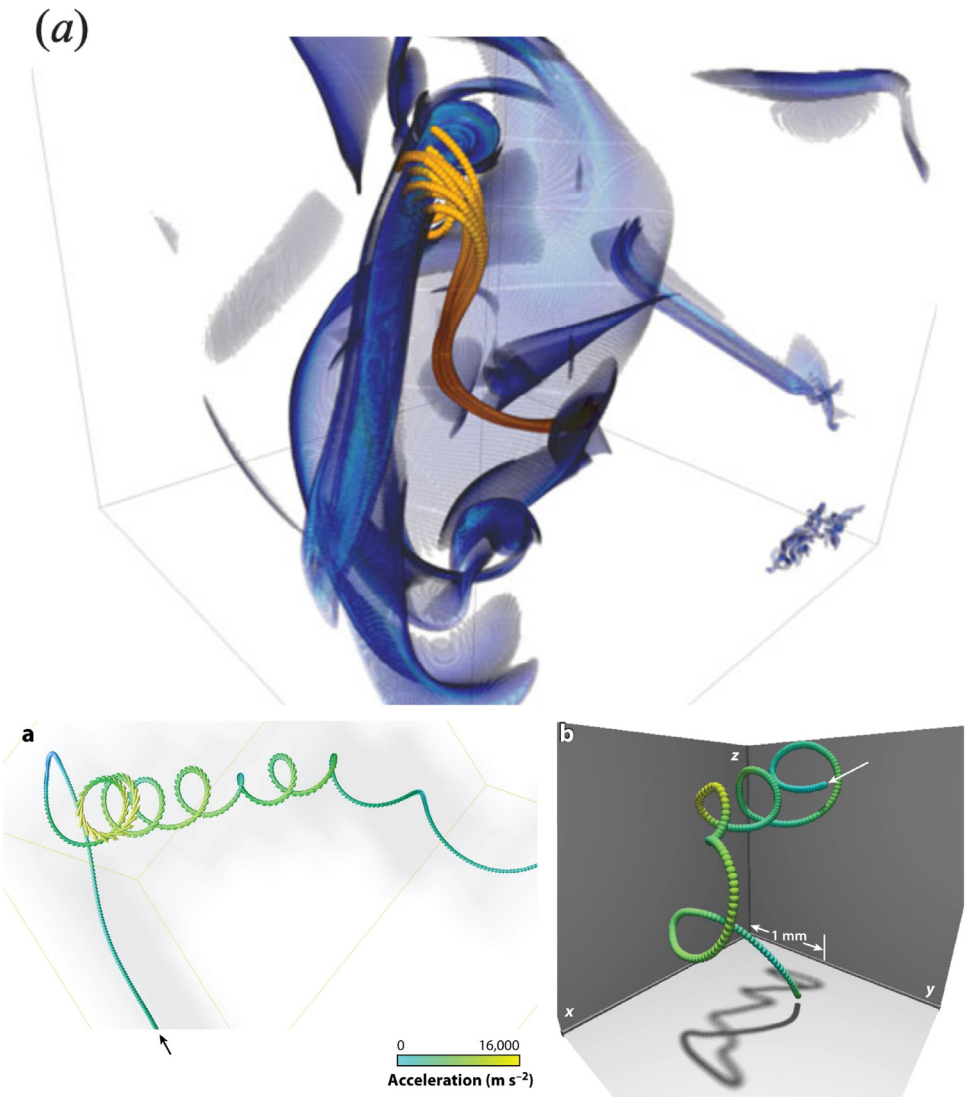

Fig. 18. (top) Example of Eulerian and Lagrangian rendering. Both the intensity of the Eulerian enstrophy field at a given time (blue isosurface) and the Lagrangian evolution of a bunch of particles with trajectories ending at the time of the Eulerian snapshots are shown. Notice that the Lagrangian particles have an initially smooth evolution because we also show the initial transient time when the underlying Eulerian field was chosen smooth and with low energy. The bunch of particles were chosen such as to encounter vortex filaments during their evolution. (bottom) A trajectory of a fluid tracer in a small-scale vortex filament in a turbulent flow from a numerical simulation at $Re_\lambda \sim 280$. Colours and arrows indicate the magnitude and direction of the velocity (see Biferale et al. 2004a, Toschi et al. 2005). (b) The trajectory of a high-acceleration event of a 46-μm-diameter tracer particle in turbulence at $Re_\lambda = 970$ recorded at a frame rate of 70,000 frames per second. The position of the particle at each of the 278 frames is represented by a sphere. The colours represent the acceleration magnitude, as indicated by the scale.
Source: (top) Figure by courtesy of B. Gallagher, reproduce from [49]. (bottom) Figures reproduced from [43], adapted from [50].

step in this direction is to start by the evidence that energy dissipation does not occur uniformly in space, rather it occurs on a subset of the three-dimensional space. One way to characterise a "complex" space pattern of a positive quantity is to consider its "fractal dimension". In our case, we assume that the field $\epsilon(\boldsymbol{x})$ of energy dissipation is characterised by a fractal dimension $D < 3$. Even if the concept of fractal dimension is rather well-known in many scientific investigations, it is worthwhile to review it shortly. Let us consider an object embedded in a d dimensional space. In our case, the object is the energy dissipation and $d = 3$. To obtain a measure of the dimension D of the object we proceed as follows: we divide the space in boxes of size r and we measure the number of boxes $N(r)$ where at least one point of our object is found. Upon changing r, the dimension D can be computed from the relation $N(r) \sim r^{-D}$. Since the total number of possible boxes are r^{-d}, we can also say that the probability to find a box where at least one point of our object is located goes as $N(r)/r^{-d} \sim r^{d-D}$. Thus the concept of fractal dimension can also be considered in a probabilistic sense. Interestingly, this definition of fractal dimension is due to Richardson.

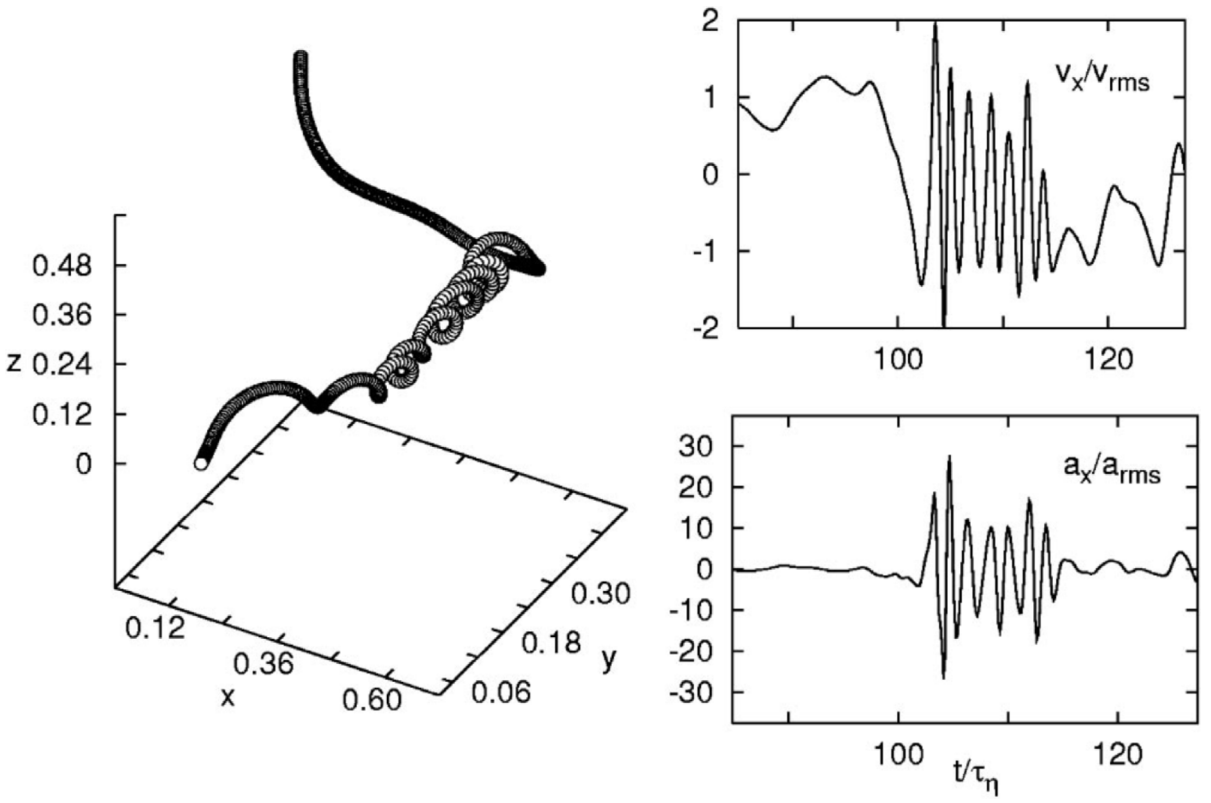

Fig. 19. Trajectory and time series. Left panel: 3D the trajectory of a trapping event in the vortex filament. Acceleration and velocity fluctuations here reach about 30 and 2 r.m.s. values, respectively (right panels).
Source: Reproduced from [51].

In applying the concept of fractal dimension to the field of turbulent energy dissipation, we should be aware that we are making a very simple approximation to the real problem. Nevertheless, we can exploit whether this idea is going in the right direction. We consider the energy dissipation an on–off field: only in a subset of dimension $D < 3$ there is a non-zero energy dissipation. The space configuration of the energy dissipation changes realisation by realisation and assuming that *on average* for each realisation we can take care of the random geometry of the energy dissipation by using the fractal dimension D. The number of boxes where the energy dissipation is non-zero is r^{-D} out of r^{-3} total number of boxes. Since on average we still assume that the energy dissipation is constant and equal to ϵ, it follows that the value of the energy dissipation in the boxes where it does not vanish is equal to ϵr^{D-3}, i.e. the energy dissipation goes as r^{D-3} with probability r^{3-D}. At this stage, we can use the RKSH to compute:

$$\langle \delta v(r)^n \rangle \sim r^{3-D} \epsilon r^{n(D-3)/3} r^{n/3} \tag{122}$$

where the first term on the r.h.s is the probability to find a box with non-zero energy dissipation. We can write (122) in the form

$$S_n(r) = \langle \delta v(r)^n \rangle \sim r^{n(D-2)/3+3-D} \tag{123}$$

Then, from Eq. (123) we obtain:

$$K(r) \equiv \frac{S_4(r)}{S_2(r)^2} \sim \frac{r^{4(D-2)/3+3-D}}{[r^{2(D-2)/3+3-D}]^2} \sim r^{D-3} \tag{124}$$

We immediately see that for $D < 3$ the kurtosis $K(r)$ should increase going from large to small scales. Eq. (123) is also referred to as the β *model* [58]and it represents the first non-trivial attempt to take into account the non-trivial random geometry of energy dissipation. Numerical simulations and experimental data are consistent with $D \sim 2.88$ using Eq. (124), i.e. the fractal dimension is not far from 3. Note that the β model for $D = 3$ is equivalent to the Kolmogorov' conjecture, $\delta v(r) \sim r^{1/3}$, as expected.

There is one special case [16] where we can assess the validity of the above ideas, namely the case of the Burgers' equation already considered in the previous lecture:

$$\partial_t u + u \partial_x u = \nu \partial^2_{xx} u \tag{125}$$

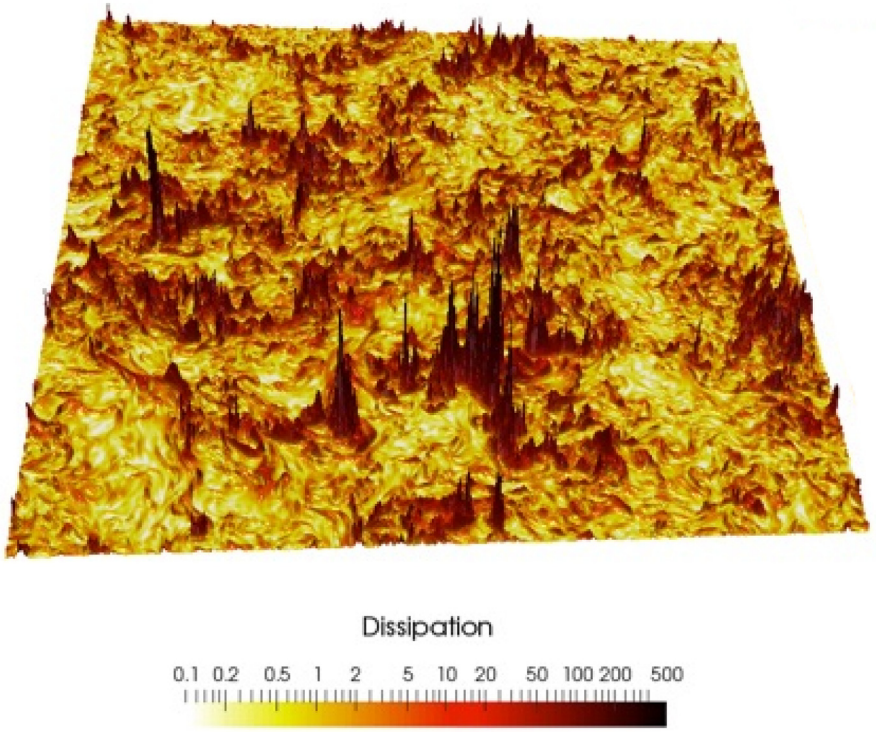

Fig. 20. 2D snapshot of the local energy dissipation field from a 3D HIT flow. *Source:* Data from a 1024^3 simulations (courtesy of M. Buzzicotti). Figure reproduced from [54].

For the case $\nu = 0$, Eq. (125) can be solved for any initial condition $f(x)$ as the solution of the equation:

$$u(x, t) = f(x - u(x, t)t) \tag{126}$$

In Fig. 22 we see that the solution of the Burgers' equation develops a singularity in a finite time. However, for $\nu > 0$ the singularity does not arise and we have the formation of shocks. The region η where the shock forms should balance advection and dissipation which leads, not surprisingly, to the relation $\eta \sim U/\nu$, where U is the characteristic velocity on the large scale due to the initial condition. The shock can be considered as regions with fractal dimension $D = 0$. Outside the shocks, the velocity field is smooth with $\delta v(r) \sim r$ while inside the shock we have $\delta v(r) \sim U$. Using the concept of fractal dimension, we can say that the probability to observe a shock goes as $p(r) \sim (r/L)^{1-D}$. Therefore we obtain:

$$\langle [\delta v(r)]^n \rangle \sim U^n [(r/L)^n (1 - p(r)) + p(r)] \sim U^n (r/L)^n \quad n \leq 1 \tag{127}$$

$$\langle [\delta v(r)]^n \rangle \sim U^n [(r/L)^n (1 - p(r)) + p(r)] \sim U^n (r/L) \quad n \geq 1 \tag{128}$$

Although for the Burgers' equation $\langle [\delta v(r)]^3 \rangle \sim r$ as in the 4/5 Kolmogorov equation, intermittency is fully dominated by the formation of shocks and the energy spectrum goes as k^{-2} since $\langle [\delta v(r)]^2 \rangle \sim r$. For the Burgers' equation we can see where intermittency comes from and why there is a strong violation of the Kolmogorov' conjecture.

The example taken from Burgers' equation suggests that intermittency is due to the formation of well-defined structures (shocks) where energy dissipation occurs. This effect shapes the scaling properties $\langle [\delta v(r)]^n \rangle$ for large n and explain why the fractal dimension, $D = 0$, of these structures enters the game. In some way, although we did not consider any structures, the β model attempts to relate the geometry of the energy dissipation in the case of three-dimensional turbulence. Let us remark that the β model implies, as for the case of the Burgers' equation, that $S_n(r) \equiv \langle [\delta v(r)]^n \rangle$ exhibit a power law behaviour with r, i.e. $S_n(r) \sim r^{\zeta(n)}$. For the β model we have from Eq. (123) $\zeta(n) = n(D - 2)/3 + (3 - D)$. To assess the validity of this approach we must:

1 - extract the values of $\zeta(n)$ from turbulent flows (either from laboratory measurements and/or from numerical simulations);
2 - understand whether or not $\zeta(n)$ are independent of *Re*.

We highlight the relevance of the second bullet from the physical point of view. One can imagine, for instance, a completely different situation where $\zeta(n)$ are weakly dependent quantities on *Re* and for $Re \to \infty$ we have $\zeta(n) \to n/3$.

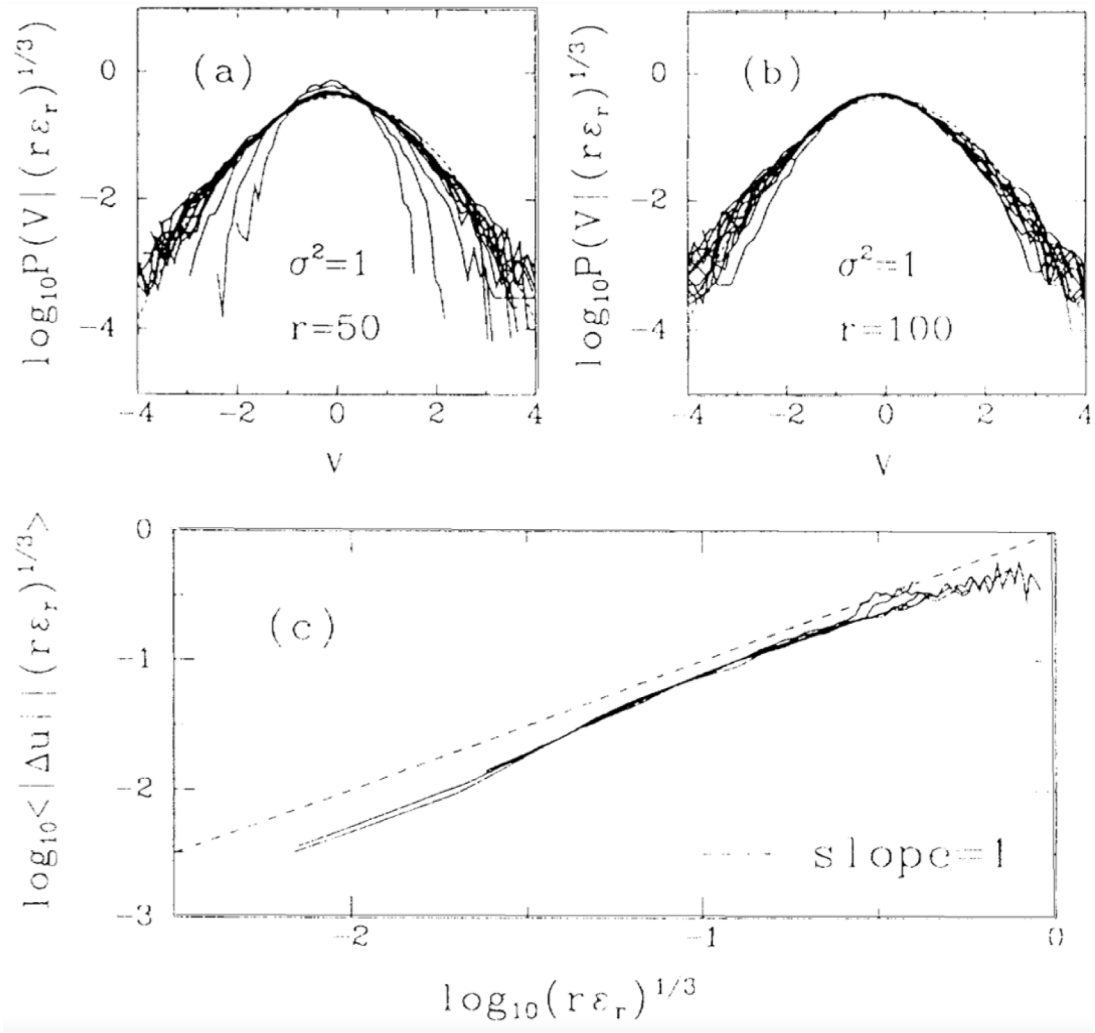

Fig. 21. (a), (b) The logarithm of the PDF of V conditioned on $(r\varepsilon_r)^{1/3}$ for different values of r. Each solid curve corresponds to a different value of the conditional parameter $(r\varepsilon_r)^{1/3}$. The value of r, the number of curves, and the minimum and maximum values of $\alpha = (r\varepsilon_r)^{1/3}/(L\langle\varepsilon\rangle)^{1/3}$ considered here are (a) st50, 14, 0.024, and 0.24; (b) 100, 15, 0.03, and 0.29. The intermediate values of a are equally spaced linearly between the minimum and maximum values. The dashed curves correspond to a Gaussian of mean zero and unity variance. 1n (a), the three innermost curves (which are distinct from the ones that collapse) correspond to the three lowermost values of $(r\varepsilon_r)^{1/3}$. (c) The logarithm of the mean value of $|\Delta u|$ conditioned on $(r\varepsilon_r)^{1/3}$ as a function of the logarithm of $(r\varepsilon_r)^{1/3}$. The four coalescing solid curves correspond to r in the inertial range of 20, 50, 100, and 200. The dashed line has a slope of I.
Source: Figure reproduced from [55].

In this scenario, the effect of intermittency as previously discussed can be considered as a *finite size effect* which vanishes at very large *Re*.

Lecture 3.5. Extended self similarity

At any rate we must take care of finite size effects. As already noted, scaling behaviour in physics is a rather general feature found in many different problems. It is also quite general that scaling behaviour is never exactly true because of finite size effects. In our case, the scaling properties of the structure functions $S_n(r) \sim r^{\zeta(n)}$ are modified when r is very large, close to the large scale L, and r is very small, close to the dissipation scale η. One can understand the issue by looking at the behaviour in r of $S_3(r)/r$ [60] which, according to the 4/5 law, is constant in the scaling region $\eta \ll r \ll L$. In Fig. 23 we show $S_3(r)/r$ for two cases at $Re_\lambda = 140$ and $Re_\lambda = 800$ respectively. Let us remember that R_λ is the *Re* number computed using the Taylor scale λ as the inner scale and it is related to a *Re* number by the scaling $Re \sim Re_\lambda^2$. At lower *Re* it is difficult to claim the existence of any scaling region whereas at relative larger *Re* one can detect a scaling region of about one decade. From the experimental data we see that the scaling region of $S_3(r)$ starts at $r \sim 50\eta$. In order

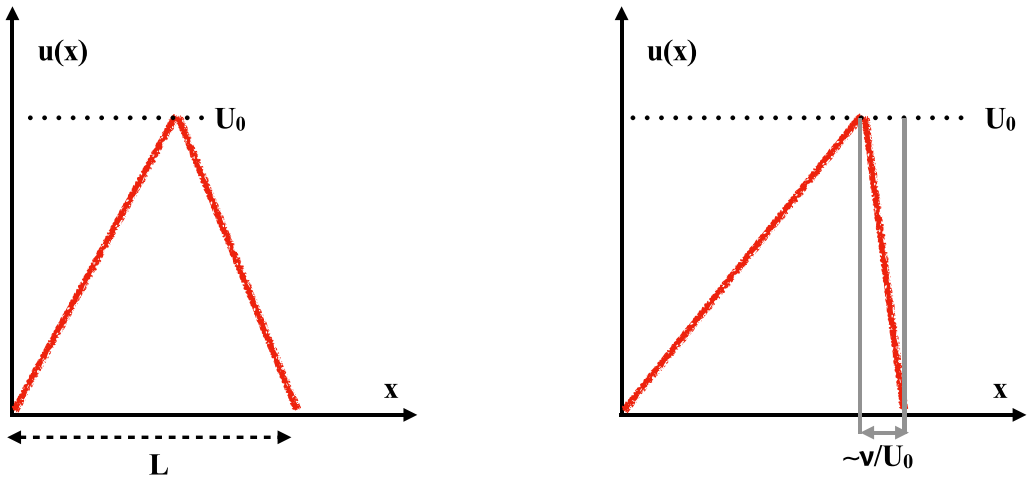

Fig. 22. The development of a singularity in the evolution of Burgers equation. As time proceeds a steep front develop (shock solution) eventually dissipated on scales controlled by the viscosity.

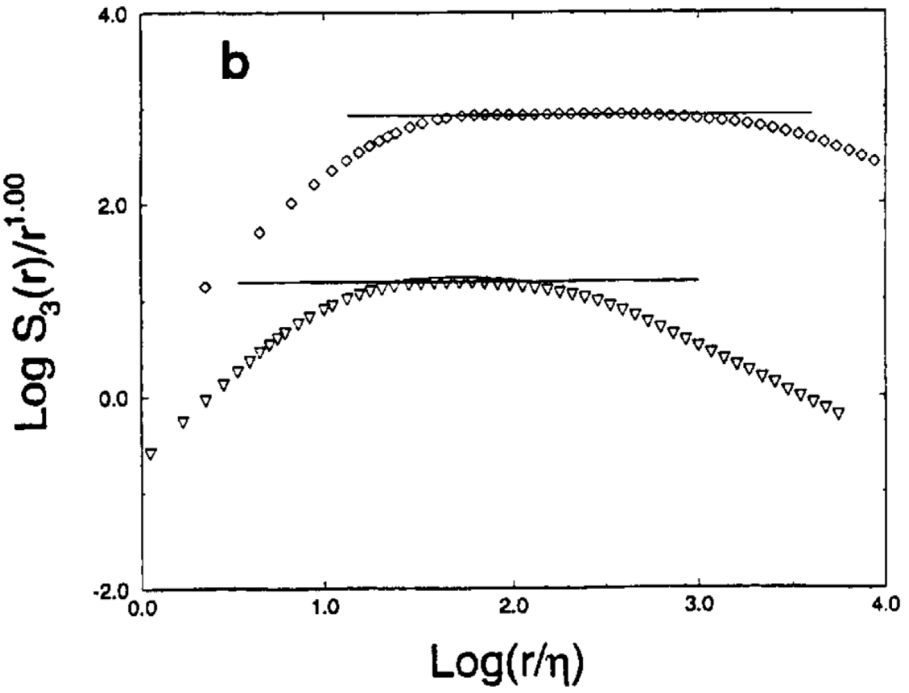

Fig. 23. Compensated structure functions $S_p(r)/r^{\zeta(p)}$, for the case $p = 3$, as a function of r.
Source: Data taken from an experiment on a jet at $R_\lambda = 800$ (O). Data taken from the wake behind a cylinder at $R_\lambda = 140$ (∇). Figure reproduced from [59].

to extract meaningful scaling values of $\zeta(n)$ we should be able to know, in principle, how $S_n(r)$ depends on the ratio r/η. Unfortunately this information is not available. However, we can use the following simple idea [61]: instead of looking at the scaling exponents of $S_n(r)$ versus r we can investigate the scaling relation:

$$S_n(r) \sim S_3(r)^{\zeta^*(n)} \tag{129}$$

Eq. (129) highlights the fact that, for $\zeta^*(n) \neq n/3$, the scaling of the structure functions $S_n(r)$ does not follow dimensional counting. This is consistent with the prediction of the β model. For this reason the exponent $\zeta^*(n)$ can be called *anomalous exponents*. Moreover, in the range where $S_3(r) \sim r$ we should have $\zeta^*(n) = \zeta(n)$. The idea is that, even if $S_3(r)$ does not show an exact scaling $S_3(r) \sim r$, the scaling (129) may still hold. If this is true, we can extend the scaling region. There is

Table 1
Scaling exponents $\zeta(n)$ of the velocity structure functions of order n obtained applying the ESS to experimental data. The error on the exponents is about $\pm 1\%$.
Source: Reproduced from table 2 in [60].

n	$\zeta(p)$
1	0.37
2	0.70
3	1.00
4	1.28
5	1.54
6	1.78
7	2.00
8	2.23

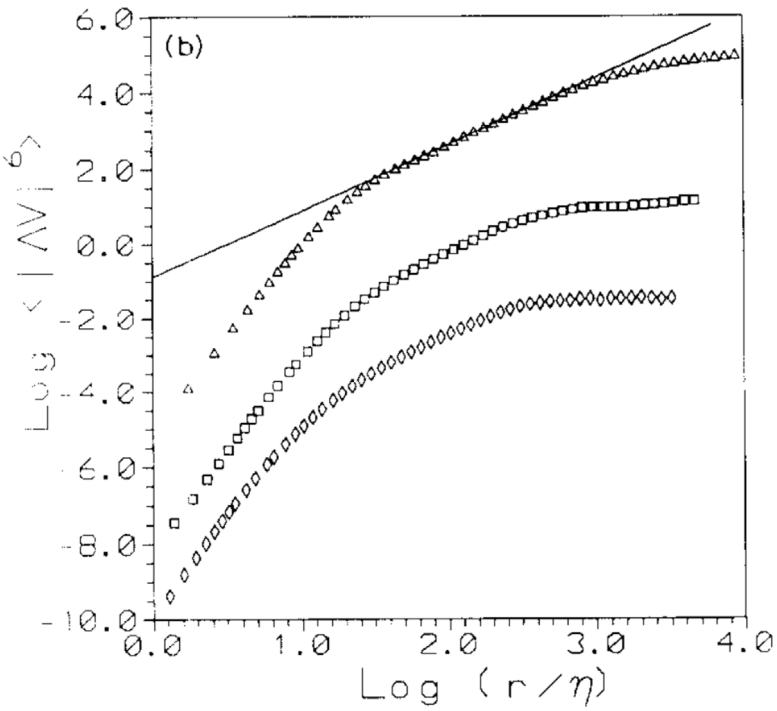

Fig. 24. Log–log plot of $S_6(r) = \langle \Delta V(r)^6 \rangle$ against r/η for the cases $Re_\lambda = 800$, $Re_\lambda = 342$ and $Re_\lambda = 225$ (from top to bottom respectively). The three cases are referred as *J*, *C*18 and *C*6 in the following. The solid lines correspond to slopes 1.79.
Source: Figure reproduced from [60].

no reason for this idea to be true but we can try whether it improves or not our estimate of $\zeta(n)$ in particular at low *Re* where $S_3(r)$ does not show any scaling at all.

Another small, although non-trivial, improvement is obtained upon using $\langle|\delta v(r)^3|\rangle$ instead of $S_3(r) = \langle \delta v(r)^3 \rangle$. The advantage is clear: $\delta v(r)$ is fluctuating between positive and negative values with zero average (for homogeneity). Thus to obtain a reliable value of $S_3(r)$ one needs a rather large statistical sample. This requirement is less demanding for any positive define structure functions $S_{2n}(r)$ and for $\langle|\delta v(r)^3|\rangle$. A detailed analysis of experimental data [60] shows that $S_3(r) \sim \langle|\delta v(r)^3|\rangle$ for all r. Thus, in practice, we use $\langle|\delta v(r)^3|\rangle$ instead of $S_3(r)$ to extract the anomalous scaling exponents $\zeta(n)$.

In Fig. 24 we show $S_6(r)$ for three different Re_λ from 225 to 800: not surprisingly only at large *Re* we observe a scaling region of about one decade whereas at lower *Re* there is little hope to make any good estimate of the scaling exponent. In Fig. 25 we show the very same data set for $S_6(r)$ plotted against the measured values of $\langle|\delta v(r)^3|\rangle$: now we can identify a very clear scaling region and we can estimate the scaling exponent using four decades. Moreover, one can show in this case that $\zeta^*(6) = \zeta(6)$. In Fig. 26 we show $S_8(r)$ against $S_3(r)$ obtained with a numerical simulation at a rather low *Re* [62]:

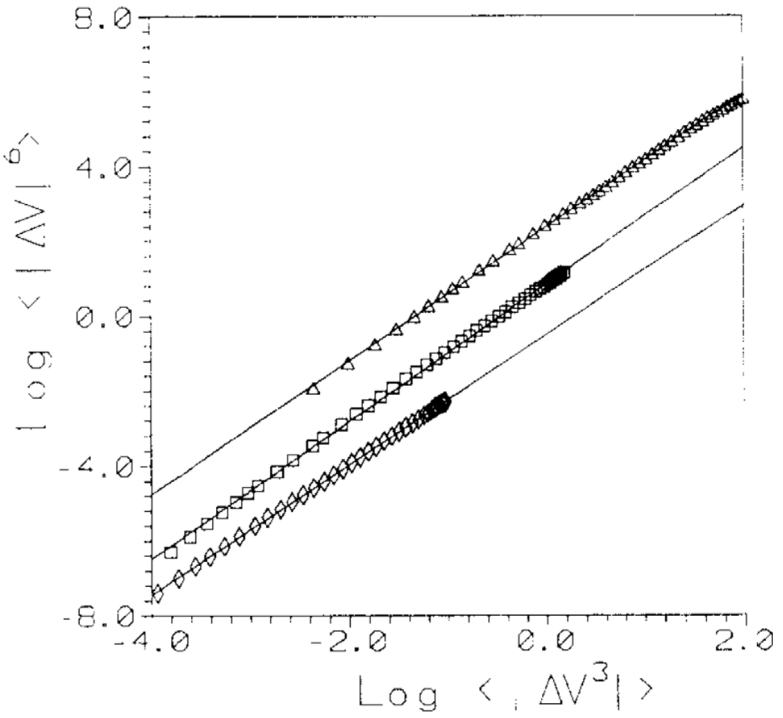

Fig. 25. Log–log plot of $S_6(r) = \langle \Delta V(r)^6 \rangle$ against $S_3(r) = \langle \Delta V(r)^3 \rangle$ for the experiments J, C18 and C6 (same symbols as Fig. 24. The solid line corresponds to a slope 1.78. In this figure the structure functions corresponding to J and C6 have been multiplied by 10 and 0.1, respectively.
Source: Figure reproduced from [60].

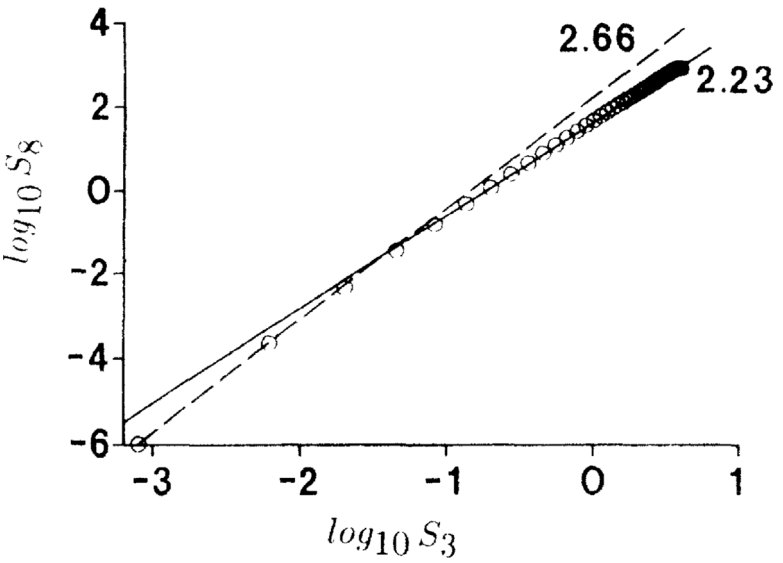

Fig. 26. Scaling of $S_8(r)$ versus $S_3(r)$ obtained with a numerical simulation at rather low *Re*. At small value of r, or equivalently of $S_3(r)$, we should observe the scaling 8/3 as indicated in the figure by the dashed line. At large r one clearly detects the anomalous scaling with exponents close to 2.23 shown by the continuous line.
Source: Figure reproduced from [62].

at small value of r, or equivalently of $S_3(r)$, we should observe the scaling 8/3 as shown in the figure by the dashed line. At large r we clearly detect the anomalous scaling with exponents close to 2.23 shown by the continuous line.

There has been extensive use of Eq. (129) in the literature to estimate the anomalous exponents from experimental data and numerical simulations. Eq. (129) has been named Extended Self Similarity (ESS). Using this method a systematic

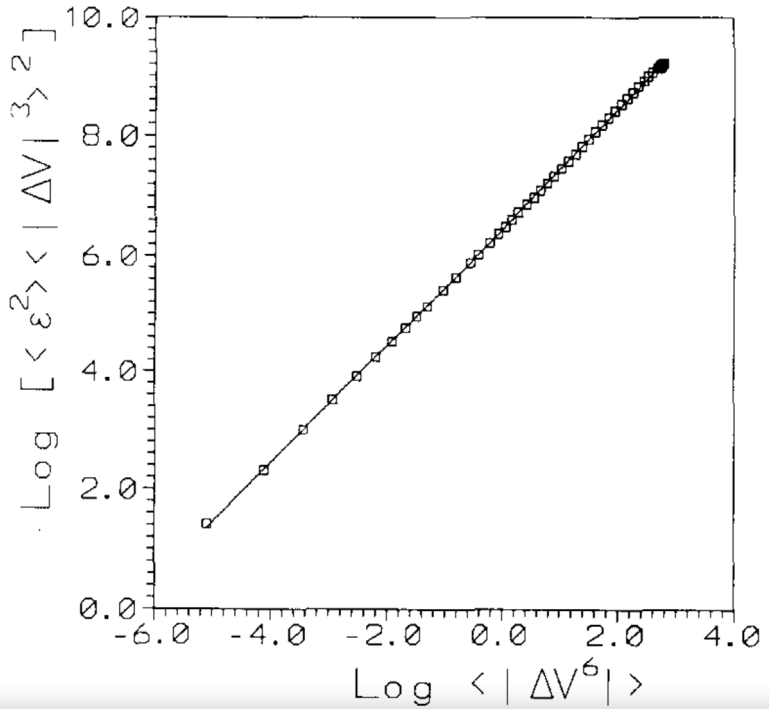

Fig. 27. Log–log plot of $\langle \varepsilon_r^2 \rangle \langle \Delta V(r)^3 \rangle^2$ against $\langle \Delta V(r)^6 \rangle$ using experimental data at $Re_\lambda = 450$. The straight line refers to the slope 1.005. *Source:* Figure reproduced from [60].

estimate of $\zeta(n)$ has been performed with Re_λ in the range [25 : 5000] [63]: the important result is that $\zeta(n)$ are independent of Re and are reported in Table 1. The relative error on $\zeta(n)$ is around a few percent and in most cases even below 1%. We remark two important points about (129): first of all, the anomalous scaling should break down for small enough r as shown in Fig. 24; secondly the use of (129) improves a lot at low Re when a clear region of scaling in r is not available and may not be extremely useful at large Re where a clear scaling is observed. Nevertheless, ESS enables us to solve our previous question: we can now state that $\zeta(n)$, being independent of Re, characterise the statistical properties of homogeneous and isotropic turbulence and the intermittency effect.

One can also improve the original form of RKSH using (129). In particular one can consider the following relation:

$$S_n(r) = \langle \epsilon(r)^{n/3} \rangle S_3(r)^{n/3} \tag{130}$$

In Fig. 27 we show the quality of the relation (130) for $n = 6$ which is extremely good (the slope is 1 with less the 1% accuracy. Therefore, the use of $S_3(r)$ instead of r improves both the estimate of the anomalous exponents and the validity of the RKSH.

The next question to answer is why there is anomalous scaling? From the table of the exponent $\zeta(n)$ we can already see that the β model cannot be correct for large n: the situation is more complex than the one described by the β model. Going back to the case of the Burgers' equation, we understand that the anomalous exponent, in this case, are $\zeta(n) = 1$ for $n \geq 1$. In the Burgers' case, anomalous exponents are dictated by the formation of shocks due to dissipative effects. In three dimensional turbulence, the situation seem to be more complex. Let us consider once again the kurtosis $K_4(r)$. At very small scales we expect $S_2(r) = G_2 r^2$ and $S_4(r) = G_4 r^4$ where $G_n \equiv \langle [\partial_x v]^n \rangle$. Using the relation (129) we can write

$$\frac{G_4}{G_2^2} = \lim_{r\to\eta} \frac{S_4(r)}{S_2(r)^2} = \lim_{r\to\eta} S_2(r)^{\zeta(4)/\zeta(2)-2} = [G_2 \eta^2]^{\zeta(4)/\zeta(2)-2} \sim Re^{0.08} \tag{131}$$

Using experimental data and numerical simulations [12] the observed behaviour is $G_4/G_2^2 \sim Re^{0.18}$: this result is definitively in contrast with the prediction (131). In other words, the anomalous exponents by themselves are not able to predict the statistical properties in the dissipation regions. This implies that we are not able to predict the statistical properties of the lagrangian acceleration. We need to improve our theoretical framework.

Lecture 3.6. Summary of Lecture 3

Let us try to summarise some of our findings in this lecture:

- there is a clear evidence of violations of the Kolmogorov scaling $\delta v(r) \sim r^{1/3}$; this implies that fully developed turbulence cannot be described by a *naive* scale invariant theory;
- deviations seem to be related to the formation of vortex tubes and/or to structures in the field of energy dissipation;
- a refined form of the Kolmogorov conjecture, the RKSH, seems to properly describe the turbulence fluctuation in the inertial range;
- it is not clear whether the correct description of the statistical properties of turbulence may be correctly understood in terms of the moments of probability distribution of $\delta v(r)$; however we do observe clear anomalous scaling in the form $S_n(r) \sim S_3(r)^{\zeta(n)}$ with $\zeta(n) \neq n/3$ for $n \neq 3$;
- we have quite good evidence that $\zeta(n)$ are universal, i.e. the anomalous exponents $\zeta(n)$ seem to be independent from *Re* and from the specific forcing mechanism;
- it is not clear how the anomalous exponents may eventually be related to the statistical properties in the dissipation range.
- it is unclear which is a possible theoretical framework able to explain why there exists anomalous exponents and why $\zeta(n)$ is a non linear function of n.

Lecture 4. Multifractal theory of turbulence

Lecture 4.1. The theory

This Lecture is one of the central conceptual points in this review: we introduce the theoretical framework known as *multifractal theory of turbulence*. Our starting point is the scaling transformation introduced in Lecture 2, namely

$$\mathbf{r} \to \lambda \mathbf{r} \tag{132}$$
$$\mathbf{v} \to \lambda^h \mathbf{v} \tag{133}$$
$$t \to \lambda^{h-1} t \tag{134}$$
$$\nu \to \lambda^{1+h} \nu \tag{135}$$
$$\epsilon \to \lambda^{3h-1} \epsilon \tag{136}$$

Although somehow abstract, using the above scale transformation we are able to obtain the Kolmogorov' conjecture assuming that ϵ is invariant with λ. This immediately gives $h = 1/3$ and the scaling $\delta v(r) \sim r^{1/3}$. Arguments like this, based on dimensional analysis can be extremely powerful or very dangerous if we do not understand the physics behind them. For Kolmogorov' theory, the physics is quite clear: ϵ represents the flux of energy from large to small scales (where it is dissipated). Then, for $\eta \ll r \ll L$, the statistical properties of the velocity fluctuations, as measured by $\delta v(r)$, should depend only on r and ϵ. Using dimensional analysis we obtain $\delta v(r) \sim r^{1/3}$. Now, let us suppose that the scale transformation (132)–(136) are still valid but in a broader sense. Somehow this is what we already did when we discuss the β model. In the β model we assumed that energy dissipation was an object of fractal dimension D. The concept of fractal dimensional is a geometrical concept. Looking at boxes of volume r^3, energy dissipation is defined on the subset of r^{-D} boxes out of r^{-3}. Thus the space average $\langle \epsilon(r) \rangle$ is proportional to $\epsilon(r) r^{3-D}$ where $\epsilon(r)$ is defined in Eq. (120). Then, from the zeroth law of turbulence, we have $\epsilon(r) r^{3-D} \sim const$. Finally using the Refined Kolmogorov Similarity Hypothesis we obtained the scaling of the structure functions with exponents $\zeta(n) = n(D-2)/3 + (3-D)$. In other words, we can look at the β model in the following way: we require scale invariance as expressed by Eqs. (132)–(136) supplemented by a *space average* procedure $\langle \dots \rangle$ which obeys the transformation

$$\langle \dots \rangle \to \lambda^{3-D} \tag{137}$$

D is the fractal dimension. Then the value of h is fixed by the zeroth law of turbulence $\langle \epsilon \rangle$ independent of λ.

Now, the basic idea is to generalise the above procedure and the concept of average as follows: let us suppose that there exists a range of exponents h and that the scaling transformation is valid with probability P_h. For $\delta v(r) \to \lambda^h \delta v(r)$ the scaling (133) holds with probability $P_h[\lambda]$. This is equivalent to saying that the scaling $\delta v(r) \sim r^h$ is true with probability $P_h[r]$. Notice that we use $\delta v(r)$ instead of Eq. (133) because we want to discuss the statistical properties of the velocity fluctuations which are obtained, for homogeneous and isotropic turbulence, from $\delta v(r)$. Next, we require that $P_h[r] \sim r^{3-D(h)}$. It follows that the scaling of the structure functions is given by:

$$\langle [\delta v(r)]^n \rangle \sim \int dh r^{nh+3-D(h)} \tag{138}$$

Since r is supposed to be small, we can perform the integral using the saddle point method and we obtain

$$\langle [\delta v(r)]^n \rangle \sim \int dh r^{nh+3-D(h)} = r^{\zeta(n)} \quad ; \zeta(n) = inf_h[nh + 3 - D(h)] \tag{139}$$

If we know $D(h)$ we can compute the anomalous exponent $\zeta(n)$. The zero law of turbulence and the 4/5 Kolmogorov' equation implies that $\zeta(3) = 1$ which is a constrain on $D(h)$. Eq. (139) is the starting point of the multifractal framework of turbulence [65,66].

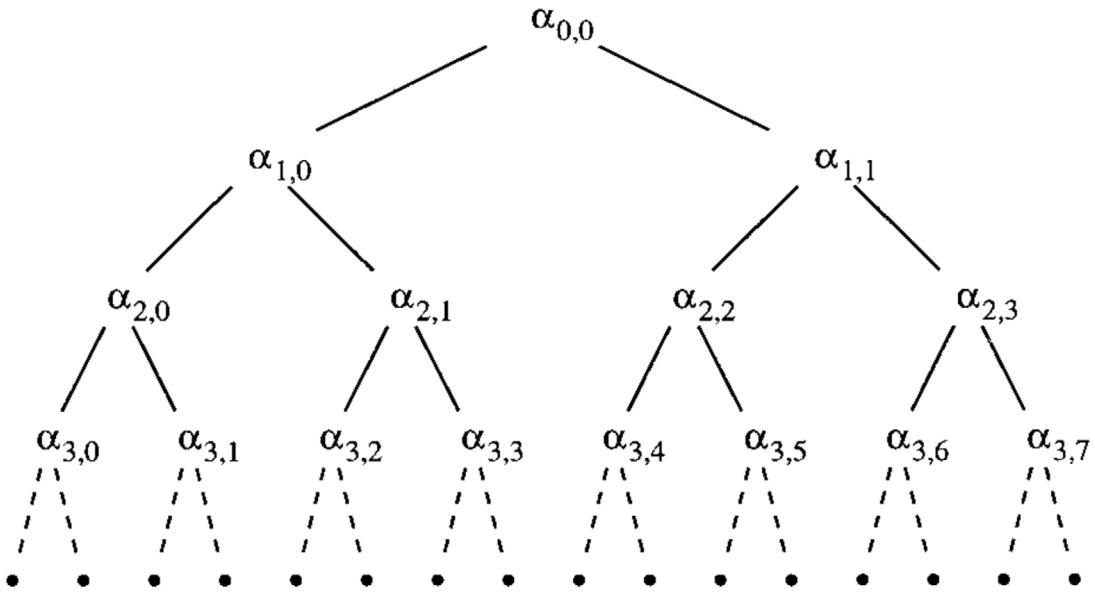

Fig. 28. Graphical representation of the dyadic cascade process for the $\alpha_{j,k}$ coefficients, where j is the level index and k is the position index of the corresponding wavelet.
Source: Reproduced from [64].

As it is written in Eq. (138), the multifractal formulation is rather obscure. We do not know $D(h)$ and we do not know the range of values of possible exponents h (i.e. the limit of the integral in (138). Our assumption is that there exists a function $D(h)$ and that the probability distribution $P_h[r]$ is itself a scaling function of r. At first sight, taking advantage of the previous discussion on the β model, we can think of $D(h)$ as a set of fractal dimensions. It is not clear, however, what are the geometrical properties we are looking at. Let us remark that relation Eq. (136) implies:

$$\epsilon(r) \sim \frac{\delta v(r)^3}{r} \quad with \;\; probability \;\; P_h[r] \tag{140}$$

From the above equation we can derive the validity of the RKSH, i.e.

$$\langle \epsilon^n(r) \rangle \sim \int dh r^{n(3h-1)+3-D(h)} = r^{\zeta(3n)-n} \sim \frac{S_{3n}}{r^n} \tag{141}$$

So far everything is abstract and we should now disentangle the physics from the formalism. To do that we want to answer a few questions, namely: (1) can we say something general on $D(h)$? (2) knowing $\zeta(n)$ can we compute $D(h)$? (3) are we able to build space dependent field showing multifractal behaviour given by (139)? After these initial questions, we need to understand whether or not the multifractal approach has any predictive value and/or whether it can explain the strong intermittency due to dissipative effects. This point is clearly more demanding and it can be investigated once we understand the physical meaning of the multifractal framework.

Lecture 4.2. From $\zeta(n)$ to $D(h)$

We start with the simplest question: knowing $\zeta(n)$ can we obtain $D(h)$? Using Eq. (139) we can compute the solution of the equation

$$\inf_h [nh + 3 - D(h)] \quad or \quad n - \frac{dD}{dh} = 0 \tag{142}$$

Let us call $h(n)$ the solution of (142). Then we have $\zeta(n) = nh(n) + 3 - D(h(n))$. Now we compute

$$\frac{d\zeta(n)}{dn} = n\frac{dh}{dn} + h(n) - \frac{dD}{dh}\frac{dh}{dn} = h(n) \tag{143}$$

Thus from this equation we can compute, in principle, the function $n = n(h)$. Next from (139) we have:

$$D(h) = n(h)h + 3 - \zeta(n(h)) \tag{144}$$

which is the result that we were looking for. Obviously the difficult part is to compute the function $n(h)$. For any practical purpose, one usually performs a fit on the exponents $\zeta(n)$ (the simplest one) and then compute $D(h)$ using (144). The other relevant information about $D(h)$ is that $D(h)$ should be a concave function of h, as it is $\zeta(n)$ with respect to n.

Lecture 4.3. The log-normal case

We now provide a very simple example to build up something similar to a multifractal behaviour [56]. This example should be considered as an exercise to understand some more physics from the formal definition. A very simple way to build up a multifractal behaviour is the following: let us consider a one-dimensional cut of the three-dimensional field associated with energy dissipation. Let L be the size of the signal and let us divide it in smaller pieces of length $l_m = 2^{-m}L$. The smallest scale available in space is denoted by l_N. We can construct a dyadic tree, see Fig. 28, with *leaves* of size l_m. For each l_m we have 2^m leaves of size l_m. We denote the position in the level by the index $i = 1, \ldots, 2^m$. Let $\epsilon_i(l_m)$ denote the *local* average of the energy dissipation at position i and level m. We now build the model in the following way: going from the level $m = 0$ (i.e. at scale L) down to the level m at scale l_m we consider one of the many possible path on the dyadic tree and, once chosen the path, we neglect for the time being the position i in each level. Along the path we can write the following equality:

$$\epsilon(l_m) = \frac{\epsilon(l_m)}{\epsilon(l_{m-1})} \ldots \frac{\epsilon(L/2)}{\epsilon(L)} \epsilon(L) \tag{145}$$

We assume $\epsilon(L)$ to be constant and, from dimensional analysis, equal to U^3/L. This assumption is equivalent to considering the limit $L \to \infty$ with $\epsilon(L)$ constant. Let us define $R_m = \epsilon(l_m)/\epsilon(l_{m-1})$ so that $\epsilon(l_m) = \Pi_{k=1,\ldots,m} R_k \epsilon(L)$. We now assume that R_k are uncorrelated random variables with $\langle R_p R_m \rangle = 0$ for $p \neq m$. This is a rather strong assumption that characterises our simplified model and we will discuss this point later on. Next, we can formally write

$$\Pi_k R_k = \exp\left[\sum_k \log(R_k)\right] = \exp\left[m\left(\frac{1}{m}\sum_k \log(R_k)\right)\right] = \exp[m\xi(m)] \tag{146}$$

$$\xi(m) = \frac{1}{m}\sum_k \log(R_k) \tag{147}$$

The quantity $\xi(m)$ is the sum of independent random variables and we can use the central limit theorem to compute the probability distribution of $\xi(m)$. The theorem tells us that $\xi(m)$ converges for large enough m to a gaussian distribution, i.e.

$$P[\xi(m)] \sim \exp\left[-\frac{m(\xi(m)-\mu)^2}{2\sigma^2}\right] \tag{148}$$

Let us recall that we are looking at a specific path on the dyadic tree. For this specific path, $\xi(m)$ is just a realisation of the probability distribution $P[\xi(m)]$. Next, it is reasonable to assume that the average over all possible paths and along the space position at the level m is equivalent to the average over the probability distribution of $\xi(m)$. Using the variable $\xi(m)$, Eq. (145) and the RKSH we can write

$$\delta v(l_m) = U\left[\frac{l_m}{L}\right]^{1/3} \exp\left[\frac{m\xi(m)}{3}\right] \tag{149}$$

Then, to compute the structure function $S_n(l_m) = \langle \delta v(l_m)^n \rangle$, we need to compute the average over $\xi(m)$. Since the integral are gaussian, this is a simple computation and we obtain:

$$S_n(l_m) \sim U^n \left[\frac{l_m}{L}\right]^{n/3} \exp\left\{m\left[\frac{n}{3}\mu + \frac{n^2\sigma^2}{18}\right]\right\} \tag{150}$$

Finally we require that $S_3(l_m) \sim l_m$ because of the 4/5 law. This implies that μ and σ^2 are not independent. This is the only point where we are using some information from the N.S. equations and in particular the Kolmogorov' equation. It is easy to see that the constrain with the 4/5 law implies $\mu = -\sigma^2/2$. Then, Eq. (150) becomes:

$$S_n(l_m) \sim U^n \left[\frac{l_m}{L}\right]^{n/3} \exp\left[m\frac{\sigma^2}{6}\left(\frac{n^2}{3} - n\right)\right] \tag{151}$$

Since $2^{-m} = l_m/L$, we can rewrite (151) in the form:

$$S_n(l_m) \sim U^n \left[\frac{l_m}{L}\right]^{\zeta(n)} \tag{152}$$

$$\zeta(n) = \frac{n}{3} + bn\left(1 - \frac{n}{3}\right) \tag{153}$$

with $b = \sigma^2/(6\log(2))$. In the region $n \in [2:4]$, Eq. (153) provides a reasonable fit with the experimental/numerical results with $b = 0.045$ a quite small deviation (as it should) from the Kolmogorov' scaling $n/3$. Expression (153) was first introduced by Kolmogorov himself. However, (153) fails to match the estimated values of the anomalous exponents

at large enough n. Before discussing the validity of (153) let us compute from it the quantity $3 - D(h)$. Introducing $h_0 = 1/3 + b$, we can write $\zeta(n) = nh_0 - bn^2/3$. For each n, we can compute the value $h(n)$ which solves Eq. (142):

$$h(n) = h_0 - \frac{2b}{3}n \rightarrow n = \frac{3}{2b}(h_0 - h) \tag{154}$$

Next we can compute $3 - D(h)$ by the knowledge of $\zeta(n)$:

$$3 - D(h) = \zeta(n) - nh = \frac{3}{2b}(h_0 - h)^2 - \frac{b}{3}\left[\frac{9}{4b^2}\right](h - h_0)^2 = \frac{3}{4b}(h - h_0)^2 \tag{155}$$

The model leading to (153) is often referred to as *log-normal model* of intermittency. The reason for this name can be understood by looking at the probability distribution of the variable $z(l_m) \equiv \epsilon(l_m)/\epsilon(L)$. Using (148) we have:

$$P[z(l_m)] \sim \frac{1}{z(l_m)} \exp\left[-\frac{(\log(z(l_m)) - m\mu)^2}{2\sigma^2 m}\right] \tag{156}$$

From (156) we see that, as we know, the variable $\log(z(l_m))$ is gaussian and this gives the name log-normal to the model. Looking at the probability distribution of $z(l_m)$, we can easily compute the moments. In particular, we already know that $\langle z(l_m)\rangle = 1$ because $\mu = -\sigma^2/2$ or equivalently $\zeta(3) = 1$. It is more interesting to compute the most probable value z_{mp} of $z(l_m)$. This value can be computed by looking at the maximum of $P[z(l_m)]$. It is easy to show that:

$$z_{mp} = \exp(-m\sigma^2) = \left[\frac{l_m}{L}\right]^{6b} \tag{157}$$

Thus at small l_m, $z_{mp} \ll \langle z\rangle = 1$. This can be interpreted by saying that in most cases $z(l_m)$ acquires a rather small value whereas in a few cases it becomes extremely large. This is the hallmark of any intermittent behaviour in physics.

We construct the random multiplicative process (145) and (146)–(147) on a dyadic tree. This geometrical feature is fundamental to providing non-trivial space correlations in the field of energy dissipation. At the smallest scale, l_N the rate of energy dissipation ϵ depends on the space position i, hereafter denoted by x_i with $l_N \equiv x_{i+1} - x_i$. Let us now consider the quantity $\epsilon(x_i + r)\epsilon(x_i)$ and let s be defined as $r = 2^{-s}L$. Then between $\epsilon(x_i)$ and $\epsilon(x_i + r)$ there are s *ancestor* in common with R_k and $N - s$ different values of the independent random variables R_k. Thus we can write

$$\epsilon(x_i)\epsilon(x_i + r) = [\Pi_{k=1,s}R_k]^2[\Pi_{j=s,s+1,\ldots,N}R_j][\Pi_{l=s,s+1,\ldots,N}R_l]\epsilon(L)^2 \tag{158}$$

Upon averaging over x_i and in the limit of large L we obtain

$$C(r) \equiv \frac{\langle\epsilon(x_i)\epsilon(x_i + r)\rangle}{\epsilon(L)^2} = \langle R^2\rangle^s \langle R\rangle^{2(N-s)} \tag{159}$$

Because $\langle R\rangle = 1$ by construction, we obtain

$$C(r) \sim \langle R^2\rangle^s = \left[\frac{l_s}{L}\right]^{\zeta(6)-2} \tag{160}$$

in agreement with the RKSH (note that we use (151)–(153)). Eq. (160) is true no matter the detail of the probability distribution $\xi(m)$ previously discussed: it can be derived from the specific dyadic tree of the random multiplicative process and from the statistical independence of the random variables R_k. Eq. (160) tells us that there is a well defined long-range correlation of the energy dissipation field. This is a feature embedded in the multifractal framework which is formulated in agreement with the RKSH. In the log-normal model of intermittency, the one leading to (153), the dyadic tree is the geometrical framework behind the multifractal statistics which is one possible, but not unique, way to obtain long range correlation in the energy dissipation field. We emphasise the fact that this is a general feature of the multifractal framework not necessarily due to the particular choice of a dyadic tree and a random multiplicative process.

Lecture 4.4. Constrain in $D(h)$ and $\zeta(n)$

Let us now come back to the specific form of $D(h)$ we obtain for the log-normal model: $D(h)$ is a parabola with negative curvature whose maximum value is 3 for $h = h_0$. It is interesting to look at $h(n)$ for different n: $h(2) = 0.318$, $h(3) = 0.288$ and $\zeta(4) = 0.258$. By increasing n the value of $h(n)$ decreases linearly and eventually becomes negative. A negative value of $h(n)$ implies that for large enough n we should have, for example, $\zeta(2n + 2) < \zeta(2n)$, i.e. the anomalous exponents $\zeta(n)$ decrease with n. Then, following [12], let us define $U_{\max}$ the maximum velocity of a turbulent flow. By definition we should have $\langle|\delta v(r)|\rangle \leq 2U_{\max}$. From this expression, it follows that

$$S_{2n+2}(r) \leq 4U_{\max}^2 S_{2n}(r) \tag{161}$$

As we know, we can write the structure-function $S_n(r) = A_n U^n (r/L)^{\zeta(n)}$, where U is the root mean square velocity of the flow at Reynolds number $Re = UL/\nu$ and A_n is a constant independent of Re. Then, using (161) we have:

$$\frac{U_{\max}^2}{U^2} \geq \frac{1}{4}\frac{A_{2n+2}}{A_{2n}}\left[\frac{r}{L}\right]^{\zeta(2n+2)-\zeta(2n)} \tag{162}$$

If $\zeta(2n+2) < \zeta(2n)$, then from (162) we have $U_{\max} \to \infty$ in the limit $r \to 0$. Moreover, from a physical point of view, denoting with c_s the sound speed of the fluid, Eq. (162) implies that the Mach number $U_{\max}/c_s$ becomes bigger for small enough r/L which violates the incompressibility requirement assumed in all our investigations. This argument, originally due to Frisch [12], shows that for the N.S. equation we expect $\zeta(n)$ to be a concave non-decreasing function of n which rules out the results (153).

Lecture 4.5. Multifractal and large deviations

The previous discussion suggests the obvious question: "where is the mistake in deriving the log-normal model"? To obtain the log-normal model we use three different pieces of information: a) the definition of the energy dissipation on a dyadic tree; b) the assumption that the variables R_k are independent random variables and (c) the central limit theorem to derive the log-normal probability distribution. Points (b) and (c) seem to be the most delicate ones. In particular, let us consider again the quantity $\xi(m)$ whose probability distribution was approximated to a gaussian in the limit $m \to \infty$. The central limit theorem is valid for *small* fluctuations of $\xi(m)$ around its mean value μ. More generally, due to the *large deviation theory* (see for example [67]), it is possible to show that the probability distribution $P[\xi(m)]$ is given by

$$P[\xi(m)] \sim \exp[-mW(\xi(m)-\mu)] \tag{163}$$

where the function $W(x)$ is a convex function with a minimum in $\xi(m) = \mu$. If we approximate $W(x)$ with a parabola we recover the central limit theorem. However, this approximation is not valid when $|\xi(m) - \mu|$ is large.

Eq. (163) can be rewritten in our case as:

$$P[\xi(m)] \sim \left[\frac{l_m}{L}\right]^{W(\xi(m)-\mu)/\log(2)} \tag{164}$$

Upon defining $h = 1/3 - \xi(m)/\log(2)$ and $3 - D(h) = W(\xi(m) - \mu)/\log(2)$ and using (149), we can finally write:

$$\delta v(l_m) \sim \left[\frac{l_m}{L}\right]^h \quad \textit{with probability } P_h[l_m/L] \sim \left[\frac{l_m}{L}\right]^{3-D(h)} \tag{165}$$

which is exactly the multifractal formulation (see [68] for the formulation at different times).

The above discussion implies that the multifractal framework may be interpreted as large deviation estimate for the probability distribution of $\delta v(r)$. This is certainly true if we assume that the multifractal is obtained by a random multiplicative process but its original formulation is not restricted to this particular case. At any rate, from the point of view of large deviations, the exponent h appearing in the statement $\delta v(r) \sim r^h$ does not imply any form of *local* (in space or time) scaling law which can be eventually observed in a turbulent flow. This also implies that given two scales $r_1 < r_2$ the most general formulation of the multifractal is given by the relation:

$$\delta v(r_1) \sim \left[\frac{r_1}{r_2}\right]^h \delta v(r_2) \quad \textit{with probability } P_h[r_1/r_2] \sim \left[\frac{r_1}{r_2}\right]^{3-D(h)} \tag{166}$$

Eq. (166) gives the probability distribution of $\delta v(r_1)$ conditioned to $\delta v(r_2)$.

As we noticed we must require $\zeta(2n+2) \geq \zeta(2n)$. Since $\zeta(n)$ is a concave function of n, for $n \to \infty$ the anomalous exponents $\zeta(n)$ should behave asymptotically as $h_0 n + 3 - D_0$ where $h_0 \geq 0$ is the smallest possible value of h and $D_0 = D(h_0)$. This behaviour does correspond to a *local* (in space) scaling of $\delta v(r)$ and it is related to the most singular value of the velocity difference $\delta v(r)$, i.e. h_0 refers to some *structure* in the flow. Using this observation and assuming that vortex filaments or tubes are responsible for h_0 plus other assumptions and information from numerical simulations, She and Lévêque [69] obtained the following estimate for the anomalous exponents

$$\zeta(n) = nh_0 + d_0[1 - \beta^{n/3}] \tag{167}$$

with $d_0 = 3 - D(h_0) = 2$, $h_0 = 1/9$ and $\beta = 2/3$. Eq. (167) is a very good approximation to the observed numerical/experimental values of the anomalous exponents and, hereafter, we assume (167) as a possible best fit of the observed anomalous exponents, $\zeta(n)$. Using Eq. (167) one can compute the corresponding function $D(h)$. After some algebra we obtain:

$$D(h) = d_0 Z(h) + 3 - d_0 - d_0 Z(h)\log[Z(h)]; \quad Z(h) \equiv \frac{h - h_0}{d_0[\log(\beta^{-1/3})]} \tag{168}$$

Expression (167) can also be derived if we assume that the random multiplicative process in (146) are log-Poisson distributed, i.e the probability distribution of $\log(R_k)$ is a Poisson distribution. For this case, one can compute exactly the function $W(x)$ appearing in the large deviation estimate (163) and the probability distribution of $\xi(m)$ is again a Poisson distribution.

Lecture 4.6. Multifractal fields

Using a random multiplicative process, we can provide examples of a synthetic turbulent signal which satisfies the multifractal scaling [70]. As before we consider a dyadic tree. Without lack of generality, we assume $L = 1$ and $\epsilon(L) = 1$. Now we label the level by j and the leaves in the level by $k = 1 \dots 2^j$. Next, we consider the function

$$\psi(x) = -\frac{d^2}{dx^2} \exp\left[-\frac{x^2}{2\sigma^2}\right] \tag{169}$$

with $\sigma \ll L$. The function $\psi(x)$ has zero average in x. Using $\psi(x)$ we define for each level j and leave k the functions

$$\psi_{j,k}(x) \equiv 2^{j/2}\psi(2^j x - k) \tag{170}$$

The function $\psi_{j,k}(x)$ is different from zero on an interval of size 2^{-j} near the point $2^{-j}k$ and it is a simple way to obtain a function which has almost compact support in each leave of our dyadic tree. Moreover, it is possible to show that:

$$\int dx\, \psi_{j,k}(x)\psi_{p,q}(x) = \delta_{jp}\delta_{kq} \tag{171}$$

i.e. the functions $\psi_{j,k}(x)$ form an orthonormal basis on the dyadic tree and it represent a local *in space and in scale* representation of the signal. There are several kinds of functions able to satisfy the above requirements and they are referred to as *wavelets* [71].

Next, we consider the following signal:

$$\Phi(x) = \Sigma_j \Sigma_k \alpha(j,k)\psi_{j,k}(x) \tag{172}$$

where the number $\alpha(j,k)$ are random variables defined on the nodes of the tree. Choosing $\alpha(0,0) = 1$ we set:

$$\begin{aligned} &\alpha(1,0) = A(1,0)\eta(1,0)\alpha(0,0) \;\; ; \alpha(1,1) = A(1,1)\eta(1,1)\alpha(0,0) \\ &\alpha(2,0) = A(2,0)\eta(2,0)\alpha(1,0) \;\; ; \alpha(2,1) = A(2,1)\eta(2,1)\alpha(1,0) \end{aligned} \tag{173}$$

and so on, where $A(i,j)$ are random variables with values ± 1 equally distributed and $\eta(j,k)$ are independent random variables taken from a given probability distribution $P[\eta]$. The scaling properties of our signal $\Phi(x)$ can now be computed upon averaging in space or, equivalently, on the probability distribution $P[\eta]$ and averaging over $A(j,k)$. For the second order structure functions we have:

$$S_2(r) \equiv \langle \left[\Sigma_{j,k}\alpha(j,k)2^{j/2}[\psi(2^j x + 2^j r - k) - \psi(2^j x - k)]\right]^2 \rangle \tag{174}$$

$$= \Sigma_{jk}\langle \alpha(j,k)^2 \rangle 2^j \langle \left[\psi(2^j x + 2^j r - k) - \psi(2^j x - k)\right]^2 \rangle \tag{175}$$

Next we define

$$\langle \left[\psi(2^j x + 2^j r - k) - \psi(2^j x - k)\right]^2 \rangle = 2^{-j} G_2(r) \tag{176}$$

and we obtain:

$$S_2(r) = \Sigma_j \langle \alpha(j,k)^2 \rangle 2^j G_2(2^j r) \tag{177}$$

Notice that the factor 2^{-j} in (176) does not appear in (177) because of the sum in k: upon averaging the factors are independent of k and the sum in k is a multiplication by a factor 2^j. Using (177) we obtain:

$$\begin{aligned} S_2(2r) &= \Sigma_j \langle \alpha(j,k)^2 \rangle 2^j G_2(2^{j+1} r) = \Sigma_j 2^{j[\log_2\langle \eta^2\rangle + 1]} G_2(2^{j+1} r) \\ &= 2^{-[\log_2\langle \eta^2\rangle + 1]} \Sigma_j 2^{(j+1)[\log_2\langle \eta^2\rangle + 1]} G_2(2^{j+1} r) \\ &= 2^{-[\log_2\langle \eta^2\rangle + 1]} S_2(r) \end{aligned} \tag{178}$$

Eq. (178) can be generalised for any structure functions showing that $\Phi(x)$ exhibits a multifractal scaling with anomalous exponents expressed in terms of the probability distribution of η:

$$\zeta(n) = -\frac{n}{2} - \log_2\langle \eta^n \rangle \tag{179}$$

A snapshot of the field $\Phi(x)$ is shown in Fig. 29.

Almost the same procedure can be used to generate a synthetic one-dimensional signal for the rate of energy dissipation $\epsilon(x)$ [64]. In this case, we use the functions

$$\psi_{j,k}(x) = 2^j \psi(2^j x - k); \qquad \psi(x) = \exp\left[-\frac{(x - 1/2)^2}{2\sigma^2}\right] \tag{180}$$

where $x \in [0:1]$ and $\sigma \ll 1$. Note that the functions $\psi_{j,k}(x)$ are no longer orthogonal. Then we define $\Phi(x)$ as in (172) and (173) with two important differences: the variables $A(j,k)$ are taken constants and equal to 1 so that $\Phi(x)$ is positive

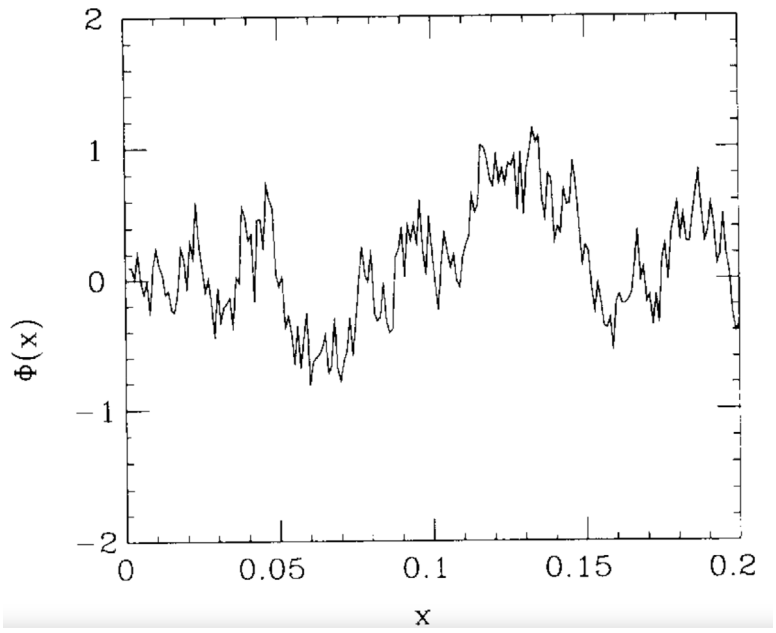

Fig. 29. A typical realisation of the multiaffine signal. The multiplicators assume two values: $2^{-5/6}$ with probability 0.875 and $2^{-1/2}$ with probability 0.125.
Source: Reproduced from [70].

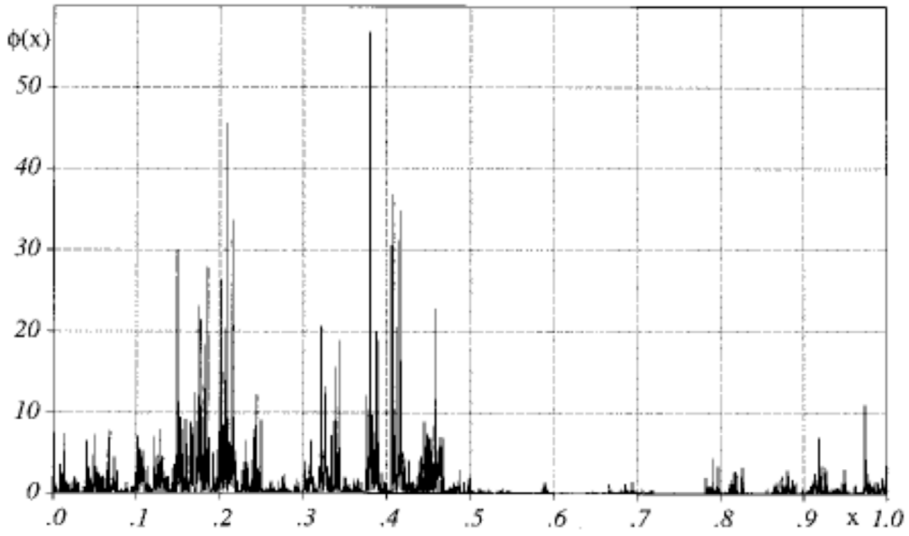

Fig. 30. A typical example of synthetic signal $\phi(x)$ generated in $x \in [0, 1]$ with the one-dimensional model and log-Poisson generator with parameters $\beta = 0.4$ and $c = 0.5$. The integral of the signal from 0 to 1 is equal to unity.
Source: Figure reproduced from [64].

defined; we require that $\int dx\Phi(x) = const \equiv C_0$. The latter constrain implies that $\alpha(0, 0)$ is given by:

$$\alpha(0,0) = \frac{C_0}{\Sigma_j 2^j \langle \eta \rangle^j} \tag{181}$$

Notice that to obtain a signal $\Phi(x)$ consistent with the observed features of the statistical properties of the energy dissipation $\epsilon(r)$, we must choose the probability distribution $P[\eta]$ in a proper way, i.e. we need to use a definition of $P[\eta]$ different from the one used for the velocity signal in (173). In Fig. 30 we show an example of $\Phi(x)$ defined by the above procedure (see Fig. 31).

We think that the possibility to build, at least in one dimension, explicit examples of a multifractal field is relevant for many reasons. The procedure is relatively easy to perform and does not require much computational power. Thus it can be used to test the statistical analysis performed on real data and provide a possible way to obtain well-defined error bars on the estimate of the scaling exponents. It can also be used to investigate the probability of *extreme events* either in the velocity difference and in the energy dissipation and eventually to perform a comparison with numerical/experimental data.

So far we have investigated the statistical and physical meaning of the multifractal theoretical framework. We want to understand whether, using the multifractal approach, we can provide any possible prediction on the observed intermittency fluctuations of homogeneous and isotropic turbulence. We assume to know $D(h)$ which can be obtained by the knowledge of $\zeta(n)$. We expect that within the scaling region where $S_n(r) \sim r^{\zeta(n)}$ the knowledge of $D(h)$ is enough to compute the probability distribution of $P[\delta v(r)]$. To see how this can be done, we use (166) with $r_1 = r$ and $r_2 = L$ where L is the largest scale in the system. We know that for homogeneous and isotropic turbulence, the velocity fluctuations $\delta v(L)$ are well approximated by a gaussian distribution:

$$P[\delta v(L)] \sim \exp\left[-\frac{\delta v(L)^2}{2\sigma^2}\right] \tag{182}$$

Then, using (166) we obtain [72]:

$$P[\delta v(r)] \sim \int dh \left[\frac{r}{L}\right]^{3-D(h)-1} \exp\left[-\frac{\delta v(r)^2}{2\sigma^2 (r/L)^{2h}}\right] \tag{183}$$

Eq. (183) shows that $P[\delta v(r)]$ is the superposition of gaussian probabilities distributions with different variance $2\sigma^2(r/L)^{2h}$. The overall effect is displayed in Fig. 31. In the figure we consider $l_n = 2^{-n}L$, with $L = 1$, and $v_n \equiv \delta v(l_n)$: going from large to small scales the probability distribution develops a higher tail (large values are more probable) which is the signature of intermittency. Notice that everything goes as if the probability distribution $P[\delta v(r)]$ exhibits a stretched exponential form, although from (183) this is not the correct interpretation.

Lecture 4.7. The dissipation range

Now we must face the most complicated issue, namely understanding how the multifractal approach is consistent with the observed statistical features near to the dissipation range, i.e. near the Kolmogorov scale. In the original Kolmogorov theory, the dissipation scales or Kolmogorov scale η can be obtained in several ways and, in particular, by saying that the Reynolds number $\delta v(r)r/\nu$ corresponding to fluctuations $\delta v(r)$ is order 1 at $r = \eta$. Using $\delta v(r) = (r/L)^{1/3}\delta v(L)$, we obtain for the Kolmogorov theory

$$\left[\frac{r}{L}\right]^{4/3} L\delta v(L) \sim \nu \to \frac{\eta}{L} \sim Re^{-3/4} \tag{184}$$

where we define $Re = \delta V(L)L/\nu$. We want to employ the same definition with the multifractal approach. However, in this case, the fluctuations $\delta v(r)$ depend on h. Thus our condition becomes [73]:

$$\left[\frac{r}{L}\right]^{h+1} L\delta v(L) \sim \nu \to \frac{\eta}{L} \sim Re^{-\frac{1}{1+h}} \tag{185}$$

Eq. (185) holds with probability

$$P_h[Re] \sim \left[\frac{\eta}{L}\right]^{3-D(h)} \sim Re^{-\frac{3-D(h)}{1+h}} \tag{186}$$

We discover that there are a number of dissipative scales each one depending on the value of h. Thus we write $\eta(h)$ to highlight this fact. Moreover, we discover that each of the different dissipative scales enters in the statistical properties of the velocity fluctuations with a probability depending on the Re number. This is a quite complicated scenario that deserves a deeper investigation.

The first thing we need to check is whether (185) and (186) are consistent with the zeroth law of turbulence. This implies that the average gradient square should be proportional to Re. Using the above definitions we obtain:

$$\langle(\nabla v)^2\rangle \sim \int dh \left[\frac{\delta v(\eta(h))^2}{\eta(h)^2}\right]\left[\frac{\eta(h)}{L}\right]^{3-D(h)} \sim \frac{U^2}{L^2}\int dh Re^{-\frac{2h-2}{1+h}} Re^{-\frac{3-D(h)}{1+h}} \tag{187}$$

where $U^2 \equiv \langle \delta v(L)^2\rangle$. To obtain the final result we need to look at the minimum value of the quantity $[2h - 2 + 3 - D(h)]/(1 + h)$. This leads to the equation for $h = h_*$ given by

$$1 + D(h_*) - (1 + h_*)\frac{dD}{dh} = 0 \tag{188}$$

Let h_3 be the value of h corresponding to the scaling exponent $\zeta(3)$. This implies that $3 = dD/dh$ at $h = h_3$ and $3h_3 + 3 - D(h_3) = 1$. It is easy to show that $h_* = h_3$ is a solution of Eq. (188). Finally, we obtain:

$$-\frac{2h_3 - 2 + 3 - D(h_3)}{1 + h_3} = -\frac{3h_3 - 2 + 3 - D(h_3) - h_3}{1 + h_3} = -\frac{-1 - h_3}{1 + h_3} = 1 \tag{189}$$

Thus using definitions (185) and (186) we are able to recover the zero law of turbulence. Note that the only assumption we use is $\zeta(3) = 1$ which is an exact value independent of the specific functional form of $D(h)$. It seems that we are on a good way in our investigations.

We can go on and we can compute the dependence on Re for all the moments of the gradients [72]. This can be done by computing the quantities:

$$\langle (\nabla v)^q \rangle \sim \frac{U^q}{L^q} \int dh Re^{-\frac{qh-q}{1+h}} Re^{-\frac{3-D(h)}{1+h}} \tag{190}$$

Now the integration over h is more complicated. Let us define:

$$\xi(q) \equiv Sup_h \left[-\frac{qh - q + 3 - D(h)}{1+h} \right] \tag{191}$$

The equation we need to solve is now:

$$2q - (1+h)\frac{dD}{dh} - 3 + D = 0 \tag{192}$$

To solve this equation we use the following trick [12]: we assume that the solution is given by $h = h_p$ where h_p is the value of h corresponding to the exponents $\zeta(p)$. Thus $p = dD/dh$ and $\zeta(p) = ph_p + 3 - D(h_p)$. Using this idea, we rewrite the r.h.s of (192) in the form $2q - (1-h_p)p - 3 + D(h_p) = 2q - p - \zeta(p)$. Then Eq. (192) can be used to write

$$q = \frac{p + \zeta(p)}{2} \tag{193}$$

Finally, we compute $\xi(q)$ from (191) and we obtain:

$$\xi(q) = -\frac{qh_p - q + 3 - D(h_p)}{1+h_p} = -\frac{q(1+h_p) - 2q + 3 - D(h_p)}{1+h_p} = -q + p = \frac{p - \zeta(p)}{2} \tag{194}$$

Although it looks a little complex, expression (193) and (194) provides us the information we need in terms of the scaling exponents $\zeta(n)$. For instance, we obtain $\xi(4) \sim 2.18$ which implies that the kurtosis of the gradients goes as $Re^{0.18}$, i.e. it increases faster than the prediction based by extrapolating the kurtosis from the inertial range down to the Kolmogorov scale (see previous lecture). This is consistent with the observation that close to the dissipation range, intermittency seems to grow faster than what we can naively predict by the scaling exponents. We are now able to understand why this happens: Eq. (185) tells us that large fluctuations (with relatively small h) dissipate at relatively small scales with respect to relatively small fluctuation which dissipates at a larger scale. The fluctuations of the dissipation scale are responsible of the increased intermittency in the dissipation range. The fluctuations of the dissipation scale are *predicted* by the knowledge of $D(h)$ through Eq. (186). Thus the knowledge of the scaling exponents $\zeta(n)$ is enough to predict or compute the most intermittent fluctuations in the dissipative range.

We are now able to compute the probability distribution of the velocity gradients $s \equiv \delta v(\eta(h))/\eta(h)$. Using $U = L = 1$ and performing the same computation as before, after some simple algebraic work, we obtain:

$$P[s] \sim \int dh \left[\frac{\nu}{s}\right]^{2-\frac{h+D(h)}{2}} \exp\left[-\frac{\nu^{1-h} s^{1+h}}{2\sigma^2} \right] \tag{195}$$

Notice that now Eq. (195) can no longer be solved by using a saddle point technique and we need a functional form of $D(h)$ consistent with the scaling exponents $\zeta(n)$. We can compare (195) against numerical simulations and the result is in agreement with numerical simulations excellent, see [72] for details.

At this stage, we can perform another non-trivial computation, namely the computation of the probability distribution $P[a]$ of a lagrangian acceleration [74]. As in the previous section we assume that $a \sim \delta v(\eta(h))/\tau_\eta$. Here the quantity τ_η depends on h as well since we can define $\tau_\eta = \eta(h)/\delta v(\eta(h))$. Thus we obtain:

$$a \sim \frac{U^2}{L} Re^{-\frac{2h-1}{1+h}} \tag{196}$$

We assume U to be gaussian distributed with $Re = UL/\nu$. Then (196) provides a link between a and U. Finally, we assume that the fluctuation of h are controlled, as before, by the dissipation scale. Putting everything together, after some work, we obtain:

$$P[a] \sim \int dh a^{\frac{h-5+D(h)}{3}} \nu^{\frac{7-2h-2D(h)}{3}} \exp\left[-\frac{a^{\frac{2(1+h)}{3}} \nu^{\frac{2(1-2h)}{3}} L^{2h}}{2\sigma^2} \right] \tag{197}$$

Once again we cannot compute the integral on h but we can compare $P[a]$ against numerical simulations as done in Fig. 17, the agreement is excellent.

Let us summarise our findings. At the beginning of this lecture, we introduced the multifractal framework of turbulence. The basic idea is that there exists a function $D(h)$ which shapes the probability distribution to observe a

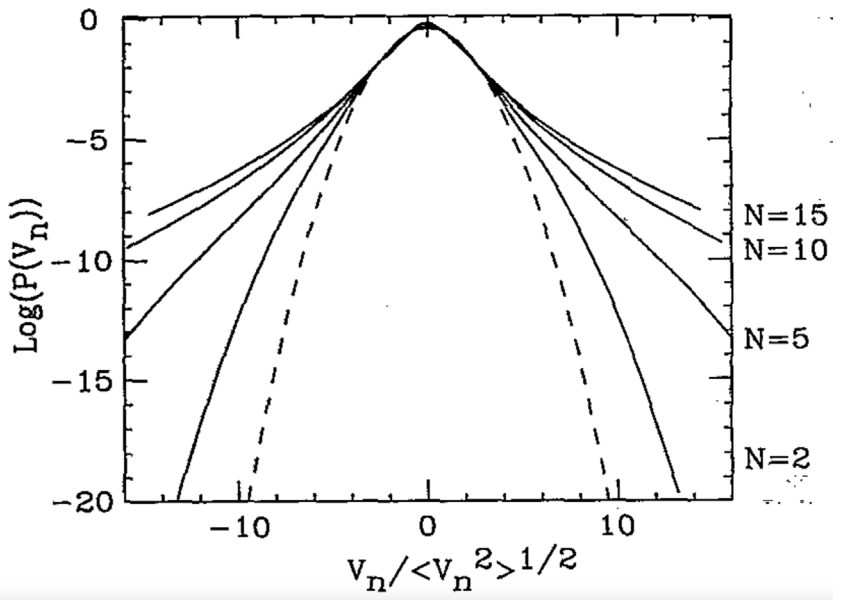

Fig. 31. Log-linear plot of the probability distribution $P(v_n)$ of the velocity increments v_n vs v_n/σ_n, where $\sigma_n^2 = \langle v_n^2 \rangle$, for $n = 2, 5, 10, 15$ (solid lines). For $n = 0$ one has a Gaussian corresponding to a parabola (dashed line). In the figure we consider $l_n = 2^{-n}L$, with $L = 1$, and $v_n \equiv \delta v(l_n)$: going from large to small scales the probability distribution develops a higher tail (large values are more probable) which is the signature of intermittency. We assume $D(h)$ given by the She–Lévêque formula (167) and $P(v_n)$ by Eq. (183).
Source: Figure reproduced from [72].

fluctuation of size $\delta v(r) \sim r^h$ at scale r. We have provided examples of (one-dimensional) multifractal field based on a random multiplicative process where $D(h)$ plays the role of *large deviation* estimate for the probability distribution of h. Our examples are constrained to (independent) random multiplicative processes while the original formulation of the multifractal framework is more general. A non-linear concave function $D(h)$ implies a non-linear behaviour of the anomalous exponent $\zeta(n)$ characterising the inertial range $\eta \ll r \ll L$ scaling of the structure functions. Next, we look at the effect of dissipation and we assume that for any h the dissipation scale $\eta(h)$ satisfies the relation $\delta v(\eta(h))\eta(h) \sim \nu$. The fluctuations of the dissipative scale $\eta(h)$ are again determined by $D(h)$ and are consistent with the zero law of turbulence. The most striking results of our analysis concern the computation of the probability distributions of the velocity gradients (195) $P[s]$ and acceleration of a lagrangian particle $P[a]$ (197). The latter quantity shows very strong intermittent fluctuations and it is probably one of the most intermittent features in a turbulent flow. In the previous lecture, we understood that intermittency in the acceleration is related to the existence of vortex filaments or tubes which are the source of large fluctuations in the lagrangian velocity. $P[a]$, from (197) shows excellent agreement with experimental/numerical results although in (197) there is no information on the existence of vortex filaments: Eq. (197) is derived assuming the existence of $D(h)$ and the fluctuation of the dissipative scale $\eta(h)$. Thus, in a way or another, whatever is the effect of vortices or any other coherent structures, their statistical significance is embedded in $D(h)$. When we look at the structure functions $\langle [\delta v(r)]^n \rangle$ we average over different fluctuation sizes $\delta v(r) \sim r^h$ with the probability $r^{3-D(h)}$. When we look at the acceleration or at the velocity gradients we perform the same computation taking into account finite size effects induced by the viscosity. We think that this is a remarkable result because it implies that $D(h)$ unifies our theoretical approach in understanding intermittency fluctuations both in the inertial range $\eta \ll r \ll L$ and near the dissipation range $r \sim \eta$ where intermittency is enhanced. One may be tempted to say that from the knowledge of inertial range fluctuations we can predict the statistical properties of the fluctuations in the dissipative region. However, this statement may be interpreted as a cause–effect relation, which, at this stage, we cannot state. The good news is that given $D(h)$ we can provide a complete description of intermittency in the N.S. equation: a rather strong and non-trivial statement.

Lecture 4.8. Constrain in ESS and finite size effects in Re

Our next step is to understand how finite size effect in *Re* can be taken into account looking at the structure functions $S_n(r) \equiv \langle [\delta v(r)]^n \rangle$. As a first approximation, we start neglecting the fluctuation in the dissipative scale, η, which is assumed to be the Kolmogorov scale. Then, following the analysis in our previous lecture, we can take into account finite size effects in $S_n(r)$ by writing [59,75,76]:

$$\delta v(r) = U_0 g_1\left(\frac{r}{\eta}\right) g_2\left(\frac{r}{\eta}\right)^h \tag{198}$$

where the functions $g_1(x)$ and $g_2(x)$ satisfy the following constrains: for $x \gg 1$ we assume $g_1(x) \sim const$ and $g_2(x) \sim r/L$ while for $x \ll 1$ $g_1(x) \sim r/\eta$ and $g_2(x) \sim const$. We also assume that (198) is true with probability:

$$P_h[r/\eta] \sim g_2(r/\eta)^{3-D(h)} \tag{199}$$

In the region $g_1(x) \sim const$, we recover from (197)–(198) the scaling properties discussed in the previous lecture, namely the Extended Self Similarity. To simplify the computation we rewrite ((198), (199)) as follows

$$\delta v(r) = U_0 \left(\frac{H(r/\eta)}{1+H(r/\eta)}\right)^{1/3} \left(\frac{\eta}{L}\right)^h (1+H(r/\eta))^h \tag{200}$$

$$P_h[r/\eta] = \left[\left(\frac{\eta}{L}\right)(1+H(r/\eta))\right]^{3-D(h)} \tag{201}$$

where $H(x) = x^3/(1+x^2)$. Using the expression (198), Eqs. (200)–(201) are equivalent to write:

$$g_1(r/\eta) = \left(\frac{H(r/\eta)}{1+H(r/\eta)}\right)^{1/3} \tag{202}$$

$$g_2(r/\eta) = \left(\frac{\eta}{L}\right)(1+H(r/\eta)) \tag{203}$$

Then from (201) we can obtain the structure functions:

$$S_n(r) = U_0^n \left(\frac{H(r/\eta)}{1+H(r/\eta)}\right)^{n/3} \left(\frac{\eta}{L}\right)^{\zeta(n)} (1+H(r/\eta))^{\zeta(n)} \tag{204}$$

Obviously this expression cannot be correct because it does not predict the correct scaling of the velocity gradients with Re. At $r \ll \eta$ we obtain from (204) $S_n(r) \sim U_0^n (r\eta)^n (\eta/L)^{\zeta(n)} \sim r^n Re^{3(n-\zeta(n))/4}$ while we know that the correct scaling should be $S_n(r) \sim r^n Re^{\chi(n)}$ where $\chi(n)$ is given by Eq. (194). The simplest way to obtain the correct result is to assume that $S_n(r)$ depends on the ratio r/η_n where η_n is the effective dissipation scale for the structure function $S_n(r)$. Then we write:

$$S_n(r) = U_0^n \left(\frac{H(r/\eta_n)}{1+H(r/\eta_n)}\right)^{n/3} \left(\frac{\eta_n}{L}\right)^{\zeta(n)} (1+H(r/\eta_n))^{\zeta(n)} \tag{205}$$

To obtain the correct scaling of the velocity gradients with Re we need to chose

$$\frac{\eta_n}{L} \sim Re^{-\frac{\chi(n)}{n-\zeta(n)}} \tag{206}$$

Eq. (206) takes into account the fluctuations of the dissipative scale $\eta(h)$ and Eq. (205) quantifies finite size effects in Re for the structure functions. Just to understand the effect of η_n, we can look at ratio η_n/η_k where η_k is the Kolmogorov scale. Then the quantity $\eta_n/\eta_k \sim Re^{\alpha(n)}$ gives us the effect of fluctuations of $\eta(h)$ in the structure functions. Using the experimental/numerical values of $\zeta(n)$ we obtain: $\alpha(2) = -0.0168$; $\alpha(3) = -0.04$; $\alpha(4) = -0.0512$; $\alpha(6) = -0.0789$.

Using (205) we can now compute the local slope $d\log[S_n(r)]/d\log[S_3(r)]$ which can be used to measure from experimental/numerical simulations the scaling exponents $\zeta(n)$ within the ESS procedure. A direct computation gives:

$$\frac{d\log[S_n(r)]}{d\log[S_3(r)]} = \left[\zeta(n) - \frac{\zeta(n)-n/3}{1+H(r/\eta_n)}\right] \frac{1+\frac{2}{1+(r/\eta_n)^2}}{1+\frac{2}{1+(r/\eta_3)^2}} \tag{207}$$

It is worth while to compare (207) against the local slope:

$$\frac{d\log[S_n(r)]}{d\log[r]} = \left[\zeta(n) - \frac{\zeta(n)-n/3}{1+H(r/\eta_n)}\right] \left(1+\frac{2}{1+(r/\eta_n)^2}\right) \tag{208}$$

The first term in the square bracket on the r.h.s of (207) goes from $\zeta(n)$, for $r \gg \eta_n$, to $n/3$, for $r \ll \eta_n$: it depends on Re rather smoothly through the quantity $H(r/\eta_n)$. The second term on the r.h.s of (207) goes from 1, for $r \gg \eta_n$, to 1, for $r \ll \eta_n$, while in the region $r \sim \eta_n$: it shows a *dip*. A detailed computation shows that the location of the dip is $r \sim (\eta_3/\eta_n)^{1/2}$ and its magnitude depends on $Re^{\alpha(n)-\alpha(3)}$. Thus at relatively small Re the ESS scaling (the first term on the r.h.s of (207)) are the dominant contribution and this result explains why a good estimate of $\zeta(n)$ can be achieved even at relatively low Re. This is also clear from the local slope (208) which change from $\zeta(n)$, for $r \gg \eta_n$, to n, at small r, see Figs. 32. On the contrary, upon increasing Re we should observe the formation of a pronounced dip in the local slope $d\log[S_n(r)]/d\log[S_3(r)]$ which is the hallmark of intermittency increases due to the fluctuation of the dissipation scale $\eta(h)$ in the system. This is a clear prediction whose validity we can investigate using experimental/numerical data in Lecture 6.

Lecture 4.9. Fusion rules

Another non-trivial prediction of the multifractal framework can be obtained using Eq. (166). Let us consider the longitudinal structure functions computed using three different points x, $x+r$ and $x+R$ with $R > r$. In particular let

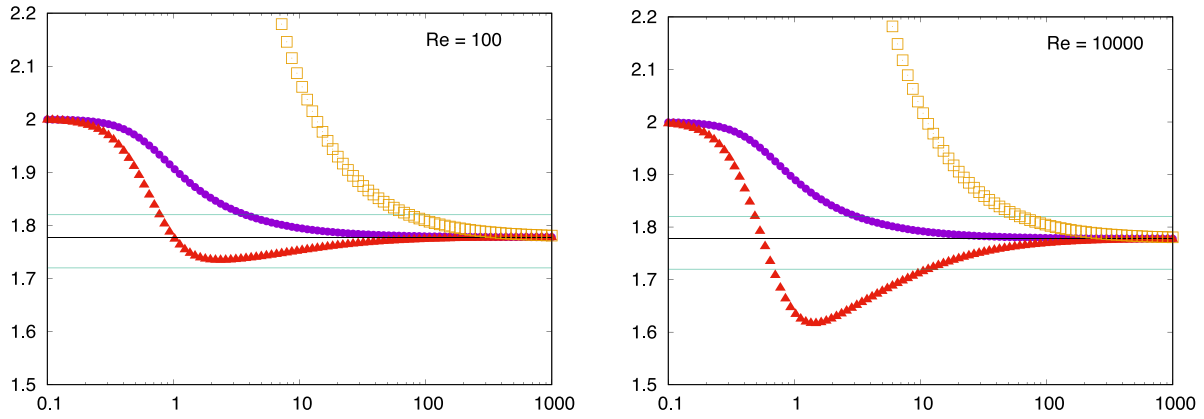

Fig. 32. In violet we show the first term in $d\log(S_6)/d\log(S_3)$, in red the full ESS slope while in yellow the local slope $d\log(S_6)/d\log(r)$. There is little doubt that ESS is very good at low Re while its validity becomes less relevant at large Re (where however the inertial range is better defined).

us consider $\delta v(r)$ and $\delta v(R)$ and the combined structure functions [77]:

$$F_{pq}(r,R) \equiv \langle \delta v(r)^p \delta v(R)^q \rangle \tag{209}$$

Using (166) we can write:

$$F_{pq}(r,R) = U_0 \left[\frac{r}{R}\right]^{\zeta(p)} \langle [\delta v(R)]^{p+q} \rangle \sim \frac{S_p(r)}{S_p(R)} S_{p+q}(R) \tag{210}$$

Eq. (210) is the multifractal prediction on $F_{pq}(r,R)$. Actually, the prediction cannot be true for all p,q. For instance, for $p=q=1$ the prediction is wrong since $S_1(r)=S_1(R)=0$ for homogeneity. For this particular case, we can use the identity:

$$S_2(R-r) = \langle [v(x+R)-v(x)-v(x+r)+v(x)]^2 \rangle = S_2(R)+S_2(r)-2F_{11}(r,R) \tag{211}$$

Similarly, we can write

$$S_3(R-r) = S_3(R) - S_3(r) + 3\frac{S_2(r)}{S_2(R)} S_3(R) - 3F_{12}(r,R) \tag{212}$$

which can be used to compute $F_{12}(r,R)$. From the above examples, we can say that (210) is valid for *even* values of p,q whereas the case of *odd* values can be obtained from a proper generalisation of (210)–(211).

For even p,q we can test the validity of (210) using numerical/experimental data [78]. For this purpose we consider the quantity

$$\tilde{F}_{pq}(r,R) \equiv \frac{F_{pq}(r,R) S_p(R)}{S_p(r) S_{p+q}(R)} \tag{213}$$

First, we fix $r = 5\eta_k$ and change R. In Fig. 33 we plot $\tilde{F}_{2,2}(r,R)$ and $\tilde{F}_{24}(r,R)$ as a function of R: we do observe that for both cases $\tilde{F}_{pq}(r,R)$ reaches a plateau as expected from (210). In Fig. 34 we plot the same quantity for fixed R and as a function of $1/r$: again for small enough r we observe a plateau as expected from (210). Both figures show that the plateau of $\tilde{F}_{pq}(r,R)$ is reached when the ratio R/r is large enough. This behaviour has to be expected. In Fig. 35 we show $\tilde{F}_{pq}(r,R)$ for both experimental data and the case of a synthetic turbulent signal obtained with a random multiplicative process: the behaviour is quite similar although the value of the plateau is slightly different.

We now generalise the previous discussion to study the quantities

$$A_n(R) \equiv \langle \Delta v(x) \delta v(R)^n \rangle \tag{214}$$

The proper behaviour of $A_n(R)$ can be obtained by computing

$$A_n(R) = \lim_{r\to 0} \left[\left(\frac{v(x+r)+v(x-r)-2v(x)}{r^2} \right) (v(x+R)-v(x))^n \right] \tag{215}$$

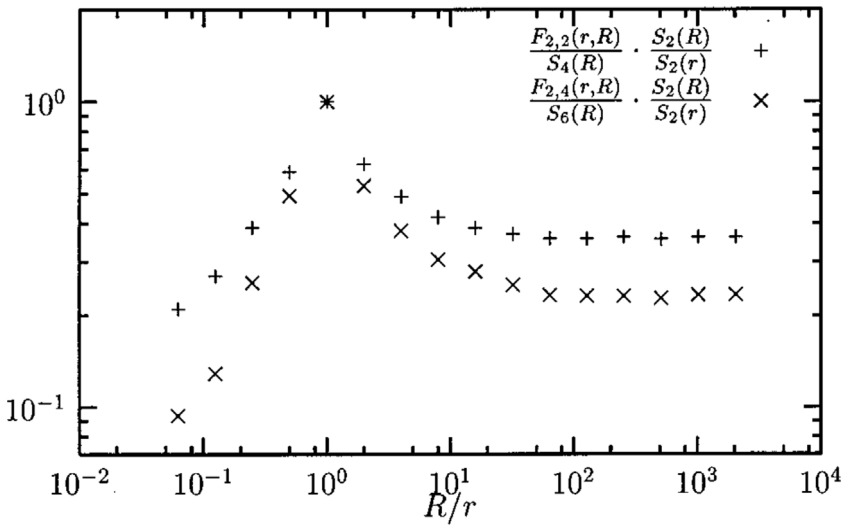

Fig. 33. Compensated $\tilde{F}_{pq}(r, R)$ at fixed $r = 5\eta$ and changing the large scale R for $p = 2$, $q = 2$ (+) and $p = 2, q = 4$ (×). Data analysis from experimental measurements at $Re_\lambda = 2000$ and $Re_\lambda = 800$ as discussed in [78] where the original figure is published.
Source: Figure reproduced from [78].

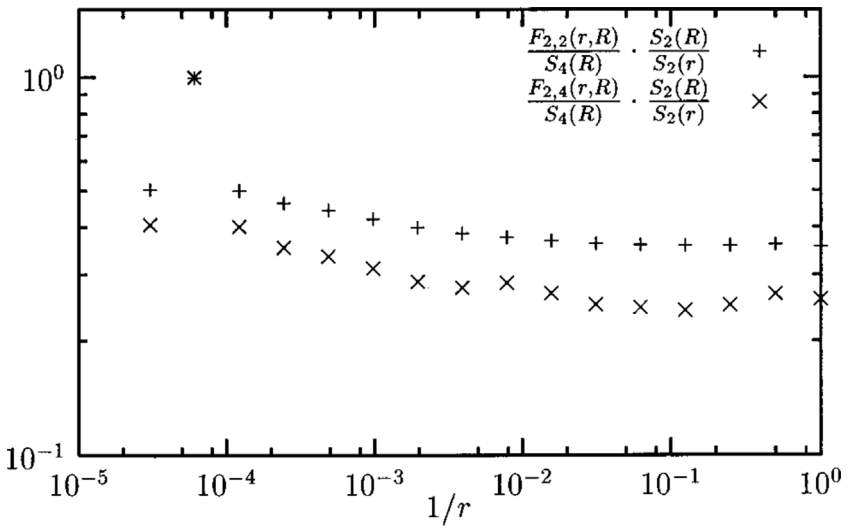

Fig. 34. Same as in Fig. 33 with R fixed and r changing. For better understanding the behaviour, data are plotted versus $1/r$.
Source: Figure reproduced from [78].

The simplest case is $n = 1$ for which we need to evaluate quantities like $F_{11}(r, R)$ before performing the limit $r \to 0$. Using (211) we obtain

$$\begin{aligned} A_1(R) &= \lim_{r\to 0} \frac{1}{2r^2}[2S_2(R) + 2S_2(r) - S_2(R-r) - S_2(R+r)] \\ &= \lim_{r\to 0} \frac{1}{r^2}\left[S_2(r) - \frac{1}{2}r^2\frac{d^2}{dR^2}S_2(R) + O(r^3)\right] \\ &= \langle(\partial_x v)^2\rangle - \frac{1}{2}\frac{d^2}{dR^2}S_2(R) \end{aligned} \tag{216}$$

For $n = 3$ we obtain:

$$\begin{aligned} A_3(R) &= \lim_{r\to 0} \frac{1}{4r^2}[2S_4(R) + 2S_4(r) + 12F_{22}(r, R) \\ &- 4F_{31}(r, R) - 4F_{31}(-r, R) - S_4(R-r) - S_4(R+r)] \\ &= \lim_{r\to 0}[3F_{22}(r, R) - \frac{r^2}{4}\frac{d^2}{dR^2}S_4(R) + O(r^3)] \end{aligned} \tag{217}$$

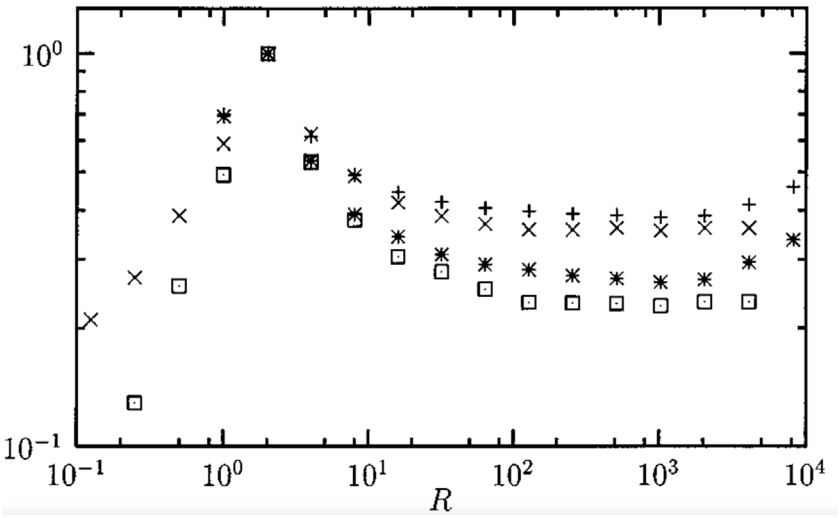

Fig. 35. Comparison of experimental data for the compensated $\tilde{F}_{pq}(r, R)$ shown in Fig. 33 with a synthetic one dimensional multifractal signal build with a random multiplicative process and $\zeta(n)$ fitted by the She–Lévêque (167) formula. Fixed r and changing R: $p = 2, q = 2$ (+) synthetic and (×) experimental; $p = 2, q = 4$ (∗) synthetic and (□).
Source: Figure reproduced from [78].

Now we need a little care in performing the first limit, i.e.

$$\lim_{r\to 0} \frac{1}{r^2} \langle \delta v(r)^2 \delta v(R)^2 \rangle \tag{218}$$

In (218) we are computing $\delta v(r)$ conditioned to $\delta v(R)$ and *after that* we perform the average. This implies that $\lim_{r\to 0} \delta v(r)^2/r^2$ is the gradient of the velocity field which we know is proportional to *Re* (zeroth law of turbulence). The crucial point is that the Reynolds number for this gradient is $R\delta v(R)/\nu$ since we are conditioning on $\delta v(R)$. Then we can write

$$\lim_{r\to 0} \frac{1}{r^2} \langle \delta v(r)^2 \delta v(R)^2 \rangle = \langle \left[\frac{R\delta v(R)}{\nu} \frac{\delta v(R)^2}{R^2} \delta v(R)^2 \right] \rangle \tag{219}$$

This gives:

$$A_3(R) \sim \frac{1}{\nu} \frac{S_5(R)}{R} - \frac{1}{4} \frac{d^2}{dR^2} S_4(R) \tag{220}$$

We can now understand how to compute the general case $A_n(R)$. The key observation is that the first term in Eq. (220) can be computed by looking at the quantity $\langle [\nu \Delta v(x) | \delta v(R)] \rangle$. Assuming that R is in the inertial range we can estimate this quantity using dimensional analysis i.e. $\langle [\nu \Delta v(x) | \delta v(R)] \rangle \sim \delta v(R)^2/R$. Then we arrive to the general formula

$$A_n(R) = \frac{C_n}{\nu} \frac{S_{n+2}(R)}{R} - \frac{1}{n+1} \frac{d^2}{dR^2} S_{n+1}(R) \tag{221}$$

We remark that it is not possible to compute the constant C_n in general (only scaling properties can be obtained!) and that it is extremely difficult (so far) to perform any experimental/numerical comparison against the prediction (221). The theory behind Eq. (221) will be used in Lecture 7 in discussing intermittency in a particular model of passive scalar.

Lecture 4.10. Summary of Lecture 4

The Multifractal theory of turbulence was introduced by Parisi and Frisch in 1983 during the Varenna Summer School on *Turbulence and Predictability in Geophysical Flows and Climate Dynamics*. The basic idea is very simple and it is a natural generalisation of the concept of fractal dimension in disordered media. Besides turbulence, multifractals have been investigated in a countless number of different problems, see also [79].

Concerning turbulence, the multifractal approach can be considered a general theoretical framework based on a probabilistic interpretation of the scaling properties of the Navier–Stokes equations. The very non-trivial point is that the multifractal framework does provide well-defined predictions on relevant quantities like the probability distribution of the lagrangian acceleration a. In the previous lecture, we argued that vortex tubes and filaments are responsible for the large fluctuations of a observed in numerical and/or experimental data. We now understand that these large fluctuations can

be predicted if we know the anomalous exponents $\zeta(n)$ observed in *inertial range* fluctuations of the velocity fields. This result is not a mathematical trick as one may think of it: physically we are speaking of very different physical properties of turbulent flows. It took a rather non-trivial effort performed over more than two decades by many research groups to reach the above conclusions.

To state it more clearly, there is no dichotomy between the statistical properties of turbulence as described by the multifractal framework and the description of turbulence flows in terms of coherent structures like vortex tubes and filaments. Even in the multifractal framework, the asymptotic scaling of the anomalous exponents is constrained to a well-defined, although rare, structure with exponent h_0, as we discussed at the beginning of this lecture. We can always choose one way or another to describe turbulent flows. The key point is whether the way we choose can be used to provide any quantitative predictions which can be verified using experimental or numerical data. The multifractal framework provides well-defined predictions, all of them in agreement with available data. Obviously, the quantity we should consider must satisfy the symmetry properties of the Navier–Stokes equation. Interesting one can employ the multifractal framework for possible turbulence model [80,81].

Finally, an important point concerns the universality of the anomalous scaling $\zeta(n)$ or equivalently $D(h)$. More properly, the question is whether the anomalous exponents are independent of the forcing and dissipation mechanism. In particular, for the time being, we consider forces that are statistically homogeneous and isotropic, whereas for the dissipation mechanism, we consider any possible mechanism of energy dissipation acting at small scales. The multifractal framework does not tell us anything about the universality of $D(h)$ with respect to forcing and dissipation. Experimental and numerical data support the statement of universality of the anomalous scaling. We will come back to this point in Lectures 7 and 8.

Lecture 5. Shell models

Lecture 5.1. A simplified approach to turbulence

In the previous lecture, we introduce and discuss in some detail the multifractal theoretical framework for turbulence. Even if the function $D(h)$ is not specified, we were able to obtain many non-trivial *predictions* or consequences. In particular, we were able to reach a unified description of intermittency in homogeneous and isotropic turbulence both in the inertial range and in the dissipation range where intermittency is observed to be stronger. The multifractal approach exploits the scale invariance of the N.S. equations $r \to \lambda r$ with $v \to \lambda^h v$ having to constrain the zero law of turbulence. The question we want to address in this lecture is whether there exists any model (possibly a simple one) which displays the same scale invariance of the N.S. and where intermittency can be observed in a qualitative or even quantitative way similar to the N.S. one. We have already discussed the Burgers equation where intermittency and anomalous scaling is observed. However, as we noticed, the Burgers equation shows two possible values of h namely $h = 0$ and $h = 1$ and it corresponds to a *bifractal* situations. The unique signature in the N.S., according to the multifractal approach, is a continuous range of possible values of h. Thus, it would be interesting to investigate a simple model (much simpler than the N.S. equations) where something similar is happening, i.e. we have both the scale invariance of the N.S. equations and anomalous scaling are described with the multifractal framework. It turns out that there exists a class of models which satisfy the above requirement: the shell models.

Usually, shell models are introduced by assuming that they represent a very simplified version of the N.S. in the Fourier Space. We prefer to think of shell models as a dynamical system where we artificially introduce velocity fluctuations at different *scales* whose dynamics are similar to real turbulence [82]. The basic idea is to build a dynamic system (with a relatively small number of degrees of freedom) that satisfies the scaling properties of the N.S. and displays chaotic behaviour in time.

To be concrete we consider the scales $l_n \equiv 1/k_n$ exponentially distributed in n, i.e. $k_n = k_0\lambda^{-n}$ where $\lambda > 1$. To each scale k_n we associate a complex variable u_n. Next, we need to write the equation for u_n. The last step is not unique and, as we shall see, there exist different proposals.

The most general formulation of the model is in the form:

$$\frac{du_n}{dt} = C_n + F_n + D_n \tag{222}$$

where F_n is the forcing term to be specified, D_n is the dissipation term and C_n is the term containing non-linear interactions. We assume $D_n = -\nu k_n^2 u_n$ to mimic the effect of dissipation in N.S. We also assume that the term C_n satisfies the Liouville equation $\partial C_n/\partial u_n = 0$ as in the case of the N.S. [26].

Lecture 5.2. The GOY model

Having identified the general requirement, the term C_n is still undetermined. A well studied case is the so-called *GOY* model [83–85] whose equations are:

$$\frac{du_n}{dt} = i[k_n u_{n+2}^* u_{n+1}^* + bk_{n-1}u_{n+1}^* u_{n-1}^* + ck_{n-2}u_{n-1}^* u_{n-2}^*] - \nu k_n^2 u_n + f_n \tag{223}$$

where usually the forcing term f_n acts on the shells corresponding to the very large scales $n = 0$ and $n = 1$. The constrain $\partial C_n/\partial u_n = 0$ is obviously satisfied for Eq. (223).

The first thing we notice is that (223), for $f_n = 0$, are invariant for the scale transformation

$$\begin{aligned} k_n &\to \Lambda^{-1} k_n \\ u_n &\to \Lambda^h u_n \\ \nu &\to \Lambda^{1+h} \nu \end{aligned} \tag{224}$$

which is one of our requirements. Notice that we now use Λ because we used the symbol λ for the ratio k_{n+1}/k_n. Let we also notice that the equation of motions are invariant for $u_n \to u_n \exp(i\theta_n)$ provided that $\theta_{n+2} + \theta_{n+1} + \theta_n = 0$. Next we assume $f_n = 0$ and $\nu = 0$ and we look at the quantities $W \equiv \Sigma_n |u_n|^2 z^n$ assuming that (223) is studied for an infinite number of shells. It is easy to show that W is conserved if:

$$1 + bz + cz^2 = 0 \tag{225}$$

If we want energy to be conserved we must require that $1 + b + c = 0$ or $c = -b - 1$. Thus the model is specified with one free parameter b. It is useful to define $\epsilon \equiv -b$ [86] Using $c = \epsilon - 1$ we can look at the equation for the energy $|u_n|^2/2$. We introduce the quantity $\Delta_n = k_{n-1} u_{n-1} u_n u_{n+1}$. Then we obtain:

$$\frac{d}{dt}\frac{|u_n|^2}{2} = \frac{1}{2}[i\Delta^*_{n+1} - i\epsilon\Delta^*_n + i(\epsilon - 1)\Delta^*_{n-1} + c.c.] + \dots \tag{226}$$

where $c.c.$ stands for complex conjugate and the dots stand for forcing and dissipative terms. Next, we introduce the quantity $J_n = \Im[-\Delta_{n+1} - (1 - \epsilon)\Delta_n]$ so that the above equation becomes

$$\frac{d}{dt}\frac{|u_n|^2}{2} = J_{n-1} - J_n + \dots \tag{227}$$

We can see from (227) that J_n can be interpreted as the rate of energy transfer for large scales (i.e. k_{n-1} and k_{n-2}) to the smaller scale k_{n+1} and k_{n+2}. Thus, $J_n > 0$ represents a positive energy transfer from large to small scales. Numerically, this is the case for $\epsilon > 0$. In the limit $\nu = 0$ and no forcing, Eq. (227) and energy conservation implies $J_n \sim const$ and therefore:

$$\Im[u_{n-1} u_n u_{n+1}] \sim k_n^{-1} \tag{228}$$

We can look at Eq. (228) or (227) as the analogous of the 4/5 Kolmogorov equation for N.S.

Next, we consider the case of forcing and finite dissipation ν. We choose $k_{n+1}/k_n = \lambda = 2$, $k_0 = 2^{-4}$, $\epsilon = 1/2$. The forcing is applied to k_0 and is equal to $5(1+i)10^{-3}$. The total number of shells is $N = 22$. For these parameters, the model (223) displays a quite clear chaotic behaviour and we are interested to estimate the scaling properties of the velocity fields. There are different and equivalent ways to estimate the analogous of the structure functions [86]:

$$s_{nq} = \left\langle |u_n|^q \right\rangle \tag{229}$$

$$S_{nq} = \left\langle |\Im(u_{n-1} u_n u_{n+1})|^{q/3} \right\rangle \tag{230}$$

$$\Sigma_{nq} = \left\langle \left| \frac{J_n}{k_n} \right|^{q/3} \right\rangle \tag{231}$$

The reason why there may be different definitions of the structure functions is clearly due to the fact that u_n does not necessarily represent the analogous of $\delta v(r)$ in turbulence. The definition (230) and in particular (231) are based on the Eq. (228): both definitions are based on the amount of energy transfer from large to small scales and they should be the physical analogous of $\delta v(r)^3$. In Fig. 36 we show $q = 6$ the scaling properties of s_{nq}, S_{nq} and Σ_{nq}: while both S_{nq} and Σ_{nq} show quite good scaling this is not true for s_{nq} which exhibits some oscillations. Thus we can assume that (230) and (231) are the correct quantities to estimate the scaling exponents $\zeta(q)$.

In Fig. 37 we show the functions S_{nq} for $q = 4$ and $q = 6$ down to the dissipation range. For $\epsilon = 1/2$ and $k_{n+1}/k_n = 2$ we obtain two interesting results: (1) the scaling exponents of the velocity fields are anomalous i.e. $\zeta(q)$ is a non-linear function of q with $\zeta(3) = 1$; (2) the values of $\zeta(q)$ are quite close (within the error bars) to the one observed from N.S. Both results are interesting and non-trivial: Eq. (223) exhibits the multifractal scaling induced by the non-linear chaotic dynamics of the system.

Going back to Eq. (225), the second possible invariant, hereafter referred to as H, corresponds to the solution $z = 1/(\epsilon - 1)$:

$$H = \Sigma_n |u_n|^2 (\epsilon - 1)^{-n} \tag{232}$$

It turns out that also the Euler equations have two invariants: the energy and the *helicity*, namely the integral over the volume of $\boldsymbol{\omega} \cdot \boldsymbol{v}$. Thus, at least dimensionally, the second invariant H in (232) becomes analogous to helicity if

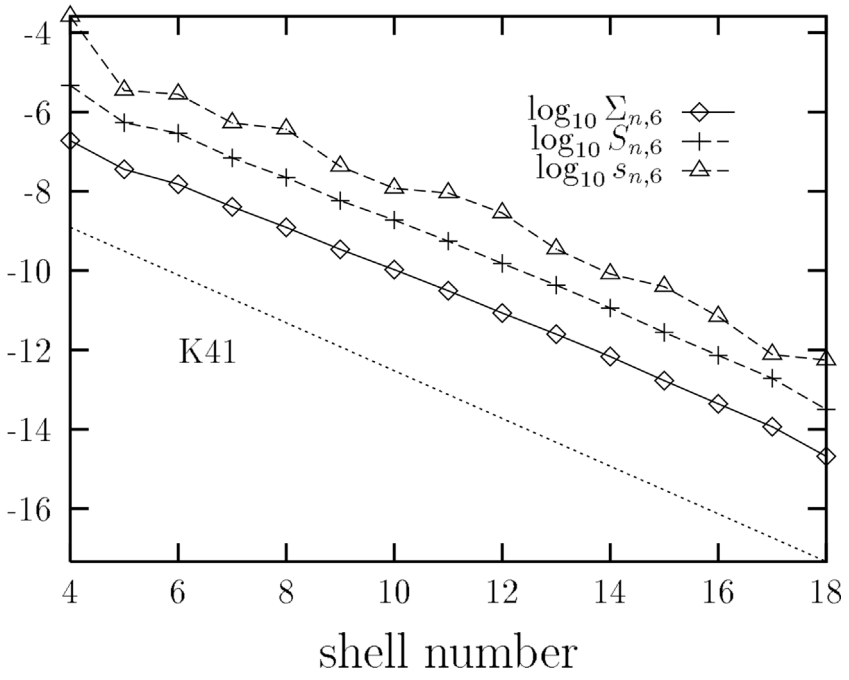

Fig. 36. Different kinds of scaling analyses with increasing accuracy: s, which is the magnitude of the velocity, S which is a cube root of the imaginary part of a product of three velocities, and X, which is the cube root of the energy flux. The upper part shows curves drawn for q = 1; the lower part for q = 6. In both cases, Z gives the longest scaling range, and hence probably the best estimates for scaling exponents. All curves are drawn for the standard parameter values. For comparison, K41 scaling is also shown.
Source: Reproduced from [86].

$(\epsilon - 1)^{-n} = (-1)^n k_n$ i.e. if:

$$\lambda = \frac{1}{1-\epsilon} \tag{233}$$

This is the case, for instance, if $\lambda = 2$ and $\epsilon = 1/2$ used for the numerical simulations shown in Figs. 36 and 37.

In general, the values of the anomalous exponents depend on both ϵ and $\lambda \equiv k_{n+1}/k_n$ as shown in Fig. 38. However, following [86] one may conjecture that, if λ and ϵ satisfy (233) the scaling exponents are independent (or at least weakly dependent) of the particular choice λ, ϵ. Fig. 38 supports this view.

The existence of anomalous scaling in the GOY model Eq. (223) is associated to other well-known features of intermittency observed in the N.S. equations. In Fig. 39 we show the probability distribution of $Re(u_n)/\langle Re(u_n)^2\rangle^{1/2}$ for different values of n: for small n (large scale) the probability distribution is close to a gaussian while, upon increasing n (small scales), we observe the development of long tails. In Fig. 40 we show the energy dissipation $\epsilon(t) \equiv \nu \Sigma_n k_n^2 |u_n|^2$ as a function of time which shows many intermittent bursts in qualitative agreement with similar features observed in the energy dissipation of turbulent flows.

Lecture 5.3. The Sabra model

To avoid the oscillations observed in the scaling properties of s_{nq}, a different version of the shell model has been introduced referred to as *Sabra* model [87]:

$$\frac{du_n}{dt} = i[k_{n+1}u_{n+2}u^*_{n+1} - \delta k_n u^*_{n-1}u_{n+1} + (1-\delta)k_{n-1}u_{n-1}u_{n-2}] - \nu k_n^2 + \dots \tag{234}$$

Eq. (234) are invariant under the transformation $u_n \to u_n \exp(i\theta_n)$ for $\theta_{n+2} - \theta_{n+1} - \theta_n = 0$. This implies that $\langle u_n u^*_m\rangle = \delta_{nm}\langle |u_n|^2\rangle$ while for the GOY model $\langle u_n u^*_{n+3}\rangle \neq 0$. The Sabra model significantly improves the estimate of the anomalous exponents from numerical simulations. For $r = 2$ and $\delta = 0.5$ the Sabra and the GOY model gives anomalous similar exponents.

Lecture 5.4. Helicity in shell models

As we already noticed, the *GOY* model is characterised by two inviscid invariants. The second invariant is not positive defined and for $\epsilon - 1 = \lambda^{-1}$ looks like, at least dimensionally, the *helicity* $H = \boldsymbol{\omega} \cdot \boldsymbol{v}$. For the Euler equation H is a local

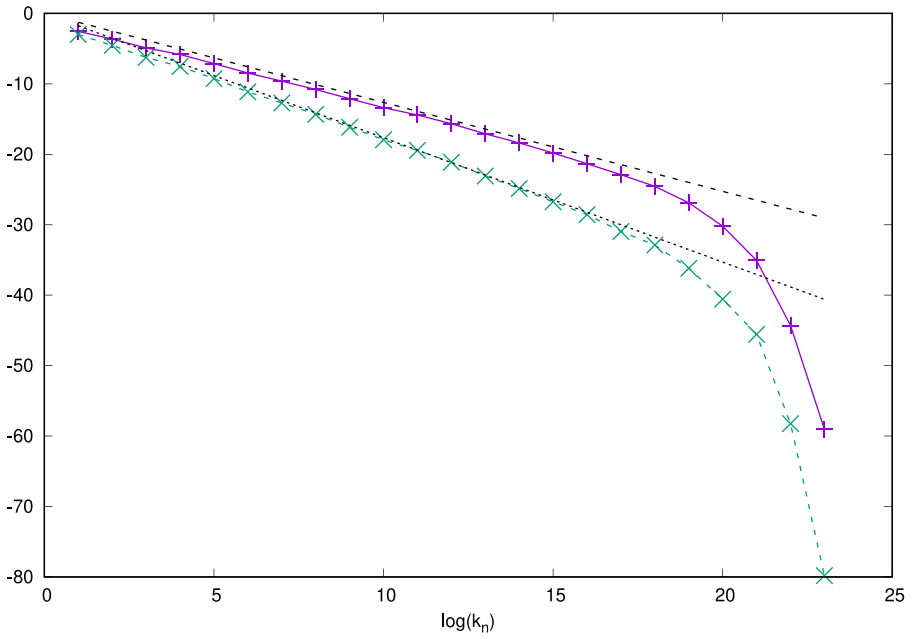

Fig. 37. Example of scaling for structure functions of 4th order (+) and 6th order (×) for the GOY shell model of turbulence. The straight lines are the best fit in the inertial range and correspond to the slopes, respectively, $\zeta(4) \sim 1.26$ and $\zeta(6) \sim 1.76$. Numerical simulations employed a total number of shells $N = 25$, viscosity $\nu = 5e-7$, and forcing $f_n = 0.1(1+i)\delta_{n,0}$, while $k_0 = 0.05$.

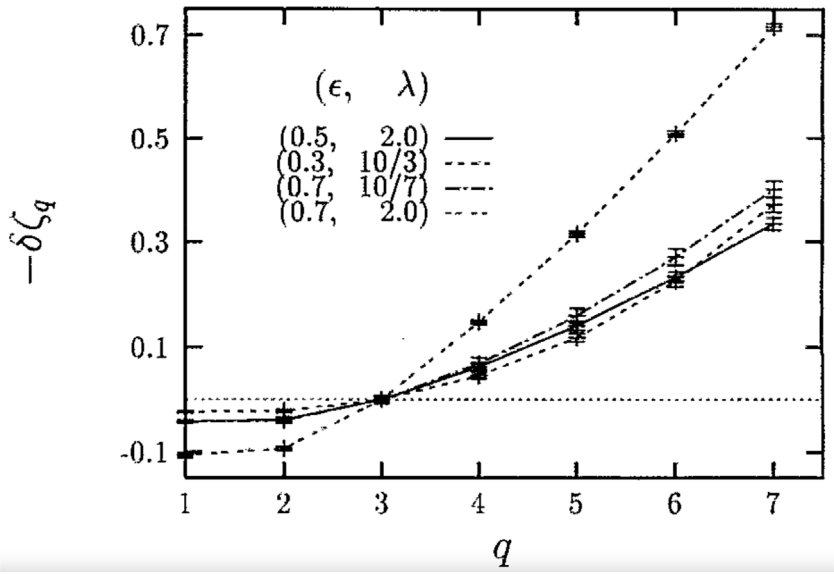

Fig. 38. $\delta\zeta_q$ versus q for four sets of parameter values. Three parameter pairs (ϵ, λ) lie on the curve (233) which defines the right value of the helicity. These have $\lambda = 10/3$ and $\lambda = 10/7$ paired with their corresponding ϵ's. The last value lies off the curve and has $\epsilon = 0.7$ with $\lambda = 2$. Note how the values on the curve stand grouped together in comparison with the other one.
Source: Reproduced from [86].

invariant on any volume Ω whose surface $S(t)$ satisfies $\boldsymbol{\omega} \cdot \hat{\boldsymbol{n}} = 0$, where $\boldsymbol{\omega}$ is the vorticity and $\hat{\boldsymbol{n}}$ is the outward normal to the surface $S(t)$. This results is obtained in two steps: (1) from the Kelvin circulation theorem [88] it is possible to show that the surface $S(t)$, while evolving in time, satisfies the condition $\boldsymbol{\omega} \cdot \hat{\boldsymbol{n}} = 0$ at any time t; (2) using the equation for the vorticity:

$$\frac{\partial \boldsymbol{\omega}}{\partial t} + \boldsymbol{v} \cdot \nabla \boldsymbol{\omega} = \boldsymbol{\omega} \cdot \nabla \boldsymbol{v} \tag{235}$$

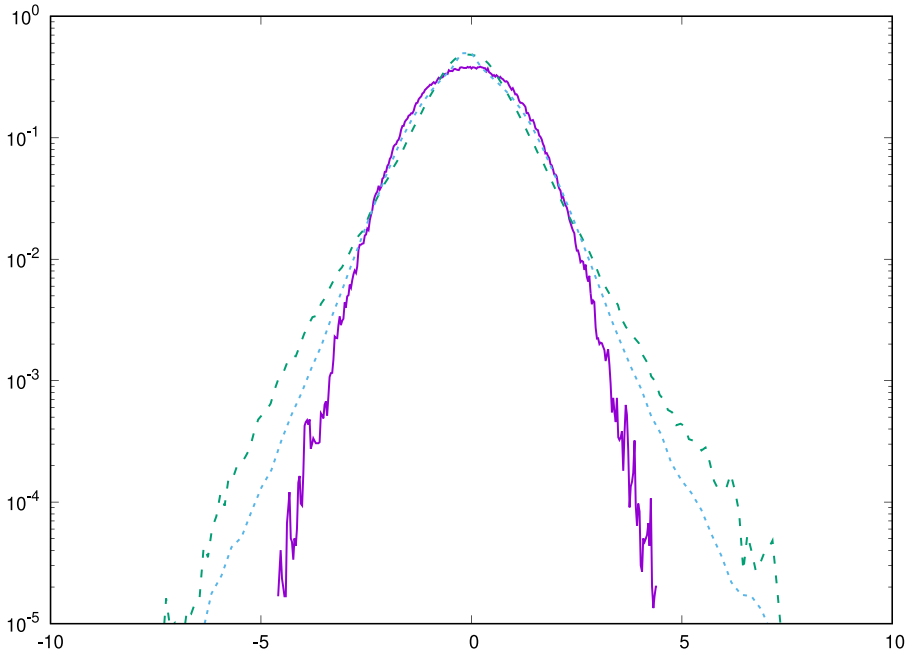

Fig. 39. Normalised PDFs of the real part of the velocity variables, $Re(u_n)$, in the GOY shell model for turbulence, for wave numbers k_n with n = 5, 10, 15. The pdf corresponding to the largest scale, $n = 5$, is represented by the solid line, the one corresponding to the intermediate scale, $n = 10$, is the long-dashed line while the smallest scale, $n = 15$ is the short-dashed line. Notice the moving to smaller and smaller scales the pdf becomes departs more and more from a Gaussian distribution.

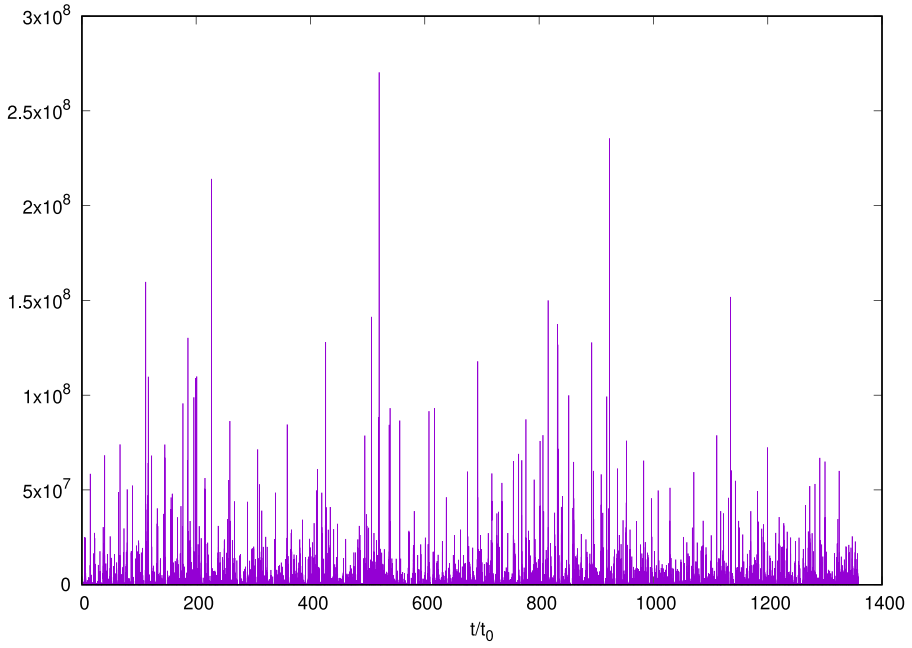

Fig. 40. Typical time evolution of the energy dissipation, $\epsilon(t) = \sum_n k_n^2 |u_n|^2$ in a GOY shell model of turbulence. Intermittency is well visible by the presence of extremely high peaks.

we can obtain the equation for H, given by

$$\frac{dH}{dt} \equiv \frac{\partial H}{\partial t} + \boldsymbol{v} \cdot \boldsymbol{\nabla} H = \boldsymbol{\nabla} \cdot \left[\boldsymbol{\omega} \left(\frac{1}{2} v^2 - \frac{p}{\rho} \right) \right] \tag{236}$$

Therefore, the integral of dH/dt in the region Ω vanishes and H is a *local* inviscid invariant of the Euler equations [89]. For periodic boundary conditions H is also a global invariant, i.e. $\langle dH/dt \rangle = 0$ where $\langle \dots \rangle$ stands for space average.

The helicity changes sign under parity transformation $\boldsymbol{r} \to -\boldsymbol{r}$ while the Euler and the N.S. equation are invariant under a parity transformation. For a turbulent flow, if the forcing mechanism is invariant for parity transformation, the average helicity should be zero and it plays no role in the statistical properties of turbulence. However, since H is a local inviscid invariants, as we previously noticed, helicity fluctuations may play some effects. From the identity $\boldsymbol{v} \cdot \nabla \boldsymbol{v} = \nabla(v^2/2) - \boldsymbol{v} \times \boldsymbol{\omega}$, relatively large (positive or negative) value of the helicity implies a decrease in the non-linear term. This may eventually produce some non-vanishing effect in the turbulent intermittency. In summary, it would be important to generalise the GOY model so that both energy and helicity are conserved by non-linear interactions and it turns out that this generalisation is possible. The basic idea is to introduce for each k_n two complex variables u_n^+ and u_n^- corresponding to positive and negative helicity modes respectively. Then at the same scale we can assume that the vorticity is proportional to $k_n(u_n^+ - u_n^-)$ and the helicity corresponds to $k_n(|u_n^+|^2 - |u_n^-|^2)$. Following this idea, the proper generalisation of Eq. (223) is given by the following equations:

$$\frac{du_n^+}{dt} = ik_n \left[u_{n+2}^- u_{n+1}^+ + b u_{n+1}^- u_{n-1}^+ + c u_{n-1}^- u_{n-2}^- \right]^* - \nu k_n^2 u_n^+ + f_n^+ \tag{237}$$

$$\frac{du_n^-}{dt} = ik_n \left[u_{n+2}^+ u_{n+1}^- + b u_{n+1}^+ u_{n-1}^- + c u_{n-1}^+ u_{n-2}^+ \right]^* - \nu k_n^2 u_n^- + f_n^- \tag{238}$$

where $f_n^{\pm}$ are the forcing terms. It is possible to show that Eqs. (237)–(238) with no forcing and dissipation conserve the two quantities

$$E = \frac{1}{2} \Sigma_n \left[|u_n^+|^2 + |u_n^-|^2 \right] \; ; \; H = \frac{1}{2} \Sigma_n k_n \left[|u_n^+|^2 - |u_n^-|^2 \right] \tag{239}$$

if we choose the parameters b and c as follows:

$$b = -\frac{\lambda^{-1} + \lambda}{\lambda^2 + \lambda} \; ; \; c = \frac{-\lambda^{-1} + \lambda^{-2}}{\lambda^2 + \lambda} \tag{240}$$

Using Eqs. (237)–(238), the anomalous exponents are not different from the ones computed from the GOY model, i.e. helicity fluctuations do not change the overall picture [90,91].

Overall shell models seem to reproduce many non-trivial features observed in real turbulence. Moreover, numerical simulations show that anomalous scaling is independent of the forcing mechanism and/or the detailed feature of the dissipation mechanism. One can read this result in two ways:

(a) it is a non-trivial check that anomalous scaling arises from the non-linear dynamics in the system characterising energy transfer in the inertial range;
(b) because in shell models there is no topological and/or geometrical features which characterises real turbulence, anomalous scaling does not capture the very essence of turbulent flows.

We feel that both statement are somehow sloppy: shell models are models where it is possible to check very general ideas on anomalous scaling. In particular, the scaling exponents depend on the parameters choices (ϵ or δ and r depending on the model). Thus, if one has a general approach on how to compute the anomalous exponents and/or $D(h)$, shell models are good candidates to make a validity test because, using numerical simulations, we can estimate the anomalous exponents with high accuracy. We remark that the comment (b) on topological and/or geometrical properties of turbulence should be specified in terms of well-defined measurable quantities whose scaling properties (if any) cannot be obtained using the multifractal model.

Lecture 5.5. Restricted Euler equation for shell model

As discussed in Lecture 2, one simple way to explore the topological properties of turbulent flows is to look at the Q, R obtained by the invariants of the matrix $A_{ij} = \partial_i u_j$. On the left panel of Fig. 41 we show sampling of Q, R using direct numerical simulations at $Re_\lambda = 180$ with a clear pronounced number of events in the vortex-stretching region (second quadrant) and in the dissipative region (fourth quadrant), see also the discussion in Lecture 2. Another interesting feature of A_{ij} is the probability distributions of the cosine between the vorticity and the eigenvectors associated with the intermediate, maximum and smallest eigenvalues of A_{ij}, shown on the left panel of Fig. 42 obtained for the same simulations used in Fig. 41. Altogether, both figures indicate, as already noticed in Lecture 2, that fully developed turbulence cannot be considered a kind of random superposition of fluctuations: structures (i.e. strong vorticity) and their space organisation plays a role. Obviously the Restricted Euler Equations (REE) do not provide any insight on this issue: REE do predict the general shape of the Q, R diagram and provide their topological interpretations but, obviously, there is no information in the REE on the energy transfer from large to small scales and the zeroth law of turbulence. Now the idea is to couple the physics described by the REE with a shell model, the results are shown on the left panels of Figs. 41 and 42. Let us highlight that, as we understood from the previous lecture, the multifractal theory takes care, statistically, of the space organisation of energy dissipation and vorticity in turbulence: using anomalous scaling exponents in the

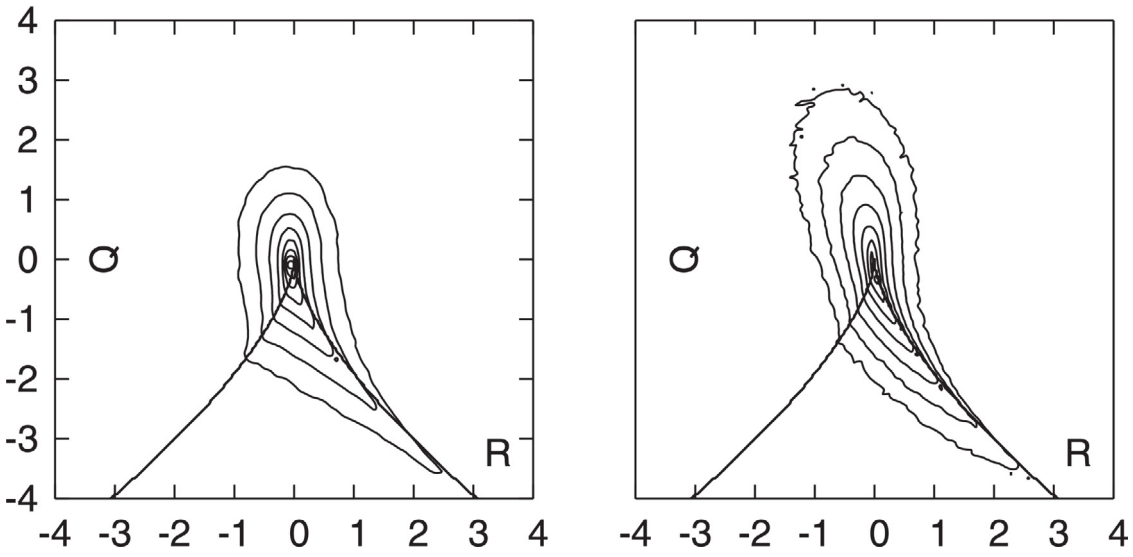

Fig. 41. Isolines of $P(R, Q)$ (normalised to have unit variance) for DNS and model data. Right-hand panel: DNS data at $Re_\lambda \sim 180$. Left-hand panel: model data at $Re_\lambda = 130$, evaluated at the dissipative scale $k_d(Re)$. The continuous line in all diagrams corresponds to the Vieillefosse zero-discriminant curve $Q^3 + 27/4R^2 = 0$.
Source: Reproduced from [92].

inertial range energy transfer we can predict the probability density in the lagrangian acceleration which is dominated by the effect of vortex filaments. However for a shell model, although anomalous scaling is observed, there is no way to think of any space organisation.

Following [92], we consider the 3×3 matrix $\boldsymbol{A}_n$ as the *coarse grained* value of A_{ij}. For simplicity, we can think of A_n as the Fourier components of A_{ij}. Next, taking inspiration from the Sabra model, we assume that $\boldsymbol{A}_n$ satisfies the equation

$$\frac{d\boldsymbol{A}_n}{dt} = \alpha\left[-\boldsymbol{A}_n{}^2 + Tr(\boldsymbol{A}_n{}^2)\frac{\boldsymbol{I}}{3}\right] + (1-\alpha)[\tilde{\boldsymbol{F}}_n - \nu k_n^2 \boldsymbol{A}_n] \tag{241}$$

$$\boldsymbol{F}_n = \boldsymbol{A}_{n+2}\boldsymbol{A}_{n+1}^T + 4b\boldsymbol{A}_{n-1}^T\boldsymbol{A}_{n+1} + 16(1-b)\boldsymbol{A}_{n-2}\boldsymbol{A}_{n-1} \tag{242}$$

where $\tilde{\boldsymbol{F}}_n \equiv \boldsymbol{F}_n - \boldsymbol{I}Tr(\boldsymbol{F}_n)/3$. In Eq. (241) $k_n = 2^n k_0$ and the parameter $\alpha = 0.5$. Also we assume $\boldsymbol{A}_n = 0$ for large scales $n = -1, n = -2$ and small scales $n = N+1, n = N+2$, with $N = 22$. For $\nu = 0$, Eq. (241)–(242) conserve the energy $\Sigma_n k_n^{-2} Tr[\boldsymbol{A}_n\boldsymbol{A}_n^T]$. To obtain a stationary probability distribution, the system is forced with a white noise in time gaussian matrix $\boldsymbol{G}$ at the largest scale $n = 0$ with variance $\langle G_{ij}G_{ml}\rangle = 2\delta_{im}jl - 0.5\delta_{ij}\delta_{ml} - 0.5\delta_{il}\delta_{jm}$ [92]. To compare the results from Eq. (241)-5.16 against numerical and/or experimental data, we should look at $\boldsymbol{A}_n$ at the dissipative scale k_d, i.e. where we observe the maximum of the energy dissipation $\langle \boldsymbol{T}r(\boldsymbol{A}_n\boldsymbol{A}_n^T)\rangle$. Then from $\boldsymbol{A}_d$ we can compute both Q and R as well as the anomalous scaling in the inertial range.

On the right panel of Fig. 41 we show the probability distribution $P(Q, R)$ obtained using the shell model (241)–(242). The two probability distributions show remarkable agreement. On the right panel of Fig. 42 we show the probability distribution of the cosine between the vorticity and intermediate, maximum and smallest eigenvalue of $\boldsymbol{A}$. In summary we can say that the topological properties of a turbulent flows as quantified by the probability distribution $P(Q, R)$ are in qualitative and quantitative agreement with the dynamics of the shell model (241)–(242). In particular, the model provides a realistic dynamics for coupling among different scales which is the driving mechanism in shaping $P(Q, R)$.

Lecture 5.6. Shell model on a tree and the refined Kolmogorov similarity hypothesis

One of the basic feature of three dimensional fully developed turbulence is the validity of the RKSH, i.e. $\delta v(r)^3 \sim \epsilon(r)r$ where $\epsilon(r) = r^{-3}\int_{B(r)} d^3x\epsilon(x)$ and $B(r)$ is a box of side r. RKSH is assumed to hold within the multifractal framework on the basis of the scaling properties of the NS equations and is observed to hold with high accuracy using experimental/numerical results. To investigate the shell models we must introduce a space dependency [93]. To this purpose, we can get a useful hint using the example of a one-dimensional multifractal field discussed in the previous lecture. In particular we can consider a dyadic tree with nodes j, n where $n = 1, \ldots$ is the level in the tree and $j = 1 \ldots 2^{(n)}$ are the nodes at level n. To each node j, n we can introduce the complex variables $u_{jn}^{\pm}$ with positive and negative helicity. Finally, we must define the interactions among the variables using the same general rules so far employed in the shell model Eqs. (237)–(238). There are several ways to do that and we consider two possible situations which are described in Figs. 44 and 45:

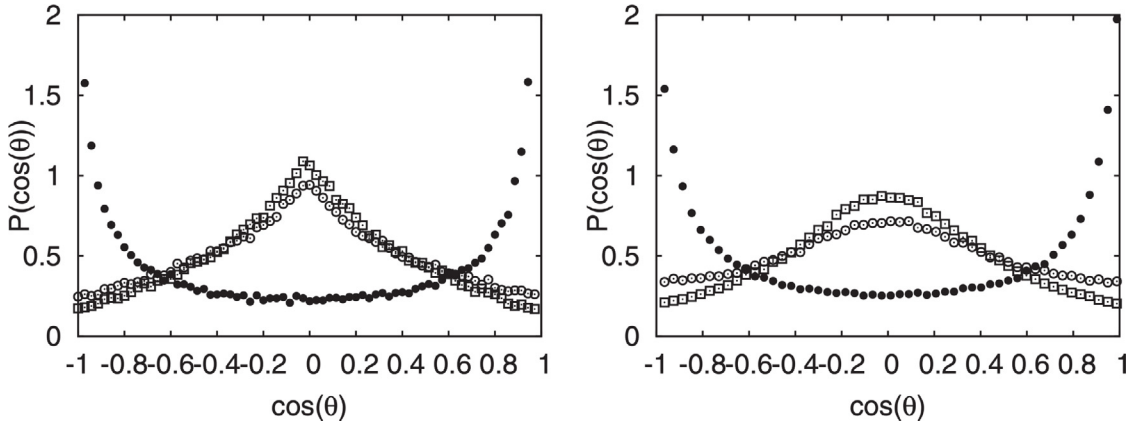

Fig. 42. PDF of the cosine between the vorticity and the eigenvectors associated with the intermediate (•), maximum (∘), and smallest (□) eigenvalues of the strain-rate matrix. Notice the good agreement between the DNS (right) data and the model data (left).
Source: Reproduced from [92].

Model A which is described by the equations:

$$\begin{aligned}\frac{du_n^+}{dt} &= ik_n\left[\frac{1}{4}u^+_{n+1,2j-1}(u^-_{n+2,4j-3}+u^-_{n+2,4j-2})+u^+_{n+1,2j}(u^-_{n+2,4j-1}+u^-_{n+2,4j})\right]^* \\ &+ ik_n\left[\frac{b}{2}u^+_{n-1,j}(u^-_{n+1,2j-1}+u^-_{n+1,2j})+cu^-_{n-1,j}u^-_{n-2,j}\right]^* - \nu k_n^2u_n^+ + f_n^+\end{aligned} \tag{243}$$

and Model B which is described by the equations:

$$\begin{aligned}\frac{du_n^+}{dt} &= ik_n\left[\frac{1}{4}u^+_{n+1,2j-1}(u^-_{n+2,4j-3}+u^-_{n+2,4j-2})+u^+_{n+1,2j}(u^-_{n+2,4j-1}+u^-_{n+2,4j})\right]^* \\ &+ ik_n\left[\frac{b}{2}u^+_{n-1,j}(u^-_{n+1,2j-1}+u^-_{n+1,2j})+cu^-_{n-1,j}u^-_{n-2,j}\right]^* \\ &+ ik_nd\left[-u^-_{n+1,2j}u^+_{n+1,2j}+e_1u^-_{n,\bar{j}}u^+_{n-1,\bar{j}}+e_2u^-_{n,\bar{j}}u^-_{n-1,\bar{j}}\right]^* \\ &+ ik_nf\left[u^+_{n,j-1}u^-_{n,j+2}-u^+_{n,j-1}u^-_{n,j+1}-u^-_{n,j-1}u^+_{n,j+1}+u^-_{n,j-2}u^+_{n,j-1}\right]^* \\ &- \nu k_n^2u^+_{n,j}+f_n^+\end{aligned} \tag{244}$$

For both models, similar equations hold by the transformations $+\to-$, $-\to+$. For model B, $\bar{j}$ is the integer part of $(j+1)/2$. For models A and B, we chose b and c as before while for model B we set $d=f=1$ and $e_1=3/4$, $e_2=1/4$. With these choices, we can obtain in the inviscid limits that both energy and helicity are invariants, see Eq. (240).

Both models A and B display anomalous scaling in the structure functions of the variables $u^\pm_{n,j}$. Note that for any level n the structure functions are build upon averaging $|u^+_{n,j}|^2+|u^-_{n,j}|^2$ over j and on time, i.e. $S_{2p}(n)=\langle[|u^+_{n,j}|^2+|u^-_{n,j}|^2]^p\rangle$ where $\langle\dots\rangle$ is the average over j and time. Model A is more intermittent than model B: for instance $\zeta_6=1.48$ for model A while it is 1.86 for model B. We remark that the variables $u^\pm_{nj}$ can be used to build a multifractal one dimensional field following the idea of previous lecture $u(x,t)=\Sigma_{nj}v_{nj}(t)\psi_{nj}(x)$ where v_{nj} are supposed to be one of the two possible dynamical variables $u^\pm_{nj}$. This implies that both models A and B provide a way to build a multifractal a one-dimensional field without employing any random multiplicative processes: randomness is supplied by the chaotic behaviour of the models.

Using both models we are able to identify the analogous of $\epsilon(r)$ for the system: at each level n we can compute the rate of energy dissipation $\eta_{nj}\equiv\nu k_n^2(|u^+_{n,j}|^2+|u^-_{n,j}|^2)$. Next, given the *length* 2^{-n+1} at the position j we need to sum all contributions at different levels n which provide a contribution to the energy dissipation rate. This procedure is represented in Fig. 43 and mathematically expressed by the following equation:

$$\epsilon_{n,j}=\eta_{n,j}+\Sigma_{m<n}\eta_{m,k(m)}+\Sigma_{m>n}\langle\eta_{m,k(m)}\rangle_{I(m)} \tag{245}$$

where $\epsilon_{n,j}$ represents the energy dissipation *averaged* at the scale 2^{-n} at the *position* j. The index $k(m)$ in the second term of rhs of (245) labels the location of larger-scale structures containing the region under consideration. In the third term, an average is performed over $k(m)\in I(m)$, where $I(m)$ labels the set of structures containing the region for any $m>n$. The rate of energy dissipation is expressed as $2^{-n+1}\Sigma_{j=1\dots2^{n-1}}\epsilon_{nj}$. From ϵ_{nj} we can build the quantities $D_p(n)\equiv\langle\epsilon^p_{nj}\rangle$. Finally,

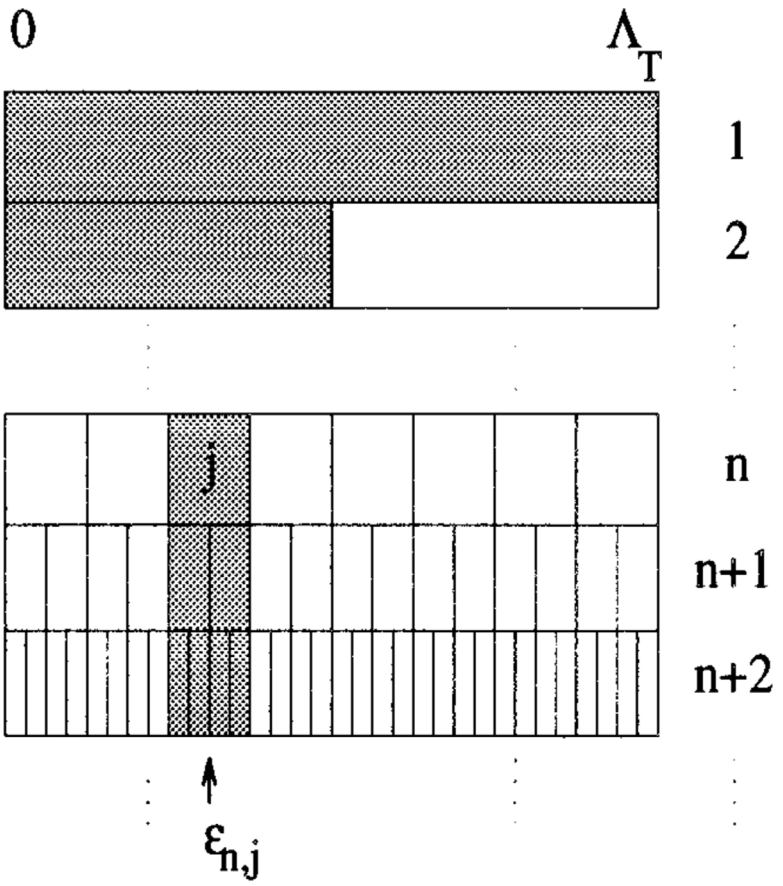

Fig. 43. A picture of the hierarchical system, covering the one-dimensional interval $[0, \Lambda_T]$.
Source: Figure reproduced from [93].

we can check the validity of the RKSH looking at the validity of the scaling relation:

$$S_{3p}(n) \sim D_p(n) S_3^p(n) \tag{246}$$

Eq. (246) is the ESS version of the RKSH discussed in the previous lecture. In Figs. 46 we show (246) for model A respectively and for $p = 4, 5, 6$ and the same result, not shown, holds for model B: in all cases, there is a clear scaling with slope 1 ± 0.01 which implies that RKSH is extremely well verified independently of the model. The basic conclusion we reach from this analysis is that RKSH is valid for shell models, i.e. the non-linear dynamics in the cascade process is consistent with the RKSH, in agreement with the scaling properties of the equation of motions. Moreover, it seems that the RKSH is independent on the horizontal interaction. If we consider the random multiplicative the process has a way to understand the geometrical structure of multifractal fields or signals, then our analysis shows that there can be other ways to generate a multifractal measure/fields which cannot be disentangled by looking at the scaling properties of the energy dissipation.

We can improve our previous analysis by looking at the correlations of the energy dissipation field at different points in space [94]. In particular, we consider the one-dimensional case i.e. the energy dissipation ϵ as a function of one space variable x and we consider $\epsilon_r(x)$ as the average of the energy dissipation on a segment of size r at the point x. Next we consider the correlation $\langle \epsilon_r(x)^q \epsilon_r(x+s)^p \rangle$ with $s > r$. Now let us assume that $\epsilon_r(x)$ is consistent with a random multiplicative process as described in the previous section or, alternatively, with the value of $\epsilon_r(x)$ obtained in the tree shell model A discussed above. Then the quantities $\epsilon_r(x)/\epsilon_s(x)$ and $\epsilon_r(x+s)/\epsilon_s(x+s)$ are statistically independent. It is always possible to write:

$$\langle \epsilon_r(x)^q \epsilon_r(x+s)^p \rangle = \langle \left[\frac{\epsilon_r(x)}{\epsilon_s(x)}\right]^q \rangle \langle \left[\frac{\epsilon_r(x+s)}{\epsilon_s(x+s)}\right]^p \rangle \langle \epsilon_s(x)^q \epsilon_s(x+s)^p \rangle \tag{247}$$

Upon defining $\tau(q) \equiv \zeta(3q) - q$ we can write $\langle [\epsilon_r(x)/\epsilon_s(x)]^q \rangle \sim (r/s)^{\tau(q)}$ and, similarly, $\langle [\epsilon_r(x+s)/\epsilon_s(x+s)]^p \rangle \sim (r/s)^{\tau(p)}$. It remains to compute the last term in (247). To do that we need to consider the common ancestor at scale l of the quantities

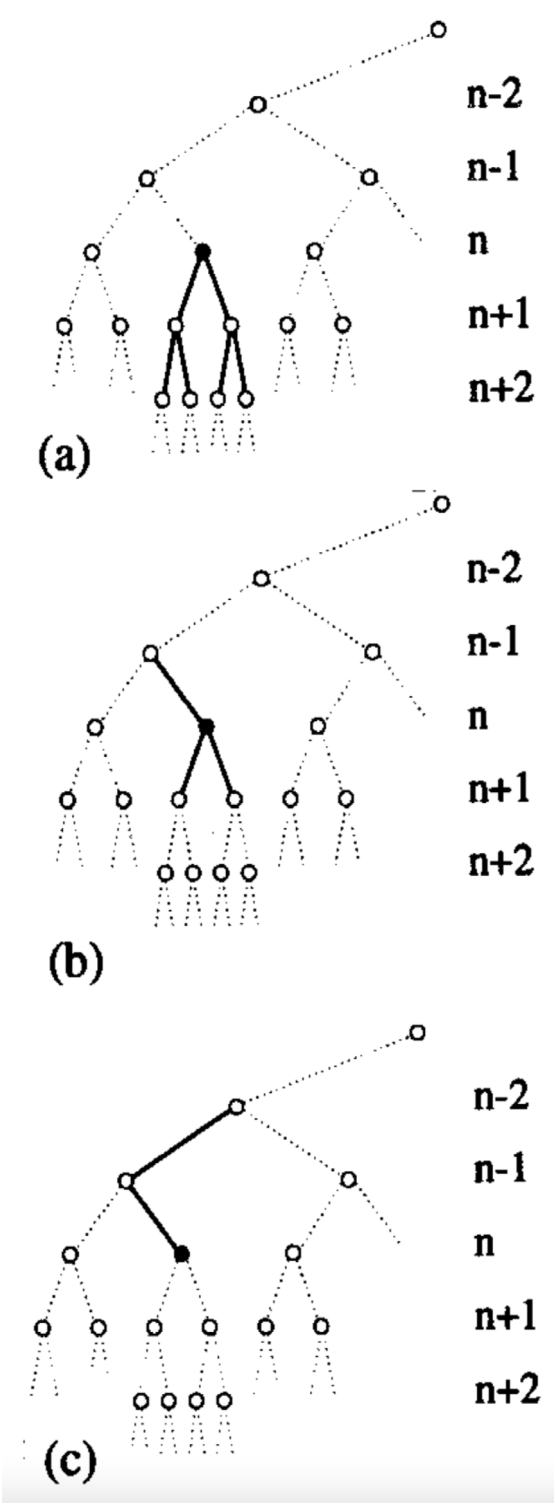

Fig. 44. Model A.
Source: Figure reproduced from [93].

$\epsilon_s(x)$ and $\epsilon_s(x+s)$. Given l (common ancestor) then we can write:

$$\langle \epsilon_s(x)^q \epsilon_s(x+s)^p \rangle = \langle \left[\frac{\epsilon_s(x)}{\epsilon_l(x)}\right]^q \rangle \langle \left[\frac{\epsilon_s(x+s)}{\epsilon_l(x+s)}\right]^p \rangle \langle \epsilon_l(x)^{q+p} \rangle_{61} \tag{248}$$

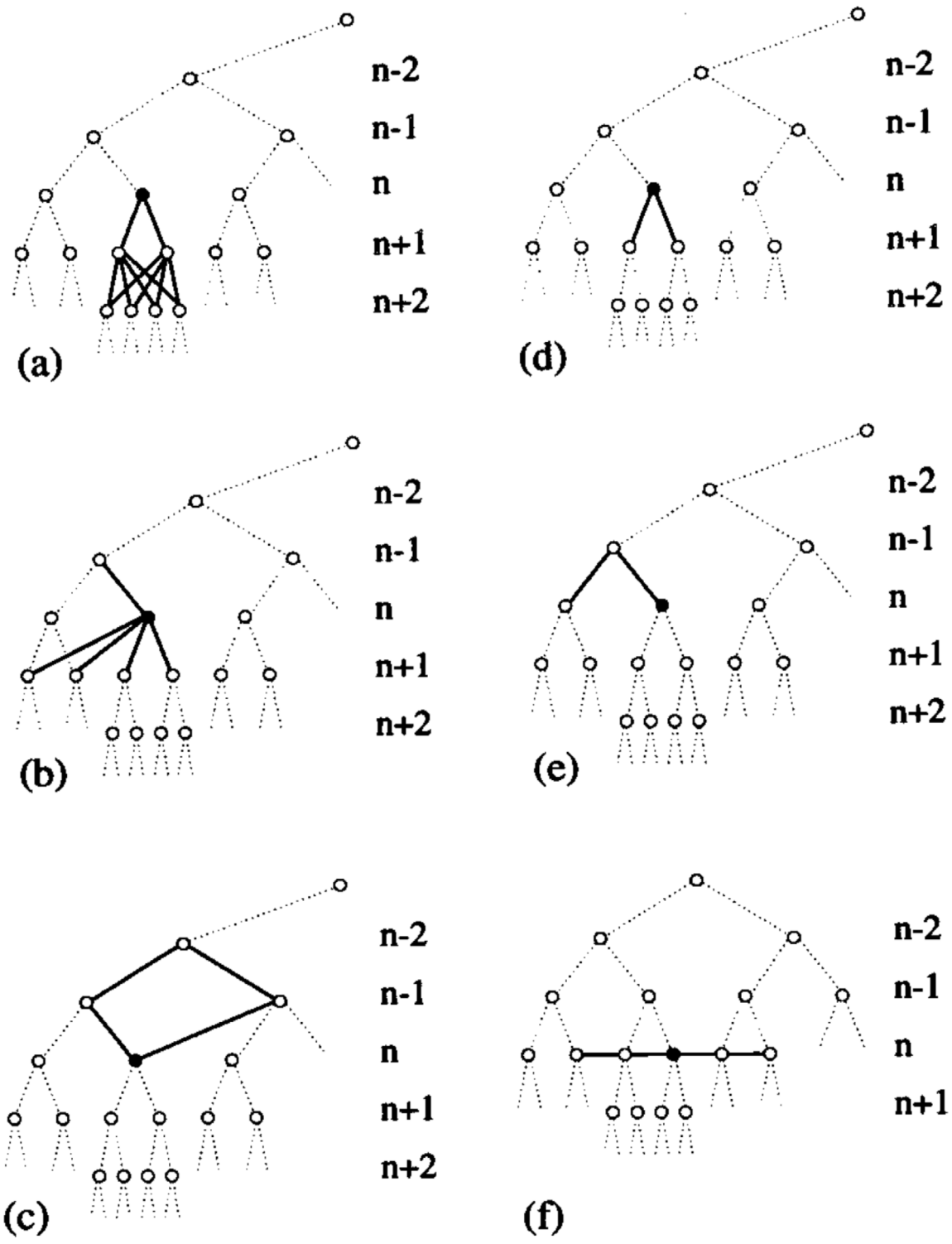

Fig. 45. Model B.
Source: Figure reproduced from [93].

Now we need to consider the probability that the points x and $x+s$ have a common ancestor of size l and we need to average (248) over this probability. Looking at Fig. 47 we understand that the probability we are looking for is simply s/l

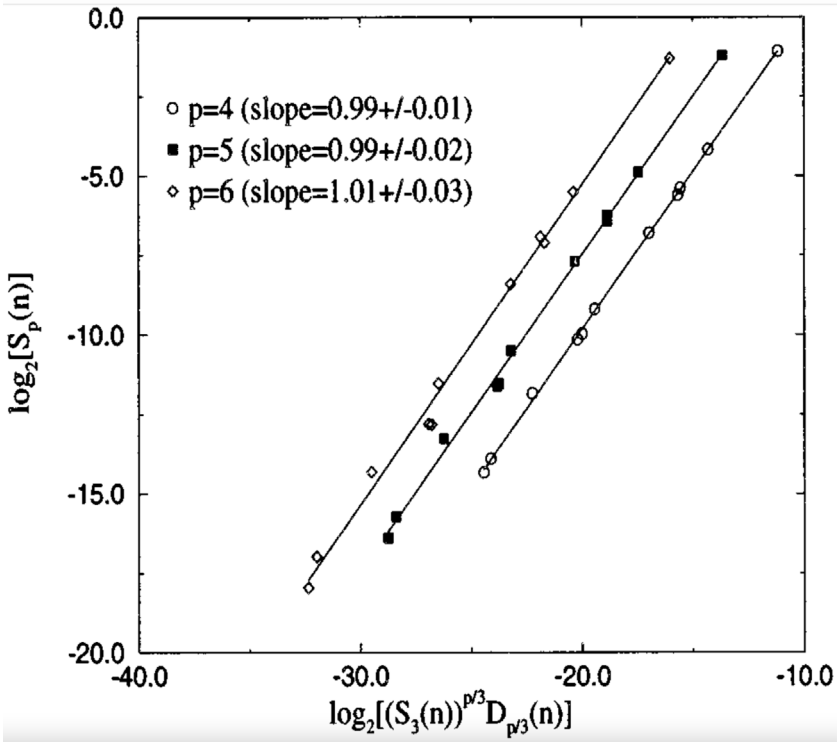

Fig. 46. Log–log plot of the velocity field structure functions, $S_p(n)$ $(p = 4, 5, 6)$, against the RKSH estimate (246).
Source: Figure reproduced from [93].

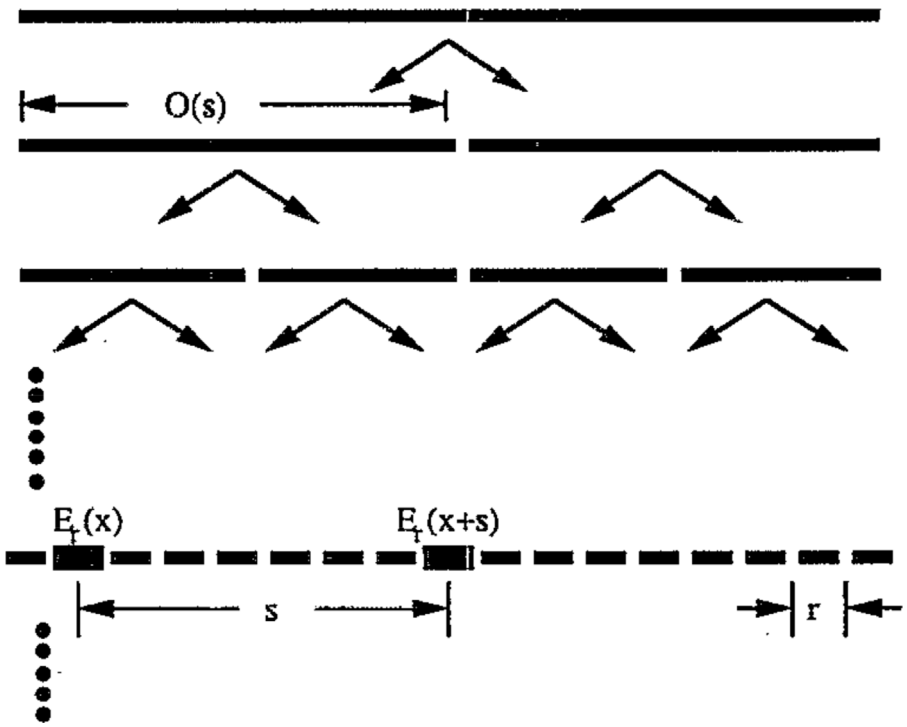

Fig. 47. Sketch of "eddies" of sizes being close together, but exhibiting no correlation because they are located at the boundary of their predecessor segments.
Source: Reproduced from [94].

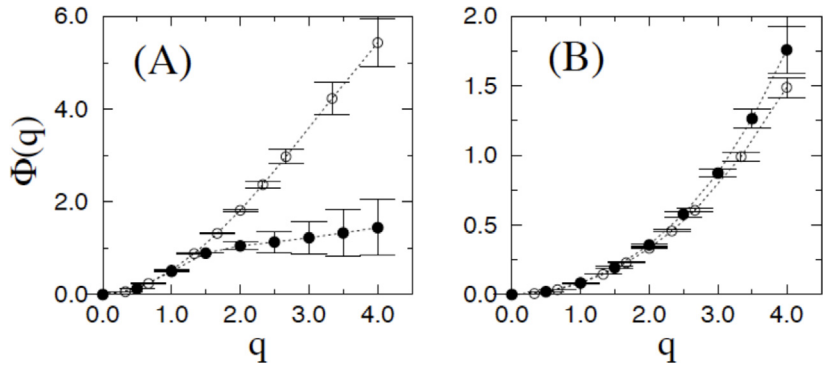

Fig. 48. Numerical results for the scaling exponent $\Phi(q)$ obtained from simulating model A (left panel) and model B (right panel). The white circles in the figure represent the quantity $-\tau(q)-\tau(-q)$.
Source: Reproduced from [95].

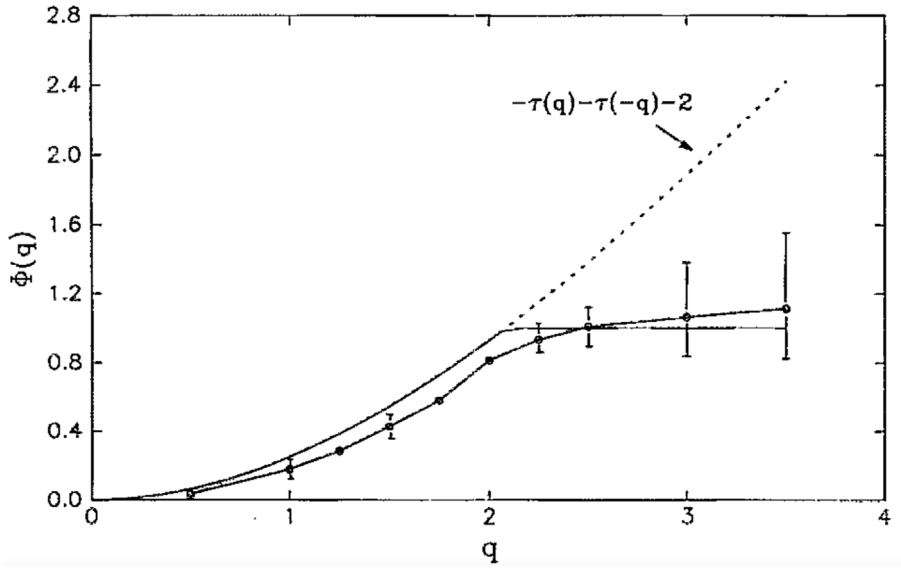

Fig. 49. Experimental and theoretical mixed scaling exponent $\phi(q)$. Circles and error bars represent the measurements and the solid line is the prediction based on the p model [96] plus the scaling transition at 1. The dashed line is the result from the p model if no scaling transition was present.
Source: Reproduced from [94].

and we must average (248) for $l = s$ to the largest scale L. This gives:

$$\langle \epsilon_s(x)^q \epsilon_s(x+s)^p \rangle \sim \Sigma_{l=s\ldots L} \left[\frac{s}{l}\right]^{\tau(q)+\tau(p)} \frac{s}{l} \left[\frac{l}{L}\right]^{\tau(q+p)} \sim \left[\frac{s}{L}\right]^{\tau(q)+\tau(p)+1} \Sigma_{l=s\ldots L} \left[\frac{l}{L}\right]^{\tau(q+p)-\tau(q)-\tau(p)-1} \tag{249}$$

We now recall that l/L in the dyadic tree can be written as 2^{-n}, i.e. the sum on the r.h.s of (249) is geometric with $s \ll L$ [94]. Although somehow trivial, the last observation enables us to reach the following conclusion: if the quantity $\tau(q+p)-\tau(q)-\tau(p)-1$ is negative then the sum is dominated by $l = s$ whereas for a positive value of $\tau(q+p)-\tau(q)-\tau(p)-1$ the sum does not scale with s (it is just a number). Putting everything together we can write (247) as:

$$\langle \epsilon_r(x)^q \epsilon_r(x+s)^p \rangle \sim \left[\frac{r}{L}\right]^{\tau(q)} \left[\frac{r}{L}\right]^{\tau(p)} \left[\frac{s}{L}\right]^{\Phi(q,p)} \tag{250}$$

where $\Phi(q,p) = \min[\tau(q+p)-\tau(q)-\tau(p), 1]$. Now we consider the case $q = -p$ for which $\tau(q+p) = 0$. Then as a function of q the quantity $\Phi(q) = \min[-\tau(q)-\tau(-q), 1]$ as sharp transition for some values of q. For instance, using the

She–Lévêque fit for the scaling exponents $\zeta(q)$, we obtain $-\tau(q)-\tau(-q) = 2\beta^q + 2\beta^{-q} - 4$ which is a positive quantity for $q > 0$. Then $\Phi(q)$ shows a sharp transition occurs around $q = 1.7$. The crucial point is that this transition (similar to a kind of thermodynamic transition) occurs if we assume that the energy dissipation is consistent with a random multiplicative process and/or the dynamics arising from model A: it is mandatory to assume a dyadic interaction on the tree for the above computations. Thus we have a way to verify our insight by computing the scaling exponents of $\langle \epsilon_r(x)^q \epsilon_s(x+s)^{-q} \rangle$ as a function of s for model A and model B. The results are displayed in Fig. 49: for model A we observe an excellent agreement with our theoretical insight (250) whereas model B does not show any sharp transition. Notes that the white circles in the figure represent the quantity $-\tau(q) - \tau(-q)$ [95].

It is now tempting to look at what happens in the experimental/numerical data. Here we consider the results discussed in [94] for a turbulent flow at high *Re* monitoring the velocity field as a function of time. The result is shown in Fig. 48 which shows a quite clear and sharp transition in qualitative and almost quantitative agreement with the dynamics given by model A. Notice that in the figure the theoretical prediction is obtained using the so-called *p model* [96] one of the possible models able to fit anomalous exponents. Regardless of the particular model, the main point here is that experimental data do show the transition as predicted by (250). We think that this is a non-trivial result which implies that our simplified view of multifractal field captures rather non-trivial *physics* of the real turbulence. Finally, let us remark that Eq. (250) and the experimental results were derived *before* the ones obtained using the space-dependent shell model.

Lecture 5.7. Summary of Lecture 5

Let us summarise our findings on shell models. Shell models demonstrate that non-linear dynamics on different *scales* can support anomalous scaling consistent with the multifractal framework of turbulent flows and the scale invariance of the equation of motions. This is a non-trivial result since it allows many theoretical investigations in simplified models. Shell models also show that anomalous scaling (i.e. multifractal) does not depend on topological/geometrical features of the energy dissipation field. Analytical computation of anomalous exponents for shell model is a the challenging theoretical problem we will discuss in the following lectures. Finally, shell models are useful tools in understanding how new general properties of turbulent flows can be described and/or analysed: if one has a new idea, shell models is a way to test this idea [97,98].

Lecture 6. Lagrangian point of view

So far we have discussed the statistical properties of turbulence discussing the Eulerian variables at a fixed position in space with the notable exception of particle acceleration analysed in Lecture 3. We want now to understand whether our approach can be extended to the statistical properties of Lagrangian turbulence when all variables are measured and/or computed (statistically) along a particle trajectory. For this purpose, the very first thing to understand is the more general form of lagrangian turbulence we want to describe.

Lecture 6.1. Motion of a lagrangian particle

To study Lagrangian turbulence we shall consider particles whose diameter a is finite and much smaller than any scale characterising turbulent fluctuations. The particle mass m_p can be equal to the mass of an equivalent volume of fluid m_f (tracer particles) or different. Since the particle is moving in a fluid we should also consider the effect of drag force on the particle velocity. A complete formulation of the equation of motions to study particle dynamics was introduced some years ago by Maxey and Riley [99]. Here we will use a simpler formulation that is enough accurate for our purpose [100]. We introduce the dimensionless numbers:

$$\beta \equiv \frac{3m_f}{m_f + 2m_p} \quad St \equiv \frac{a^2 U}{3\beta \nu L} \tag{251}$$

The quantity St is called *Stokes number* and it takes into account the drag force and the finite size a of the particle. In terms of β and St the equation of motion are:

$$\frac{d\boldsymbol{X}}{dt} = \beta \boldsymbol{u}(\boldsymbol{X}, t) + \boldsymbol{V} \tag{252}$$

$$\frac{d\boldsymbol{V}}{dt} = \frac{1}{St}[(1-\beta)\boldsymbol{u}(\boldsymbol{X}, t) - \boldsymbol{V}] \tag{253}$$

where $\boldsymbol{u}$ it the fluid velocity and $\boldsymbol{V}$ is the covelocity defined in Eq. (252). For $\beta = 1$ the first term on the r.h.s of (253) vanishes and $\boldsymbol{V}$ becomes zero on a time scale that depends on the drag effect parametrised by the Stokes number. In this case, i.e. for tracers, particle distribution is uniformly spread in space by turbulence. Then we can apply the Richardson "eddy" diffusion to describe the system. The situation is different for $\beta \neq 1$.

Let us consider the phase space $\Psi \equiv (\mathbf{X}, \mathbf{V})$ of Eqs. (252)–(253). Then it is easy to see that

$$\frac{\partial}{\partial \Psi_i} \frac{d\Psi_i}{dt} < 0 \tag{254}$$

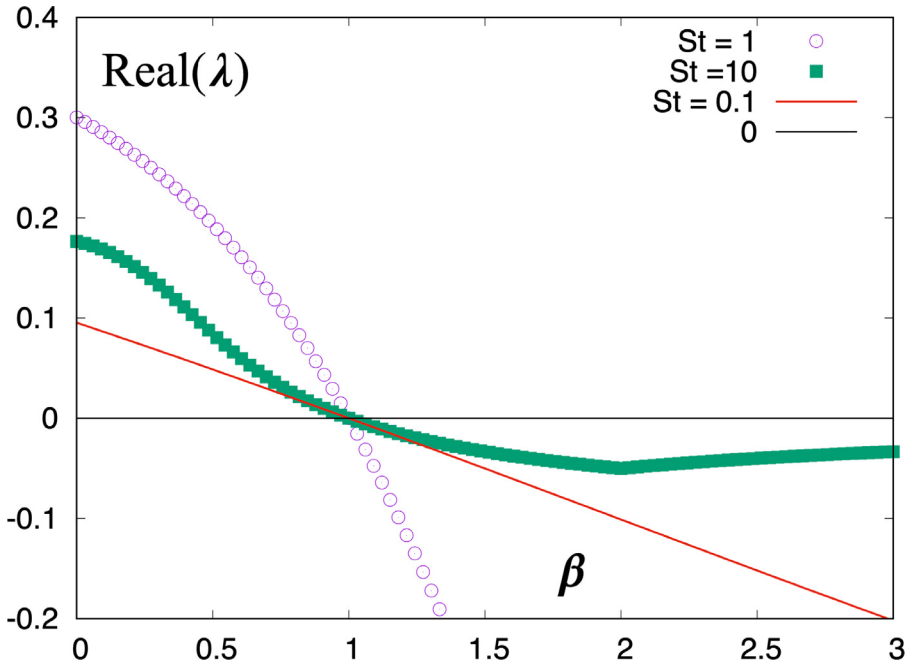

Fig. 50. Solution of Eq. (261) referring to a stationary vortex in two dimensions.

Thus we expect that $\boldsymbol{\Psi}$ (in the 2d phase space) will be asymptotic to some subset of the phase space (attractors) with a (fractal) dimension D_f usually smaller than 2d. To fix the idea, we assume that the motion is in a closed basin or with periodic boundary conditions. To understand what may happen, let us consider some simple cases and let us assume that the velocity field $\boldsymbol{u}$ is a two-dimensional flow with vorticity ω, $\boldsymbol{u} = (-\omega y, \omega x)$. Then, using (252)–(253) we obtain:

$$\frac{dX}{dt} = -\beta\omega Y + V_x \;\; ; \frac{dV_x}{dt} = \frac{1}{St}[-(1-\beta)\omega Y - V_x] \tag{255}$$

$$\frac{dY}{dt} = \beta\omega X + V_y \;\; ; \frac{dV_y}{dt} = \frac{1}{St}[(1-\beta)\omega X - V_y] \tag{256}$$

To solve these equations we use the variables $Z \equiv X + iY$ and $W \equiv V_x + iV_y$. Then the equations of motion become

$$\frac{dZ}{dt} = i\beta\omega Z + W \tag{257}$$

$$\frac{dW}{dt} = \frac{1}{St}[i(1-\beta)\omega Z - W] \tag{258}$$

The eigenvalues λ for the above equations are given by:

$$St\lambda^2 - \lambda[i\beta\omega St - 1] - i\omega = 0 \tag{259}$$

Now we look at the real part of λ which can be solved as a function of ω, St and β. In Fig. 50 we show $\Re(\lambda)$ as a function of β for different values of St and for $\omega = 1$. For $\beta < 1$ we look at *heavy particles* ($m_p > m_f$ from (251)) while for $\beta > 1$ we look at *light particles*. The information we obtain from Fig. 50 is that heavy particles tend to move out of the vortex while light particles tend to concentrate in the vortex region. Next, we look to a simple strain flow (still in two dimensions) with velocity $(\gamma x, -\gamma y)$. Following the same approach we can compute the eigenvalues of the systems from the equation:

$$St\lambda^2 + (1 - \beta St(\pm\gamma))\lambda - (\pm\gamma) = 0 \tag{260}$$

where $\pm\gamma$ are the eigenvalues of the flow. In this case, the particle follows the instability of the flow associated to the eigenvalue $\gamma > 0$.

In general [100] for both two and three-dimensional flows, if χ is an eigenvalue of the flow field, the local stability analysis for the equation in the space $(\boldsymbol{X}, \boldsymbol{V})$ can be discussed in terms of the eigenvalue λ satisfying the equation

$$St\lambda^2 + (1 - \beta St\chi)\lambda - \chi = 0 \tag{261}$$

Thus, heavy particles tend to concentrate outside the vorticity regions while light particles tend to concentrate inside the vorticity regions.

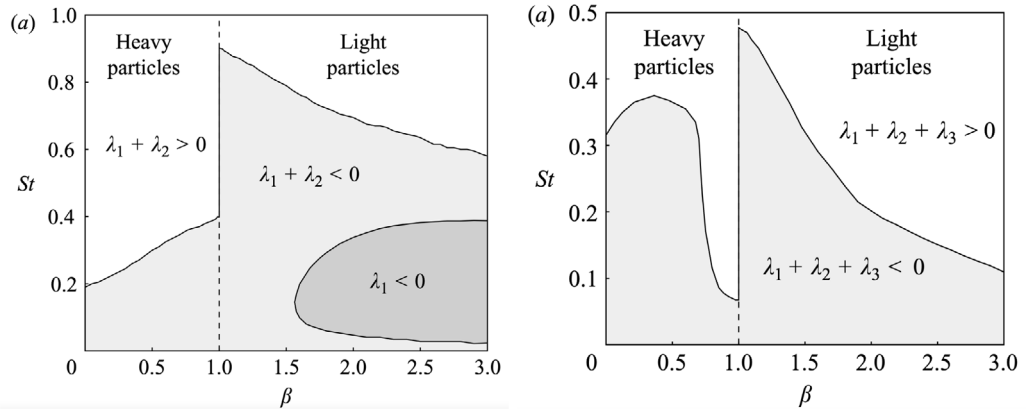

Fig. 51. Phase diagrams in the parameter space St, β for $d = 2$ (a) and $d = 3$ (b) representing the different regimes of the dynamics corresponding to different behaviours of the Lyapunov exponents.
Source: Reproduced from [100].

If the flow is non-stationary, Eq. (261) become meaningless. In principle, to understand the dynamics of particles in non-stationary or turbulent flows, we must compute all the Lyapunov exponents of the dynamical system (252)–(253), see [100,101] for details. Upon denoting by d the space dimension, there are $2d$ Lyapunov exponents of (255)–(256) which we denote by λ_i with $i = 1, 2, \ldots, 2d$ and $\lambda_1 > \lambda_2 > \ldots$. The values of the Lyapunov exponents λ_i is obtained numerically using well-established procedure. Because of (255), we know that $\Sigma_{i=1,\ldots,2d}\lambda_i < 0$ and the particle motion asymptotically occurs on an *attractor* whose dimensionality d_H is smaller than $2d$. Now the quantity $\Lambda_d \equiv \Sigma_{i=1,\ldots,d}\lambda_i$ is the rate of expansion ($\Lambda_d > 0$) or contraction ($\Lambda_d < 0$) of a volume of d dimension in the $2d$ phase space. If $\Lambda_d > 0$ then particles should uniformly spread in the *physical* d-dimensional space whereas for $\Lambda_d < 0$ particles form fractal clusters. A complete analysis of the solutions for Eq. (261) give the results shown in Fig. 51: both in two and three dimension depending on the possible Lyapunov exponents, particles tend to spread differently depending on St and β. In particular there exists regions in the parameter space where particle distribution (heavy or light) is not uniform and, eventually, show *fractal clusters* in space [101]. In Fig. 52 we show examples from direct numerical simulations for different values of St and $\beta = 0$.

We want to stress the importance of the above discussion. The non-uniformity in the particle distribution of light/heavy particles is relevant for many reasons. First of all, there exist a number of physical problems where clustering is providing the key information to understanding the physics. For instance, rain formation in clouds occurs because water vapour molecules (heavy particles) tend to cluster which provides an efficient mechanism to drop formation on a relative short time scale: tracer particles need a much longer time scale for aggregation to occur. Secondly, the statistical properties of light/heavy particles are important to probe the relevance of vortex dynamics in turbulent flows as we shall discuss later on in this lecture.

Lecture 6.2. Scaling properties of lagrangian velocity fluctuations

We now turn our attention to the velocity of a lagrangian particle and in particular of a tracer. We expect to find intermittent fluctuations in the velocity difference $\delta v(\tau) = v(t+\tau) - v(t)$ where $v(t)$ is the velocity of the tracer [102]. In Fig. 53 [43,46] we show the probability distribution of $\delta v(\tau)/\langle[\delta v(\tau)]^2\rangle^{1/2}$ for different values of τ: as expected intermittency is observed quite clearly. Can we provide any predictions on the statistical properties of $\delta v(\tau)$? According to the multifractal framework we should be able to obtain a quantitative *prediction* on intermittency for the lagrangian tracers using the scaling relation $r \to \lambda r$, $v \to \lambda^h v$. It follows that $\tau \sim r/\delta v(r) \sim r^{1-h}$. Thus, the lagrangian velocity structure functions should be obtained by the relation

$$\delta v(\tau) \sim \tau^{\frac{h}{1-h}} \quad with \quad probability \quad P_h(\tau) \sim \tau^{\frac{3-D(h)}{1-h}} \tag{262}$$

Then it follows that

$$S_n^L(\tau) \equiv \langle[\delta v(\tau)]^n\rangle \sim U_0 \left[\frac{\tau}{T}\right]^{\zeta_L(n)} \tag{263}$$

$$\zeta_L(n) = inf_h \left[\frac{nh + 3 - D(h)}{1-h}\right] \tag{264}$$

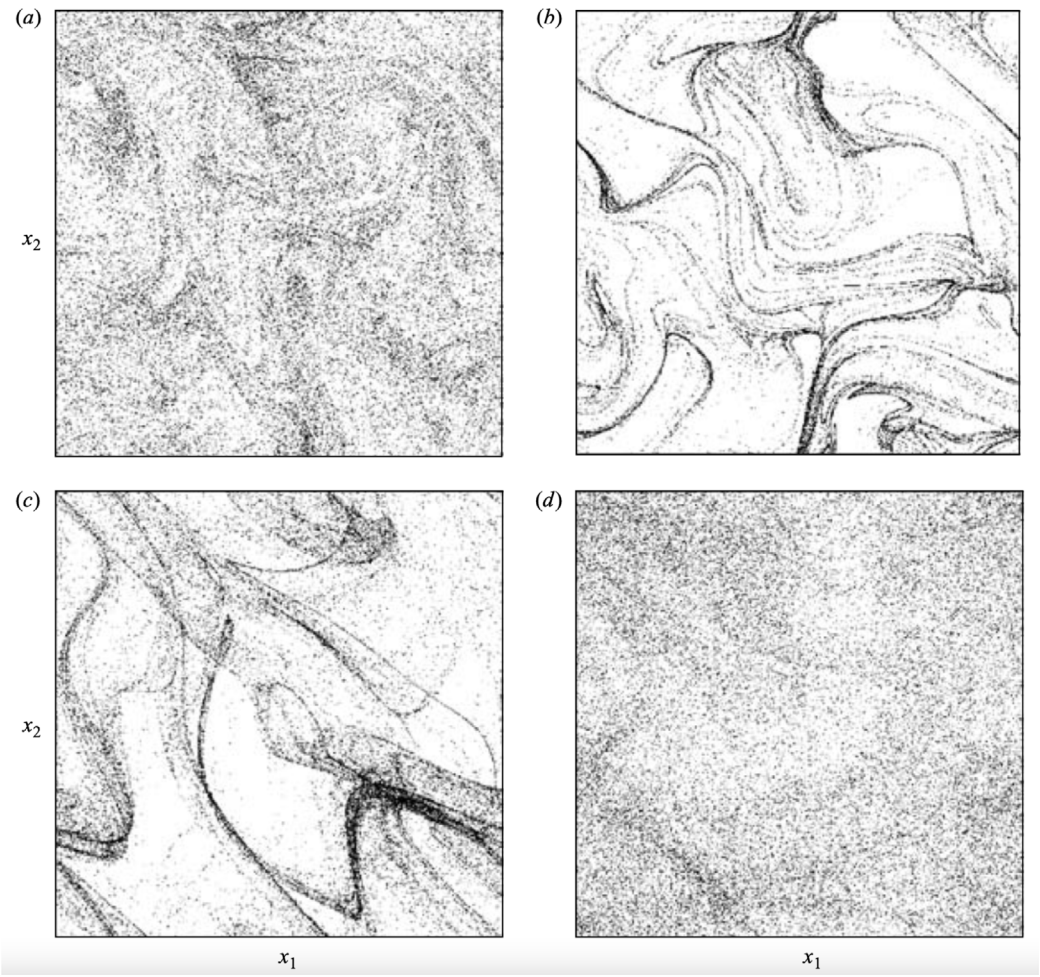

Fig. 52. Snapshots of the positions of $N = 10^5$ heavy particles ($\beta = 0$) associated to four different Stokes numbers. (a) $St = 10^{-3}$, (b) 10^{-2}, (c) 10^{-1}, (d) 1. (a), (b) and (c) correspond to values smaller than the threshold, so that particles form fractal clusters. (d) corresponds to a Stokes number larger than the critical value, so that the particles fill the whole domain.
Source: Reproduced from [100].

We highlight that Eq. (264) is a simple, remarkable and non-trivial prediction of the multifractal framework. For $n = 2$, (264) gives:

$$\left(2 - \frac{dD}{dh}\right)(1 - h) + (2h + 3 - D) = 0 \tag{265}$$

which is easily solved by using the value of $h = h_3$ for which $\zeta(3) = 1$ for the Eulerian structure-function: $dD/dh = 3$ and $3h_3 + 3 - D(h_3) = 1$. Thus we immediately obtain $\zeta_L(2) = 1$ which is the equivalent in the lagrangian case of the scaling $S_3(r) \sim r$ of Kolmogorov equation. At variance with the 4/5 equation, we cannot predict the coefficient of $S_2^L(\tau)$, i.e. we can write

$$S_2^L(\tau) \sim \epsilon\tau \tag{266}$$

Can we show that the prediction (264) is correct? This is a rather non-trivial issue both numerically and experimentally [49]. The point is that we must know the value of $D(h)$ and from there we compute $\zeta_L(n)$ to be compared against the scaling exponents observed for $S_n^L(\tau)$. Thus we have two different source of errors which sum together: the first one corresponds to the uncertainty in $D(h)$ and the second one to the scaling exponent $\zeta_L(n)$. The error on $D(h)$ is not easy to be computed in this case and an extensive study on this problem can be accurately performed using numerical simulations where the lagrangian structure functions can be computed using order 10^8 different particles [49].

The main problem comes from the isotropy condition. In Eulerian framework, isotropy can be checked on the structure functions and, upon increasing the order n of the structure-function, non-isotropic contribution can be observed for finite Re even if one uses random isotropic forcing. This has to be expected and we discuss the issue in Lecture 8. Here we

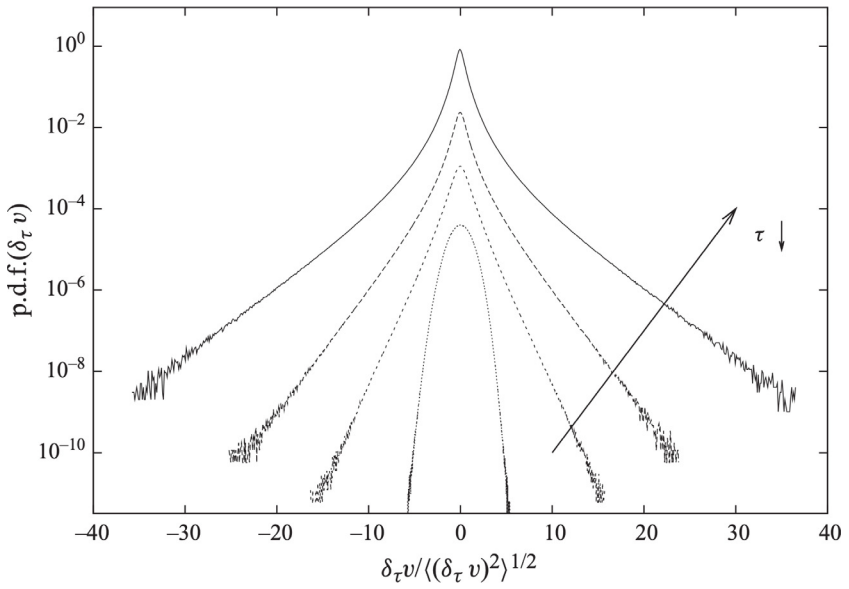

Fig. 53. Lagrangian p.d.f. for a single component velocity increments along particle trajectories, over different time increments, $\tau \in [2 : 400]\tau_\eta$. Curves are shifted along the y-axis for presentation purposes.
Source: Reproduced from [49].

use a rather pragmatic procedure: we can define two sets of scaling exponents: $\zeta_l(n)$ which refer to the *longitudinal* structure functions and $\zeta_t(n)$ which refer to the *transversal* structure functions. They should be the same for isotropic turbulence. However, at large n there is some difference induced by the error in estimating the scaling exponents and the non-isotropic contribution which cannot be avoided at finite Re. This is shown in Fig. 54 using the numerical simulations described in [49]: notice that up to $n = 6$ the difference between $\zeta_l(n)$ and $\zeta_t(n)$ is inside error bars whereas this is not the case for $n = 8, 10$. Starting from the two different sets of the exponents, we can define $D_L(h)$ and $D_T(h)$ obtained from $\zeta_l(n)$ and $\zeta_t(n)$ respectively. This requires some fitting procedure which introduces other errors anyway [49]. From $D_L(h)$ and $D_T(h)$ we can compute two possible estimates of the lagrangian exponents $\zeta_L(n)$: the two values represent the theoretical prediction with the uncertainty (error) due to finite Re and statistical errors. To estimate $\zeta_L(n)$ we use the lagrangian version of the ESS already discussed in Lecture 3: we compute the exponent $\chi^{(n)} \equiv \zeta_L(n)/\zeta_L(2)$ as a proper estimate of $\zeta_L(n)$ because of the scaling ansatz (266). The final result is shown in Fig. 55: up to $n = 8$ and within the error bars, there is a quite good agreement between $\zeta_L(n)$ computed from (264) and the observed scaling exponents (the error in estimating $\zeta_L(10)$ is too large for any possible comparison). The final outcome of this rather complex data analysis is that Eq. (264), with the *same* function $D(h)$ used for Eulerian intermittency, is consistent with the anomalous scaling of Lagrangian structure functions.

As a final remark let us note that this is a clear example where the computation of known uncertainty should be taken into account to obtain a fair comparison between a quantitative *prediction* and the experimental/numerical data.

Lecture 6.3. Dissipation range in lagrangian turbulence

There is another important point to explore using lagrangian turbulence. The Kolmogorov theory as well as the multifractal framework predicts that viscous effect becomes relevant at the Kolmogorov scale plus multifractal fluctuations. In the *time* domain, which is the one we use for the lagrangian structure functions $S_n^L(\tau)$, the proper quantity to consider is the Kolmogorov time τ_k. We observe that $\tau_k/T \sim Re^{-1/2}$ whereas in the *space* domain the viscous effect depends on Re through the ratio $\eta_k/L \sim Re^{-3/4}$. The observation is that viscous effect is more pronounced for the lagrangian structure functions $S_n^L(\tau)$ with respect to the Eulerian ones. This implies that the lagrangian turbulence is most suited to study the multifractal predictions on the fluctuations of the viscous scale.

We expect that the dissipation time scale τ_η depends on h in analogy to the Eulerian case. The dissipative scale $\tau_\eta(h)$ can be computed using the same approach followed in Lecture 4 on the intermittency in the dissipation range. Using Eq. (262) the condition for the dissipative time scale reads:

$$U\left(\frac{\tau}{T}\right)^{h/(1-h)}\left(\frac{\tau}{T}\right)^{h/(1-h)} L \sim \nu \rightarrow \left(\frac{\tau_\eta(h)}{T}\right) \sim Re^{-(1-h)/(1+h)} \tag{267}$$

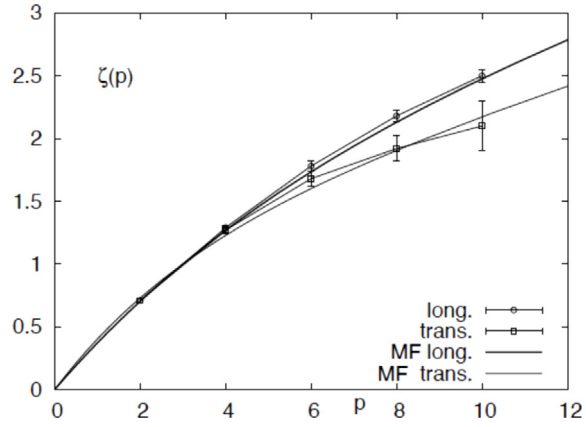

Fig. 54. Comparison between Eulerian scaling exponents for longitudinal, $\zeta_l(p)$, and transverse, $\zeta_t(p)$ Structure Function together with two different multifractal predictions (MF) obtained with two different choices of $D(h)$.
Source: Reproduced from [76].

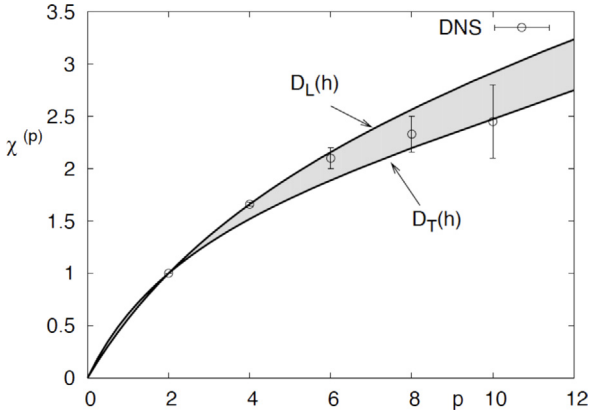

Fig. 55. Summary of the Lagrangian scaling exponents, $\xi(p) = \zeta(p)/\zeta(2)$ (circles), as measured in the inertial range in our numerics, together with the prediction obtained from the Eulerian statistics by using the bridge relation either with the longitudinal Eulerian statistics (upper limit of the shadowed area) or with the transverse one (lower limit of the shadowed area). The previous measurement of Lagrangian scaling exponents are also shown (see Table 2).
Source: Reproduced from [49].

where $U = L/T$ is the characteristic large scale velocity. Eq. (267) is valid with probability

$$P_h[Re] \sim \left(\frac{\tau_\eta(h)}{T}\right)^{(3-D(h))/(1-h)} = Re^{-(3-D(h))/(1+h)} \tag{268}$$

Actually, we use the above equations to compute the probability distribution of the acceleration of Lagrangian particles. As a first check for the validity of (267) and (268), we can compute the average of $\delta(\tau)^2/\tau$ in the dissipation time scale:

$$\begin{aligned}\left\langle \frac{\delta v(\tau)^2}{\tau} \right\rangle &\sim \int_h dh Re^{-(3h-1)(1-h)/(1+h)(1-h)} Re^{-(3-D(h))/(1+h)} \\ &= \int_h dh Re^{-(3h-1+3-D(h))/(1+h)} = const\end{aligned} \tag{269}$$

The above result follows from the constrain $\zeta_E(3) = 1$ and it is consistent with the fact that

$$\epsilon = \left\langle \frac{\delta v(\tau)^2}{\tau} \right\rangle$$

Following the analysis done in Lecture 4 we already know that the quantities

$$a_n(\tau) \equiv \frac{d\log[S_n^L(\tau)]}{d\log[S_2^L(\tau)]} \tag{270}$$

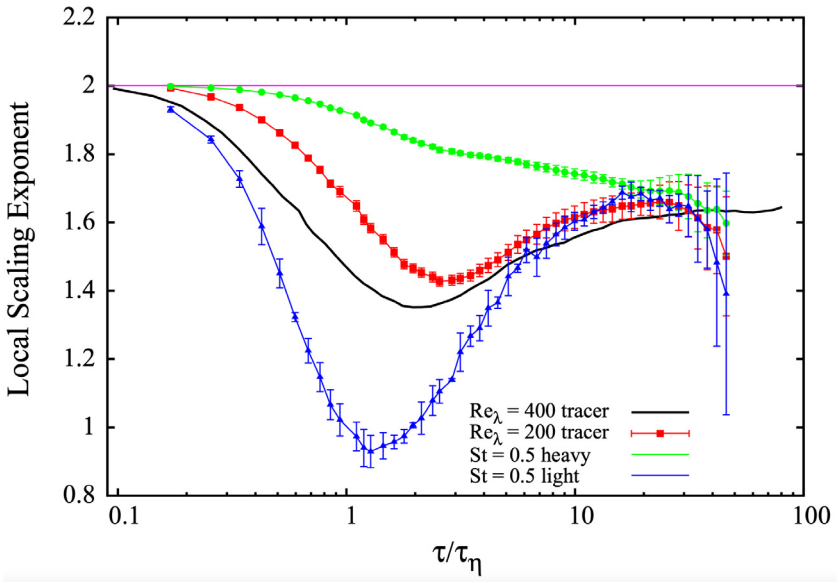

Fig. 56. Comparison of local scaling exponents for the 4th order Lagrangian Flatness between: (i) tracers particles at two different Reynolds numbers (ii) one light and (iii) one heavy particle. Notice the enhancement (depletion) of the bottleneck around $\tau/\tau_\eta \sim 1$ for light (heavy) particles with respect to the tracers' statistics. The horizontal line corresponds to the K41 non-intermittent prediction = 2.
Source: Figure reproduced from [76].

should show, for $n > 2$, a dip in the dissipative region. In Fig. 56 we show $a_4(\tau)$ for three kinds of particles: heavy, tracers and light particles [103,104]. As we previously discussed, heavy particles move *outside* vortex filaments and light particles *inside*. From the figure, we see that a clear dip is observed for both tracers and light particles, the latter shows a more pronounced dip while we do not observe any dip for the heavy particles. From this observation we can *naively* deduce that vortex filaments are responsible for the intermittency increase (dip) in the dissipation range. This conclusion is however misleading. In fact, we have already shown that the probability distribution of particle accelerations is well explained by the multifractal framework, Eqs. (267)–(268), even if we do observe strong fluctuations of the velocity when particles are inside a vortex filament. In other words, the information about vortex filaments are *statistically* embedded in the multifractal framework. This is not something strange since, physically, it is simply a consequence of the zeroth law of turbulence and the NS invariance under the transformation $r \to \lambda r$, $v \to \lambda^h v$ with the multifractal probability distribution $\lambda^{3-D(h)}$. Light and heavy particles sample different region of the turbulent flows and the effective advection field is compressible. This implies that their lagrangian velocity fluctuations are subject to different cutoff time scales in the dissipation range.

Next, using the same reasoning of Lecture 4, we can now employ our knowledge of $D(h)$ coming from the scaling exponents of the Eulerian structure functions to predict the dip observed for tracers in the figure. The idea is to assume the velocity increments $\delta v(\tau)$ can be expressed as $G(\tau,\tau_\eta)F(\tau,\tau_\eta)^{h/1-h}$ with probability $F(\tau,\tau_\eta)^{(3-D(h))/(1-h)}$ where $G \sim const$, $F \sim \tau$ for large τ while $G \sim \tau$ and $F \sim const$ for small τ. Obviously, some best fit over the functions F and G is needed taking into account the *known* uncertainty on the estimate for $D(h)$. For this case [105], a good result is obtained using:

$$\delta v(\tau) \sim U \left[\frac{K(x)}{1+K(x)}\right]^{1/\beta} \left(\frac{\tau_\eta}{T}\right)^{h/(1-h)} \left[(1+K(x))^{1/\beta}\right]^{h/(1-h)} \tag{271}$$

$$P_h\left(\frac{\tau}{T}\right) \sim \left[\left(\frac{\tau_\eta}{T}\right)(1+K(x))^{1/\beta}\right]^{(3-D(h))/(1-h)} \tag{272}$$

$$x \equiv \frac{\tau}{\tau_\eta} \tag{273}$$

$$K(x) \equiv x^\beta \tag{274}$$

where τ_η is a function of h from (267) and $\beta = 4$. Although different from what we did in Lecture 4, the above choices in Eqs. (271)–(274) provides similar results. In particular, $a_n(\tau)$ given by (270) shows a minimum (dip) in the dissipation region. In Fig. 57 we show the final result for $a_4(\tau)$ [105]: several experimental and numerical data are plotted in the same figure together with the coloured area which represents the theoretical predictions with their uncertainty. One observes a clear collapse of all data on the same curve *within the error bars* as well as the agreement with the theoretical prediction using the above fitting procedure. Note that the data comes from different values of $Re_\lambda \sim Re^{1/2}$ and one can wonder whether the dip is somehow independent of Re. According to our discussion in Lecture 4 there should be a very

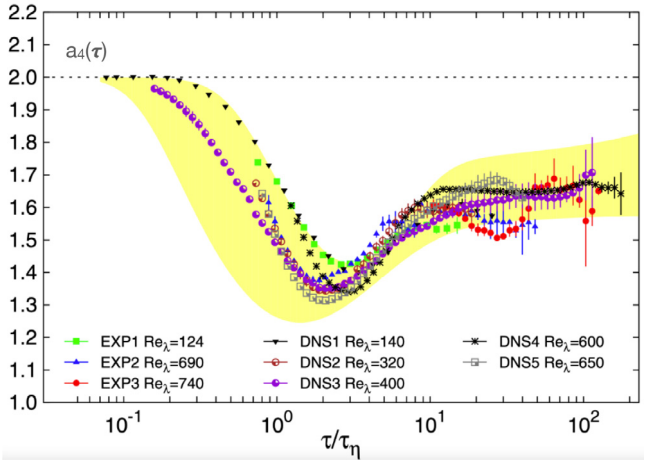

Fig. 57. The quantity $a_4(\tau)$ obtained from different numerical simulations and experimental data (see symbols). The coloured area shows the theoretical prediction with the error bars, see [105] for details from which this figure is reproduced.
Source: Figure reproduced from [105].

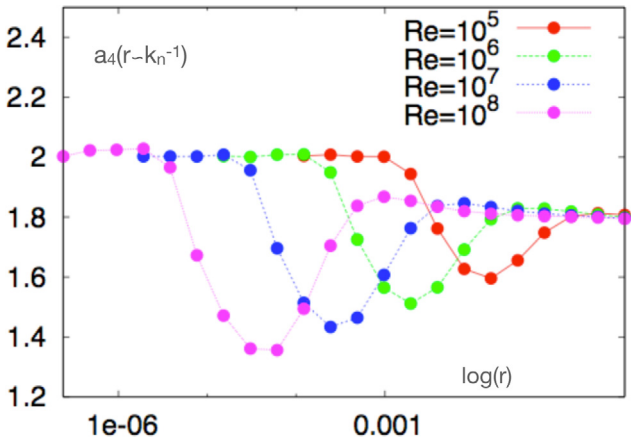

Fig. 58. The quantity $a_4(r) = d\log S_4(r)/d\log S_2(r)$ computed using the *Sabra* shell model for different *Re*. Here r is taken as k_n^{-1}.

weak dependence on *Re* which cannot be observed in the range of *Re* shown in the figure. Fig. 57 refers to many different experimental/numerical cases and highlight the statement of universality in anomalous scaling.

We want to remark that the increase of intermittency (dip) within the dissipation range can also be studied in shell models. In Fig. 58 we show $a_4(r)$ computed for the Eulerian structure functions for a Sabra model at different *Re* with $r \sim k_n^{-1}$. Note that $r \sim k_n^{-1}$ in the figure. The dip is clearly observed and it becomes deeper upon increasing *Re* although the *Re* dependence is extremely weak. We also notice that in the shell model there is no vortex structure whereas the dip in the dissipation range is clearly similar to the one previously observed.

Lecture 6.4. Large eddy simulations

As we have seen, using lagrangian trajectories we can test the prediction of the multifractal framework in the dissipation range with a rather good accuracy and we can validate, within error bars, the "strong" statement that all the statistical properties, i.e. scaling, of turbulence can be derived from the knowledge of $D(h)$. Although vortex filaments or other fluid structures are present in any turbulent flow, their relevance in the statistical picture of turbulence is embedded in $D(h)$. One important question to answer is whether $D(h)$ is dependent or not on the dissipation mechanism [106]. Let us recall that we can compute $D(h)$ from the anomalous scaling exponents $\zeta(n)$ in the inertial range. Can we show that, upon changing the way turbulence is dissipated, $D(h)$ is unchanged? This is a question that can be investigated using numerical simulations.

We consider homogeneous and isotropic turbulence at two different resolutions 1024 and 8192 grid points corresponding to $Re = 2 \times 10^4$ and $Re = 3 \times 10^5$ respectively. We refer to these cases as *DNSx1* and *DNSx8*. For each simulation

we compute the scaling exponents in the inertial range and we look at the quantities $a_n(r) \equiv d\log S_4(r)/d\log S_2(r) \equiv \xi_n(r)/\xi_2(r)$ for all numerical simulations and for $n = 4, 6$, where $\xi_n(r)$ refers to the local scaling exponents of $S_n(r)$ defined as $\xi_n(r) = d\log S_n(r)/d\log(r)$. We use $a_n(r)$ as a proper measure of the intermittency. Next, we consider a completely different set of simulations based on the following idea. We solve the NS equations in the spectral domain at resolution 1024 corresponding to a maximum wave number $k_m = 512$ and we neglect the dissipation term $-\nu k^2$ in the dynamics. Next, we assume that the turbulent energy $E(k)$ for $k > k_c$ follows the inertial range dynamics. This can be done by imposing that $E(k)$, for $k > k_c$, follows the same dynamics of $E(k_c)$:

$$\frac{dE_k(t)}{dt} = \left(\frac{k_c}{k}\right)^{5/3} \frac{dE_{k_c}(t)}{dt} \tag{275}$$

Let us define by $\hat{T}_k(t)$ the Fourier projection of the non-linear terms (including pressure) of the NS equations and by $T_k(t) = \Sigma_{|k|=k} u_k^*(t)\hat{T}_k(t)$ where $u_k(t)$ is the Fourier projection of the velocity field. Then we solve the dynamics of $u_k(t)$ using the equations:

$$\partial_t u_k(t) = \hat{T}_k(t) - \gamma_k\lambda_k(t)u_k(t) + \dots \tag{276}$$

$$\lambda_k(t) = \frac{1}{2}\frac{T_k(t) - (k_c/k)^{5/3}T_{k_c}(t)}{E_k(t)} \tag{277}$$

with $\gamma_k = 0$ for $k < k_c$ and $\gamma_k = 1$ for $k_m > k > k_c$ and the dots in (276) represent the forcing term acting on the large scale. Upon multiplying by $u_k^*(t)$ Eq. (276) and summing over all wave numbers with $|k| = k$ and recalling that $E_k(t) = 1/2\,\Sigma_{|k|=k}u_k(t)u_k^*(t)$ we obtain:

$$\frac{dE_k}{dt} = T_k(t) - [T_k(t) - (k_c/k)^{5/3}T_{k_c}(t)] = \left(\frac{k_c}{k}\right)^{5/3}\frac{dE_{k_c}(t)}{dt} \tag{278}$$

which is the desired result. We call this simulation *SGSM-sharp* where *sharp* refers to the change form 0 to 1 of γ_k. We can also smooth the *sharpness* of γ_k by assuming some smoothing function, whose details are irrelevant in this discussion, and we refer to this case as *SGSM-smooth*. Here *SGSM* refers to *sub-grid scale modelling*. Using this idea we can achieve with a resolution of 1024 points the value $Re = 2 \times 10^5$ for *SGSM-sharp* and $Re = 4 \times 10^5$ for *SGSM-smooth*.

In Fig. 59 we show the value of $a_n(r) \equiv d\log S_4(r)/d\log S_2(r) \equiv \xi_n(r)/\xi_2(r)$ for all numerical simulations and for $n = 4, 6$. For DNSx1 and DNSx8 we observe a rather clear plateau of $a_n(r)$ in the inertial range followed by a dip which is increasing (very weakly) upon increasing the value of *Re*. In the same figure we show $a_n(r)$ for SGSM-sharp and SGSM-smooth: again we can see the plateau for almost the same values observed in the DNSx1 and DNSx8 but now there is no dip because the viscous range is suppressed in the system. Finally in the insets we show $F_n(r) \equiv S_n(r)/S_n(r)^{n/2}$ for $n = 4, 6$. Note that, using the known anomalous exponents discussed in Lecture 3 or the She–Lévêque fit (167), we have in the inertial range $F_r(r) \sim r^{-0.11}$ and $F_6(r) \sim r^{-0.31}$. Obviously, for *SGSM* either sharp or smooth, $F_n(r)$ are not defined in the dissipation range, although their scaling behaviour is consistent with the known experimental/numerical results in the inertial range. This is clear-cut evidence that the anomalous scaling in the inertial range is independent on the detail dynamics of the dissipation range. In other words, the function $D(h)$ is independent of the dissipation mechanism, a very non-trivial statement.

Lecture 6.5. Summary of Lecture 6

There is a lot of interesting physics which we can understand by looking at the properties of lagrangian particles in fully developed flows. In this lecture, we have discussed some (but not all) of them. We consider an important achievement that, within the experimental/numerical uncertainties, the multifractal theoretical framework is able to give well-defined predictions. In particular, we have shown how lagrangian turbulence can be considered a *magnifying glass* to understand fluctuations in the dissipation range. In general, intermittency is enhanced for lagrangian velocity fluctuations and this effect is even stronger in the dissipation range. Our analysis shows that intermittency in the dissipation range can be explained using the very same $D(h)$ obtained from Eulerian inertial range scaling of the structure functions, at least within terror bars. This is an important achievement in understanding turbulent flows and it is important to increase the quality of numerical simulations and experimental results to enhance the overall accuracy. A related question we were able to answer is whether intermittency is driven by strong fluctuations in the dissipation range or the other way round strong intermittency in the dissipation range are generated by fluctuations in the energy transfer *within the inertial range*. Numerical simulations show that inertial range intermittency is the mechanism driving the fluctuations in the dissipation range. From the physical point of view, this implies that scale invariance properties of the Euler equations, supplemented by the zeroth law of turbulence, are acting behind the intermittent fluctuations independently of the formation of vortex filaments and/or tubes characterising the dissipation range.

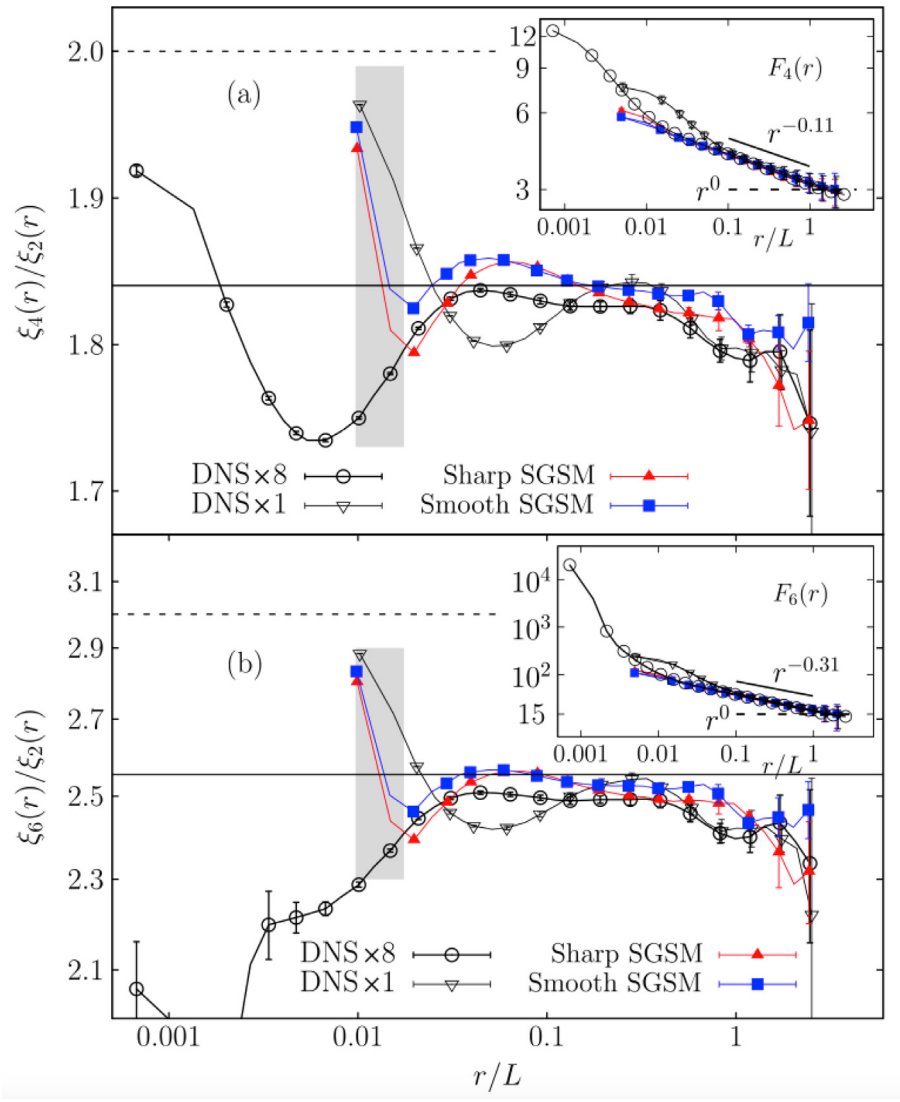

Fig. 59. Log-lin plot of $\xi_4(r)/\xi_2(r)$ for (a) $n = 4$ and (b) $n = 6$ for SGSM and DNS data. The dashed line is the Kolmogorov scaling while the solid line refers to the anomalous scaling. In grey, we indicate the range of scales where the closure is applied. Inset: log–log plot of $F_n(r) \equiv S_n(r)/S_2(r)^{n/2}$ versus r.
Source: Reproduced from [106].

Lecture 7. Passive scalar turbulence

Lecture 7.1. Scaling and intermittency in the advection of a passive scalar

We already introduced the equation for a passive scalar $\theta(x + r)$ advected by a flow $\boldsymbol{v}$:

$$\partial_t \theta + \boldsymbol{v} \cdot \boldsymbol{\nabla} \theta = \kappa \Delta \theta + f_\theta \tag{279}$$

We are interested in understanding the statistical properties of the "passive turbulence" described by θ assuming that $\boldsymbol{v}$ is a homogeneous and isotropic turbulent velocity field. This implies that we assume the forcing f_θ in Eq. (279) to be a large-scale homogeneous and isotropic forcing. We meanly focus on three-dimensional flows. In analogy to the study developed for homogeneous and isotropic velocity fluctuations in turbulence, we consider the quantities

$$F_p(r) \equiv \langle [\delta\theta(r)]^p \rangle \tag{280}$$

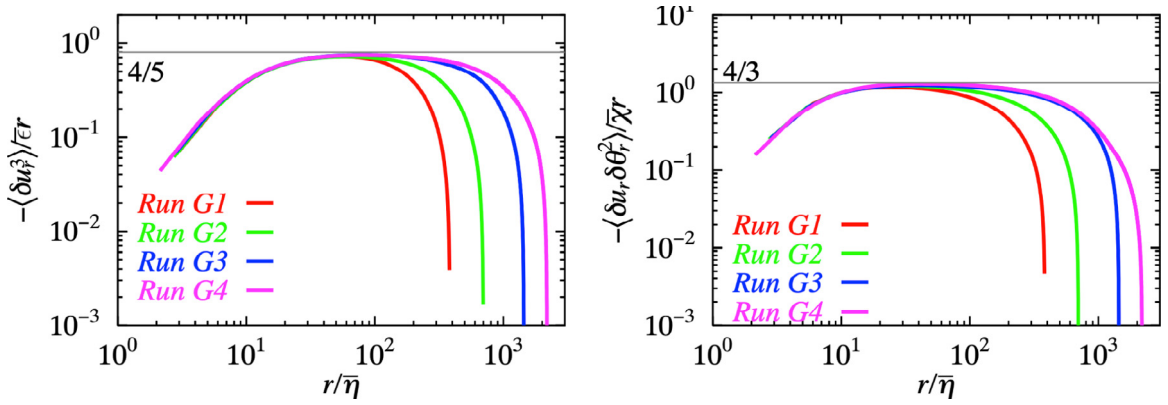

Fig. 60. Approach to the 4/5 and 4/3 laws at the increasing of R_λ. Left: The 4/5 law, Right: the 4/3 law. G1: $R_\lambda = 174$, G2: $R_\lambda = 263$, G3: $R_\lambda = 468$, G4: $R_\lambda = 586$.
Source: Figure reproduced from [107].

with $\delta\theta(r) = \theta(x + r) - \theta(x)$. We expect that $\delta\theta(r)$ shows intermittency fluctuations. We first notice that Eq. (279) is invariant under the transformation

$$r \to \lambda r \tag{281}$$
$$v \to \lambda^h v \tag{282}$$
$$t \to \lambda^{1-h} t \tag{283}$$
$$\theta \to \lambda^{h_1} \theta \tag{284}$$
$$\kappa \to \lambda^{h+1} \kappa \tag{285}$$

In other words, the scaling of θ is not linked to the one of the velocity fields. For Eq. (279) there exists the analogous of the 4/5 law for the passive scalar, namely;

$$\langle \delta v(r) \delta\theta(r)^2 \rangle \sim -Nr \tag{286}$$

where N is the rate of "passive scalar dissipation" in the system, see Fig. 60 [36]. We are assuming, in analogy to the velocity field, that N is independent of Re and κ, which is well documented in experimental/numerical data. Let us remark that under the transformation (281), we have $N \to \lambda^{2h_1+h-1} N$. Thus, assuming Kolmogorov scaling $h = 1/3$, we expect that $h_1 = 1/3$ as well. However, according to the multifractal framework, the constraint $2h_1 + h - 1 = 0$ is true *on average* and it does not imply any well-defined relation between h_1 and h.

The above discussion has several consequences:

- The passive scalar may show intermittent fluctuations with anomalous exponent for $F_{2p}(r)$; however, there is no simple link between the anomalous scaling for the passive scalar and the one characterising the velocity field.
- Intermittency for the passive scalar may be described by the multifractal framework, i.e. assuming that $\delta\theta(r) \sim r^{h_1}$ with $P_{h_1}[r] \sim r^{3-D(h_1)}$; however we do not know how $D(h_1)$ is linked with the analogous function $D(h)$ for the velocity field.
- The passive scalar may be intermittent *even if the velocity field is not*.
- In general we need to know the joint probability distribution $P_{h,h_1}[r]$ for $\delta v(r)$ and $\delta\theta(r)$.

As we can see, intermittency for the passive scalar may be more complex than the one observed in the N.S. equation.

For three-dimensional turbulence, intermittency in the passive scalar fluctuations is well documented from both experimental and numerical data (see Fig. 63) [36,39,109]. Upon defining

$$F_{2p}(r) \sim r^{\xi(2p)} \tag{287}$$

we observe that $\xi(2p)$ are smaller than the corresponding scaling exponents of the velocity field [109] (see Fig. 61 and Table 2).

For $p = 1$ we can obtain a lower bound to the exponent $\xi(2)$ by assuming that the fluctuations $\epsilon(r)$ of energy dissipation at scale r and the fluctuations of passive dissipation $N(r)$ are uncorrelated, where

$$N(r) = \frac{1}{r^3} \int_{B(r)} \kappa (\nabla\theta)^2 d^3 r \tag{288}$$

Then, following [110], we obtain

$$F_2(r) \sim r^{2/3} \epsilon(r)^{-1//3} N(r) \sim r^{1+\xi(-1)} \tag{289}$$

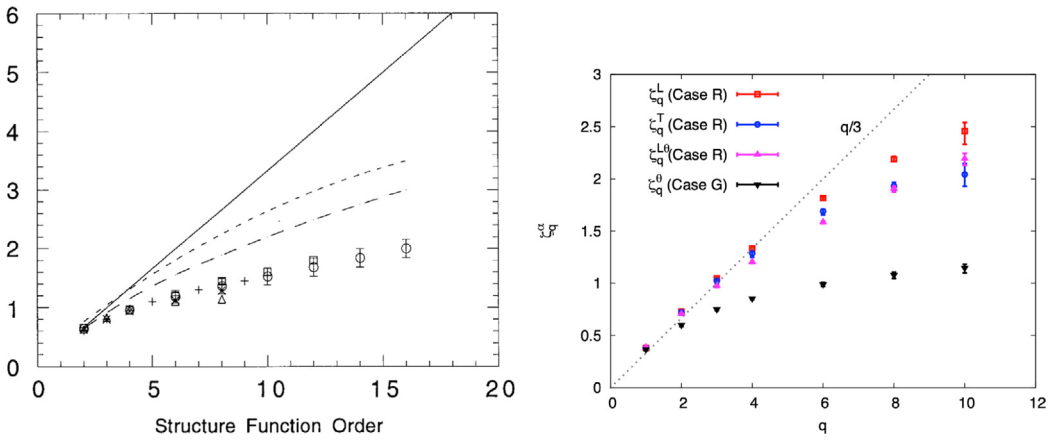

Fig. 61. (Left) The scaling exponent ζ_n for the scalar structure function $\langle[\Delta\theta(r)]^n\rangle$ within the inertial subrange as a function of n. Different symbols correspond to different experiments and fully resolved numerical simulations. The long-dashed line is the white-noise estimate from Kraichnan (1994) while the short-dashed line is for the velocity field from Anselmet (1984). The solid line is the Kolmogorov–Obukhov–Corrsin (KOC) prediction. (Right) Scaling exponents ζ_q^L, ζ_q^T and ζ_q^θ for $q = 1, \ldots, 10$. The straight line shows the Obkhov–Corrsin scaling.
Source: (Left) Figure reproduced from [39]. (Right) Figure reproduced from [107].

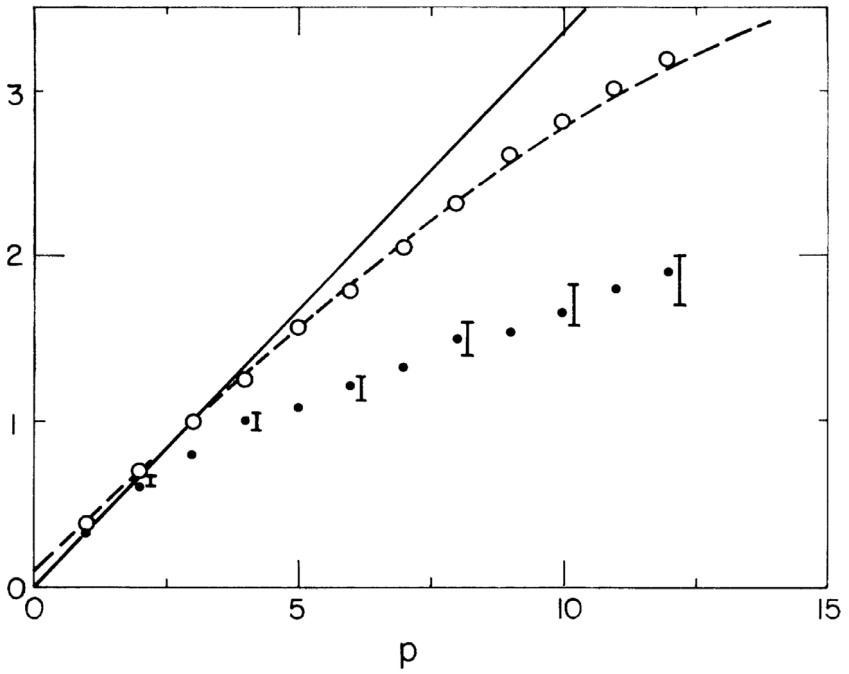

Fig. 62. The open circles show the scaling exponent of the *GOY* shell model while the dots represent the scaling exponents for the shell model of the passive scalar Eq. (290). The continuous line is the K41 theory while the dashed line shows a possible best fit of the anomalous exponents for the shell model. The vertical bars correspond to the experimental values of the anomalous exponents for the passive scalar. The shell model of the passive scalar seems to reproduce qualitatively and almost quantitatively the behaviour observed for the 3d case.
Source: Figure reproduced from [108].

Using the She–Lévêque fit for the exponents $\zeta(p)$ we obtain $F_2(r) \sim r^{0.6}$, not far from the experimental estimates. The above argument provides a simple hint on why we should expect $\xi(2p)$ to be smaller than $\zeta(2p)$.

Lecture 7.2. Passive scalar for shell model

An interesting point is to consider the same problem within the context of shell models [111]. It is possible to define an analogous of the passive scalar for shell model by using the equations:

$$\frac{d\theta_n}{dt} = i[h_n(u_{n+1}\theta_{n+2} + u_{n+2}\theta_{n+1}) + e_n(u_{n-1}\theta_{n+1} - u_{n+1}\theta_{n-1}) + g_n(u_{n-2}\theta_{n-1} + u_{n-1}\theta_{n-2})]^* \tag{290}$$

Table 2
Exponents of the temperature and velocity structure functions.
Source: Values reproduced from [109].

Order	$\xi(n)$	$\zeta(n)$
1	0.37 ± 0.003	0.37 ± 0.003
2	0.62 ± 0.005	0.70 ± 0.005
3	0.80 ± 0.008	1.00 ± 0.010
4	0.94 ± 0.010	1.28 ± 0.020
5	1.04 ± 0.010	1.54 ± 0.030
6	1.12 ± 0.020	1.78 ± 0.050
7	1.20 ± 0.020	2.00 ± 0.070
8	1.29 ± 0.020	2.23 ± 0.080

where h_n, e_n and g_n are chosen in such a way that, for $\kappa = 0$, the quantity $\Sigma_n|\theta_n|^2$ is conserved. For instance, assuming we choose u_n obtained from the GOY model with $b = 1/2$, then the proper choice is $h_n = 1/2 = e_n = -g_n$. The scaling exponents for the passive scalar in the shell models seems to reproduce qualitatively and almost quantitatively the behaviour observed for the three-dimensional case (see Fig. 62).

Lecture 7.3. The Kraichnan model

A deep insight in the study of passive scalar turbulence and more generally in understanding the physical properties of intermittency can be achieved working on the so-called Kraichnan model [112]. As already noted, there is no reason to believe that anomalous scaling for the passive scalar should be observed if and only if the velocity field shows intermittent behaviour. Kraichnan had the very bright and non-trivial idea to consider a velocity field $\vec{v}$ in Eq. (279) as a gaussian random variable δ-correlated in time supplemented with some known scaling behaviour for the two-point correlation function. In particular, following Kraichnan, let us assume to be in $d \geq 2$ dimensions and let us consider the velocity correlation:

$$S_{ij}(r) = \int_0^\infty \left\langle [v_i(x+r,s) - v_i(x,s)][v_j(x+r,0) - v_j(x,0)] \right\rangle ds \tag{291}$$

Assuming isotropy, $S_{ij}(r)$ is consistent with a divergence-free velocity field if:

$$S_{ij} \sim D r^\xi \left[(d - 1 + \xi)\delta_{i,j} - \xi \frac{r_i r_j}{r^2} \right] \tag{292}$$

with $\xi \in [0:2]$. Then, upon assuming a large-scale isotropic forcing, it is possible to show that the structure functions $F_{2p}(r)$ satisfy, in a statistically stationary state, the following equations:

$$-\frac{2}{r^{d-1}} \frac{\partial}{\partial r} \left(r^{d-1+\xi} \frac{\partial F_{2p}(r)}{\partial r} \right) = \kappa J_{2p}(r) \tag{293}$$

where

$$J_{2p}(r) = 2p \langle [\delta\theta(r)]^{2p-1} H[\delta\theta(r)] \rangle \tag{294}$$

$$H[\delta\theta(r)] \equiv \langle [\Delta_x + \Delta_{x'}] \delta\theta(r) | \delta\theta(r) \rangle \tag{295}$$

The last expression means that *given* $\delta\theta(r)$ we compute the fusion rules with $\Delta\theta$ in a way similar to what we already discussed in the previous lecture for the multifractal approach. Then Kraichnan provided an ansatz on the function $J_{2p}(r)$ from which he derived the scaling exponents of $F_{2p}(r)$. The remarkable point, *assuming the Kraichnan ansatz*, is that $F_{2p}(r)$ show anomalous scaling. The existence of anomalous scaling is supported by numerical integration of the Kraichnan model and is shown in Fig. 63.

It turns out that the Kraichnan ansatz is not correct but something new was discovered: there exists anomalous scaling in the Kraichnan model due to some new mechanism. A detailed account of this important result is discussed in [1] where the proper and elegant mathematical techniques are presented and reviewed. Here we limit ourselves to an overview of the most important outcomes using a very simplified model to decrease the mathematical difficulties.

Before discussing the physics behind the Kraichnan ansatz and its validity, let us comment on the final results. Was it true, the Kraichnan's model is the first (and only) case where we can understand *physically* how anomalous scaling arises in a turbulent-like flow. However, we need to understand how eq. (293) has been obtained and explained in detail the Kraichnan ansatz on $J_{2p}(r)$. This requires some non-trivial mathematics which, as we already said, we develop for a simple (but non-trivial) case. We consider an extremely simplified version of the Kraichnan model given by a shell model [114]:

$$\frac{d\theta_n}{dt} = i[k_{n+1}\theta_{n+1}u_n - k_n\theta_{n-1}u_{n-1}]^* - \kappa k_n^2 \theta_n + f(t)\delta_{1,n} \tag{296}$$

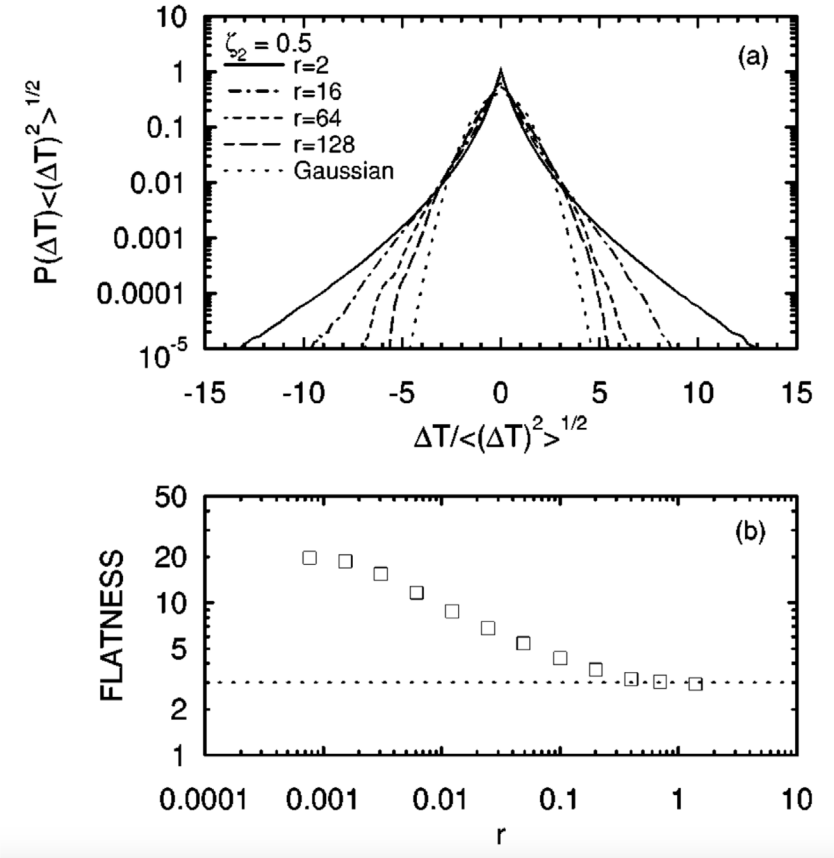

Fig. 63. (a) The probability density function (pdf) of the passive scalar difference $\Delta\theta(r)/ < [\Delta\theta(r)]^2 >^{1/2}$ as a function of r within the inertial subrange. The solid curve is the derivative pdf ($r \sim \eta$) and as r increases the curves tend towards Gaussian. (b) The kurtosis, K, of the scalar difference as a function of r for the same data as for (a). For the smallest r this is the derivative kurtosis. (For this figure r is normalised by the integral scale.) Both (a) and (b) are from the direct numerical simulations of Chen & Kraichnan (1998) using a white-noise velocity field. [For these statistics white-noise computations compare well with laboratory measurements, reproducing similar values of K at the same R_λ (see for example Mydlarski & Warhaft 1998a).
Source: Figure reproduced from [113].

First of all, let us show that in the limit $\kappa \to 0$ and $f(t) \to 0$ the system conserves energy. We have

$$\frac{d}{dt}\langle\theta_n\theta_n^*\rangle = k_{n+1}\Pi_{n,n+1} - k_n\Pi_{n-1,n} \tag{297}$$

with

$$\Pi_{n,n+1} = i\langle u_n^*\theta_n^*\theta_{n+1}^*\rangle - i\langle u_n\theta_n\theta_{n+1}\rangle$$

Note that for $\langle\theta_n\theta_n^*\rangle$ to be stationary we need $k_{n+1}\Pi_{n,n+1} \sim const$, i.e. $\Pi_{n,n+1} \sim k_{n+1}^{-1}$ which is equivalent to Eq. (286). Now we assume that u_n are random variables δ-correlated in time and with $D_n \equiv \langle|u_n|^2\rangle = k_n^{-\xi}$. This implies that, in Eq. (296), the "noise" (i.e. u_n) acts as a multiplicative noise in the system.

Lecture 7.4. Mathematical interlude

It is not trivial to work with multiplicative noise in physics and there are various prescriptions to follow which correspond to different interpretations. Although there are several textbooks and review papers on the problem [115], we think it is worthwhile to understand it using some simple examples. First, we recall some useful information when the noise is addictive. We start by introducing the Itô-calculus. Let us consider the stochastic differential equations:

$$dx = h(x)dt + \sqrt{\epsilon}dW \tag{298}$$

Following Itô we assume that $dW(t)$ is a gaussian process with zero mean and variance dt (i.e. $W(t)$ is nowhere a differential). Eq. (298) can be numerically simulated by integrating the deterministic part over a time step dt and then

adding a random number with gaussian distribution with variance ϵdt. The probability distribution $P[x,t]$ associated to eqn. (298) is given by the solution of the Fokker–Planck equation:

$$\partial_t P + \frac{\partial}{\partial x}[hP] = \frac{1}{2}\epsilon \frac{\partial^2}{\partial x^2} P \tag{299}$$

Next we consider the quantity $f(x,t)$ for which we want to write an equation. The Itô calculus says that

$$df(x,t) = \left[\partial_t f + \partial_x(fh(x)) + \frac{1}{2}\epsilon \partial^2_{xx} f\right] dt + \partial_x f \sqrt{\epsilon} dW \tag{300}$$

Notice that the third term on the r.h.s of (300) does not appear in ordinary calculus and it is called Itô term. For instance, let us suppose that $h(x) = -ax$ which implies that the stationary solution of the Fokker–Planck Eq. (299) is a gaussian with zero mean and variance $\epsilon/(2a)$. Now, let us consider $f(x) = x^2$. Upon applying the Itô calculus (300) we have

$$dx^2 = [-2ax^2 + \epsilon]dt + 2x\sqrt{\epsilon} dW$$

Upon averaging on the noise we obtain $\langle 2x^2\rangle - \epsilon = 0$, i.e. $\langle x^2\rangle = \epsilon/(2a)$ as expected.
In general, given the set of stochastic differential equations:

$$dx_i = h_i dt + \Sigma_j b_{ij} dw_j \tag{301}$$

the Itô calculus for $f(x_1, x_2, \ldots, t)$ reads

$$df = \left[\frac{\partial f}{\partial t} + \Sigma_i \frac{\partial f}{\partial x_i} h_i + \frac{1}{2}\Sigma_{ij}\sigma_{ij}\frac{\partial^2 f}{\partial x_i \partial x_j}\right] dt + \Sigma_{ij} b_{ij} \frac{\partial f}{\partial x_i} dw_j \tag{302}$$

with

$$\sigma_{ij} = [bb^T]_{ij} \tag{303}$$

Now let us consider the equation

$$\frac{dx}{dt} = -ax + x\eta(t) \tag{304}$$

where $\eta(t)$ is a gaussian noise. In physics, we usually think of noise as the outcome of some physical process whose time scale is much shorter than the one characterising the macroscopic behaviour. Having this observation in mind, we want to understand what does it mean for $\eta(t)$ to be a noise with short correlation time with respect to $1/a$ (the macroscopic time scale of the system). So we write:

$$d\eta = -\frac{1}{\tau}\eta dt + \frac{1}{\tau} dW(t) \tag{305}$$

and we consider the case $\tau \to 0$. Now we can integrate Eq. (304) and we obtain

$$x(t) = x(0)\exp\left[-at + \int_0^t \eta(s) ds\right] \tag{306}$$

Then we consider Eq. (305) in the limit $\tau \to 0$. Notice that $\langle \eta^2\rangle = 1/2$ (one can use the above example to derive it). Thus $d\eta$ is at most of order 1 and $-\eta dt + dW$ should be close to zero for $\tau \to 0$. Therefore we can write $\eta dt = dW + \mathcal{O}(\tau)$ and we obtain

$$x(t) = x(0)\exp\left[-at + \int_0^t dW(s)\right] \tag{307}$$

The quantity $\int_0^t dW(s) = W(t) - W(0)$ is a gaussian variable with zero mean and variance t, following the definition of the Wiener process. Using gaussian integration we obtain

$$\langle x(t)^n\rangle = x(0)^n \exp\left[-nat + \frac{n^2}{2}t\right] \tag{308}$$

Now we consider the stochastic differential equation:

$$dx = \left[-ax + \frac{1}{2}x\right] dt + x dW \tag{309}$$

Using the Itô formula (300) we obtain

$$dx^n = \left[-nax^n + \frac{n}{2}x^n + \frac{1}{2}n(n-1)x^n\right] dt + nx^n dW \tag{310}$$

Upon averaging we obtain:

$$\frac{d\langle x^n\rangle}{dt} = -na\langle x^n\rangle + \frac{n^2}{2}\langle x^n\rangle$$

which is the equivalent, in differential form, of Eq. (308) Thus Eq. (309) is the correct way to write (304) in the limit $\tau \to 0$. The term $x/2$ is called the Stratonovich term and Eq. (309) is interpreted in the Itô sense as discussed before.

Let us now discuss a slightly more difficult case, namely

$$\frac{dx}{dt} = -ax + y\eta \tag{311}$$

$$\frac{dy}{dt} = -ay - x\eta \tag{312}$$

For $a = 0$ the system conserves the quantity $x^2 + y^2$. To deal with this equation, we introduce the quantity $z = x + iy$ and we obtain:

$$\frac{dz}{dt} = -az - iz\eta$$

Then we can proceed exactly as before and we obtain:

$$z(t) = z(0)exp\left[-at - i\int_0^t \eta(s)ds\right]$$

Notice that zz^* is constant for $a \to 0$. Using the same technique as before, it is easy to see that (311) is equivalent to

$$dx = \left[-ax - \frac{1}{2}x\right]dt + ydW \tag{313}$$

$$dy = \left[-ay - \frac{1}{2}y\right]dt - xdW \tag{314}$$

Let us understand how to obtain this result in a more general way. We consider the term $y\eta$ in (311) and we want to compute how the Stratonovich term is obtained. What we need to do is to look to at the r.h.s of the equation dy/dt and take (with the sign) the term $\partial dy/dt/\partial\eta$, i.e. the term proportional to the "noise" η which is correlated to the noise $y\eta$ in equation for dx/dt. This term is, for our simple case, $-x$. After that we divide by the factor 2. Using the Itô calculus in Eq. (313) we get

$$dx^2 = \left[-2ax^2 - x^2 + y^2\right]dt + 2xydW$$

$$dy^2 = \left[-2ay^2 - y^2 + x^2\right]dt - 2xydW$$

So on the average, in the limit $a \to 0$ the quantity $\langle x^2 + y^2\rangle$ is conserved as it should.

In general, we can define the Stratonovich terms for the equation:

$$\frac{dx_i}{dt} = h_i(\boldsymbol{x}) + \Sigma_j b_{ij}(\boldsymbol{x})\eta_j \tag{315}$$

where $\boldsymbol{x}$ is a shorthand notation for $x_1, x_2, \ldots$. Using our rules we obtain:

$$dx_i = \left[h_i(\mathbf{x}) + \frac{1}{2}\Sigma_k\Sigma_j b_{kj}(\mathbf{x})\frac{\partial}{\partial x_k}b_{ij}(\mathbf{x})\right]dt + \Sigma_j b_{ij}(\mathbf{x})dW_j \tag{316}$$

Lecture 7.5. Going back to physics

Now, at least for the shell model, we can understand what is the logic of our computations. Let us remember that the only non vanishing correlation for u_n are $\langle u_n u_m^*\rangle = k_m^{-\xi}\delta_{m,n}$. Let us do it for Eq. (296). We consider the multiplicative term which are $ik_{n+1}\theta_{n+1}^* u_n^*$ and $-ik_n\theta_{n-1}^* u_{n-1}^*$. Let us take the first term which is multiplied by u_n^* and look for the equation of θ_{n+1}^*:

$$\frac{d\theta_{n+1}^*}{dt} = -i\left[k_{n+2}\theta_{n+2}u_{n+1} - k_{n+1}\theta_n u_n\right] + \ldots \tag{317}$$

where the dots do not depend on u_n. The only term proportional to u_n (which correlates with $u_n{}^*$) is given by $+ik_{n+1}\theta_n$. Thus the contribution due to the first term (Stratonovich contribution) is given by $-k_{n+1}^2 D_n\theta_n/2$. Analogously the contribution of the second term is given by $-k_n^2 D_{n-1}\theta_n/2$. Thus, Eq. (296) should be written as

$$d\theta_n = \left[-\frac{k_{n+1}^2 D_n}{2}\theta_n - \frac{k_n^2 D_{n-1}}{2}\theta_n - \kappa k_n^2\theta_n\right]dt + i\left[k_{n+1}\theta_{n+1}D_n dW_n - k_n\theta_{n-1}D_{n-1}dW_{n-1}\right]^* \tag{318}$$

Notice that the effect of Stratonovich is to introduce an effect of diffusion (proportional to k_n^2) due to the velocity. This, in the language of the passive scalar equation, is usually referred to as effective diffusivity or eddy diffusivity.

We can now use Eq. (318) to compute the quantity $E_n \equiv \langle \theta_n \theta_n^* \rangle$. First we need to obtain the equation for $\theta_n \theta_n^*$ using the Itô calculus (302) and then we have to average over the noise. The Itô calculus contains two times the derivative with respect to θ_n and θ_n^*. The computation is a little long but at the very end we obtain after averaging:

$$\frac{dE_n}{dt} = k_{n+1}^2 D_n [E_{n+1} - E_n] - k_n^2 D_{n-1} [E_n - E_{n-1}] + \dots \tag{319}$$

where now the dots include a term proportional to κ. We immediately see that a stationary solution implies

$$[E_n - E_{n-1}] k_n^2 D_{n-1} \sim const \rightarrow E_n - E_{n-1} \sim k_n^{\xi - 2}$$

or equivalently

$$E_n \sim k_n^{-\xi(2)} \ ; \xi(2) = 2 - \xi \tag{320}$$

This ends our computation in the so-called "simplified" case.

We can now go back to the Kraichnan model. We did not derive Eq. (293) but we now know which tools are needed to derive it. In fact, not surprisingly, we find on the r.h.s of Eq. (293) the divergence in d dimensional space of $S_{i,j}$ multiplied by the structure functions, in complete analogy with the term $k_n^2 D_{n-1}$ obtained in our simplified model. We rewrite Eq. (293):

$$-\frac{2}{r^{d-1}} \frac{\partial}{\partial r} \left(r^{d-1+\xi} \frac{\partial F_{2p}(r)}{\partial r} \right) = \kappa J_{2p}(r) \tag{321}$$

To solve the problem, we first consider the case $p = 1$. Then the term $\kappa J_2(r)$ is constant since it corresponds to the analogous of the viscous anomalies for the $3d$ N.S. equation. Integrating eqn. (293) from 0 to r we obtain

$$r^{d-1+\xi} \frac{\partial F_2(r)}{\partial r} \sim r$$

which gives $F_2(r) \sim r^{2-\xi}$. This is in analogy with our extremely simplified shell model Eq. (319). We want now to compute the scaling of $F_{2p}(r)$ for any $p > 1$. To do that, we need to know $J_{2p}(r)$. Let us remember that $J_{2p}(r)$ depends on the fusion rules between $\delta\theta(r)^{2p-1}$ and $\Delta\theta$. Kraichnan made the ansatz

$$J_{2p}(r) = \eta J_2(r) \frac{F_{2p}(r)}{F_2(r)} \tag{322}$$

Using Eq. (322) into Eq. (321) we obtain:

$$nd\xi(2) = \xi(2p)(\xi(2p) + d - \xi(2))$$

from which we obtain

$$\xi(2p) = \frac{1}{2} \left[\sqrt{4nd\xi(2) + (d - \xi(2))^2} - (d - \xi(2)) \right] \tag{323}$$

The above expression means that $F_{2p}(r)$ shows anomalous scaling for $\xi(2) > 0$. As said, for the first time we have an explicit computation of the anomalous scaling obtained directly from the equation of motions. We now need to understand what is the physics behind it and whether it is correct.

We observe that the anomalous scaling is obtained by balancing the inertial term dynamics (l.h.s of Eq. (321)) with the fusion rules for J_{2p}. The fusion rules should be evaluated in the "diffusion" range (analogous of the viscous range). Thus the way the diffusion affects the behaviour of $\delta\theta$ at small scales is crucial for the anomalous scaling to hold. We also notice that using the multifractal framework, we have computed fusion rules like $\langle \delta v(r)^{2n+1} \Delta v \rangle$ for the velocity. The computations involve the effect of fluctuating viscous length in the system and we did not control exactly the constant in front of the fusion rules.

We can take a different point of view and consider the correlation functions of $2p$ scalar fields in $2p$ different positions. For instance, consider Fig. 64: fusion rules in the diffusion dominated regime are needed if we want to study the limit $\Delta \rightarrow 0$ where Δ is the separation between two points which eventually merge. However, we can more generally consider the correlation function $C_4 = \langle \theta(x_1)\theta(x_2)\theta(x_3)\theta(x_4) \rangle$ and, assuming homogeneity and isotropy, we can study the equation of C_4 and, in particular, the scaling properties of the correlation function as a function of $r_{ij} = |x_i - x_j|$.

It is in general non trivial to write the equations for the correlation functions and, more importantly, to solve them. At the formal level, for the correlation C_4, the general structure of the equation becomes:

$$\partial_t C_4 + M_4 C_4 = O(\kappa) + forcing \tag{324}$$

where the r.h.s. takes care of the terms due to diffusivity κ and the effect of the forcing. The quantity M_4 is a *linear* (in C_4) differential operator acting on the correlation functions (on all its argument) and it can be computed from the advection term $\boldsymbol{v} \cdot \nabla\theta$ using the Stratonovich–Itô rules. The solution of (324) is formally given by

$$C_4 = \Psi_4 + \Psi_4(\kappa, F) \tag{325}$$

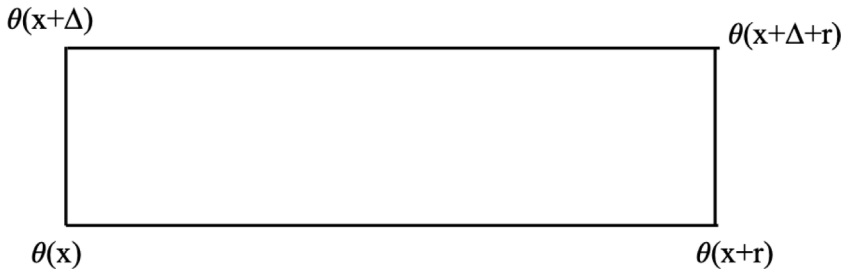

Fig. 64. Distribution of points and fields for the correlation of 2p scalars in 2p different positions.

where Ψ_4 satisfies the equation $M_4\Psi_4 = 0$ and $\Psi_4(\kappa, F)$ is the solution of (324) for non zero values of κ and the forcing F. Although this is all very formal and almost trivial, there is a clear physical interpretation: Ψ_4 is independent both on forcing and diffusion (in the limit $\kappa \to 0$) and it is controlled by inertial term (i.e. terms derived from $\boldsymbol{v}\cdot\boldsymbol{\nabla}\theta$) whereas this is not the case for $\Psi_4(\kappa, F)$. Assuming the forcing to be statistically isotropic and homogeneous, we also expect Ψ_4 to be a scaling function of it arguments r_{ij} in the inertial range (r_{ij} much smaller than the characteristic scale of the forcing and much larger than the diffusive scale). If in the inertial range Ψ_4 dominates over $\Psi_4(\kappa, F)$ then the scaling properties and intermittency of the passive scalar are not the one predicted by the Kraichnan ansatz. In a remarkable effort discussed in [116–118], it was shown that this is exactly what happen: the function Ψ_4 has anomalous scaling which differs from the one obtained using the Kraichnan ansatz Eq. (322), it is independent on forcing and diffusion and dominates the scaling properties of the inertial range quantities. In other words, anomalous scaling in the Kraichnan model is not due to balancing the diffusion term with the inertial dynamics but it is only due to the inertial dynamics!

The computation needed to obtain the above (exciting) results are highly non-trivial. Here we will show [114] how the above result can be reached in the much simpler case of the shell model introduced in Eq. (296). In particular we want to compute the solution for the quantities $\left\langle |\theta_m|^2 |\theta_q|^2 \right\rangle \equiv P_{m,q}$. To do that we need to write the equations for $P_{m,q}$ which can be done using the same tools as we already employed to compute the equation for E_m.

$$\frac{dP_{m,q}}{dt} = [- P_{m,q}k_{m+1}^2 D_m((1+\delta_{q,m+1}) + \lambda^{\xi-2}(1+\delta_{q,m-1})) + \tag{326}$$

$$+ P_{m+1,q}k_{m+1}^2 D_m(1+\delta_{q,m}) + P_{m-1,q}k_m^2 D_{m-1}(1+\delta_{q,m}) \tag{327}$$

$$+ (q \to m; m \to q)] \tag{328}$$

$$+ (\delta_{1,m}E_m + \delta_{1,q}E_q)F_1 - \kappa(k_m^2 + k_q^2)P_{m,q} \tag{329}$$

The symbol $(q \to m; m \to q)$ means that we write the same expression by exchanging m and q. For F_1 and $\kappa \to 0$, Eq. (326) is an infinite set of linear equations which we are interested to solve.

Before discouraging, let us try to rewrite the equations in a simpler way. First, we introduce the quantities:

$$P_{n,n+l} = C_l P_{n,n} \tag{330}$$

$$P_{n,n-l} = D_l P_{n,n} \tag{331}$$

Then we observe that $P_{m,q}$ is a symmetric function of m and q. So we can write

$$P_{n+l,n} = D_l P_{n+l,n+l} = P_{n,n+l} = C_l P_{n,n}$$

This implies that

$$\frac{P_{n+l,n+l}}{P_{n,n}} = \frac{C_l}{D_l} \tag{332}$$

Using the identity

$$\frac{P_{n+l+1,n+l+1}}{P_{n,n}} \frac{P_{n+l,n+l}}{P_{n+l+1,n+l+1}} \frac{P_{n,n}}{P_{n+l,n+l}} = 1$$

We obtain:

$$\frac{C_{l+1}}{C_l C_1} = \frac{D_{l+1}}{D_l D_1} \tag{333}$$

Upon denoting $R = C_1/D_1$ the scaling properties of $P_{n,n}$ are controlled by R i.e. by C_1 and D_1. Let us notice that C_l and D_l are nothing else than the fusion rules (in the inertial range) of the structure functions of θ within the shell model.

Now introduce the quantity $x = \lambda^{\xi-2}$ and we can write the equations for $P_{m,m}$ and $P_{m,m-1}$:

$$\frac{dP_{m,m}}{dt} = 2P_{m,m}k_{m+1}^2 D_m[1 + x - 2(C_1 + D_1 x)] = 0 \tag{334}$$

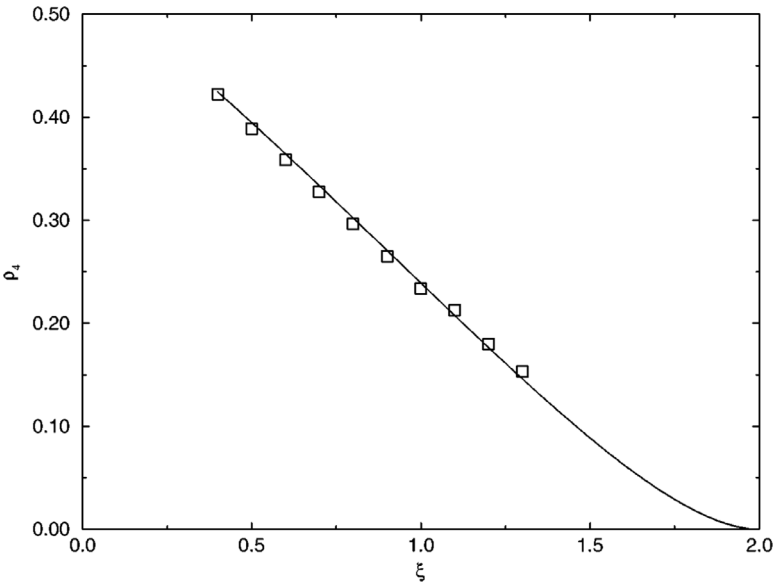

Fig. 65. Analytical ansatz (continuous line) and numerical results (squares) for ζ_4 are plotted for various values of ζ. *Source:* Figure reproduced from [114].

$$\frac{dP_{m,m-1}}{dt} = 2P_{m,m-1}k_{m+1}^2 D_m \left[-1-4x-x^2+\frac{x}{D_1}+\frac{x+C_2+x^2C_2/R}{C_1}\right]=0 \tag{335}$$

From Eqs. (334) we can easily see our problem: we have 2 equations for 3 unknown C_1, D_1 and C_2.

To make progress, we consider the quantity $\gamma_l = D_{l+1}/D_l$ and $\delta_l = C_{l+1}/C_l$ and we rewrite the Eqs. (326) in the form:

$$\gamma_l\left(R+x^{l+1}\right) \quad +\frac{1}{\gamma_{l-1}}\left(x^l+\frac{x}{R}\right)=0 \tag{336}$$

$$\delta_l\left(1+\frac{x^{l+1}}{R}\right)+\frac{1}{\delta_{l-1}}(Rx^l+x)-(1+x)(1+x^l)=0 \tag{337}$$

Finally we observe that Eqs. (334) are maps which define the "evolution" of γ_l and δ_l by iterations. The two maps are the same once we notice that $\delta_l = R\gamma_l$. Therefore, we focus only on γ_l.

Let us recall that $\gamma_l = D_{l+1}/D_l$ and D_l is defined by the relation $P_{n,n-l} = D_l P_{n,n}$. So if we go from $l-1$ to l we are moving from the diagonal part of the matrix $P_{n,n}$ to the boundary at $l=0$ hereafter referred to as *infrared boundary* or simply as *IR boundary*. Similarly, we can use the map of γ_l as a map to move from l to $l-1$ (remember we have an infinite set of equations!) and in this case we are moving from the *IR boundary* to the diagonal. The same is true for the map δ_l: iterating from l to $l+1$ we move from the diagonal to the boundary which, in this case, is a boundary for large l i.e. an *ultraviolet boundary* referred to as *UV boundary* and iterating from l to $l-1$ we move from the *UV boundary* to the diagonal.

Next we consider the fixed points of the map for γ_l. One has two fixed points $\gamma_1^* = x/R$ and $\gamma_2^* = 1/R$. It is easy to show that γ_1^* is a stable fixed point for the iteration from l to $l-1$, i.e. moving from the *IR boundary* to the diagonal. Analogously, a stable fixed point is observed for δ_l iterating from l to $l-1$ i.e. moving from the *UV boundary* to the diagonal.

At this stage, it is clear how to proceed. We fix a value of R and we can iterate the maps in order to reach the fixed points. This allows us to compute C_2/C_1 and D_2/D_1 near the fixed points. From Eqs. (334) we compute the new value of R and we repeat the operation until we converge to the stable fixed point. In this way, we can solve the infinite equations. Once we have R we can obtain the scaling of $P_{n,n} \sim R^n$ or equivalently $R = \lambda^{-\xi(4)}$.

In Fig. 65 we show the quantity $\rho_4 = \xi(4) - 2\xi(2)$, which is the part responsible for the anomalous scaling, computed from our procedure with a continuous line against the numerical results obtained by directly simulating the model (squares). The agreement is almost perfect.

Let us try to summarise what we found so far:

- anomalous scaling can be computed almost analytically;
- anomalous scaling does not require any balance between inertial range dynamics and diffusion; it is a property of the inertial range dynamics alone;
- anomalous scaling is universal since it is stable for large and small scale perturbations.

The last point comes from the fact that our solution is *UV* and *IR* stable, i.e. it is stable by changing the boundary conditions.

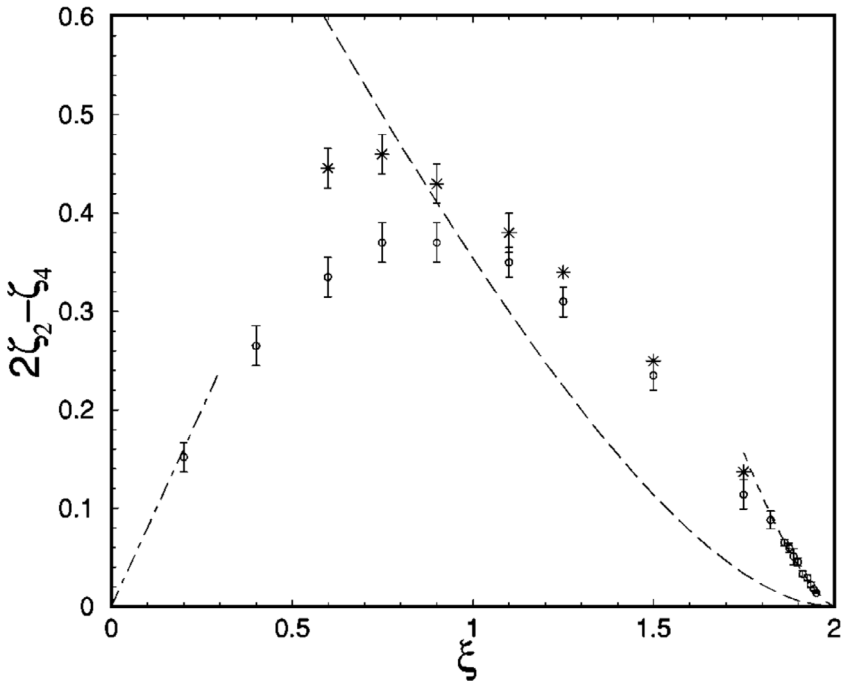

Fig. 66. The anomaly $2\zeta_2 - \zeta_4$ for the fourth-order structure function in two dimensions stars, upper graph and three dimensions circles, lower graph. Error bars in 2D shown only for $\zeta < 1.1$. The dashed line is the three-dimensional linear ansatz prediction by Kraichnan [112].
Source: Figure reproduced from [119].

Our starting Eqs. (326) can be formally written as in (324), i.e. we can write

$$\partial_t P_{m,q} + M^{(4)}_{n,m,p,q} P_{n,p} = O(\kappa) + Forcing \tag{338}$$

Our solution correspond to find the solution of the equation

$$M^{(4)}_{n,m,p,q} P_{n,p} = 0 \tag{339}$$

The solution of this equation are called *zero modes*.

It is much more difficult to find the zero modes for the original Kraichnan model [1]. However, this can be done "perturbatively" in ξ, near $\xi = 0$, and in $2 - \xi$ near $\xi = 2$. As already noted, the solution of Eq. (338) or (324) is composed of two contributions: one is the zero mode and the other one depends on the forcing and dissipation. The zero modes, however, are the leading terms in the inertial range behaviour of the correlation functions showing anomalous scaling.

The above picture shows the results in $d = 2$ and $d = 3$ of the numerical simulations against the theoretical estimate (dashed lines), see Fig. 66.

For the Kraichnan model, the basic idea to perform analytical computation and numerical simulations [119], is to use lagrangian dynamics. We consider a (very large) ensemble of lagrangian particles moving in the velocity field:

$$\frac{d\vec{x}}{dt} = u(\vec{x}) + \sqrt{2\kappa}\eta(t) \tag{340}$$

Each particle carries the passive scalar information θ which "feels" the forcing through the equation:

$$\frac{d\theta}{dt} = f(\vec{x}, t) \tag{341}$$

Then the quantity we are in general interested to compute is $\langle \theta(\vec{x}_1)\theta(\vec{x}_2)\dots \rangle$ which can be computed upon averaging on different lagrangian trajectories.

Lecture 7.6. Zero modes in a realistic case

Even if interesting, all the above discussion refers to the Kraichnan model whose velocity field has little resemblance to real turbulence. Does the same picture hold for a realistic case? To answer this question, following Celani and Vergassola

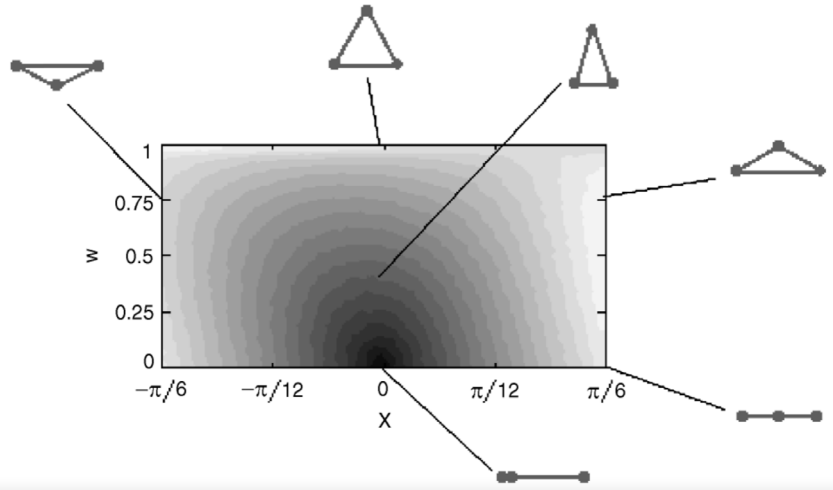

Fig. 67. Contour lines in the $\xi - w$ plane of the third order shape function f appearing in (5).
Source: Figure reproduced from [120].

[120], we consider a two-dimensional turbulent flow and we consider a passive scalar where an external non-vanishing gradient $\boldsymbol{g}$ of the passive scalar is applied. Then we define θ as the solution of the equation

$$\frac{\partial \theta}{\partial t} + \boldsymbol{v} \cdot \nabla \theta + \boldsymbol{v} \cdot \boldsymbol{g} = \kappa \Delta \theta + f \tag{342}$$

where the external forcing f is a random gaussian field concentrated to large scale. In two dimensions, kinetic energy is transferred from small to large scale, as we discussed in Lecture 2, the energy spectrum goes as $E(k) \sim k^{-5/3}$, i.e. $\delta v(r) \sim r^{1/3}$. For this particular case the quantity $\langle \theta(\boldsymbol{r}_1)\theta(\boldsymbol{r}_2)\theta(\boldsymbol{r}_3)\rangle$ is not vanishing because of the term $\boldsymbol{v} \cdot \boldsymbol{g}$. In particular we consider three points forming a triangle which can be characterised by a length scale $R^2 = (r_{12}^2 + r_{23}^2 + r_{13}^3)/3$ and two angles χ and ω so that $\langle \theta(\boldsymbol{r}_1)\theta(\boldsymbol{r}_2)\theta(\boldsymbol{r}_3)\rangle \equiv C_3(R, \chi, \omega)$. First, let us consider the Eulerian point of view, where we fix the points and look how C_3 changes, say, with R. A geometrical analysis of the possible triangular shapes shows that $C_3(R, \chi, \omega) = R^{\xi_3} f(\chi, \omega) cos(\phi)$ where ϕ is the orientation of the triangle with respect to the mean gradient $\boldsymbol{g}$. The figure shows the function $f(\chi, \omega)$ and the corresponding triangular shapes, see Fig. 67.

From numerical simulations, we can obtain C_3 as a function of R in the Eulerian case, shown in Fig. 68. We observe a clear scaling law $C_3 \sim R^{\xi_3}$ and exponent $\xi_3 = 1.25$.

Now we consider the lagrangian dynamics, i.e. we consider 3 particles and we evaluate $\langle \theta(\boldsymbol{r}_1)\theta(\boldsymbol{r}_2)\theta(\boldsymbol{r}_3)\rangle \equiv C_3(R, \chi, \omega)$ *averaging over the lagrangian realisations* hereafter denoted by $\langle C_3 \rangle_{Lag}$. Obviously R should grow (Richardson like diffusion), see Fig. 69. In particular, the Richardson diffusion predicts that $R^2 \sim t^3$. Thus we expect that $R^{\xi_3} \sim t^{3\xi_3/2}$ as shown in the figure. This is not the case for $\langle C_3 \rangle_{Lag}$.

What is the physical meaning of Fig. 69 ? While R is growing the quantity $f(\chi, \omega)$ should decrease to compensate the increasing value of R. This means that the shape of the triangles should change: the smaller is ξ_3 the longer the triangles remains degenerate, i.e. the longer the three points are closer to each other.

According to our previous discussion for the Kraichnan models, the scaling properties of the inertial range are controlled by the zero modes. In this particular case, $\langle C_3 \rangle_{Lag}$ is the three point correlation. Since zero modes are steady solutions of the equation of motions (with forcing and dissipation and in the limit of $\kappa \to 0$), they are also constant during the system evolution. Thus we may argue that $\langle C_3 \rangle_{Lag}$ is a zero modes in our specific case and it is a *distribution on the space of the triangle configurations, that are statistically invariant to the turbulent dynamics*. This is a very non trivial result because it gives a numerical proof that the concept of *zero modes* is behind the anomalous scaling of passive scalar with realistic turbulence flow.

Lecture 7.7. Statistically preserved structures

We want now to extend the previous result and for this purpose we start considering the shell model introduced by Eq. (296). Let us define with $\Psi^{(n)}$ the zero modes for the model. For the Kraichnan random velocity field, $\langle u_n u_m^* \rangle = \delta_{nm} k_n^{-\xi}$,

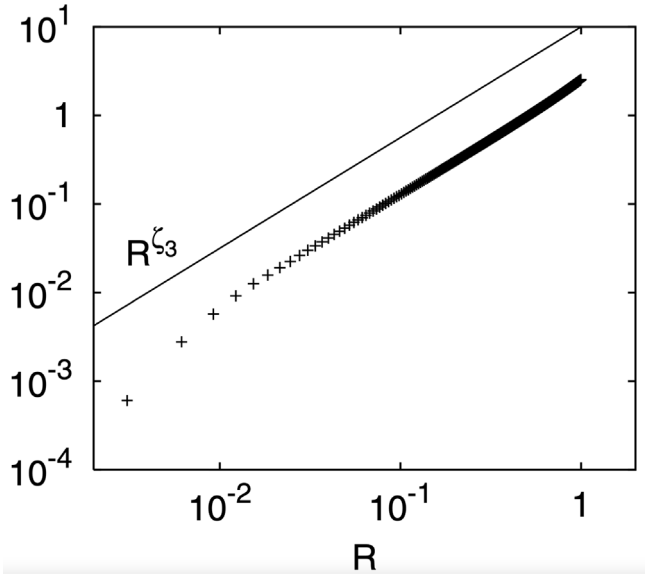

Fig. 68. The Lagrangian average of the correlation function C_3 compared against the average of $R^{\zeta_3} \sim |t|^{3/2\zeta_3}$.
Source: Figure reproduced from [120].

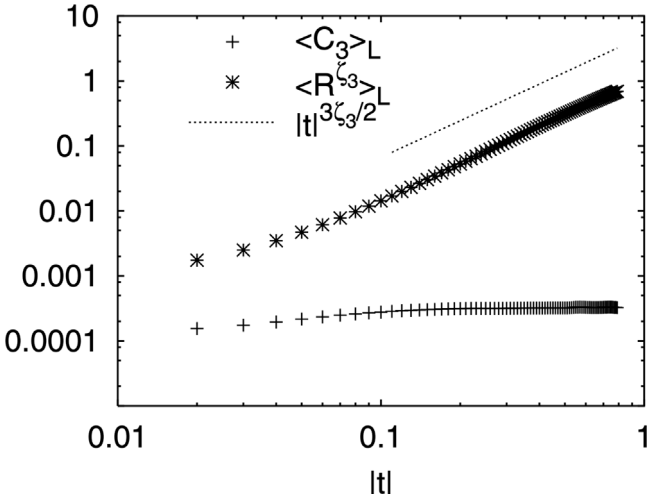

Fig. 69. The dependence of the third-order correlation function C_3 with respect to the size of the triangle R. The straight line is the power law behaviour $R^{1.25}$.
Source: Figure reproduced from [120].

we have computed $\Psi^{(2)}$ and $\Psi^{(4)}$ by solving the equations:

$$\partial_t \Psi^{(2)}_m = M^2_{mn} \Psi^2_n = 0 \tag{343}$$

$$\partial_t \Psi^{(4)}_{m,q} = M^{(4)}_{n,m,p,q} \Psi^4_{n,p} = 0 \tag{344}$$

The zero modes are eigenvector of eigenvalue 0 of the operator $M^{(n)}$. Let us now consider the Kraichnan random flow with no forcing. The initial energy of the system $E_m(0)$ starts to decreases for small but finite κ. Formally the evolution equation of $E_m(0)$ is given by Eq. (343) in the form

$$E_m(t) = P^{(2)}_{mn}(t) E_n(0) \tag{345}$$

where $P^{(2)}_{mn}$ is a formal way to write $[exp(tM^{(2)})]_{mn}$. Then we can say that $\Psi^{(n)}$ are eigenvectors of eigenvalue 1 of the operator $P^{(n)}$. In this case, the zero modes are both *right and left eigenvectors* of the evolution operators $M^{(n)}$. Using $\Psi^{(2)}$

we can easily show that:

$$\Sigma_m E_m(t)\Psi_m^{(2)} = \Sigma_{m,n} P_{mn}^{(2)} E_n(0)\Psi_m^{(2)} = \Sigma_n E_n(0)\Psi_n^{(2)} \tag{346}$$

In other words, *projecting the decaying function E_m on the proper zero modes $\Psi_m^{(2)}$, we obtain a conserved quantity*. Obviously this conservation holds up until some *large* time scale, of order $1/\kappa$ is reached. The same argument can be done for the *4th* order correlation functions $\langle|\theta_n|^2|\theta_m|^2\rangle$.

Let us try to summarise the previous argument: in the Kraichnan model the simultaneous N*th*-order correlation function satisfies a linear differential equation, which is inhomogeneous in the presence of the forcing. The general solution is the sum of the inhomogeneous and homogeneous parts. It turns out that the scaling exponent of the homogeneous part (the zero modes) is the leading term (smaller scaling exponent) compared to the other. Let us now consider the decaying problem for the Kraichnan model. Then, upon projecting the *time dependent* decaying correlation functions on the proper zero modes we obtain *statistically conserved structures* (in the limit $\kappa \to 0$). It is crucial to remember that the conservation occurs upon averaging over different initial conditions. This is the meaning of Eq. (346) and its generalisation to the correlation of order N.

We can now consider the more general case of passive scalar advected by a turbulent flow. Then, based on the above discussion, following [121], we can make the following two conjectures:

- there exist a set of *time independent* special functions Z_n which are left eigenvalue of the evolution operator (whatever it is);
- Z_n corresponds to the correlation functions of the *forced* dynamics of the passive scalar.

Using the two conjectures, the projection of the correlation functions on the Z_n, *averaged* over the different initial conditions, are *statistically preserved structures*. The reason why the above statements are conjectures is that for the generic case of a turbulent flow advecting a passive scalar, we have no analytical control of the time evolution operator as in the Kraichnan model. We should consider the two conjectures as the *physical* synthesis of our investigations of the Kraichnan model.

Although we cannot prove the two conjectures, we can provide evidence (at least in the case of shell model) that they are correct. For this purpose, we consider the Sabra shell model for u_n advecting the passive scalar θ_n:

$$\frac{d\theta_n}{dt} = i(k_{n+1}u_{n+1}\theta_{n+1} + k_n\theta_{n-1}u_n^*) - \kappa k_n^2\theta_n \tag{347}$$

Let us remark that u_n is not a random flow. Next, we consider the forced case. The non-zero correlation functions up to order 6 are

$$F_2(m) = \langle|\theta_m|^2\rangle \tag{348}$$

$$F_{4a}(m,n) = \langle|\theta_m|^2|\theta_n|^2\rangle;\ \ F_{4b}(n) = \langle\theta_{n+2}\theta_{n+1}^*\theta_{n+1}^*\theta_{n-1}\rangle \tag{349}$$

$$F_6(m,n,k) = \langle|\theta_m|^2|\theta_n|^2|\theta_k|^2\rangle \tag{350}$$

According to our second conjecture the F_l are the functions we need to use to construct the statistically preserved structures. Then, we consider the same problem in Eq. (347) *without forcing* and for the same κ and we define the time-dependent quantities:

$$C_2(m,t) = \langle|\tilde\theta(t)_m|^2\rangle \tag{351}$$

$$C_{4a}(m,n,t) = \langle|\tilde\theta(t)_m|^2|\tilde\theta(t)_n|^2\rangle;\ \ C_{4b}(n,t) = \langle\tilde\theta(t)_{n+2}\tilde\theta(t)_{n+1}^*\tilde\theta(t)_{n+1}^*\theta_{n-1}\rangle$$

$$C_6(m,n,k,t) = \langle|\tilde\theta(t)_m|^2|\tilde\theta(t)_n|^2|\tilde\theta(t)_k|^2\rangle$$

with $\tilde\theta(t)$ the "decaying solutions". In (351) the averaging is done over different initial conditions.

If our conjectures are correct, we should observe that the quantities:

$$I_2 \equiv \Sigma_n C_2(m,t)F_2(m) \tag{352}$$

$$I_4 \equiv \Sigma_{nm} C_{4a}(m,n,t)F_{4a}(m,n) + \Sigma_n C_{4b}(n,t)F_{4b}(n) \tag{353}$$

$$I_6 \equiv \Sigma_{nmk} C_6(m,n,k,t)F_6(m,n,k) \tag{354}$$

are conserved quantities. The numerical simulations support this idea, see Fig. 70. The final result demonstrates that I_l as defined in (352)–(354) are conserved quantities (in the limit $\kappa \to 0$) in agreement with our conjectures. This is an important result because it provides evidence that for the generic case of a turbulent flow, the passive scalar intermittency (anomalous scaling) is due to the same mechanism discussed for the Kraichnan model, namely the relevance of the zero modes that dominate inertial range dynamics. This also implies that the anomalous scaling is universal, i.e. independent of the large-scale forcing and dissipation.

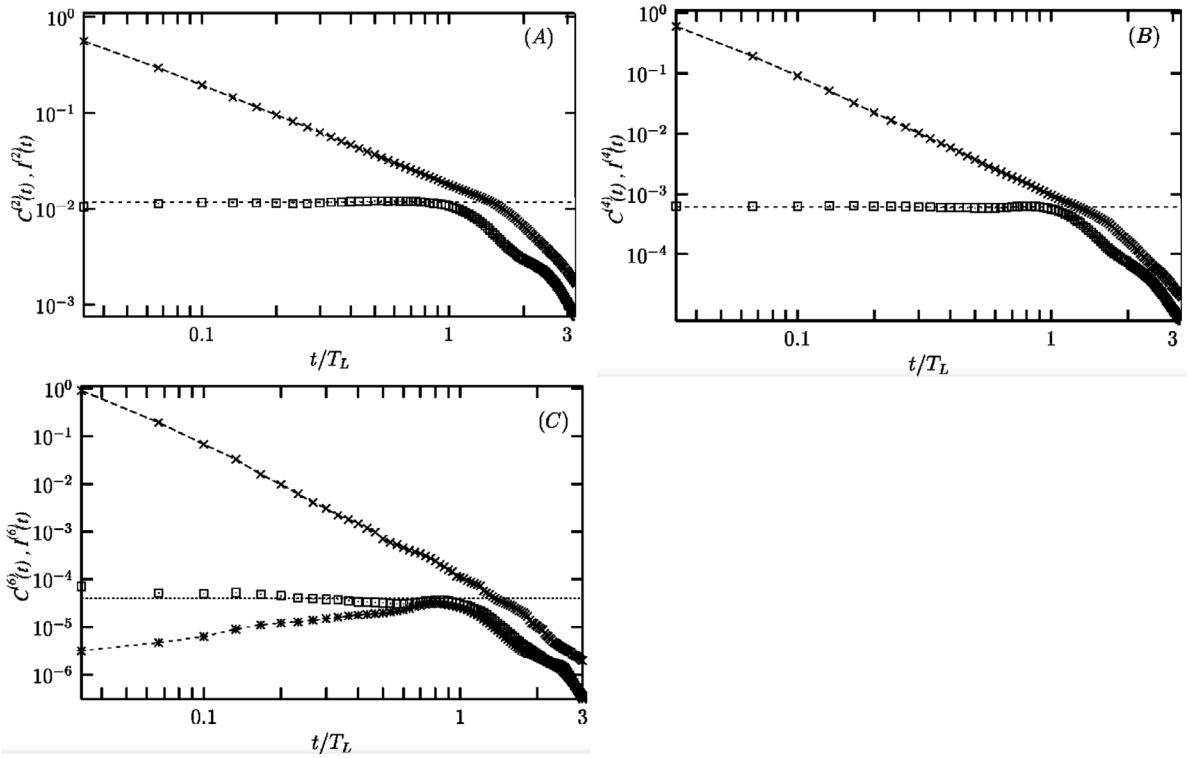

Fig. 70. Panel (*A*) time dependence of the decaying second order correlation functions, together with the time dependence of the statistically conserved quantities I_2. The equations have been integrated with a total number of shells $N = 33$. Time in the horizontal axis is given in units of the eddy turnover time T_L. Panel (*B*): the same as panel (*A*) but for the fourth-order correlation function and with $N = 25$. Panel (*C*): the same as panel (*B*) but for the sixth-order correlation function. Here we also present I_6 when we replace the forced solution $F_6(n, m, k)$ with its dimensional prediction.
Source: Figure reproduced from [121].

Lecture 7.8. The non-linear case

The previous results strongly point out that zero modes are the leading contribution to the (anomalous) scaling properties of a passive scalar. Is there any way to extend this feature to the N.S. equations? Here we make the first step in this direction [122]. Let us consider a vector field $\boldsymbol{w}$ subjected to the condition $\nabla \cdot \boldsymbol{w} = 0$ and satisfying the equations

$$\begin{aligned} &\partial_t \boldsymbol{w} + \boldsymbol{v} \cdot \nabla \boldsymbol{w} + \lambda \boldsymbol{w} \cdot \nabla \boldsymbol{w} = -\nabla \pi + \nu \Delta \boldsymbol{w} + f_w \\ &\frac{\partial \boldsymbol{v}}{\partial t} + \boldsymbol{v} \cdot \nabla \boldsymbol{v} + \lambda \boldsymbol{w} \cdot \nabla \boldsymbol{v} = -\nabla p + \nu \Delta \boldsymbol{v} + f_v \end{aligned} \tag{355}$$

where we assume the density $\rho = 1$. Eq. (355), in the limit $\lambda \to 0$, tends to the N.S. equations for $\boldsymbol{v}$ advecting a passive vector $\boldsymbol{w}$. For any $\lambda > 0$ we expect that the scaling properties of $\boldsymbol{v}$ and $\boldsymbol{w}$ are the same and we also expect that the limit $\lambda \to 0$ is not singular. In other words, we expect that the scaling properties of a passive vector advected by a turbulent flow are the same as the scaling properties of the advection field. We can also reach the same conclusions by considering the two fields $\boldsymbol{u}_+ = \boldsymbol{v} + \lambda \boldsymbol{w}$ and $\boldsymbol{u}_- = \boldsymbol{v} - \lambda \boldsymbol{w}$. Then the equation for $\boldsymbol{u}_+$ are the N.S. equations with forcing $f_+ = f_v + f_w$ while the equations for $\boldsymbol{u}_-$ are those of a passive vector with forcing $f_- = f_v - f_w$. Provided we choose the forcing f_v and f_w such that f_+ and f_- to be uncorrelated, we end up from (355) with the equation of a passive vector advected by a turbulent flow. By construction, we know that the scaling of $\boldsymbol{u}_+$ and $\boldsymbol{u}_-$ should be the same, as it is the case from the numerical simulations, see Fig. 71.

Next, we can use our previous idea for the statistically preserved structures to show that the correlation functions of the N.S. equations are zero modes for the passive vector. For this problem it is much simpler to work with a shell model. We consider the following equations:

$$\frac{du_n}{dt} = -\nu k_n^2 + \frac{i}{3} \Phi_n(u, u) + f_n^{(u)} \tag{356}$$

$$\frac{dw_n}{dt} = -\nu k_n^2 + \frac{i}{3} \Phi_n(u, w) + f_n^{(w)} \tag{357}$$

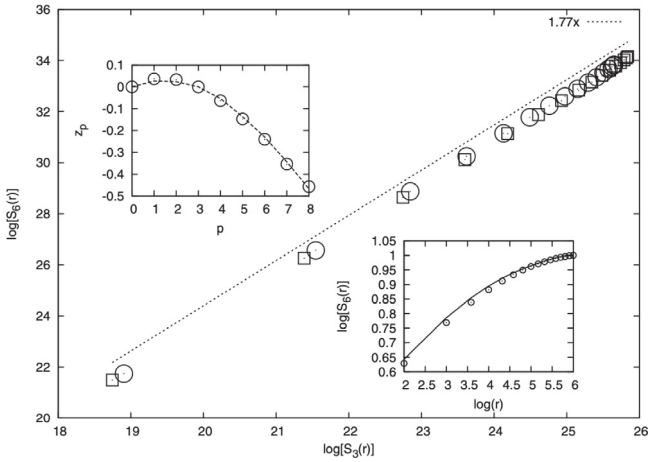

Fig. 71. Log–log plot of the sixth order structure functions of the fields $\boldsymbol{u}_-$ and $\boldsymbol{u}_+$ (circles and squares, respectively), for $\mu = 1$, as a function of the third order structure functions. The dashed line corresponds to the best fit in the scaling region with slopes 1.77. Lower inset: the sixth-order structure function of the two fields as a function of r. Upper inset: $z_p = \zeta_p/\zeta_3 - p/3$ computed for the structures functions of $\boldsymbol{u}_+$ and $\boldsymbol{u}_-$(circles).
Source: Figure reproduced from [122].

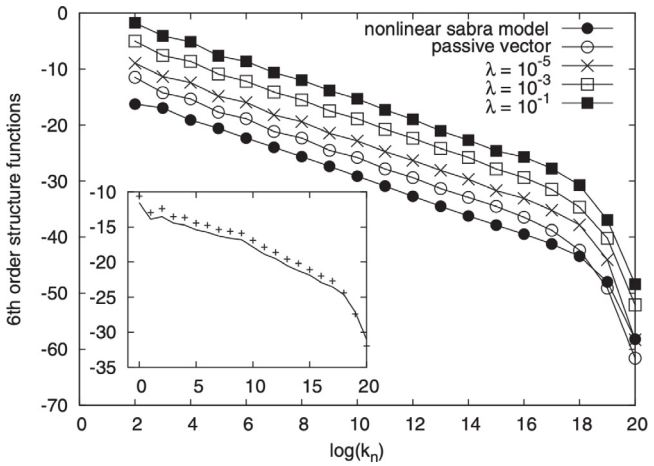

Fig. 72. The sixth order structure function of the field w_n for $\lambda = 10^{-1}$, 10^{-3} and 10^{-5} together with the sixth-order structure function for the Sabra model and for the linear model, respectively. The structure functions of the field u_n for $\lambda > 0$ are not shown since they are indistinguishable from those of the w_n. Inset: log–log plot of the fourth-order correlation function $F_{2,2}(k_n, k_7)$ vs k_7 calculated for the linear field $(+)$ and for the nonlinear field (solid line) at $\lambda = 0$.
Source: Figure reproduced from [122].

$$\begin{aligned}\Phi_n(u,w) &= k_{n+1}[(1+\delta)u_{n+2}w^*_{n+1} + (2-\delta)u^*_{n+1}w_{n+2}] \\ &+ k_n[(1-2\delta)u^*_{n-1}w_{n+1} - (1+\delta)u_{n+1}w^*_{n-1}] \\ &+ k_{n-1}[(2-\delta)u_{n-1}w_{n-2} + (1-2\delta)u_{n-2}w_{n-1}]\end{aligned} \tag{358}$$

Expression (358) is obtained by taking the antisymmetric part of the original Sabra model. It is easy to see that $\Sigma_n|u_n|^2$, $\Sigma_n|w_n|^2$ an $\Sigma_n u_n w^*_n + w_n u^*_n + c.c$ are conserved quantities for $\nu = 0$ and no forcing as for the passive vector, as in the case of Eqs. (355). In Fig. 72 we show the sixth order structure functions for the non linear Sabra model and for the passive vector at different value of λ: this is a clear check (at least for the shell model) that the limit $\lambda \to 0$ is not singular and that the anomalous exponents of the passive vector are the same of the non-linear Sabra model.

We can do more. Using the previous discussion on the statistical preserved quantities, we know that the same argument applied to the passive vector, namely we can use the correlation functions *of the forced case* to build the statistically preserved quantities for the *decaying case*. Instead of doing that, we now use the correlation function of the non-linear forced Sabra model. More precisely, let us define

$$Z^{(2)}(n) = \langle |u_n|^2 \rangle \tag{359}$$

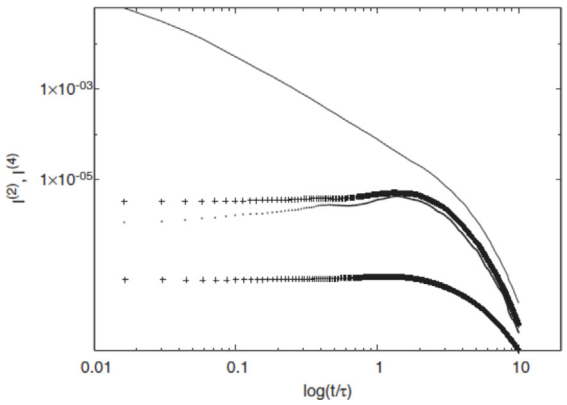

Fig. 73. We show in the figure with the symbols (+) the constants $I^{(2)}$ (bottom) and $I^{(4)}$ (top) constructed by projecting the decaying structure function of the linear model on the forced structure function of the nonlinear model. To emphasise the importance of using the correct SPS, we also show the result for $I^{(4)}$ using the dimensional Kolmogorov prediction for $Z^{(4)}$ (small dots) and $Z^{(4)} = 1$ corresponding to decaying behaviour (solid line).
Source: Figure reproduced from [122].

$$Z^{(4a)}(n,m) = \langle |u_n|^2 |u_m|^2 \rangle \tag{360}$$
$$Z^{(4b)}(n) = \langle u_n u_{n+1}^2 u_{n+3}^* \rangle \tag{361}$$
$$Z^{(4c)}(n) = \langle u_n u_{n+1} u_{n+3} u_{n+4}^* \rangle \tag{362}$$

for the forced non linear Sabra model. Then, we now compute the same quantity for $f^{(w)} = 0$ so that the vector field is decaying in time:

$$F_2(n,t) = \langle |w_n|^2 \rangle \tag{363}$$
$$F_{4a}(n,m,t) = \langle |w_n|^2 |w_m|^2 \rangle \tag{364}$$
$$F_{4b}(n,t) = \langle w_n w_{n+1}^2 w_{n+3}^* \rangle \tag{365}$$
$$F_{4c}(n,t) = \langle w_n w_{n+1} u_{n+3} w_{n+4}^* \rangle \tag{366}$$

The last step is to evaluate the two quantities:

$$I_2 = \Sigma_n F_2(n,t) Z^{(2)}(n) \tag{367}$$
$$I_4 = \Sigma_{nm} Z^{(4a)}(m,n) F_{4a}(m,n,t) + \Sigma_n [Z^{(4b)}(n) F_{4b}(n,t) + Z^{(4c)}(n) F_{4c}(n,t)] \tag{368}$$

The crucial and non trivial observation is that if the non linear Sabra model has the same anomalous scaling of the passive vector, then both I_2 and I_4 should be constant *on average*. Numerical simulations show that this is the case 73: the correlation functions of the non linear Sabra model plays the role of the zero modes (that we know to exist) for the passive vector. This result strongly points out that the non linear model exhibits the same class of properties (universality with respect to forcing and dissipation mechanism) which characterise the existence of the zero modes and their role in anomalous scaling. This result implies that the anomalous scaling of the non-linear Sabra model can be computed by knowing the scaling properties of the zero modes of the passive vector. The last problem is mathematically difficult although well-defined conceptually and one may try to employ different perturbation approaches to solve it.

Lecture 7.9. Summary of Lecture 7

In this lecture, we have seen a number of new concepts and results. It is quite clear that the Kraichnan model is an important breakthrough to understanding intermittency in the passive scalar. Although the velocity field in the Kraichnan model is rather unrealistic (gaussian and δ-correlated in time), it is *rough* in the sense that $\delta v(r)$ does not scale as r. Then, the arguments discussed in Lecture 1 for the Richardson diffusion can be applied and intermittency in the passive scalar can be linked to the breaking of lagrangian trajectories. This is the physical reason behind the solution of the Kraichnan model, namely the dominating role of *zero modes* in the anomalous scaling of the passive scalar correlation functions in the inertial range dynamics. A proper mathematical framework for these ideas is reviewed in [1]. To simplify the discussion, we decided to illustrate how to compute zero modes using a simplified shell model. However, all the concepts we introduce are general and shell models are used just as a simple way to avoid mathematical difficulties. This is also true for the discussion of *statistically preserved structures* which opens the way to extend the results obtained in the Kraichnan model for the passive scalar turbulence advected in realistic flows. In [120] it is shown how statistically

preserved structures arise in the case of two-dimensional passive scalar turbulence taking advantage of the lagrangian formulation for the dynamics. The same idea can be successfully applied in shell models for passive scalar and extended to the non-linear case. One natural question is whether the results discussed in this chapter provide a physical interpretation of intermittency that is different from the one discussed using the multifractal framework. We argue that, in fact, the results on passive scalar turbulence complement the multifractal framework showing that intermittency is a fundamental property of inertial range dynamics whose statistical features are independent of large-scale forcing and small-scale dissipation. New concepts like zero modes and statistically preserved structures highlight the physical reason which supports our claim of universality in the anomalous scaling.

Lecture 8. Non isotropic turbulence

In many interesting problems turbulence is produced by an external non-isotropic forcing. This is the case, for instance, in channel flow turbulence or in natural convection for Rayleigh–Bénard turbulence. How can we deal with non-isotropic turbulence? In this lecture, we provide some answers to this question.

The issue of non-isotropic fluctuations is in fact more general. Even in the numerical simulations, no matter how accurately we can design the large scale forcing, some degrees of non-isotropic fluctuations is always present in the system. This is obviously true for experimental conditions like, for instance, turbulence in the wake of a solid body in wind tunnel experiments. Thus the first question to answer is can we say anything from a theoretical point of view? The basic idea, as pioneered in the original Kolmogorov's theory of turbulence, is that for large enough Re and small enough scale r, the statistical properties of turbulence are *locally* homogeneous and isotropic. However, this is a rather general statement that needs to be defined in a better way. Fortunately, we have at least one simple case where the statistical properties of turbulence are under some control, namely the case discussed in detail in the previous lecture concerning the Kraichnan model of a passive scalar. We will use this model to make some general remarks and then we can apply our findings to discuss some specific cases.

Lecture 8.1. The SO(3) decomposition

The equation of motions, both the N.S. and/or Kraichnan's model, are invariants under rotations. This is true unless the external forcing introduces a specific preferential direction as, for instance, in the case of a forcing induced by an external gradient in the velocity field. Thus we immediately understand we are facing two different problems: the first one is associated to the case of a statistically isotropic forcing where invariance under rotation holds *statistically*; the second one deals specifically with the case of non-isotropic forcing like those previously mentioned, i.e. channel flow turbulence or Rayleigh–Bénard system.

Let us focus on the first class of problems where rotational invariance holds statistically. The basic idea underlying our approach has been discussed in detail in [123,124] and it is hereafter shortly sketched. Let us consider a generic multipoint correlation function $C^{(n)}_{\alpha_1,\alpha_2,\ldots,\alpha_n}(\vec{x}_1,\vec{x}_2,\ldots,\vec{x}_n) = \langle u_{\alpha_1}(\vec{x}_1)u_{\alpha_2}(\vec{x}_2)\ldots u_{\alpha_n}(\vec{x}_n)\rangle$. Under rotation $C^{(n)}_{\alpha_1,\alpha_2,\ldots,\alpha_n}(\vec{x}_1,\vec{x}_2,\ldots\vec{x}_n)$ transforms as the product of n vector, i.e. a tensor of order n. In general $C^{(n)}_{\alpha_1,\alpha_2,\ldots\alpha_n}(\vec{x}_1,\vec{x}_2,\ldots\vec{x}_n)$ depends on the size $x_i = |\vec{x}_i|$ and the orientation $\hat{x}_i$ of the vectors $\vec{x}_i$. We are interested to understand how rotation can change the functional form of $C^{(n)}_{\alpha_1,\alpha_2,\ldots\alpha_n}(\vec{x}_1,\vec{x}_2,\ldots\vec{x}_n)$ on the orientations $\hat{x}_i$. This can be easily achieved if we can *represent* $C^{(n)}_{\alpha_1,\alpha_2,\ldots\alpha_n}(\vec{x}_1,\vec{x}_2,\ldots\vec{x}_n)$ in some general way as a function of the orientation $\hat{x}_i$. Now, the crucial observation is that rotations in a three-dimensional space forms a group, the $SO(3)$ group. Then, mathematics tells us that the angular dependence of $C^{(n)}_{\alpha_1,\alpha_2,\ldots\alpha_n}(\vec{x}_1,\vec{x}_2,\ldots\vec{x}_n)$ can be decomposed on a suitable orthogonal basis of functions that can be derived using spherical harmonics $Y_{jm}(\hat{r})$ (we refer to [123] for the proper discussion). The index j in the decomposition of $C^{(n)}_{\alpha_1,\alpha_2,\alpha_n}(\vec{x}_1,\vec{x}_2,\ldots\vec{x}_n)$ refers to the *angular momentum* of the configuration $\hat{x}_i$. A this stage, mathematics becomes rather complex. However, the relevant and highly non-trivial conclusion is that every j component of the representation satisfies equations which do not mix with different values of j. This statement can be proved for the Kraichnan model and it is argued to hold for the N.S. equation. In other words, the basic conclusion is that $C^{(n)}_{\alpha_1,\alpha_2,\ldots\alpha_n}(\vec{x}_1,\vec{x}_2,\ldots\vec{x}_n)$ can be represented as the sum of different correlation functions with their own j. For our purpose, this implies that the general form of the scaling of structure functions can be represented as:

$$S^{(n)}(\vec{r}) = \sum_{jm} S^{(n)}_{jm}(r)Y_{jm}(\hat{r}) \tag{369}$$

The functions $S^{(n)}_{jm}(r)$ have their own scaling exponents for small r referred to as $\zeta^{(n)}_j$. The important result is that one can show the following inequality:

$$\zeta^{(n)}_0 < \zeta^{(n)}_{j>0} \tag{370}$$

Besides their mathematical derivation, Eqs. (369) and (370) represent the solution to our first problem. Notice that Eq. (370) holds in general, i.e. for $\zeta^{(n)}$ not necessarily equal to Kolmogorov's theory and its generalisation. Eq. (369) tells us that the proper way to study non isotropic effects in turbulence is to decompose the structure functions in their different j sector. Moreover, because of (370), we understand that for large enough Re and small enough scales r, the

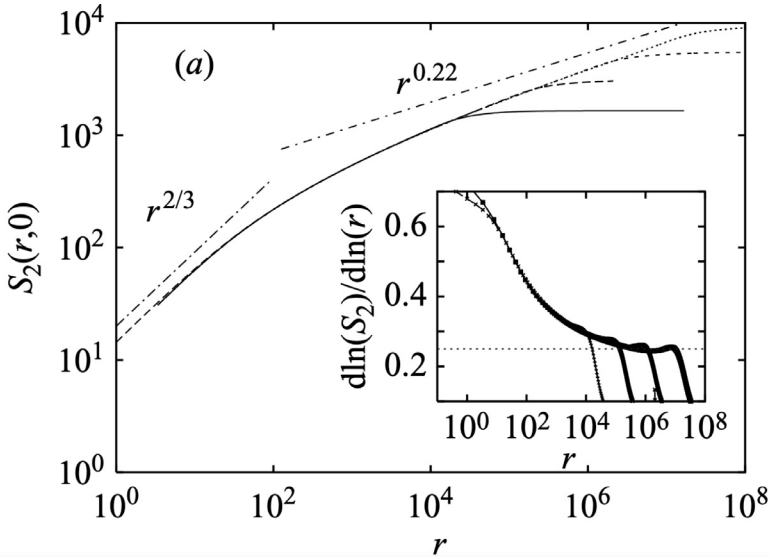

Fig. 74. The scalar second-order structure function measured in the x-direction, $S2(r,0)$, fixing σ and varying L_f. The inset shows the local slopes. Note that the approach to the asymptotic scaling $r^{0.22}$ is even slower than in the spectra.
Source: Figure reproduced from [125].

isotropic contribution is the dominant one. Thus Eqs. (369) and (370) should be considered as rather general and non-trivial results derived from the invariant properties of the N.S. equations under $SO(3)$ transformations. In general, however, the computation of $\zeta_j^{(n)}$ cannot be done exactly and some results are available for a few specific cases (see again [123]).

One interesting outcome of Eqs. (369) and (370) concerns the effect of non-isotropy in the intermittent properties of the passive scalar advected by turbulent flows. In the past, one quantity used to discuss the relevance of non-isotropic effects was to consider the quantity

$$S(r) \equiv \frac{\langle \delta\theta(r)^3 \rangle}{(\langle \delta\theta(r)^2 \rangle)^{3/2}} \tag{371}$$

i.e. the skewness of $\delta\theta(r)$, which can be easily computed from any experimental and/or numerical simulations. In some cases, $S(r)$ does not decrease for $r \to 0$ and, in fact, it can even increase at small r. From Eqs. (369) and (370) we understand that the behaviour of $S(r)$ for small r does not tell us anything about isotropy versus non-isotropy. Assuming that the forcing can be considered statistically stationary, we should compute the quantity $S_{jm}^{(n)}$ to assess the proper relevance of the isotropic fluctuations. In other words, the statistical properties of $\delta\theta(r)$ are not suitable to study the relevance of non-isotropic effects using expressions like Eq. (372). Eqs. (369) and (370) clarify this point in a clean and elegant way.

Lecture 8.2. Shear effects in passive scalar

We now turn our attention to the second problem, namely, we do have a non-isotropic forcing in the system and we would like to know if and how intermittency may depend on the effect of anisotropy. We start by analysing a relatively simple problem for a passive scalar to understand how non-isotropic forcing can change the scaling properties of $S_2(r) = \langle \delta\theta(r)^2 \rangle$ [125]. We assume that the velocity field advecting the scalar θ is given by:

$$\vec{v} = Sy\hat{x} + \vec{u} \tag{372}$$

The aim is to compute how the scaling properties of $\langle \delta\theta(r)^2 \rangle$ depend on S knowing the scaling properties of $\vec{u}$. First of all let us compute $\langle \delta\theta(r)^2 \rangle$ for $S = 0$. We already did it in the previous lecture pointing out the difficulties in estimating intermittency corrections. Here we want to use a different approach which is particularly useful when $\vec{u}$ is the one prescribed by Kraichnan's model.

The quantity $\langle \delta\theta(r)^2 \rangle$ is related to the correlation of $C(\vec{r}) = \langle \theta(\vec{r}_1)\theta(\vec{r}_2) \rangle$ which depends on $\vec{r} = \vec{r}_2 - \vec{r}_1$. From the point of view of lagrangian dynamics, the passive scalar is described in the limit $\kappa \to 0$ by the equation:

$$\frac{d\theta}{dt} = f(r/L, t) \tag{373}$$

where $f(r/L, t)$ is a shorthand notation for the large-scale forcing applied to θ. Each particle carries on the value of θ according to (373) while being advected by the velocity field $\vec{u}$. Then the correlation $C(\vec{r})$ depends on the probability for

two particles being at separation $\boldsymbol{r} \equiv \boldsymbol{r}_1 - \boldsymbol{r}_2$. The latter quantity should be proportional to the time $T(\boldsymbol{r})$ spent *on average* by the two particles at a separation $\boldsymbol{r}$. This intuitive result is discussed in [1,119], with the proper mathematical formalism, and it enables us to obtain the scaling of $\langle \delta\theta(r)^2 \rangle$ using Richardson diffusion. To see how it works, let us consider the case of a passive scalar advected by a velocity field satisfying the Kolmogorov scaling. We consider two particles separated by a distance R whose evolution is given by

$$\frac{dR}{dt} = \delta u(R) \sim R^{1/3} \tag{374}$$

Now we assume $R \sim t^\alpha$. According to our previous argument, the scaling of $\langle \delta\theta(R)^2 \rangle \sim t(R) \sim R^{1/\alpha}$. Thus we need to compute α. In this case, upon substituting $R \sim t^\alpha$ in Eq. (374) we obtain:

$$t^{\alpha-1} \sim t^{\alpha/3}$$

from which we obtain $\alpha = 3/2$. Then $\langle \delta\theta(R)^2 \rangle \sim t \sim R^{2/3}$ is in agreement with the known result.

Now, we want to apply the above procedure to the case (372) where $\vec{u}$ is the velocity field of Kraichnan's model. For the Kraichnan's model $\delta u(R)$ is a random velocity field δ-correlated in time. Then, from $dR/dt = \delta u(R)$ we obtain:

$$R(t) = \int ds \delta u(R,s) \rightarrow \langle R^2(t) \rangle = \left\langle \int ds_2 \int ds_1 \delta u(R,s_1) \delta u(R,s_2) \right\rangle \tag{375}$$

Next we use the identity $\langle \delta(R,s_1)\delta(R,s_2) \rangle = \langle \delta u(R)^2 \rangle \delta(s_2 - s_1)$. From this expression we obtain:

$$\langle R^2 \rangle = \int ds \langle \delta u(R)^2 \rangle \rightarrow \frac{d\langle R^2 \rangle}{dt} = \left\langle \delta u(R)^2 \right\rangle \tag{376}$$

For the Kraichnan's model we know that $\langle \delta u(R)^2 \rangle = R^\xi$. Then we assume $R \sim t^\alpha$ and using (376) we obtain $\alpha = 1/(2-\xi)$. This implies, according to our previous discussion, that $\langle \delta\theta(R)^2 \rangle \sim t \sim R^{1/\alpha} = R^{2-\xi}$ as expected.

We are now ready to compute what happens for $S \neq 0$. We introduce the equations:

$$\dot{R}_x = S R_y + \delta u_x(R) \tag{377}$$

$$\dot{R}_t = \delta u_t(R) \tag{378}$$

where the subscript t (not to be confused with time) stands for the transversal direction with respect to $\hat{x}$. We now assume $R_x \sim t^\alpha$ and $R_t \sim t^\beta$. Then from (377) the leading contribution for large S gives $\alpha - 1 = \beta$ while from (378) we have $2\beta - 1 = \alpha\xi$. The latter equation comes from:

$$\frac{d\langle R_t^2 \rangle}{dt} = \left\langle \delta u_t(R)^2 \right\rangle \sim R_x^\xi.$$

The final results is $\alpha = 3/(2-\xi)$ and $\beta = (1+\xi)/(2-\xi)$. Since R_x is dominating with respect to R_t, we can easily argue that for large enough R the scaling of $\langle \delta\theta(R)^2 \rangle$ goes as $R^{(2-\xi)/3}$. For small enough R, we can neglect the first term on the r.h.s. of (377) and we recover the scaling $R^{2-\xi}$. Thus the effect of the external shear S introduces a scale L_S above which the scaling properties (and the intermittency as well) change because of the shear, S. For $R < L_S$ we expect to recover the isotropic scaling. We expect L_S to decrease for increasing values of S. This can be deduced using the balance equation $SL_S = \delta u(L_S)$ from Eq. (377). For $\xi = 4/3$, equivalent to the Kolmogorov scaling $\langle \delta u(R)^2 \rangle \sim R^{2/3}$, all the expectations from (377)–(378) are nicely confirmed by numerical simulations shown in Fig. 74. Notice that we expect $\delta\theta(R)^2 \sim R^{2/9}$ at large enough R and $R^{2/3}$ at small R.

Lecture 8.3. Intermittency in shear flows and boundary layers

Now, we want to understand if something similar is happening in the case of N.S. equation. For this purpose, we consider the rather theoretical situation of a homogeneous shear flow (HS) in the direction $\hat{x}$ described by the equation:

$$\frac{\partial \boldsymbol{v}}{\partial t} + \boldsymbol{v} \cdot \nabla \boldsymbol{v} + Sy \frac{\partial \boldsymbol{v}}{\partial y} + v_y S \hat{x} = -\frac{1}{\rho} \nabla p + \nu \Delta \boldsymbol{v} \tag{379}$$

Although artificial, homogeneous shear flows can be simulated numerically by using a quite ingenious trick with periodic boundary conditions [38]. It turns out that many physical features observed in HS are also observed in properly designed laboratory experiments. In the following, we will discuss both cases.

Looking at Eq. (379) one immediately understands that the shear S plays a double role: on one hand it is the source of turbulence in the system (as in boundary layer turbulence) and on the other hand it modifies the energy transfer from large to small scales because it modifies the Kolmogorov 4/5 equations. The last statement is quite complicated to discuss since for HS one cannot make any claim of isotropy. Here we refrain to discuss what is the proper mathematical objects which should be considered in the 4/5 equation for HS. The final result of this investigation is however important. For HS the 4/5 equation is modified as follows [126]:

$$\left\langle \delta v(r)^3 \right\rangle + \alpha S r \langle \delta v(r)^2 \rangle \sim \epsilon r \tag{380}$$

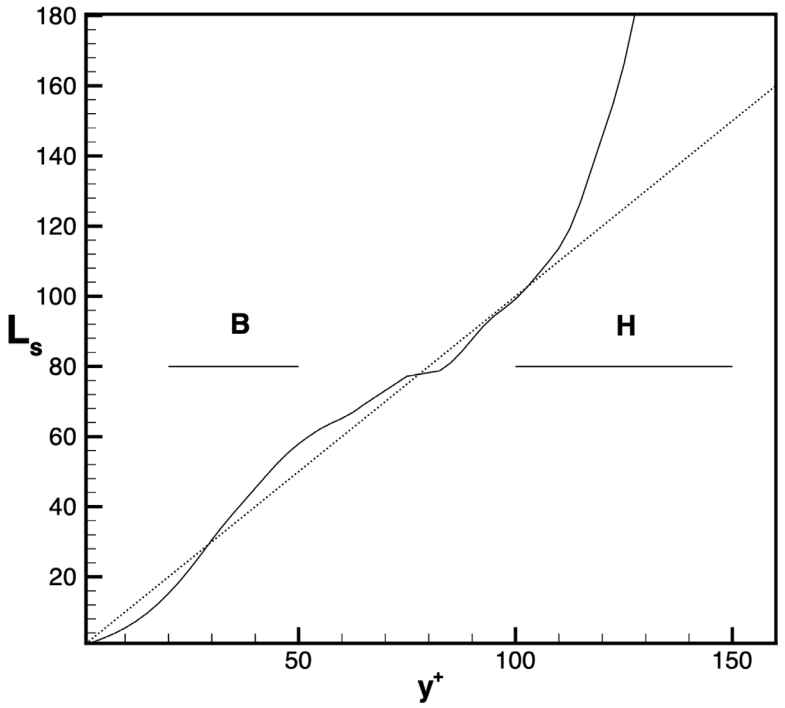

Fig. 75. The characteristic scale $L_s(y^+)$ as a function of y^+ (continuous line). The dotted line is reported to enlighten the growth of L_s out of the wall region.
Source: Figure reproduced from [128].

where α is a number order 1 independent on S. For boundary layer turbulence S should be replaced by a y-dependent local shear rate $S(y)$. Eq. (380) is a simplified version of the more cumbersome one obtained by (379) [127]. Even if simplified, Eq. (380) tells us two important things: A) the energy dissipation ϵ plays some role already discussed in homogeneous and isotropic turbulence; B) there exists some scale L_S such that for $r > L_S$ the statistical properties of turbulence should be modified by the presence of the shear S. To compute L_S we can use the K41 estimate $\delta v(r) \sim \epsilon^{1/3} r^{1/3}$ and compute L_S by solving $\langle \delta v(L_S)^3 \rangle \sim \alpha S r \langle \delta v(L_S)^2 \rangle$. This gives [128]:

$$L_S = \sqrt{\frac{\epsilon}{S^3}} \tag{381}$$

Actually, the presence of the shear S introduces a momentum flux q^2 in the y direction as we already discussed in the first lecture for boundary layer turbulence. Then we can introduce the scale $L_0 \equiv q^3/\epsilon$ which is the *large scale* associated to the forcing mechanism *as if* we consider the case of homogeneous and isotropic turbulence. Finally, upon defining $S_* = Sq^2/\epsilon$, it is easy to see that

$$S_* = \left[\frac{L_0}{L_S}\right]^{2/3} \tag{382}$$

The physical meaning of the dimensionless parameter S_* is clear [129,130]: for large S_* there exists a range of scale $\in [L_S, L_0]$ where turbulence is modified by the effect of the shear whereas for small S_* we should recover the case of homogeneous and isotropic turbulence. In analogy with (382) we can introduce the parameter $S_c \equiv (\eta/L_S)^{2/3}$. Then for large *Re* number we expect S_c to be very small: in the limit of small S_c and large S_* one should observe two different kind of turbulence: one dominated by the shear effect S and the other one close to the homogeneous and isotropic case. This result is already non-trivial and is obtained essentially by dimensional analysis applied to Eq. (380) and it is qualitatively in agreement with the case of passive scalar discussed above. In Fig. 75 we show L_S as a function of wall distance y^+ for boundary layer turbulence while in Fig. 76 we show the velocity profile of the boundary layer turbulence. Upon increasing y^+, L_S increases and becomes larger than y^+ and we can identify two possible regions in the system indicated by H for homogeneous isotropic turbulence and B for shear-dominated turbulence.

We want now to understand what are the turbulence properties in the shear-dominated range. say the region B where for boundary layer turbulence in Fig. 75 and/or for large shear values of S_* in homogeneous shear flow. In particular, we are interested in understanding if and how intermittency is different when the (local) shear rate is large. We start by looking at the most elementary measure of intermittency, namely the kurtosis. In Fig. 77 we show $k(r) = \langle \delta u(r)^4 \rangle / \langle \delta u(r)^2 \rangle^2$ at

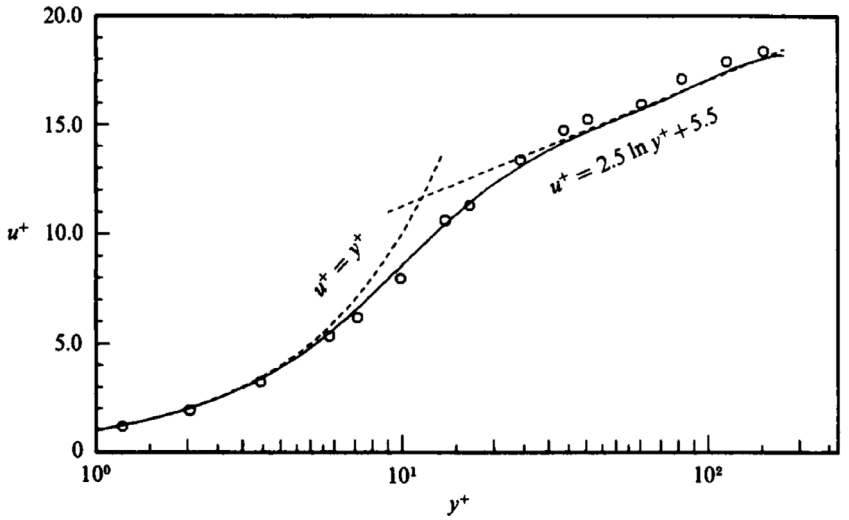

Fig. 76. Mean-velocity profiles (continuous line), symbols correspond to the 'corrected' data of Eckelmann (1974).
Source: Figure reproduced from [131].

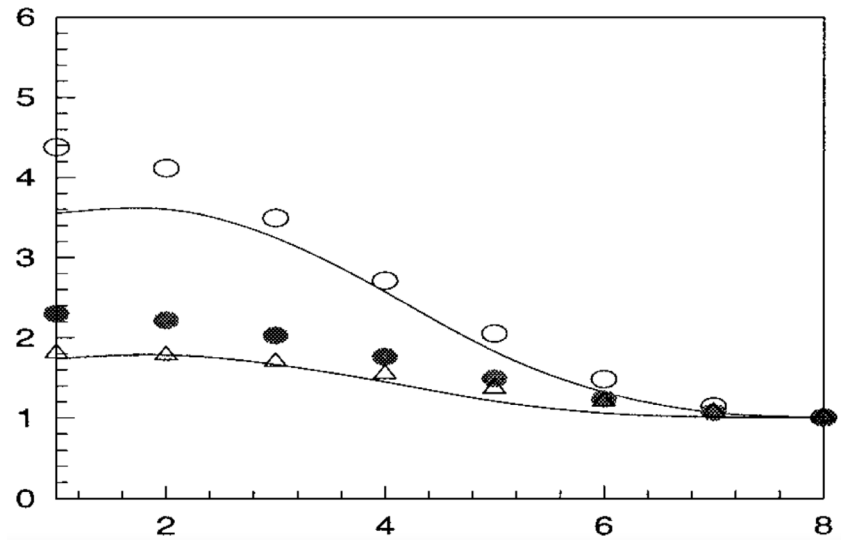

Fig. 77. Flatness, $F = \langle \delta V^4 \rangle / \langle \delta V^2 \rangle^2$ vs. $\log_2(r^+/D_x^+)$, $D_x^+ = 2.5$, at $y^+ = 151$ (open triangles) and at $y^+ = 31$ (open circles), as evaluated using F_b and F_w, respectively, see Eqs. (385)–(386). For comparison, filled circles, F_b applied at $y^+ = 31$. Correspondingly, the solid lines give the flatness as evaluated directly in terms of velocity.
Source: Figure reproduced from [130].

two points in the boundary layer turbulence in regions H and B (continuous lines) while in Fig. 78 we show $k(r)$ for homogeneous shear flow as compared with the same result for homogeneous and isotropic turbulence. Quite clearly we observe an increase of intermittency in the system for large shear flow. The next question to answer is why intermittency increases when S (local or not) becomes large enough.

To provide an answer to this question let us come back to Eq. (380). In the shear-dominated region, the second term on the r.h.s should become the dominant one. Then we can wonder whether a new form of RKSH is working. Using the notation $S_n(r) \equiv \langle \delta u(r)^n \rangle$ and $\epsilon(r) = r^{-3} \int_{B(r)} \epsilon(x) d^3x$, the RKSH in its generalised form for homogeneous and isotropic turbulence reads:

$$S_{3n}(r) = \frac{\langle \epsilon(r)^n \rangle}{\langle \epsilon \rangle^n} S_3(r)^n \tag{383}$$

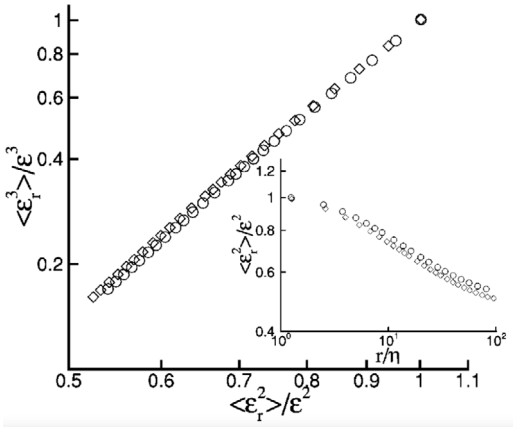

Fig. 78. $\langle\epsilon_r^3\rangle$ vs $\langle\epsilon_r^2\rangle$ in the homogeneous shear flow (circles) and in homogeneous isotropic turbulence (diamonds). In the inset $\langle\epsilon_r^2\rangle$ vs r/η for the two cases.
Source: Figure reproduced from [132].

The form of RKSH in (383) takes advantage of the ESS scaling discussed in Lecture 4 which mitigates the issue of finite size effects. In the shear-dominated region, we expect that the new form of RKSH should be

$$S_{2n}(r) = \frac{\langle\epsilon(r)^n\rangle}{\langle\epsilon\rangle^n} S_2(r)^n \tag{384}$$

Thus in the shear-dominated region we expect that the kurtosis is given by $\langle\epsilon(r)^2\rangle/\langle\epsilon\rangle^2$ at variance with the homogeneous and isotropic case where the kurtosis is given by $\langle\epsilon(r)^{4/3}\rangle/\langle\epsilon^{2/3}\rangle^2$. Using (383) and (384) we can write how the flatness $F(r)$ changes when the shear is relatively weak or large. Upon denoting $F_b(r)$ and $F_w(r)$ the two different cases, we obtain:

$$F_b(r) = \frac{\langle\epsilon(r)^{4/3}\rangle}{\langle\epsilon(r)^{2/3}\rangle^2} \tag{385}$$

$$F_w(r) = \frac{\langle\epsilon(r)^{4/2}\rangle}{\langle\epsilon(r)^{2/2}\rangle^2} \tag{386}$$

In Fig. 77 the open symbols refers to expression (385)–(386) for the boundary layer at $y^+ = 31$ (open circles in shear-dominated region using $F_w(r)$) and $y^+ = 151$ (open triangles in the region of weak shear effects where $F_b(r)$ is used). For comparison we plot $F_b(r)$ in the shear dominated region $y^+ = 31$ in filled circles.

Now, *if the scaling of* $\epsilon(r)$ *does not change* in the shear-dominated region with respect to the homogeneous and isotropic turbulence, we may think to explain the increase of the kurtosis as shown in the Figs. 77 and 15 To make progress, first, we need to understand if the statistical properties of $\epsilon(r)$ are different in the two cases (shear dominated and homogeneous isotropic case); second, we need to verify whether the new for of RKSH given by Eq. (384) is correct and finally whether we can explain quantitatively the increase of intermittency in the shear dominate range.

Upon defining $\Pi_n \equiv \langle\epsilon(r)^n\rangle/\langle\epsilon\rangle^n$, in Fig. 78 we show Π_3 versus Π_2 for both homogeneous and isotropic turbulence and shear flows whereas in the inset of Fig. 78 we show Π_2 versus r/η or the two different cases. Altogether the figure provides evidence that the statistical properties of $\epsilon(r)$ do not change for shear dominated turbulence. Next, in Figs. 79 we check the validity of the standard form of RKSH and in particular we look at $S_6(r)$ versus $\langle\epsilon(r)^2\rangle S_3(r)^2$ at two different points in the boundary layers, i.e. $y^+ = 151$ (open triangles) and $y^+ = 31$ (open circles). While in the region of weak shear ($y^+ = 151$) RKSH holds with very good precision, this is not true in the shear-dominated region at $y^+ = 31$. We now look at the validity of the new form of RKSH and in Fig. 80 we look at the relation $S_4(r)$ versus $\langle\epsilon(r)^2\rangle S_2(r)$: while the original RKSH (383) does not hold, the new version of RKSH seems to be extremely well verified in the shear-dominated case. The same result holds for turbulence in a homogeneous shear. In Figs. 81 we show the very same analysis for the new form of RKSH with an excellent agreement.

We are now able to provide another quantitative result demonstrating the validity of (384). Let us define, using ESS, the anomalous scaling ζ_n by the relation:

$$S_n(r) \sim S_3(r)^{\zeta_n} \tag{387}$$

In homogeneous isotropic turbulence, ζ_n are the numbers we discussed in the previous lectures. For shear-dominated flows, we still use (387) and refer to the anomalous exponents as $\hat{\zeta}_n$ to highlight the difference with the isotropic case.

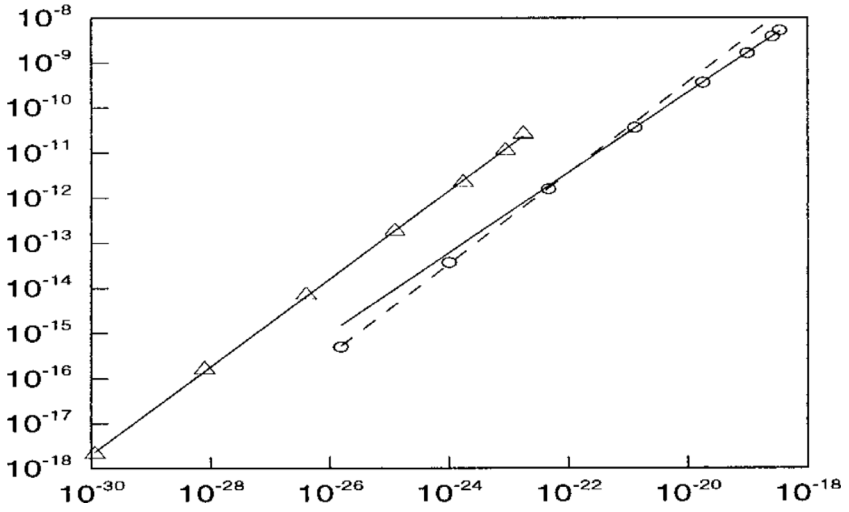

Fig. 79. Check of the RKHS in boundary layer: $S_6(r)$ versus $\langle\epsilon(r)^2\rangle S_3(r)^2$ at $y^+ = 151$ (open triangles) and $y^+ = 31$ (open circles).
Source: Figure reproduced from [130].

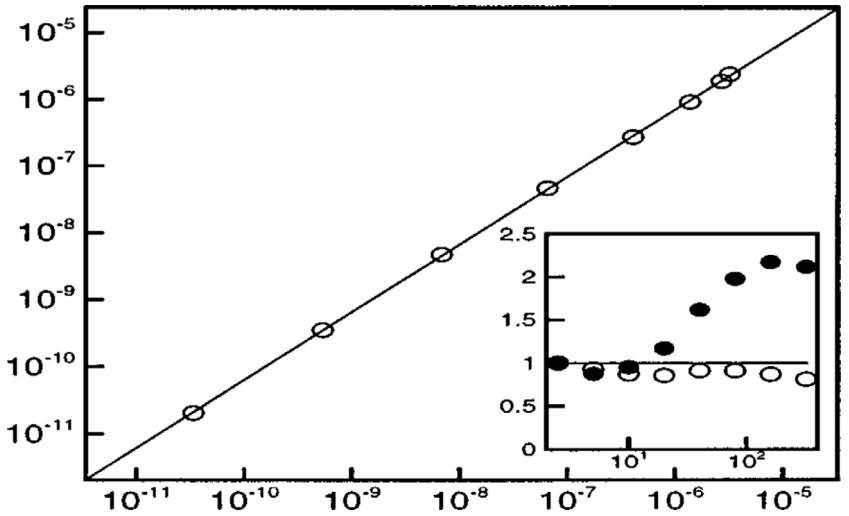

Fig. 80. Validity of the new form of RKHS in the shear dominated region of the boundary layer $y^+ = 31$. The main figure shows $S_4(r)$ versus $\langle\epsilon(r)^2\rangle S_2(r)^2$. In the inset we plot $S_2(r)^2\langle\epsilon(r)^2\rangle/S_4(r)$ (open circles) and $S_3(r)^2\langle\epsilon(r)^2\rangle/S_6 r$ as a function of r.
Source: Figure reproduced from [130].

We want to compute $\hat{\zeta}_n$ as a function of ζ_n. For this purpose we observe that, using (384), the following identity should be true [132]:

$$\hat{\zeta}_{2n} - n\hat{\zeta}_2 = \zeta(3n) - n \equiv \tau(n) \tag{388}$$

Since $\hat{\zeta}_3 = 1$ anyway, using (388) with $n = 3/2$ we obtain:

$$\hat{\zeta}_2 = \frac{2}{3}[1 - \tau(3/2)] \tag{389}$$

Then from (388) we obtain:

$$\hat{\zeta}_n = \zeta_{3n/2} - \frac{n}{2} + \frac{n}{3}[1 - \tau(3/2)] \tag{390}$$

This equation is the result we were looking for. If our arguments (i.e. Eq. (384)) is correct), we should observe for large S_* and large *Re* two different scaling regimes for the structure functions: at large scale $r > L_S$ the scaling is given by $\hat{\zeta}_n$ in Eq. (390) while at the small scale we should recover the scaling ζ_n.

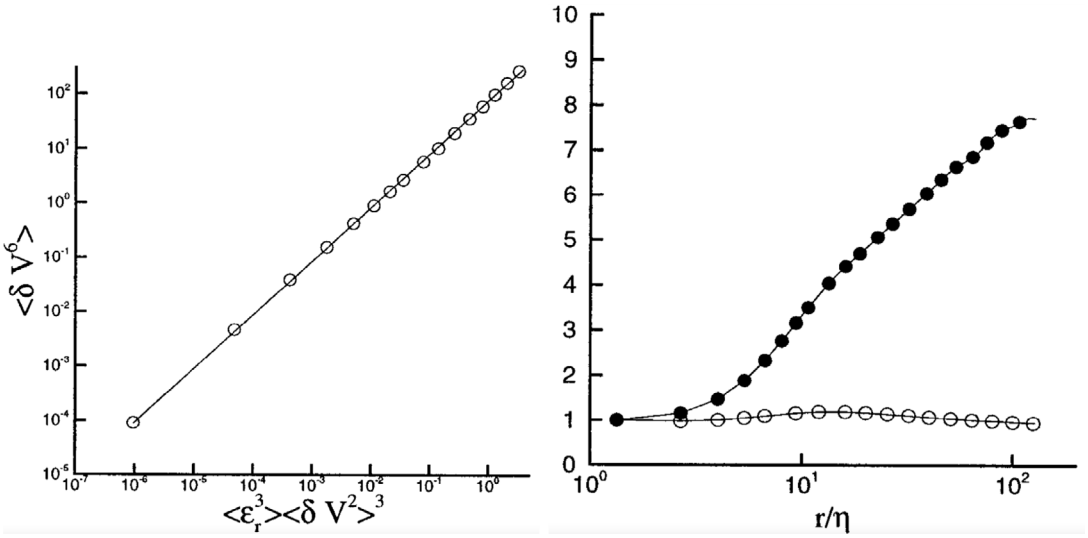

Fig. 81. Validity of the new for of RKSH for homogeneous shear: on the left we show $S_4(r)$ versus $\langle\epsilon(r)^2\rangle S_2(r)^2$ while on the right we plot $S_2(r)^2\langle\epsilon(r)^2\rangle/S_4(r)$ (open circles) and $S_3(r)^2\langle\epsilon(r)^2\rangle/S_6(r)$ as a function of r.
Source: Figures reproduced from [129].

Table 3
Scaling exponents of structure functions (DNS) above and below the shear scale L_s. Data are compared with those of homogeneous and isotropic turbulence and with the prediction of Eq. (390).
Source: Reproduced from [132].

p	1	2	3	4	5	6
$r < L_s$	0.36	0.69	1.00	1.28	1.54	1.78
$r > L_s$	0.38	0.72	1.00	1.23	1.42	1.56
hom.iso	0.36	0.69	1.00	1.28	1.54	1.78
Eq. (390)	0.39	0.73	1.00	1.23	1.42	1.58

In Table 3 we show the numerical values of the different ζ_n and $\zeta_n(S)$ computed using (390). We now consider the scaling and the local slopes for $\sigma_p \equiv S_p(r)/S_2(r)^{p/2}$ and $\rho_p \equiv S_p(r)/S_3(r)^{p/3}$ which, according to (390), should gives different scaling in different regions. In particular we have:

$$\sigma_n = S_3(r)^{\tau(n/2)} \; for \quad r \gg L_S \tag{391}$$
$$\sigma_n = S_3(r)^{\tau(n/3)-n\tau(2/3)/2} \; for \quad r \ll L_S \tag{392}$$

and

$$\rho_n = S_3(r)^{\tau(n/2)-n\tau(3/2)/3} \; for \quad r \gg L_S \tag{393}$$
$$\rho_n = S_3(r)^{\tau(n/3)} \; for \quad r \ll L_S \tag{394}$$

In Fig. 82 we show the scaling behaviour of σ_n and ρ_n versus $S_3(r)$ with $n = 6$, while in the inset of the figures the local slopes $d\log(\sigma_n)/d\log S_3$ and $d\log(\rho_n)/d\log S_3$ respectively [132]. Although the range of scaling is not large, there is quite clear evidence that there are two different scaling regions depending on if r is larger or smaller than L_S and that the scaling exponent (within the ESS framework) are in agreement with Eqs. (391)–(394). Notice that the two sets of curves shown in the figures refers to the homogeneous shear flow and boundary layer turbulence. Overall we can safely reach the conclusion that in shear-dominated flows there is an increase of intermittency and that this increase can be explained in terms of a new form of the RKSH. Physically this implies that the whole framework developed in the previous lectures remains valid provided we do change the relation between $\delta v(r)$ and $\epsilon(r)$ following Eq. (384). This is a quite non-trivial result and it is in complete analogy, from the physical point of view, to the discussion of a passive scalar in shear flow for Kraichnan's model.

We can wonder whether our previous discussion on SO(3) decomposition can add something to our findings. To this purpose, we consider a numerical simulation of homogeneous shear performed at *Re* rather large using highly resolved large eddy simulations, that is an eddy viscosity at small scales aimed at increasing the inertial range resolution L/η [133]. In particular we consider three values of S_*, namely 2.2 (low), 5.4 (intermediate) and 7 (large). At variance with the previous analysis, we now look at the scaling in r and we compute the $S_n^{(0,0)}$ in the isotropic sector. In Fig. 83 we show

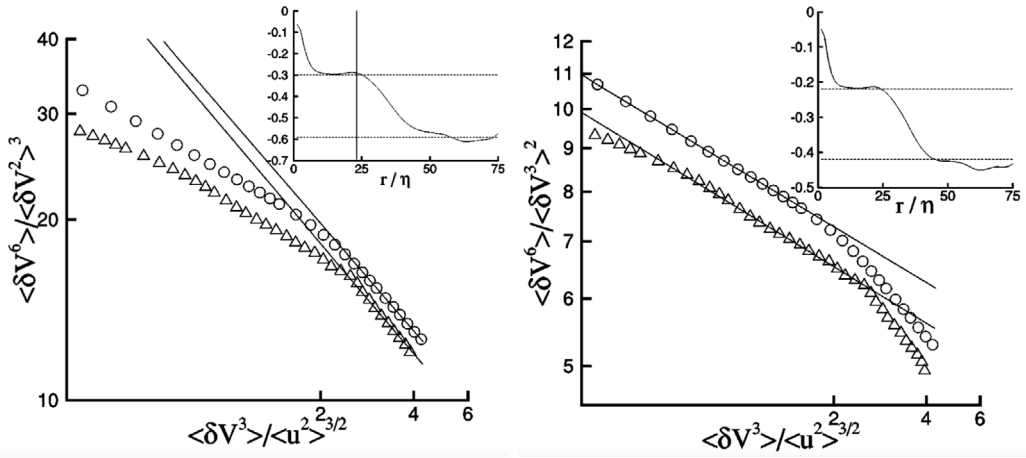

Fig. 82. The figure shows the scaling behaviour of σ_n and ρ_n versus $S_3(r)$ with $n = 6$, while in the inset of the figures the local slopes $d\log(\sigma_n)/d\log S_3$ and $d\log(\rho_n)/d\log S_3$ respectively [132]. Although the range of scaling is not large, there is quite clear evidence that there are two different scaling regions above and below the shear length scale L_S.
Source: Reproduced from [132].

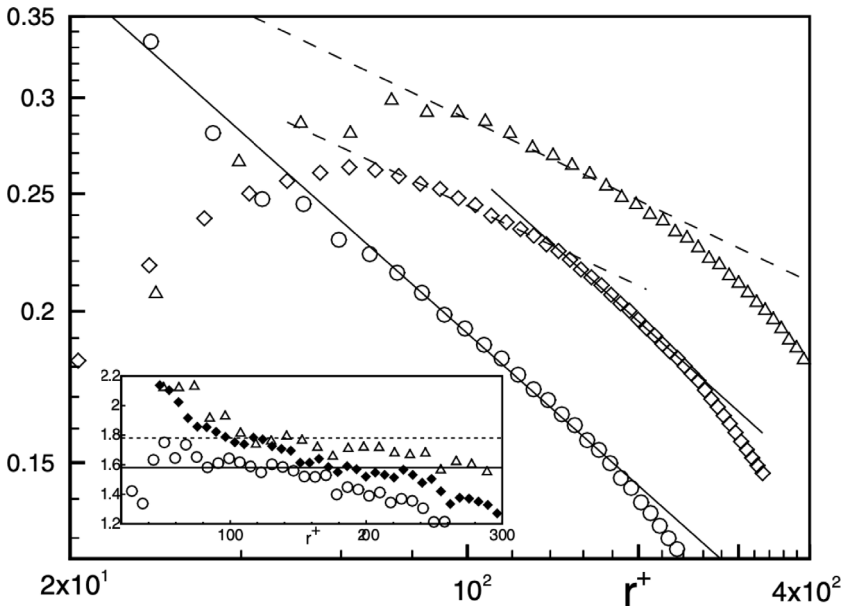

Fig. 83. Isotropic component of the sixth order longitudinal structure function normalised by its dimensional scaling, $S_{00}^{(6)}/r^2$. High shear case: circles, $S^* = 7$, $Re_\lambda = 150$, $\Delta^+ = \Delta/\eta = 17$. Low shear case: triangles, $S^* = 2.2$, $Re_\lambda = 160$ and $\Delta^+ = \Delta/\eta = 20$. Intermediate shear case: diamonds, $S^* = 5.4$, $Re_\lambda = 150$ $L_x^+ = 1320$, $\Delta^+ = \Delta/\eta = 17$. The slope of the solid lines is -0.42 corresponding to an anomalous exponents $\zeta(6) = 1.58 \pm 0.08$ while for the dashed line is -0.22 corresponding to an anomalous exponent $\zeta(6) = 1.78 \pm 0.08$.
Source: Reproduced from [133].

$S_6^{(0,0)}/r^2$ for the three cases. At low $S_* = 2.2$ there is evidence of a scaling region of slope -0.22 corresponding to $\zeta_6 = 1.78$ consistent with homogeneous and isotropic turbulence. At high $S_* = 7$ we observe a much steeper slope around -0.42 which gives $\zeta_6 = 1.58$ as predicted by Eq. (390). This result completes our assessment of shear-dominated turbulence. We have shown that, besides the strong anisotropy induced by the shear, we can still investigate the statistical properties of turbulence using the same conceptual framework introduced for homogeneous and isotropic turbulence. However, we can do more.

Lecture 8.4. Application to large eddy simulations in boundary layers

We want to investigate in more detail intermittency properties for boundary layer turbulence. In this case, the shear is a function of the distance y^+ from the boundary at $y^+ = 0$, where we recall that $y^+ = yv_*/\nu$ and $-v_*^2$ is the momentum

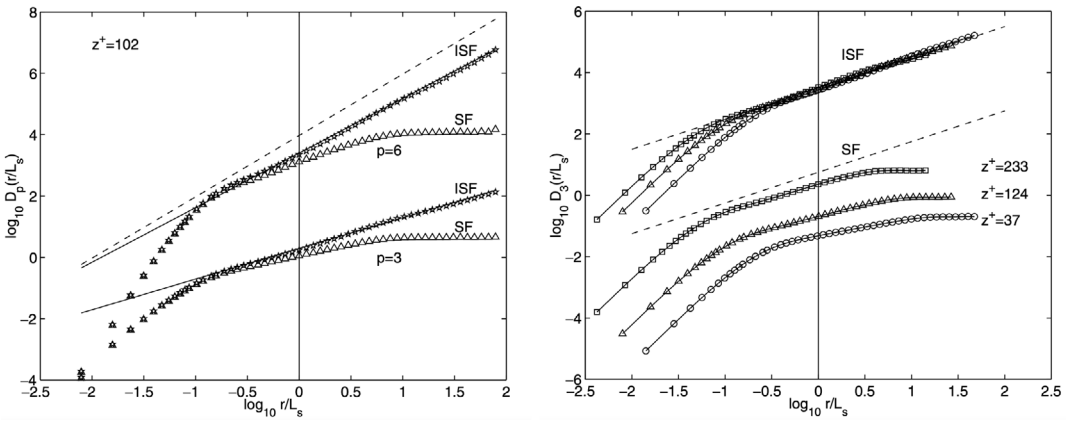

Fig. 84. From the boundary layer experiment, third-order structure function at various distances from the wall: $z^+ = 37$ (○), $z^+ = 124$ (△) and $z^+ = 233$ (□). The scaling properties of D_3 (SF) do depend on the distance z^+. On the contrary, $\tilde{D}_3$ (ISF) displays the same scaling behaviour for all z^+. The dashed line has a slope 1. The curves have been shifted vertically for convenience.
Source: Reproduced from [126].

flux towards the wall. Following our previous discussion we now introduce structure functions which depend on y^+:

$$D_n(y^+, r) \equiv \langle [\delta v(y^+, r)^3 + \alpha S(y^+)\delta v(y^+, r)^2]^{n/3} \rangle \tag{395}$$

where $S(y^+) = \partial_y^+ U(y^+)$ and $U(y^+)$ is the mean flow in the x direction [126]. We refer to the expression (395) as ISF (integral structure functions) to distinguish from the standard structure functions (SF). The parameter α in (395) is an empirical factor order 1. We expect that *for any* y^+ $D_n(y^+, r)$ show the same scaling properties of homogeneous and isotropic turbulence. This is a consequence of the fact that the statistical properties of $\epsilon(r)$ do not depend on the shear as previously discussed. In Fig. 84 we show experimental data for turbulent boundary layers from [126]. Velocity measurements are taken at various distances from the wall: on the right panel we show both the ISF $D_3(y^+, r)$ and the standard SF $S_3(y^+, r)$ while on the left panel, we focus on ISF $D_6(y^+, r)$ and SF $S_6(y^+, r)$. For any value of y^+ we observe for $n = 3$ the same scaling proportional to r. In Fig. 85 we show the quantity $\log[D_n(y^+, r)/r^{\zeta_n}]$ versus $\log(r/L_S)$ where ζ_n are the anomalous exponents observed in homogeneous and isotropic turbulence. All the shown results are obtained with $\alpha = 0.2$. The value of α, which may not be a universal number, can be fixed by the requirement $D_3(y^+, r) \sim r$ for all y^+. From the two figures, we understand that the statistical properties of $D_n(y^+, r)$ are consistent with the ones observed in homogeneous and isotropic turbulence. This non-trivial information can now be used to compute the *eddy viscosity* following the same arguments discussed in Lecture 2.

Let Δ denote the smallest resolved scale in the computation. We can introduce the eddy viscosity ν_{eddy} using the identity [134]:

$$\delta U(\Delta)^3 + A\langle S(y^+)\rangle \Delta \delta U(\Delta)^2 = \nu_{eddy} \frac{\delta U(\Delta)^2}{\Delta^2} \Delta \tag{396}$$

where $S_m(y^+) \equiv \langle S(y^+)\rangle$ is the average (in the homogeneous direction or in time) shear rate. At the smallest scale Δ we have $\delta U(\Delta) = \Delta \tilde{S}$ where $\tilde{S}$ is the instantaneous local shear rate. The parameter A needs to be computed. From (396) we find:

$$\nu_{eddy} = \Delta^2 \tilde{S}(y^+) + A\Delta^2 S_m(y^+) = \Delta^2 [\tilde{S}(y^+) + A S_m(y^+)] \tag{397}$$

If there is no turbulence then we expect $\tilde{S} = S_m$. In this case, we also expect the flow to be smooth and ν_{eddy} should be zero (recall the overall viscosity is $\nu + \nu_{eddy}$). This requirement fixes the value of $A = -1$. Then we finally obtain

$$\nu_{eddy} = \Delta^2 [\tilde{S}(y^+) - S_m(y^+)] \tag{398}$$

Expression (398) is referred to as *shear improved Smagorinsky model* (SISM), its idea was originally proposed in [126] and it was first tested on a backward-facing step in [135] and later also on channel flow turbulence [134]. The SISM model requires the knowledge of the "instantaneous" average shear, something that can easily be estimated e.g. via adaptive low-pass Kalman filter [136]. The SISM model can be used in numerical simulations with excellent results. In Fig. 86 we show the velocity profile obtained by using (398) a rather popular model for eddy viscosity and DNS. The agreement is quite excellent. Overall one can obtain an accurate simulation of turbulent channel flows with a computational cost reduced by a factor 50.

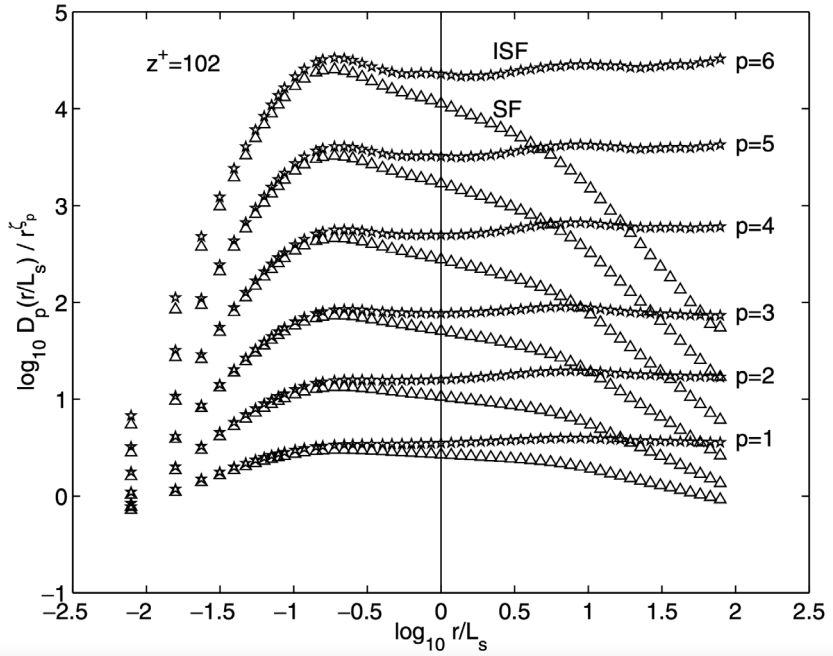

Fig. 85. In the experimental boundary layer at $z^+ = 102$. SF and ISF, compensated by homogeneous and isotropic scalings, are displayed for p=1 . . . 6.
Source: Reproduced from [126].

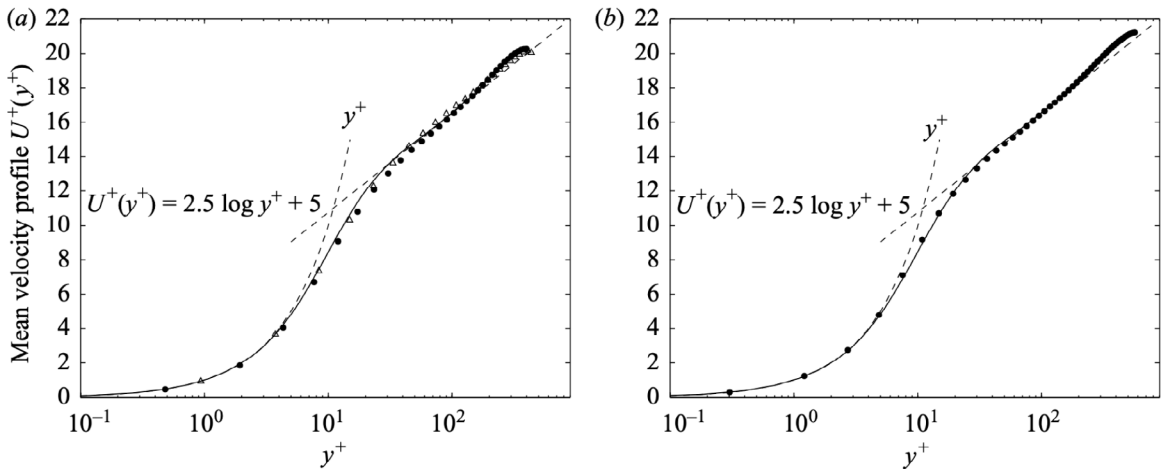

Fig. 86. (•) mean-velocity profile (in wall units) at $Re_\tau = 395$. The computational domain (in outer units) is $4\pi H \times 2H \times 2\pi H$ with $64 \times 65 \times 64$ grid points. In comparison with (-) the DNS data obtained in the domain $2\pi H \times 2H \times \pi H$ with $256 \times 193 \times 192$ grid points, and (△) a computation of the dynamic Smagorinsky model carried out by Piomelli (private communication) in the domain $5\pi H/2 \times 2H \times \pi H/2$ with $48 \times 49 \times 48$ grid points (using a pseudo-spectral solver). (b) (•) mean-velocity profile at $Re_\tau = 590$ with $96 \times 97 \times 96$ grid points. In comparison with (-) the DNS data with $384 \times 257 \times 384$ grid points.
Source: Reproduced from [134].

Lecture 8.5. Summary of Lecture 8

In this lecture, we have discussed two different cases concerning homogeneous non-isotropic turbulence:

A how to disentangle in the statistical properties of turbulence isotropic contribution from non-isotropic components;
B how to investigate scaling and intermittency in shear flows.

It is important to realise the basic difference between the two cases: at variance with (A), in case (B) the external shear introduces a dynamical scale L_S and we focus on scaling and intermittency on scales *larger than* L_S for L_S small with

respect to the domain size L_0, i.e. in the shear dominated range of scales. This result is nicely supported by the study of homogeneous shear flow in passive scalar turbulence using Kraichnan's model. In case (A) we consider the effect of anisotropy for small scales. The two cases are somehow complementary. Also, shear flows are just one, although important, case of non-isotropic turbulence, and the considerations developed in this lecture may be considered as a starting point to consider different situations.

Having said that, we discussed many non-trivial results obtained in our analysis. First of all, we now understand that issue related to non-isotropic contributions to inertial range dynamics can be properly discussed for $r \to 0$ and $Re \to \infty$ using the SO(3) decomposition which provides well defined answers to the questions. Then we show that for homogeneous shear flows and boundary layer turbulence, the statistical properties of coarse-grained energy dissipation $\epsilon(r)$, in the shear dominated scales range, are the same of homogeneous and isotropic turbulence. We argue that this is an important result that allows us to generalise the multifractal framework for these problems. As a side product, following the original idea of Smagorinsky model for eddy viscosity, we discussed how to generalise the concept of eddy viscosity in the shear dominated range of scales.

Altogether, the picture which emerge from our discussion, provided we take care of the proper generalisations, support our view of anomalous scaling and intermittency developed for homogeneous and isotropic turbulence and no new theoretical framework is required. Whether this is always the case, i.e. for different classes of non-isotropic forcing, is an open question.

Conclusion

In this review, we mostly confine our discussions to the case of three-dimensional homogeneous and isotropic turbulence. In this case, there is a general consensus and good experimental evidence that turbulence exhibits the phenomenon of the dissipative anomaly: by increasing the Reynolds (Re) number the rate of energy dissipation remains constant. This effect, also known by the name of zero-th law of turbulence or dissipative anomaly, implies that turbulence is self-generating its own ultraviolet (small-scale) divergences: in the limit of large Re the velocity gradients become singular. Mathematically, it is not so strange that there is some singular behaviour when the viscosity goes to zero. After all, the viscous one is the only term that multiplies a second space derivative in the Navier–Stokes equations, and some strange results in the limit of zero viscosity could be expected. In some sense, the most fundamental turbulence problem is the explanation or the proof that the zeroth law of turbulence is exact. Actually, the problem of dissipative anomaly has been solved for the passive scalar in Kraichnan's model. Although far from the Navier–Stokes equations, the solution of Kraichnan's model tells us something interesting, and along this line, we can hope that some breakthrough results can be obtained in the future.

We can also take a different point of view. We can start assuming that based on experimental and/or numerical results the zeroth law of turbulence is exact. Then the question is whether there are still some problems to be solved. From this point of view, homogeneous and isotropic turbulence may be considered a rather narrow choice to investigate. Yet, one observes a rather rich and very non-trivial phenomenology in homogeneous isotropic turbulent flows which cannot be explained by the zeroth law: we must face the problem of intermittency. The first question we need to understand is whether it is true or not that dissipative anomaly must be associated with intermittency for fluid phenomena.

No matter how one defines intermittency, the basic question (even for homogeneous and isotropic turbulence) is whether intermittency is independent or not of the large-scale forcing and the detailed dissipation mechanism. In more abstract terms, we want to understand whether intermittency is independent of large-scale (infrared) forcing and small-scale (ultraviolet) cutoff. This is by far the most relevant and important question we need to solve.

Obviously, intermittency is observed and investigated in many different kinds of turbulent flows, for instance in rotating turbulence, magnetohydrodynamics, or two-phase flows. Yet we feel that only if we can answer this question in the case of homogeneous and isotropic turbulence we can eventually approach the same problem in more complex situations. The case of passive scalar for Kraichnan's model is illuminating. In fact, the original solution proposed by Kraichnan is a balance between the effects due to inertial terms and those due to dissipation (in this case diffusivity). This solution turns out to be wrong and the correct solution can be found in the anomalous scaling due to the inertial range dynamics. There are claims, suggestions, and/or speculations that something similar happens for the Navier–Stokes equation.

Related to the above problem there is the problem to compute (at least in one case) the anomalous scaling exponents measured in many laboratory experiments and numerical simulations. So far it is not very clear whether the computation of anomalous exponents is a problem that needs radically new ideas in order to be solved. In other words, it strongly depends on how the solution, if any, may be obtained, i.e. whether it opens a new approach to turbulence-like problems (e.g. as it has been for the renormalisation group) or not.

Although there may still be some debates, the multifractal description of turbulence had provided us, over the years, with a powerful tool to unify different results. We can now reasonably state that knowing the entropy-like function $3 - D(h)$ one may be able to compute all the scaling properties of turbulence variables, both in the inertial and in the dissipation range, for lagrangian as well as eulerian quantities. The only constraint in the multifractal approach is that the quantities we are considering are invariant for the same group of transformations of the Navier–Stokes equation. So far, to our knowledge, there is no evidence of discrepancy with the above statement. At any rate, it is worth performing further investigation on this point.

Obviously, there are still non-trivial questions that should be understood better. Among them, we would like to mention two different issues. The first one is related to the spectacular agreement of the so-called Refined Kolmogorov Similarity. In the multifractal approach, although never stated clearly, it is the basic assumption connecting the inertial properties and the dissipative phenomena in turbulence. For this problem, clearly observed in eulerian and lagrangian dynamics, there is simply no explanation besides dimensional arguments.

The second problem, important in many applications, is related to the understanding of systems where large space non-homogeneities lead to the presence of spatial fluxes, such as the heat flux in Rayleigh–Bénard convection, the momentum flux and drag in turbulence boundary layers, and similar cases in MHD. In these systems, the zeroth law of turbulence alone, may not be enough to quantitatively explain the observed phenomenology.

The homogeneous and isotropic case is the starting point to understand the complexity of turbulent flows. Assuming that we reached enough physical accuracy in understanding the statistical properties of homogeneous and isotropic turbulence, we can now start from this basic knowledge to work on many other problems in turbulence. As an example, a few of the most relevant directions to be addressed include: thermally and density-driven flows [137–146], magnetohydrodynamics (MHD) [147–151], combustion [152–154], plasma turbulence [155,156], geophysical and rotating turbulence [157], superfluid turbulence [158,159], turbulence in complex and/or structured fluids [160–165], supersonic turbulence [166].

Declaration of competing interest

The authors declare the following financial interests/personal relationships which may be considered as potential competing interests: Federico Toschi reports travel was provided by Dutch Research Council. Roberto Benzi reports equipment, drugs, or supplies and travel were provided by European Research Council.

Acknowledgements

We would like to warmly acknowledge all the many collaborators, friends, and colleagues with whom we have interacted during the journey that took us here. While it is simply impossible to individually mention all of them special gratitude goes to Luca Biferale, Massimo Vergassola, Angelo Vulpiani and Uriel Frisch. This publication is part of the project “Shaping turbulence with smart particles” (with project number OCENW.GROOT.2019.031 of the research programme Open Competitie ENW XL which is (partly) financed by the Dutch Research Council (NWO). This work was partially supported by the European Research Council (ERC) under the European Union’s Horizon 2020 research and innovation programme (grant agreement No. 882340).

References

[1] G. Falkovich, K. Gawedzki, M. Vergassola, Particles and fields in fluid turbulence, Rev. Modern Phys. 73 (4) (2001) 913.
[2] C. Navier, Resume Des Lecons Donnees a L'Ecole Des Ponts Et Chaussees sur L'Application de la Mecanique a L'Etablissement Des Constructions Et Des Machines Par Navier, Societe Belge de librairie, 1839.
[3] G.G. Stokes, On the steady motion of incompressible fluids, Trans. Camb. Philos. Soc. 7 (1848) 439.
[4] O. Reynolds, IV. On the dynamical theory of incompressible viscous fluids and the determination of the criterion, Philos. Trans. R. Soc. London.(A.) (186) (1895) 123–164.
[5] Y. Kaneda, T. Ishihara, M. Yokokawa, K. Itakura, A. Uno, Energy dissipation rate and energy spectrum in high resolution direct numerical simulations of turbulence in a periodic box, Phys. Fluids 15 (2) (2003) L21–L24.
[6] T. Von Karman, Zeitschrift für angewandte mathematik und mechanik, 1921, I.
[7] I. Procaccia, K. Sreenivasan, The state of the art in hydrodynamic turbulence: Past successes and future challenges, Physica D 237 (14–17) (2008) 2167–2183.
[8] L.F. Richardson, Atmospheric diffusion shown on a distance-neighbour graph, Proc. R. Soc. Lond. Ser. A, Contain. Pap. A Math. Phys. Character 110 (756) (1926) 709–737.
[9] G. Boffetta, I.M. Sokolov, Relative dispersion in fully developed turbulence: The Richardson’s law and intermittency corrections, Phys. Rev. Lett. 88 (9) (2002) 094501.
[10] P.A. Davidson, Y. Kaneda, K. Moffatt, K.R. Sreenivasan, A voyage through turbulence, Cambridge University Press, 2011.
[11] L.D. Landau, E.M. Lifshitz, Theoretical physics, in: Fluid Mechanics,Vol. 6, Pergamon, London, 1987.
[12] U. Frisch, Turbulence: The Legacy of an Kolmogorov, Cambridge University Press, 1995.
[13] H. Tennekes, J.L. Lumley, J.L. Lumley, et al., A first course in turbulence, MIT Press, 1972.
[14] A. Vulpiani, F. Cecconi, M. Cencini, Chaos: From Simple Models to Complex Systems, Vol. 17, World Scientific, 2009.
[15] A.N. Kolmogorov, The local structure of turbulence in incompressible viscous fluid for very large Reynolds numbers, Proc. R. Soc. Lond. Ser. A: Math. Phys. Sci. 434 (1890) (1991) 9–13.
[16] U. Frisch, J. Bec, Burgulence, in: New Trends in Turbulence Turbulence: Nouveaux Aspects, Springer, 2001, pp. 341–383.
[17] T. Ishihara, T. Gotoh, Y. Kaneda, Study of high-Reynolds number isotropic turbulence by direct numerical simulation, Annu. Rev. Fluid Mech. 41 (1) (2009) 165–180.
[18] P. Vieillefosse, Local interaction between vorticity and shear in a perfect incompressible fluid, J. Physique 43 (6) (1982) 837–842.
[19] C. Meneveau, Lagrangian dynamics and models of the velocity gradient tensor in turbulent flows, Annu. Rev. Fluid Mech. 43 (1) (2011) 219–245.
[20] B.J. Cantwell, Exact solution of a restricted Euler equation for the velocity gradient tensor, Phys. Fluids A: Fluid Dyn. 4 (4) (1992) 782–793.
[21] A. Ooi, J. Martin, J. Soria, M.S. Chong, A study of the evolution and characteristics of the invariants of the velocity-gradient tensor in isotropic turbulence, J. Fluid Mech. 381 (1999) 141–174.
[22] M. Chertkov, A. Pumir, B.I. Shraiman, Lagrangian tetrad dynamics and the phenomenology of turbulence, Phys. Fluids 11 (8) (1999) 2394–2410.

[23] F. van der Bos, B. Tao, C. Meneveau, J. Katz, Effects of small-scale turbulent motions on the filtered velocity gradient tensor as deduced from holographic particle image velocimetry measurements, Phys. Fluids 14 (7) (2002) 2456–2474.
[24] G. Gulitski, M. Kholmyansky, W. Kinzelbach, B. Lüthi, A. Tsinober, S. Yorish, Velocity and temperature derivatives in high-Reynolds-number turbulent flows in the atmospheric surface layer. Part 1. Facilities, methods and some general results, J. Fluid Mech. 589 (2007) 57–81.
[25] F. Champagne, The fine-scale structure of the turbulent velocity field, J. Fluid Mech. 86 (1) (1978) 67–108.
[26] U. Frisch, On the singularity structure of fully developed turbulence, Turbul. Predict. Geophy. Fluid Dyn. Clim. Dyn. (1985).
[27] G.K. Batchelor, Small-scale variation of convected quantities like temperature in turbulent fluid part 1. General discussion and the case of small conductivity, J. Fluid Mech. 5 (1) (1959) 113–133.
[28] G. Boffetta, A. Celani, M. Vergassola, Inverse energy cascade in two-dimensional turbulence: Deviations from Gaussian behavior, Phys. Rev. E 61 (1) (2000) R29.
[29] R. Benzi, S. Patarnello, P. Santangelo, On the statistical properties of two-dimensional decaying turbulence, Europhys. Lett. 3 (7) (1987) 811.
[30] R. Benzi, G. Paladin, S. Patarnello, P. Santangelo, A. Vulpiani, Intermittency and coherent structures in two-dimensional turbulence, J. Phys. A: Math. Gen. 19 (18) (1986) 3771.
[31] R. Benzi, S. Patarnello, P. Santangelo, Self-similar coherent structures in two-dimensional decaying turbulence, J. Phys. A: Math. Gen. 21 (5) (1988) 1221.
[32] B. Legras, P. Santangelo, R. Benzi, High-resolution numerical experiments for forced two-dimensional turbulence, Europhysics Letters 5 (1) (1988) 37.
[33] G. Boffetta, R.E. Ecke, et al., Two-dimensional turbulence, Annu. Rev. Fluid Mech. 44 (1) (2012) 427–451.
[34] D. Bernard, G. Boffetta, A. Celani, G. Falkovich, Conformal invariance in two-dimensional turbulence, Nat. Phys. 2 (2) (2006) 124–128.
[35] A.S. Monin, A.M. Yaglom, Statistical Fluid Mechanics, Volume II: Mechanics of Turbulence, Vol. 2, Courier Corporation, 2013.
[36] T. Watanabe, T. Gotoh, Statistics of a passive scalar in homogeneous turbulence, New J. Phys. 6 (1) (2004) 40.
[37] J. Martın, C. Dopazo, L. Valiño, Dynamics of velocity gradient invariants in turbulence: Restricted Euler and linear diffusion models, Phys. Fluids 10 (8) (1998) 2012–2025.
[38] A. Naso, A. Pumir, M. Chertkov, Scale dependence of the coarse-grained velocity derivative tensor: Influence of large-scale shear on small-scale turbulence, J. Turbul. (7) (2006) N41.
[39] Z. Warhaft, Passive scalars in turbulent flows, Annu. Rev. Fluid Mech. 32 (1) (2000) 203–240.
[40] U. Frisch, A. Pomyalov, I. Procaccia, S.S. Ray, Turbulence in noninteger dimensions by fractal Fourier decimation, Phys. Rev. Lett. 108 (7) (2012) 074501.
[41] A. Celani, S. Musacchio, D. Vincenzi, Turbulence in more than two and less than three dimensions, Phys. Rev. Lett. 104 (18) (2010) 184506.
[42] C. Casciola, P. Gualtieri, R. Benzi, R. Piva, Scale-by-scale budget and similarity laws for shear turbulence, J. Fluid Mech. 476 (2003) 105–114.
[43] F. Toschi, E. Bodenschatz, Lagrangian properties of particles in turbulence, Annu. Rev. Fluid Mech. 41 (2009) 375–404.
[44] R. Benzi, C. Casciola, P. Gualtieri, R. Piva, Numerical evidence of a new similarity law in shear dominated flows, Comput. Math. Appl. 46 (4) (2003) 617–631.
[45] T. Gotoh, D. Fukayama, T. Nakano, Velocity field statistics in homogeneous steady turbulence obtained using a high-resolution direct numerical simulation, Phys. Fluids 14 (3) (2002) 1065–1081.
[46] L. Biferale, G. Boffetta, A. Celani, B. Devenish, A. Lanotte, F. Toschi, Multifractal statistics of Lagrangian velocity and acceleration in turbulence, Phys. Rev. Lett. 93 (6) (2004) 064502.
[47] J. Bec, L. Biferale, G. Boffetta, A. Celani, M. Cencini, A. Lanotte, S. Musacchio, F. Toschi, Acceleration statistics of heavy particles in turbulence, J. Fluid Mech. 550 (2006) 349–358.
[48] A. La Porta, G.A. Voth, A.M. Crawford, J. Alexander, E. Bodenschatz, Fluid particle accelerations in fully developed turbulence, Nature 409 (6823) (2001) 1017–1019.
[49] R. Benzi, L. Biferale, R. Fisher, D. Lamb, F. Toschi, Inertial range Eulerian and Lagrangian statistics from numerical simulations of isotropic turbulence, J. Fluid Mech. 653 (2010) 221–244.
[50] G.A. Voth, A. La Porta, A.M. Crawford, J. Alexander, E. Bodenschatz, Measurement of particle accelerations in fully developed turbulence, J. Fluid Mech. 469 (2002) 121–160.
[51] L. Biferale, G. Boffetta, A. Celani, A. Lanotte, F. Toschi, Particle trapping in three-dimensional fully developed turbulence, Phys. Fluids 17 (2) (2005) 021701.
[52] S. Douady, Y. Couder, M. Brachet, Direct observation of the intermittency of intense vorticity filaments in turbulence, Phys. Rev. Lett. 67 (8) (1991) 983.
[53] P. Constantin, I. Procaccia, D. Segel, Creation and dynamics of vortex tubes in three-dimensional turbulence, Phys. Rev. E 51 (4) (1995) 3207.
[54] A. Alexakis, L. Biferale, Cascades and transitions in turbulent flows, Phys. Rep. 767 (2018) 1–101.
[55] G. Stolovitzky, P. Kailasnath, K. Sreenivasan, Kolmogorov's refined similarity hypotheses, Phys. Rev. Lett. 69 (8) (1992) 1178.
[56] A.N. Kolmogorov, A refinement of previous hypotheses concerning the local structure of turbulence in a viscous incompressible fluid at high Reynolds number, J. Fluid Mech. 13 (1) (1962) 82–85.
[57] P. Kailasnath, K. Sreenivasan, G. Stolovitzky, Probability density of velocity increments in turbulent flows, Phys. Rev. Lett. 68 (18) (1992) 2766.
[58] U. Frisch, P.-L. Sulem, M. Nelkin, A simple dynamical model of intermittent fully developed turbulence, J. Fluid Mech. 87 (4) (1978) 719–736.
[59] R. Benzi, L. Biferale, S. Ciliberto, M. Struglia, R. Tripiccione, Generalized scaling in fully developed turbulence, Physica D 96 (1–4) (1996) 162–181.
[60] R. Benzi, S. Ciliberto, C. Baudet, G.R. Chavarria, On the scaling of three-dimensional homogeneous and isotropic turbulence, Physica D 80 (4) (1995) 385–398.
[61] R. Benzi, S. Ciliberto, R. Tripiccione, C. Baudet, F. Massaioli, S. Succi, Extended self-similarity in turbulent flows, Phys. Rev. E 48 (1) (1993) R29.
[62] M. Briscolini, P. Santangelo, S. Succi, R. Benzi, Extended self-similarity in the numerical simulation of three-dimensional homogeneous flows, Phys. Rev. E 50 (3) (1994) R1745.
[63] A. Arneodo, C. Baudet, F. Belin, R. Benzi, B. Castaing, B. Chabaud, R. Chavarria, S. Ciliberto, R. Camussi, F. Chilla, et al., Structure functions in turbulence, in various flow configurations, at Reynolds number between 30 and 5000, using extended self-similarity, Europhys. Lett. 34 (6) (1996) 411.
[64] R. Deidda, R. Benzi, F. Siccardi, Multifractal modeling of anomalous scaling laws in rainfall, Water Resour. Res. 35 (6) (1999) 1853–1867.
[65] U. Frisch, G. Parisi, Fully developed turbulence and intermittency, New York Acad. Sci. Ann. 357 (1980) 359–367.
[66] R. Benzi, G. Paladin, G. Parisi, A. Vulpiani, On the multifractal nature of fully developed turbulence and chaotic systems, J. Phys. A: Math. Gen. 17 (18) (1984) 3521.
[67] H. Touchette, The large deviation approach to statistical mechanics, Phys. Rep. 478 (1–3) (2009) 1–69.
[68] V.S. L'vov, E. Podivilov, I. Procaccia, Temporal multiscaling in hydrodynamic turbulence, Phys. Rev. E 55 (6) (1997) 7030.
[69] Z.-S. She, E. Leveque, Universal scaling laws in fully developed turbulence, Phys. Rev. Lett. 72 (3) (1994) 336.

[70] R. Benzi, L. Biferale, A. Crisanti, G. Paladin, M. Vergassola, A. Vulpiani, A random process for the construction of multiaffine fields, Physica D 65 (4) (1993) 352–358.
[71] and others, Wavelet transforms and their applications to turbulence, Annu. Rev. Fluid Mech. 24 (1) (1992) 395–458.
[72] R. Benzi, L. Biferale, G. Paladin, A. Vulpiani, M. Vergassola, Multifractality in the statistics of the velocity gradients in turbulence, Phys. Rev. Lett. 67 (17) (1991) 2299.
[73] U. Frisch, M. Vergassola, A prediction of the multifractal model: The intermediate dissipation range, in: New Approaches and Concepts in Turbulence, Springer, 1993, pp. 29–34.
[74] F. Toschi, L. Biferale, G. Boffetta, A. Celani, B. Devenish, A. Lanotte, Acceleration and vortex filaments in turbulence, J. Turbul. (6) (2005) N15.
[75] R. Benzi, L. Biferale, Fully developed turbulence and the multifractal conjecture, J. Stat. Phys. 135 (5) (2009) 977–990.
[76] R. Benzi, L. Biferale, Homogeneous and isotropic turbulence: A short survey on recent developments, J. Stat. Phys. 161 (6) (2015) 1351–1365.
[77] R. Benzi, L. Biferale, F. Toschi, Multiscale velocity correlations in turbulence, Phys. Rev. Lett. 80 (15) (1998) 3244.
[78] R. Benzi, L. Biferale, G. Ruiz-Chavarria, S. Ciliberto, F. Toschi, Multiscale velocity correlation in turbulence: Experiments, numerical simulations, synthetic signals, Phys. Fluids 11 (8) (1999) 2215–2224.
[79] G. Paladin, A. Vulpiani, Anomalous scaling laws in multifractal objects, Phys. Rep. 156 (4) (1987) 147–225.
[80] C. Meneveau, J. Katz, Scale-invariance and turbulence models for large-eddy simulation, Annu. Rev. Fluid Mech. 32 (1) (2000) 1–32.
[81] C. Meneveau, T.S. Lund, W.H. Cabot, A Lagrangian dynamic subgrid-scale model of turbulence, J. Fluid Mech. 319 (1996) 353–385.
[82] T. Bohr, M.H. Jensen, G. Paladin, A. Vulpiani, Dynamical systems approach to turbulence, 1998.
[83] L. Biferale, Shell models of energy cascade in turbulence, Annu. Rev. Fluid Mech. 35 (1) (2003) 441–468.
[84] E.B. Gledzer, System of hydrodynamic type admitting two quadratic integrals of motion, in: Sov. Phys. Dokl., Vol. 18, 1973, pp. 216–217.
[85] K. Ohkitani, M. Yamada, Temporal intermittency in the energy cascade process and local Lyapunov analysis in fully-developed model turbulence, Progr. Theoret. Phys. 81 (2) (1989) 329–341.
[86] L. Kadanoff, D. Lohse, J. Wang, R. Benzi, Scaling and dissipation in the GOY shell model, Phys. Fluids 7 (3) (1995) 617–629.
[87] V.S. L'vov, E. Podivilov, A. Pomyalov, I. Procaccia, D. Vandembroucq, Improved shell model of turbulence, Phys. Rev. E 58 (2) (1998) 1811.
[88] L. Kelvin, On vortex atoms, in: Proc. R. Soc. Edin, Vol. 6, 1867, pp. 94–105.
[89] H. Moffatt, A. Tsinober, Helicity in laminar and turbulent flow, Annu. Rev. Fluid Mech. 24 (1) (1992) 281–312.
[90] R. Benzi, L. Biferale, R. Kerr, E. Trovatore, Helical shell models for three-dimensional turbulence, Phys. Rev. E 53 (4) (1996) 3541.
[91] L. Biferale, D. Pierotti, F. Toschi, Helicity transfer in turbulent models, Phys. Rev. E 57 (3) (1998) R2515.
[92] L. Biferale, L. Chevillard, C. Meneveau, F. Toschi, Multiscale model of gradient evolution in turbulent flows, Phys. Rev. Lett. 98 (21) (2007) 214501.
[93] R. Benzi, L. Biferale, R. Tripiccione, E. Trovatore, (1+ 1)-dimensional turbulence, Phys. Fluids 9 (8) (1997) 2355–2363.
[94] J. O'Neil, C. Meneveau, Spatial correlations in turbulence: Predictions from the multifractal formalism and comparison with experiments, Phys. Fluids A: Fluid Dyn. 5 (1) (1993) 158–172.
[95] R. Benzi, L. Biferale, E. Trovatore, Ultrametric structure of multiscale energy correlations in turbulent models, Physical review letters 79 (9) (1997) 1670.
[96] C. Meneveau, K. Sreenivasan, Simple multifractal cascade model for fully developed turbulence, Phys. Rev. Lett. 59 (13) (1987) 1424.
[97] R. Benzi, L. Biferale, G. Parisi, On intermittency in a cascade model for turbulence, Physica D 65 (1–2) (1993) 163–171.
[98] A.A. Mailybaev, Shell model intermittency is the hidden self-similarity, Phys. Rev. Fluids 7 (3) (2022) 034604.
[99] M.R. Maxey, J.J. Riley, Equation of motion for a small rigid sphere in a nonuniform flow, Phys. Fluids 26 (4) (1983) 883–889.
[100] J. Bec, Multifractal concentrations of inertial particles in smooth random flows, J. Fluid Mech. 528 (2005) 255–277.
[101] J. Bec, K. Gawedzki, P. Horvai, Intermittent distribution of tracers advected by a compressible random flow, 2003, ArXiv Preprint Nlin/0310015.
[102] M. Borgas, The multifractal Lagrangian nature of turbulence, Philos. Trans. R. Soc. Lond. Ser.A: Phys. Eng. Sci. 342 (1665) (1993) 379–411.
[103] L. Biferale, G. Boffetta, A. Celani, A. Lanotte, F. Toschi, Particle trapping in three-dimensional fully developed turbulence, Phys. Fluids 17 (2) (2005) 021701.
[104] J. Bec, L. Biferale, M. Cencini, A.S. Lanotte, F. Toschi, Effects of vortex filaments on the velocity of tracers and heavy particles in turbulence, Phys. Fluids 18 (8) (2006) 081702.
[105] A. Arnéodo, R. Benzi, J. Berg, L. Biferale, E. Bodenschatz, A. Busse, E. Calzavarini, B. Castaing, M. Cencini, L. Chevillard, et al., Universal intermittent properties of particle trajectories in highly turbulent flows, Phys. Rev. Lett. 100 (25) (2008) 254504.
[106] L. Biferale, F. Bonaccorso, M. Buzzicotti, K.P. Iyer, Self-similar subgrid-scale models for inertial range turbulence and accurate measurements of intermittency, Phys. Rev. Lett. 123 (1) (2019) 014503.
[107] T. Gotoh, T. Watanabe, Y. Suzuki, Universality and anisotropy in passive scalar fluctuations in turbulence with uniform mean gradient, Journal of Turbulence (12) (2011) N48.
[108] M. Jensen, G. Paladin, A. Vulpiani, Shell model for turbulent advection of passive-scalar fields, Physical Review A 45 (10) (1992) 7214.
[109] C. Baudet, S. Ciliberto, G. Ruíz Chavarria, Scaling laws and dissipation scale of a passive scalar in fully developed turbulence, 1996.
[110] R. Benzi, L. Biferale, G. Parisi, Intermittency correction to the Obukhov-Corrsin theory of a passive scalar, Europhys. Lett. 18 (3) (1992) 213.
[111] M. Jensen, G. Paladin, A. Vulpiani, Intermittency effects of energy cascade and passive scalar fields, in: Pattern Formation in Complex Dissipative Systems: Fluid Patterns, Liquid Crystals, Chemical Reactions, World Scientific, 1992, p. 387.
[112] R.H. Kraichnan, Anomalous scaling of a randomly advected passive scalar, Phys. Rev. Lett. 72 (7) (1994) 1016.
[113] S. Chen, R.H. Kraichnan, Simulations of a randomly advected passive scalar field, Phys. Fluids 10 (11) (1998) 2867–2884.
[114] R. Benzi, L. Biferale, A. Wirth, Analytic calculation of anomalous scaling in random shell models for a passive scalar, Phys. Rev. Lett. 78 (26) (1997) 4926.
[115] Z. Schuss, Theory and Applications of Stochastic Processes: An Analytical Approach, Vol. 170, Springer Science & Business Media, 2009.
[116] K. Gawedzki, A. Kupiainen, Anomalous scaling of the passive scalar, Phys. Rev. Lett. 75 (21) (1995) 3834.
[117] B.I. Shraiman, E.D. Siggia, Anomalous scaling of a passive scalar in turbulent flow, Comptes Rendus de L'AcadÉMie Des Sci. SÉRie II, MÉCanique, Physique, Chimie, Astronomie 321 (7) (1995) 279–284.
[118] M. Chertkov, G. Falkovich, Anomalous scaling exponents of a white-advected passive scalar, Phys. Rev. Lett. 76 (15) (1996) 2706.
[119] U. Frisch, A. Mazzino, A. Noullez, M. Vergassola, Lagrangian method for multiple correlations in passive scalar advection, Phys. Fluids 11 (8) (1999) 2178–2186.
[120] A. Celani, M. Vergassola, Statistical geometry in scalar turbulence, Phys. Rev. Lett. 86 (3) (2001) 424.
[121] I. Arad, L. Biferale, A. Celani, I. Procaccia, M. Vergassola, Statistical conservation laws in turbulent transport, Phys. Rev. Lett. 87 (16) (2001) 164502.
[122] L. Angheluta, R. Benzi, L. Biferale, I. Procaccia, F. Toschi, Anomalous scaling exponents in nonlinear models of turbulence, Phys. Rev. Lett. 97 (16) (2006) 160601.
[123] L. Biferale, I. Procaccia, Anisotropy in turbulent flows and in turbulent transport, Phys. Rep. 414 (2–3) (2005) 43–164.
[124] I. Arad, B. Dhruva, S. Kurien, V.S. L'vov, I. Procaccia, K. Sreenivasan, Extraction of anisotropic contributions in turbulent flows, Phys. Rev. Lett. 81 (24) (1998) 5330.

[125] A. Celani, M. Cencini, M. Vergassola, E. Villermaux, D. Vincenzi, Shear effects on passive scalar spectra, J. Fluid Mech. 523 (2005) 99–108.
[126] F. Toschi, E. Leveque, G. Ruiz-Chavarria, Shear effects in nonhomogeneous turbulence, Phys. Rev. Lett. 85 (7) (2000) 1436.
[127] C. Casciola, P. Gualtieri, R. Benzi, R. Piva, Scale-by-scale budget and similarity laws for shear turbulence, J. Fluid Mech. 476 (2003) 105–114.
[128] F. Toschi, G. Amati, S. Succi, R. Benzi, R. Piva, Intermittency and structure functions in channel flow turbulence, Phys. Rev. Lett. 82 (25) (1999) 5044.
[129] P. Gualtieri, C. Casciola, R. Benzi, G. Amati, R. Piva, Scaling laws and intermittency in homogeneous shear flow, Phys. Fluids 14 (2) (2002) 583–596.
[130] R. Benzi, G. Amati, C. Casciola, F. Toschi, R. Piva, Intermittency and scaling laws for wall bounded turbulence, Phys. Fluids 11 (6) (1999) 1284–1286.
[131] J. Kim, P. Moin, R. Moser, Turbulence statistics in fully developed channel flow at low Reynolds number, J. Fluid Mech. 177 (1987) 133–166.
[132] C. Casciola, R. Benzi, P. Gualtieri, B. Jacob, R. Piva, Double scaling and intermittency in shear dominated flows, Phys. Rev. E 65 (1) (2001) 015301.
[133] C. Casciola, P. Gualtieri, B. Jacob, R. Piva, Scaling properties in the production range of shear dominated flows, Phys. Rev. Lett. 95 (2) (2005) 024503.
[134] E. Lévêque, F. Toschi, L. Shao, J.-P. Bertoglio, Shear-improved Smagorinsky model for large-eddy simulation of wall-bounded turbulent flows, J. Fluid Mech. 570 (2007) 491–502.
[135] F. Toschi, H. Kobayashi, U. Piomelli, G. Iaccarino, Backward-facing step calculations using the shear improved Smagorinsky model Proceedings of the Summer Program 2006, Center for Turbulent Research, 2006.
[136] A. Cahuzac, J. Boudet, P. Borgnat, E. Lévêque, Smoothing algorithms for mean-flow extraction in large-eddy simulation of complex turbulent flows, Phys. Fluids 22 (12) (2010) 125104.
[137] G. Ahlers, S. Grossmann, D. Lohse, Heat transfer and large scale dynamics in turbulent Rayleigh-Bénard convection, Rev. Modern Phys. 81 (2) (2009) 503.
[138] D. Lohse, K.-Q. Xia, Small-scale properties of turbulent Rayleigh-Bénard convection, Annu. Rev. Fluid Mech. 42 (2010) 335–364.
[139] E.D. Siggia, High Rayleigh number convection, Annu. Rev. Fluid Mech. 26 (1) (1994) 137–168.
[140] P. Garaud, Double-diffusive convection at low Prandtl number, Annu. Rev. Fluid Mech. 50 (2018) 275–298.
[141] M.G. Worster, Convection in mushy layers, Annu. Rev. Fluid Mech. 29 (1) (1997) 91–122.
[142] E. Bodenschatz, W. Pesch, G. Ahlers, Recent developments in Rayleigh-Bénard convection, Annu. Rev. Fluid Mech. 32 (1) (2000) 709–778.
[143] D. Livescu, Turbulence with large thermal and compositional density variations, Annu. Rev. Fluid Mech. 52 (2020) 309–341.
[144] M.G. Wells, R.M. Dorrell, Turbulence processes within turbidity currents, Annu. Rev. Fluid Mech. 53 (2021) 59–83.
[145] S. Grossmann, D. Lohse, C. Sun, High–reynolds number Taylor-Couette turbulence, Annu. Rev. Fluid Mech. 48 (2016) 53–80.
[146] S. Grossmann, D. Lohse, Scaling in thermal convection: A unifying theory, J. Fluid Mech. 407 (2000) 27–56.
[147] A. Beresnyak, MHD turbulence, Living Rev. Comput. Astrophys. 5 (1) (2019) 1–59.
[148] D. Biskamp, Magnetohydrodynamic Turbulence, Cambridge University Press, 2003.
[149] D. Biskamp, Magnetic reconnection, Phys. Rep. 237 (4) (1994) 179–247.
[150] M.K. Verma, Statistical theory of magnetohydrodynamic turbulence: Recent results, Phys. Rep. 401 (5–6) (2004) 229–380.
[151] P.D. Mininni, Scale interactions in magnetohydrodynamic turbulence, Annu. Rev. Fluid Mech. 43 (2011) 377–397.
[152] H. Pitsch, Large-eddy simulation of turbulent combustion, Annu. Rev. Fluid Mech. 38 (2006) 453–482.
[153] N. Peters, Turbulent Combustion, Cambridge University Press, 2000.
[154] A. Giusti, E. Mastorakos, Turbulent combustion modelling and experiments: Recent trends and developments, Flow Turbul. Combust. 103 (4) (2019) 847–869.
[155] R. Marino, L. Sorriso-Valvo, Scaling laws for the energy transfer in space plasma turbulence, Phys. Rep. 1006 (2023) 1–144.
[156] J.A. Krommes, Fundamental statistical descriptions of plasma turbulence in magnetic fields, Phys. Rep. 360 (1–4) (2002) 1–352.
[157] F. Bouchet, A. Venaille, Statistical mechanics of two-dimensional and geophysical flows, Phys. Rep. 515 (5) (2012) 227–295.
[158] M.S. Paoletti, D.P. Lathrop, Quantum turbulence, Annu. Rev. Condens. Matter Phys. 2 (1) (2011) 213234.
[159] C.F. Barenghi, N.G. Parker, A Primer on Quantum Fluids, Springer, 2016.
[160] R. Benzi, E.S. Ching, Polymers in fluid flows, Ann. Rev. Condens. Matter Phys. 9 (2018) 163–181.
[161] S. Balachandar, J.K. Eaton, Turbulent dispersed multiphase flow, Annu. Rev. Fluid Mech. 42 (2010) 111–133.
[162] L. Brandt, F. Coletti, Particle-laden turbulence: Progress and perspectives, Annu. Rev. Fluid Mech. 54 (2022) 159–189.
[163] I. Procaccia, V.S. L'vov, R. Benzi, Colloquium: Theory of drag reduction by polymers in wall-bounded turbulence, Rev. Modern Phys. 80 (1) (2008) 225.
[164] Y. Dubief, V.E. Terrapon, B. Hof, Elasto-inertial turbulence, Annu. Rev. Fluid Mech. 55 (2023).
[165] A. Gupta, D. Vincenzi, Effect of polymer-stress diffusion in the numerical simulation of elastic turbulence, J. Fluid Mech. 870 (2019) 405–418.
[166] S.K. Lele, Compressibility effects on turbulence, Annu. Rev. Fluid Mech. 26 (1) (1994) 211–254.